2018

DIRECTIONAL NON-COVALENT INTERACTIONS: EXPLORING THE NUANCES OF HALOGEN BONDS AND HYDROGEN BONDS IN SOLUTION AND THE SOLID-STATE

Nicholas Blouin Wageling

DIRECTIONAL NON-COVALENT INTERACTIONS: EXPLORING THE NUANCES OF HALOGEN BONDS AND HYDROGEN BONDS IN SOLUTION AND THE SOLID-STATE

By

NICHOLAS BLOUIN WAGELING

Bachelor of Science, University of New Hampshire, Durham, New Hampshire, 2012

Dissertation

presented in partial fulfillment of the requirements
for the degree of

Doctor of Philosophy
in Organic Chemistry

The University of Montana
Missoula, MT

July 2018

Approved by:

Scott Whittenburg, PhD, Dean of The Graduate School
Graduate School

Christopher Palmer, PhD, Chair
Department of Chemistry and Biochemistry

Orion Berryman, PhD, Advisor
Department of Chemistry and Biochemistry

Nigel Priestley, PhD
Department of Chemistry and Biochemistry

Mark Cracolice, PhD
Department of Chemistry and Biochemistry

Andrea Stierle, PhD
Department of Biomedical and Pharmaceutical Sciences

Wageling, Nicholas, PhD, July 2018 Organic Chemistry

DIRECTIONAL NON-COVALENT INTERACTIONS: EXPLORING THE NUANCES OF HALOGEN BONDS AND HYDROGEN BONDS IN SOLUTION AND THE SOLID-STATE

Advisor: Orion Berryman

Chairperson: Christopher Palmer

Molecules interact in numerous ways. Halogen bonding is one of the most newly discovered and poorly understood non-covalent interactions. However, this attractive force may be a useful tool for chemists in various disciplines. The directional nature, and competitive strength of the interaction makes it a promising alternative to hydrogen bonding based molecules. Indeed, through crystal structures and solution phase anion titrations, this work has shown that a halogen bonding scaffold can outperform its hydrogen bonding analogue not only in overall interaction strength, but also in resistance to inactivation from polar solvents (an important feature in anion receptors, organocatalysts, and many other applications).

Crystal structures of another bidentate, halogen bonding receptor revealed an orthogonal binding mode within the active site. This previously unseen orientation is also found in biological catalysts that contain an oxyanion hole. This finding prompted small molecule solid-state investigations and solution phase catalysis screens in an attempt to mimic biological oxyanion-hole geometry.

Due to the synthetic obstacles related to modifying the halogen bonding molecule, a different scaffold was developed to explore orthogonal binding of oxyanions. Urea based receptors were designed to be conformationally locked, with systematically increasing steric groups affixed just next to the active site. The increasing sterics were correctly predicted to direct certain planar guests into orthogonal orientations, as determined through single crystal X-ray diffraction. The orthogonal guest binding of trifluoroacetate closely resembles the carbonyl substrate orientation in biological oxyanion holes. This similarity validated a reaction screen with various carbonyl guests in different reaction types. Additionally, the ureas were added to the reaction of *N*-methylindole and *trans*-β-nitrostyrene, a commonly screened reaction in organocatalyst development. The findings showed that urea catalytic activity decreases as the steric bulk adjacent to the active site increases. This finding was not present for the reaction with carbonyls, which showed no catalytic activity difference between the ureas.

The findings here demonstrate the numerous hurdles to overcome when designing a catalyst. The capabilities and advantages of halogen bonding receptors were explored, revealing high binding strength and solvent resistance. The unique solid-state data may foreshadow unknown or overlooked binding modes in future organocatalyst design.

ACKNOWLEDGEMENTS

First and foremost, I would like to thank my advisor, Orion Berryman, for his guidance and support through my graduate career. Orion is one of the most driven, tenacious, and intelligent people I have ever met. I learned from him, not only chemistry, but a better way to approach problems, deal with stress, and push myself in all aspects of my life. For that I will be eternally grateful, and am surely a better person for it. I would also like to extend my gratitude to the other members of my committee: Christopher Palmer, Mark Cracolice, Nigel Priestley, and Andrea Stierle. All of you were frequently available to answer my questions, provide moral support, and expose me to alternative ideas. That degree of availability is a laudable feat, and you have my sincere appreciation. Of course, I must also extend my thanks to the entire faculty and staff of the Department of Chemistry and Biochemistry. For your help with everything, big and small, I am extremely appreciative of all of you.

I would also like to thank the Berryman Research Group. Asia, Casey, Jiyu, Eric, and James have been invaluable resources in my day-to-day laboratory experiences. The constructive criticism they gave (and received) during our group meetings and halogen-bonding meetings helped make me a more-well rounded scientist and person. I would like to extend special thanks to George Neuhaus for his exceptional work on the XB portion of this project. I would also like to specially thank Daniel Decato for his tireless hours in the X-ray diffraction lab. I am sure I submitted broken glass or sodium chloride to him multiple times, and he refrained from telling me to spare my pride. Crystal structures are a large part of my research, and I would not have so many were it not for the work he put in.

Finally, I cannot imagine how I would have made it through graduate school without the love and support of my family and friends. The emotional and financial support of my family, Mark, Marguerite, and Anna Wageling was invaluable, and I am so grateful to have you in my corner. Last, but not least, I would like to thank my girlfriend Jill. Thank you for letting me bounce ideas off you, for challenging me, and for being my partner in all adventures, epic and mundane.

The funding for this research was provided by the following grants: NSF CARRER CHE-1555324, NSF-MRI CHE-1337908, and CoBRE P20GM103546. Nicholas Wageling was also supported in the 2014-2015 academic year by the UM CBSD (NIH CoBRE) fellowship: NIGMS P20GM103546.

TABLE OF CONTENTS

LIST OF FIGURES

LIST OF TABLES

LIST OF EQUATIONS

LIST OF ABBREVIATIONS

∠ – angle
Å – angstrom (10^{-10} m)
$CDCl_3$ – chloroform-*d* (deuterated)
CSD – Cambridge Structural Database
DCM – dichloromethane
e.g. – exempli gratia, "for example"
ESI Q-TOF – electrospray ionization, quadrupole/time-of-flight
G – guest
H – host
HB – hydrogen bond
HSAB – hard-soft acid-base
Hz – hertz
i.e. – id est, "that is"
IUPAC – International Union of Pure and Applied Chemistry
IUPAC – International Union of Pure and Applied Chemistry
J – coupling constant(s)
K_a – association constant
kcal – kilocalorie
kJ – kilojoule
Me – methyl
MeCN – acetonitrile
MeCN-d3 – acetonitrile-*d3* (deuterated)
MeOH – methanol
NaBARF – sodium tetrakis[3,5-(trifluoromethyl)phenyl]borate
n-BuLi – *n*-butyllithium
NMR – nuclear magnetic resonance (spectroscopy)
Ph – phenyl
ppm – parts per million
TBABr – tetrabutylammonium bromide
TBACl – tetrabutylammonium chloride
TBAI – tetrabutylammonium iodide
TFA/TFA^- – trifluoroacetic acid/trifluoroacetate
XB – halogen bond
δ – NMR shift, in ppm
ΔG – change in Gibbs free energy
σ-bond – σ bond
σ-hole – σ hole
Σr_{VDW} – sum of the van der Waals radii

Chapter 1

Hydrogen Bonds, Halogen Bonds, and the Connection Between Anion Recognition and Catalysis

Matter can interact in a myriad of ways, from the strong-nuclear-force, all the way down to the comparatively weak gravitational attraction. In chemistry, the forces that are studied fall in between those two extremes, under the overarching electromagnetic force. Of the spectrum of different molecular interactions that exist, this work will focus on hydrogen bonding (HB) and halogen bonding (XB). This chapter will discuss the history of the two interactions, how they have already been exploited, and into what future applications they can be incorporated.

1.1 Introduction to non-covalent interactions

Non-covalent interactions occupy a region of physical study that is overarched by the electro-weak force, specifically electromagnetism. The underlying cause of this interaction is based on Coulombic attraction and repulsion. That is, opposing charges will attract one another, and like charges will be repelled. This basic concept will also be referred to as an "electrostatic effect" in this work.

Distortions in the electronic "cloud" surrounding an atom (or molecule) will expose or shield the atomic nuclei to different extents. The random translocation of electrons due to the Heisenberg uncertainty principle dictates that the density of electrons will not be uniform over a molecular surface, at least not for long. This process is responsible for the weakest, yet universal, non-covalent interaction: the London

dispersion force.[1–5] Instantaneous repositioning of electrons can lead to aligned polarity, causing two molecules to be drawn to each other. However, the rapid repositioning of the electrons makes this attraction fleeting, hence why it is the weakest interaction (when considered singly). This is the dominant, attractive, intermolecular interaction in uniform mixtures of alkanes, noble gases, and other molecules without a permanent dipole or charge.

When a compound contains elements of sufficiently different electronegativities, the electron cloud is distorted toward the more electronegative atom. This distortion causes a permanent dipole to form, drawing polar molecules towards one another to pair their partial charges.[6,7] While London dispersion still plays a role, this interaction is the dominant attractive force between molecules of chemicals like acetone and dimethyl sulfoxide. The higher boiling points of these liquids, relative to their non-polar analogues propane and dimethyl sulfide respectively, is a testament to the strength of a dipole-dipole interaction.

A very specific type of dipole can form when one of the atoms involved is a hydrogen. Hydrogen atoms that are covalently bonded in an organic molecule have a few distinguishing characteristics: 1) Being the smallest element, the hydrogen nucleus does not have layers of electrons to shield it. Its electron cloud can be easily distorted to expose the nucleus, and therefore more positive charge. 2) With few exceptions, hydrogen only forms one covalent bond, leaving its distal end available to interact with other atoms or molecules. 3) Compared to other elements, hydrogen has intermediate electronegativity. There are many elements that can unevenly draw electron density off

the hydrogen atom when they are covalently bonded to it. Because of these characteristics, and the ubiquity of hydrogen in nature, a special type of interaction was defined: the hydrogen bond (HB).

1.2 The Hydrogen Bond

The first mention of hydrogen bonding was by Huggins[8] in 1919, followed shortly by Latimer and Rodebush,[9] and then Pauling,[10] who popularized the term in mainstream chemistry.[11] Interestingly, these scientists describe the HB as a hydrogen nucleus held between two Lewis Basic species. That is, the hydrogen nucleus itself is the bond between the two electron rich atoms, keeping them in close contact. This description of a HB is rarely discussed in modern chemistry. The modern IUPAC definition[12] of the HB is:

> *The hydrogen bond is an attractive interaction between a hydrogen atom from a molecule or a molecular fragment X–H in which X is more electronegative than H, and an atom or a group of atoms in the same or a different molecule, in which there is evidence of bond formation.*

The HB must contain two entities: a donor and an acceptor. The nomenclature for a HB dictates that the electron-deficient hydrogen acting as a Lewis acid is called a hydrogen bond donor, and the electron rich Lewis basic species attractively interacting with it is the hydrogen bond acceptor. In text, it is pictorially represented as such: D-H···A. Here, the donor (D) is covalently bonded to the hydrogen (H), and the hydrogen forms a HB (···) with the HBA (A).

The two most important factors when considering a HB are the distance and the angle. Stronger HBs have shorter H···A distances, and more linear D-H···A angles. As the HB grows weaker, the distance increases, and the angle of interaction moves farther away from linearity. Additionally, the forces dominating the interaction change depending on the system. The strongest HBs have a degree of covalency to the interaction, whereas the weakest HBs are composed of mainly electrostatic and dispersion forces. The classifications defined by Jeffrey[13] can be found in table 1.1.

Table 1.1 Hydrogen bond classifications, lengths, angles and energies

	Strong	**Moderate**	**Weak**
Interaction type	Strongly covalent	Mostly electrostatic	Electrostatic/dispersion
Bond lengths (Å)	1.2 – 1.5	1.5 – 2.2	> 2.2
Bond angles (°)	170 – 180	> 130	> 90
Bond E (kcal·mol^{-1})	15 – 40	4 – 15	< 4

Due to the strength of HBs, they can impart stability in small molecules, such as a β-diketone, where intramolecular HBing can stabilize one conformation over another, leading to preorganization. Intramolecular HBing to impart deliberate conformation has also been seen in supramolecular structures such as resorcinarenes[14] and multidentate, XBing anion receptors.[15,16] Some examples of structures have complex networks of HBs that run along the seams of the supramolecular monomers, and are persistent when assembled in non-polar solvents. These structures can be designed to have a variety of different shapes, each with their own unique properties. This technology allows chemists to predict and design molecules with specific conformations in mind.

HBs can also direct molecular structure at an intramolecular level. In biology, nucleic acid helices and protein secondary structures such as β-sheets and α-helices are mainly stabilized by many HBs working cooperatively. HBs also play a role in biological catalysts. Inside the hydrophobic cores of many catalysts exists a web of HB donor/acceptor sites. They are ideally located to donate and accept HBs to guests with complimentary structure.

1.2.1 Hydrogen Bond Based Anion Recognition

Since the HB is a strong, directional interaction, it seems well suited as the active component of an anion receptor. Unlike cations, many anions are polyatomic, and more charge diffuse. This increases the difficulty of designing an effective anion receptor. By designing receptors that direct hydrogen bonds towards the electron rich regions of polyatomic anions, some receptor designs have been successful at selectively binding polyatomic anions over the more charge dense monoatomic ones in solution.[17] Highly discriminatory guest binding can even be exploited in the solid phase to selectively bind tetrahedral oxoanions in complex aqueous mixtures.[18]

1.2.2 Hydrogen Bonding Catalysis

Acidic proton catalysis has been known for over a century.[19] However, it was not acknowledged as such (the term HB wasn't even coined until 1930) until much later. In the 1970s, Hajos and Parrish proposed that HBing could be an important feature in proline catalysis.[20] HB catalysis became the topic of more widespread research in the 1990s, with the discovery that electron deficient ureas could catalyze reactions.[21–26]

Since then, the scope of small molecule HBing catalyst scaffolds has grown to include other prolines,[27–31] binaphthols (BINOLs),[32–34] biphenylenediols,[35,36] guanadiniums and amidiniums,[37–39] lactams,[40–43] tetraaryl dioxolane diols (TADDOLs),[44–46] phosphoric acids,[47–49] and cinchona alkaloids.[50–53]

The mechanisms through which HB catalysis operates vary from system to system. Typically, however, HB catalysis proceeds through a process known as Lewis-acid catalysis. In this mechanism, the hydrogen bonding catalyst interacts with an electron-rich portion of the electrophile in the transition state of the reaction. As the electrophile is attacked by some nucleophilic species, the high electron density on the molecule is stabilized by accepting hydrogen bonds from the catalyst.

1.3 The Halogen Bond

Like the hydrogen bond, the halogen bond (XB) is a directional, non-covalent interaction. Generally, halogens that participate in XBing are similar to hydrogens that participate in HBing: 1) With few exceptions, halogens are covalently bonded to terminal points of an organic molecule through only one bond. 2) The halogens that form the strongest XBs have moderate electronegativity. A definition was recommended to IUPAC[54] in 2013:

> *A halogen bond occurs when there is evidence of a net attractive interaction between an electrophilic region associated with a halogen atom in a molecular entity and a nucleophilic region in another, or the same, molecular entity.*

One of the major differences between the interactions, however, is in abundance. The strongest XBs are formed by the larger halogens (iodine and bromine), and halogenated organic compounds are scarce in nature. Additionally, halogens do not often "cap" electronegative atoms such as oxygen and nitrogen the same way hydrogen does. This limits the chances of halogens forming a significant dipole to more deliberate structures.

The theory behind XBing is similar to HBing, but with some subtle differences (some of the major comparisons can be found in figure 1.1). First, the halogen must be bound to something more electronegative. Sometimes this is another halogen, like in the case of the dihalogens. In fact, the publication considered to be the launching-off point for XB studies included elemental bromine (Br_2) as a halogen bond donor.[55] Other times the halogen is bound to an aromatic or conjugated system with several electron-

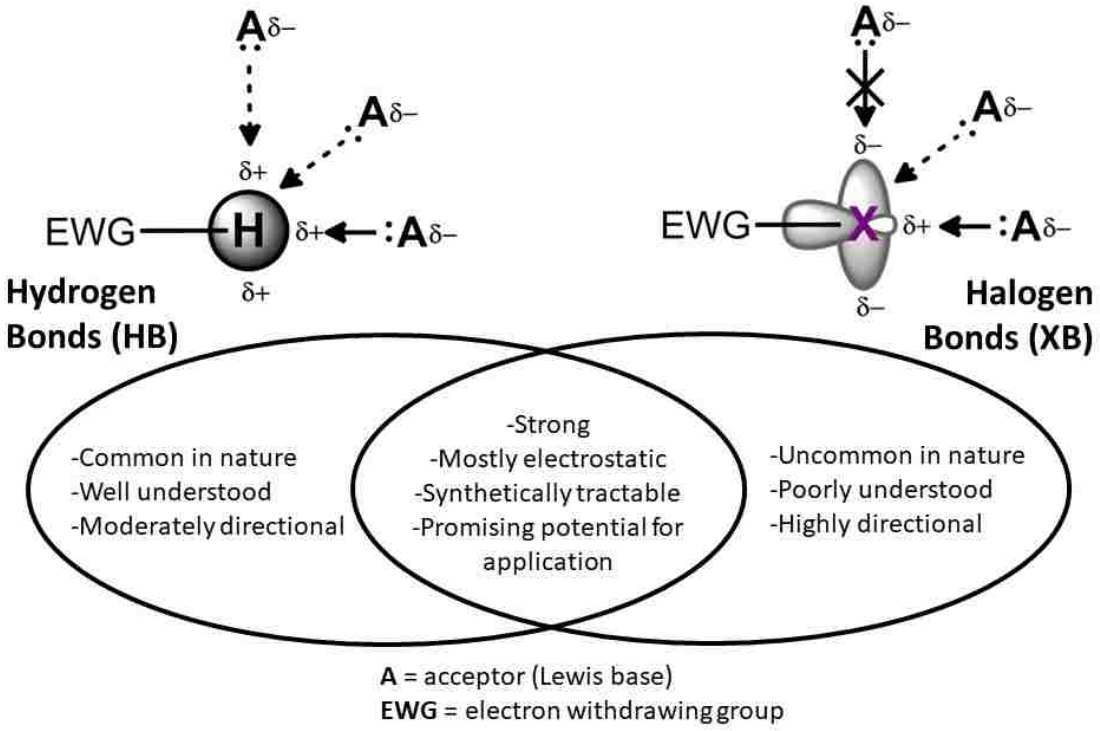

Figure 1.1 Comparison of HBs and XBs

withdrawing groups on it. Positively charged aromatic/conjugated systems (e.g pyridinium, imidazolium, etc.) also work well as strong electron withdrawing groups.

While hydrogen atoms only have a small electron cloud to displace, the heavier halogens have many layers of stabilized electrons that cannot be disrupted easily. Therefore, even when a halogen is covalently bonded to a strong electron-withdrawing group, only the outer layers of electrons are displaced. This creates a smaller surface of relative partial positive charge on the surface of the halogen, as opposed to the more widespread partial positive charge that appears on hydrogens in a similar chemical environment. This small area of partial positive charge on the halogen viewed more

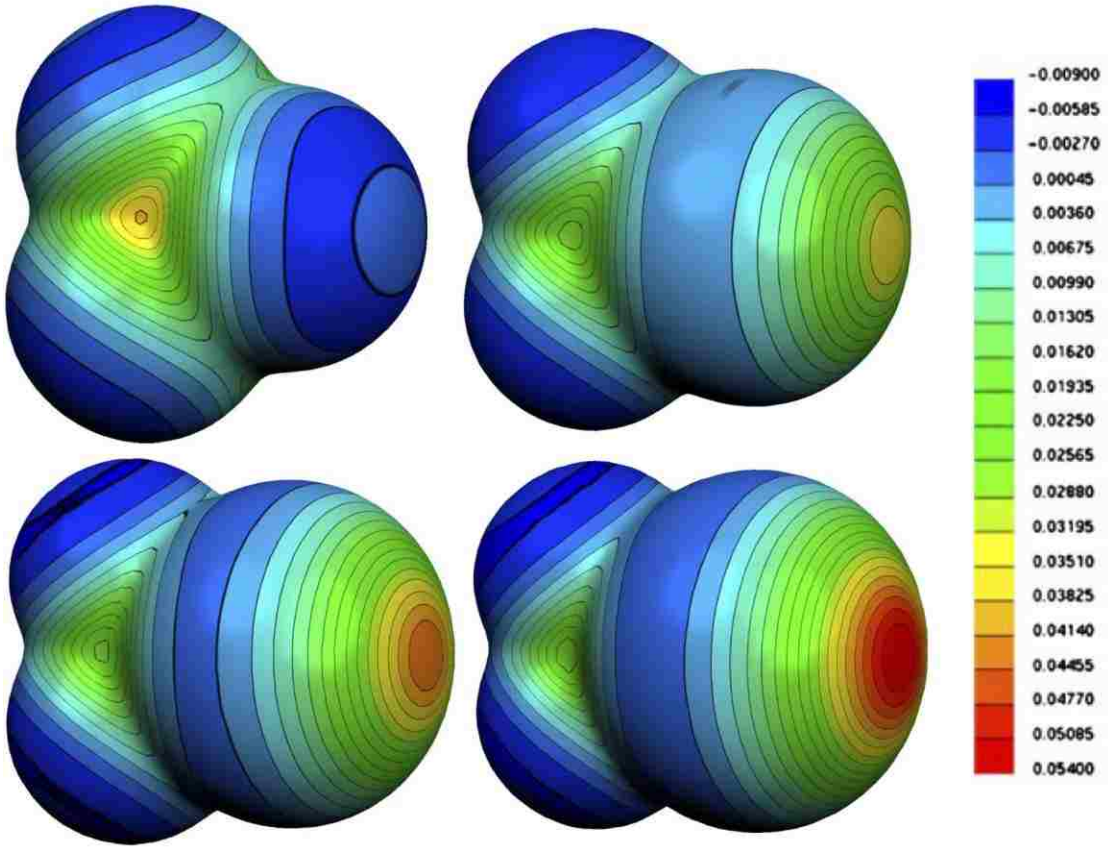

Figure 1.2 Electrostatic potential surfaces for CF_4 (top left), CF_3Cl (top right), CF_3Br (bottom left), and CF_3I (bottom right). Adapted with permission from T. Clark, et al. *J. Mol. Model.* **2007**, 13, 291-296. Copyright © 2007, Springer-Verlag.

clearly in figure 1.2, has been dubbed the "σ-hole." The σ-hole can also be described from a molecular orbital perspective as a decrease in energy of the C-X bonding orbitals. Much of the computational study of XBs has been focused on how to properly model the σ-hole. Clark, Politzer, and Murray,[56–58] Hobza,[59,60] and Taylor[61] have made significant contributions to the field of XB as it pertains to computational studies.

The large electron cloud around halogens plays another important role. As the electron cloud is drawn away from the halogen, it bunches around the equator of the atom, perpendicular to the σ-bond. This electronic anisotropy contributes to the directionality of the XB by interacting repulsively with Lewis basic species that interact with the atom.[62] Additionally, an examination of the CSD performed by Beer et al.[63]

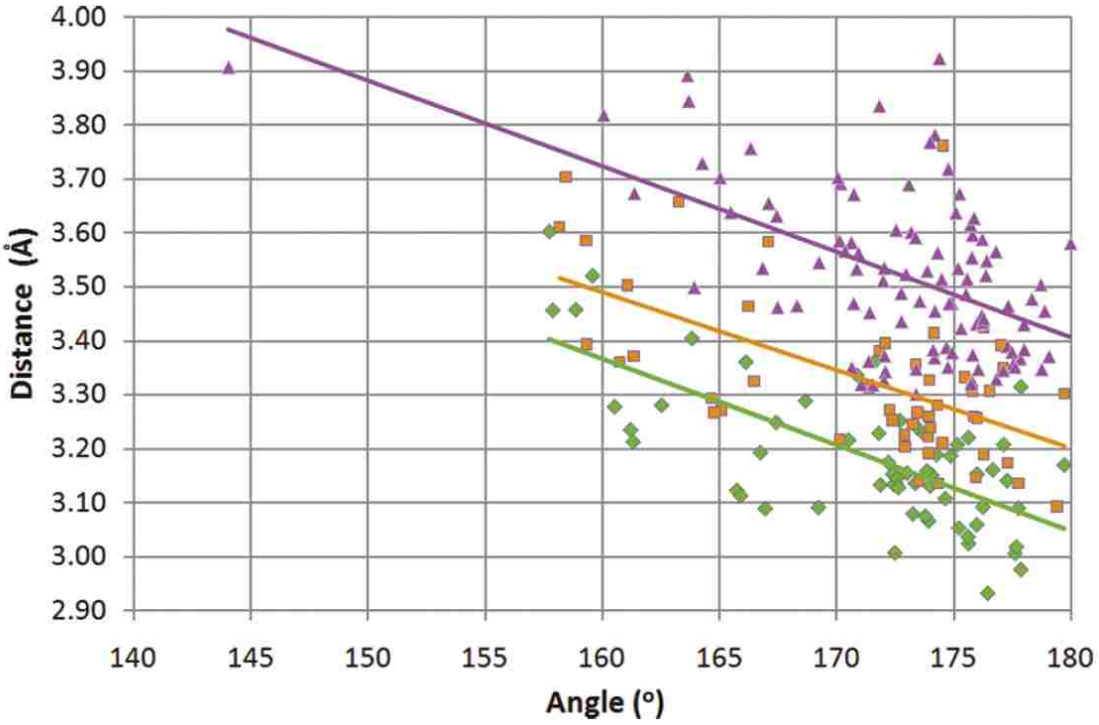

Figure 1.3 Scatterplot of CSD study demonstrating the relationship between XB length and angle. R = non-metal, non-halogen. Reprinted with permission from P. D. Beer, et al., *Cryst. Growth Des*. **2011**, 11, 4565-4571. Copyright © 2011 American Chemical Society.

demonstrates the strict directionality of the XB. The majority of the structures have a XB angle of greater than 170°, with few structures forming contacts below 165° (figure 1.3).

1.3.1 Halogen Bonds in Crystal Engineering

After Hassel's discovery of the bromine-1,4-dioxane cocrystal,[55] much of the literature was on the subject of XB in the solid-state. Metrangolo, Resnati, and Terraneo,[64,65] Rissanen,[66,67] Pennington,[68,69] and Aakeröy[70] have made numerous advances in the study of crystals with XB directed structure. Much of the early experimental evidence for the existence of XBs is from solid-state data. In crystal structures, the distance between a XB donor and an acceptor can help predict the strength of a XB. At minimum, the distance between XB donor and acceptor atoms must be less than the sum of their van der Waals radii (equation 1). Any van der Waals radii used in this work will be those calculated by Alvarez.[71]

$$r_{XB} \leq \sum r_{vdW} \tag{1.1}$$

As with most supramolecular chemistry, X-ray diffraction is an invaluable resource to take advantage of. Crystal structures can help determine molecular conformation, XBing ability, and experimental binding pocket size. The high number of XBing crystal structures allowed chemists to make general guidelines about the interaction. Naturally, studies of this interaction eventually migrated to the solution phase.

1.3.2 Halogen Bond Based Anion Recognition

A large portion of XB research has been focused on the solid-state. Naturally, crystal structures have been informative of XB receptor active sites. The information gathered from solid-state data (preferred guest orientation, XB bond distances, application of HSAB theory, etc.) laid the groundwork for solution phase studies of this mostly unknown interaction. Recent reviews nicely highlight the various receptors, and their ability to selectively bind anions.[72–74] The design of these receptors include neutral, iodo-perfluoroarenes (monodentate[75] and multidentate[76]), charged, multidentate, iodo pyridiniums,[77,78] imidazoliums,[79,80] and triazoliums,[80] and multidentate mixed-interaction rotaxanes.[81]

1.3.3 Halogen Bonding Catalysis

As mentioned earlier, HBing catalysis is abundant in the literature. Due to its similarity to HBing, XBing was quickly explored as an alternative in organocatalysts. It was discovered that XBing catalysts, could outperform HBing catalysts in comparable structures.[82] Inorganic XB catalysts saw early success in the form of elemental iodine.[83–85] Unlike inorganic XB donors, utilizing an organic framework allows for greater control of the active site. Despite this, the recent literature has not contained many new XB organocatalyst frameworks since Huber's 1,3-bis(*N*-alkyl-2-iodoimidazolium)benzene.[82,86–88] The other active XBing molecules used in organocatalysis are all monodentate: iodo-imidazoliums,[89,90] iodoalkynes,[91] N-fluoropyridinium,[92] and CBr_4.[93] The degree of complexity and specificity in HBing

organocatalysts surely foreshadows the future of XBing organocatalysis. The field is in its infancy, and there is much to discover.

1.4 Anion Recognition and Catalysis

Anion recognition and organocatalysis are closely related to each other.[94] Many reactions proceed through an anionic transition state (e.g., nucleophilic addition into a carbonyl). Like typical Lewis acid catalysts (BF_3, $AlCl_3$, etc.), XBing and HBing receptors that perform well in anion recognition also have potential as active organocatalysts. However, the inherent design of some anion receptors makes them improbable as catalysts (e.g., rotaxanes necessarily have a small active site that is ideal for anions but are not large enough to fit most of the molecules/transition states that are often targeted in catalysis). Other designs leave the active site open enough to bind reagents that are the subject of catalysis screens. In competition with an open active site is the fact that many studies on HBing have shown that multidentate receptors are better at binding anions, and therefore, are more active organocatalysts.[95] Therefore, it is important to balance the number of interactions and active site availability when designing an organocatalyst.

Much of the research that has already been performed has been invaluable in designing new, and better receptors. Solid-state studies reveal low energy conformations and limitations on binding geometry, which are both important factors to consider when designing an anion receptor or organocatalyst. Growing diffraction quality crystals and obtaining crystal structures of new molecules is a crucial component of our progress in understanding new receptors and organocatalysts.

In order to further grasp the full potential of organocatalysts and anion receptors, more studies need to be performed on multidentate receptors. The active site of these molecules is still a mystery. Utilizing poorly understood, but strong, interactions such as XBs may result in significant advances to the field. XBing will be able to distinguish itself as a competitive and unique design strategy for receptors once the scope of its capabilities has been expanded. One of the most exciting aspects of XBing research comes from HB comparison studies. Observing significant differences between a XBing receptor and its isostructural HBing counterpart will demonstrate the need for continued studies of not only these receptors, but the active site as a whole.

Chapter 2

Halogen bonding host: Synthesis, Computations, Crystal Structures, and Anion Binding Study in a Competitive Solvent

2.1 Preface

The syntheses, characterizations, diffraction quality crystallizations, and anion titrations in this chapter were performed by Nicholas Wageling and George Neuhaus. The crystallographic data were obtained and solved by Daniel A. Decato. The computational studies were performed by Ariana M. Rose. This chapter was written by Nicholas Wageling, and includes work that was published in *Supramolecular Chemistry* (**2016**, 28, 665-672).

2.2 Introduction

The halogen bond (XB) has been growing more prevalent in the literature in the last 20 years. The strict directionality requirements and potential to form strong interactions has made it a competitive alternative to structures containing hydrogen bonds (HB). Additionally, XB receptors have different synthetic strategies associated with them compared to HB donors (e.g., cannot use traditional donor motifs such as ureas, sulfonamides, etc.). This synthetic difference has led to XB receptors with novel design features.

The majority of solution-phase organic XB donor studies have focused on anion recognition which led to applications in chemical sensing, anion transport, and ion extraction. Much of this early research involved XBs in non-polar organic solvents, due to the difficulty in designing a receptor that is competitive in polar solvents. In non-polar

solvents, a polar interaction like XBing will be more pronounced and facilitate proof of principle studies. Hunter and coworkers have shown that XBing may show higher resistance to polar-solvent inhibition than HB receptors.[96]

XBing receptors that bind anions in competitive solvents demonstrate the potential for XBing organocatalysts. In the same way that a simple Brønsted acid or HB donor can catalyze a reaction, structures with XB donors should also be able to effectively catalyze reactions. However, up until this point, XBing organocatalysts have been scarce in the literature. XB molecules as organocatalysts, with their stricter directionality requirement and solvent-inhibition resistance, have the potential to become a new paradigm in non-covalent catalyst design.

In order to balance the synthetic ease of a monodentate receptor with the increased stabilization of a multidentate receptor, a bidentate XB scaffold was chosen for this structural design and has proven effective at binding anionic guests. Since many reactions proceed through an anionic transition state, anion-binding studies can often predict the catalytic effectiveness of a host molecule. Higher association constants (K_a) typically correlate to higher-performance catalysts. However, associations constants that are too large may indicate that the receptor will bind the guest too strongly, in which case the reaction will not proceed. Other features must also be considered: accessibility of the host active site, guest geometry, and product binding ability (i.e., product inhibition).

This chapter will discuss the design and synthesis of four bidentate receptors. The properties of the molecules will be collected through computations, X-ray

diffraction, and anion titrations. The anion titration data can be used to determine association constants and structural binding information. The association constants will help determine whether the receptor is a viable candidate for catalysis.

2.3 Synthesis of XB Receptors

One must take certain structural restrictions into consideration when designing XB anion receptors. First, the halogen donor must be electron deficient enough to have a sufficient partial positive region (the σ-hole). In HB systems, a traditional HB donor is typically bonded to a more electronegative atom such as nitrogen or oxygen, which is sufficient to generate a significant dipole. Halogens bonded to an oxygen or nitrogen on an organic framework are uncommon, and synthetically untenable presently. Therefore, the halogen is usually covalently bonded to a carbon atom that can be made electron withdrawing through various means. Two common approaches are to use iodo-perfluorinated alkyl chains/phenyl rings, or to use some sort of positively charged iodo-annulene (see figure 2.1 for other examples). Since charged annulenes are better electron-withdrawing groups, they will be used in this study. Specifically, *N*-methylated imidazolium will be used, as there is literature precedence of it performing well as the electron withdrawing group for XB activation.

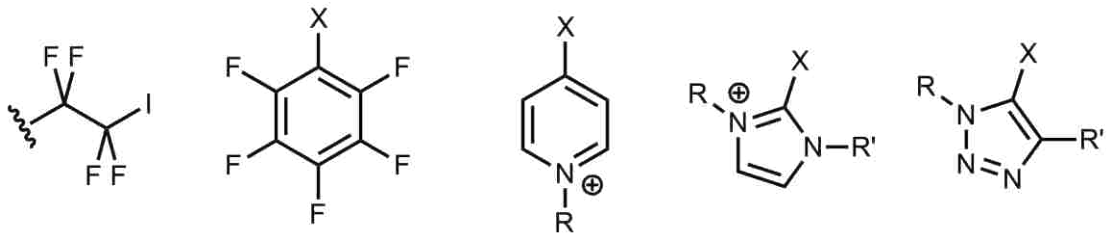

Figure 2.1 Examples of carbon based EWGs to activate halogens (X) for XBing.

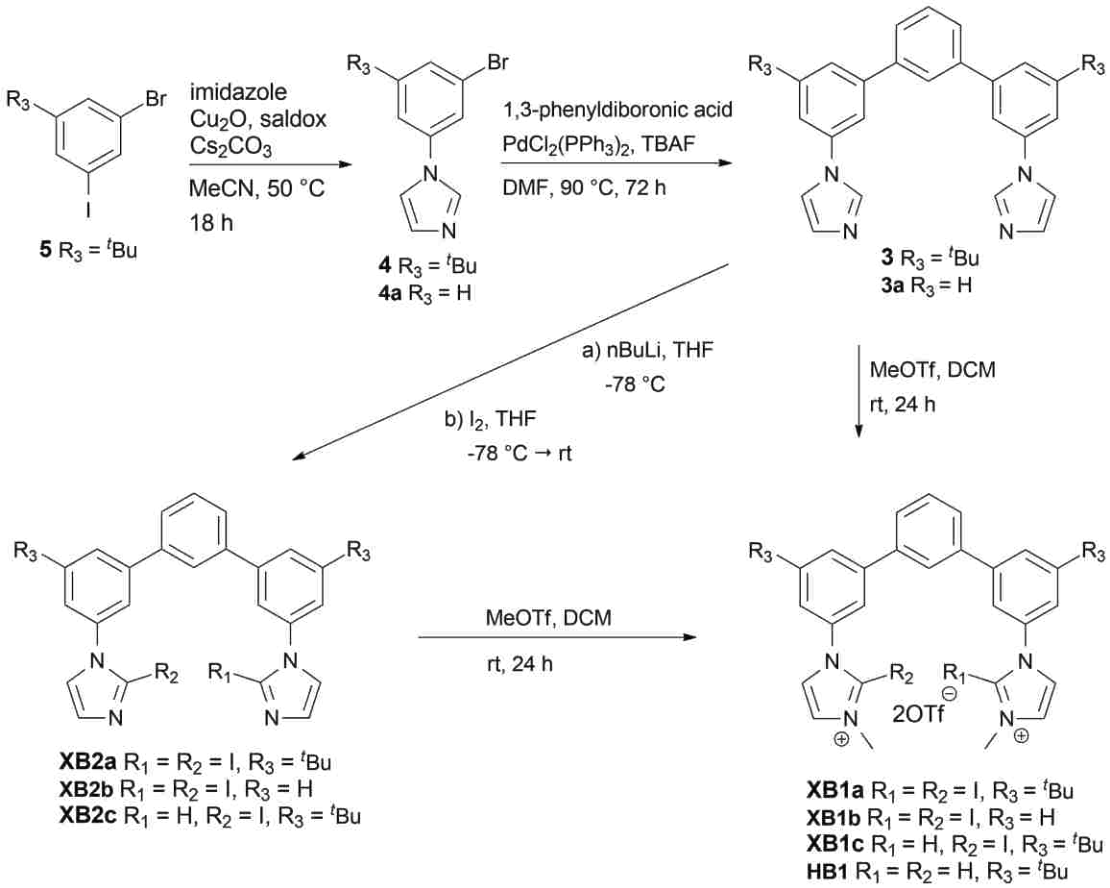

Figure 2.2 Synthesis of the XB and HB anion receptors.

The next feature to consider is the size of the halogen. Iodine, the best XB donor atom, is much larger than hydrogen. This means the scaffold must be larger, and must be designed in a way that allows multiple iodines to coordinate to a single guest. Failing to account for this can even result in a scaffold that is conformationally locked in a divergent arrangement.[97] A *meta*-terphenyl backbone should provide the separation necessary to prevent the iodines from repulsively interacting with one another, while still providing a degree of conformational rigidity to keep them convergent on a guest.

Bidentate XB scaffold **XB1** and controls **XB2** and **HB3** were prepared by regioselective *N*-arylation of **5** or **5a** with imidazole (figure 2.2). Selectively coupling the

two rings at the iodinated carbon leaves the brominated carbon available for further chemistry. In this case, the aryl-imidazole product (**4**/**4a**) was then allowed to react with 1,3-phenyldiboronic acid through a twofold palladium catalyzed Suzuki-Miyaura cross-coupling reaction. This *meta*-terphenyl scaffold with terminal imidazoles (**3**/**3a**) is the base structure for the molecules studied in this chapter. The HBing analogue (**HB1**) was prepared by *N*-alkylation of the imidazoles at the peripheral nitrogen with methyl triflate. To iodinate the neutral scaffold, the imidazole C2 carbons were deprotonated using *n*-BuLi, and the resultant di-carbanion was quenched with elemental iodine. This reaction generated the neutral (and inactive) XBing penultimate products (**XB2a**/**XB2b**). A byproduct of the iodination is the monoiodinated species (**XB2c**), which was collected during purification to study the receptor with mixed HB/XB donors. The neutral iodinated structures were then activated by methylation of both imidazoles to give the active XB-donor receptors **XB1a** and **XB1b**, and the monoiodinated **XB1c**.

2.4 Crystal Structures of XB Receptors

X-ray diffraction is an invaluable tool for evaluating structural features in the solid-state. The receptor conformation in the solid-state can be informative of the preferred conformation in solution. In this study, crystal structures of **XB1b** (with triflate counteranions), **HB1** (with triflate counteranions), and **XB1a** (with iodide counter anions, **XB1a·2I**) were obtained from diffraction quality single crystals. Crystals of **XB1b** were grown from the slow evaporation of an acetone solution. **HB1** crystals were grown from vapor diffusion of THF into a MeOH solution. **XB1a·2I** crystals were grown from the slow evaporation of the receptor and TBAI in 1 % D_2O:CD_3CN.

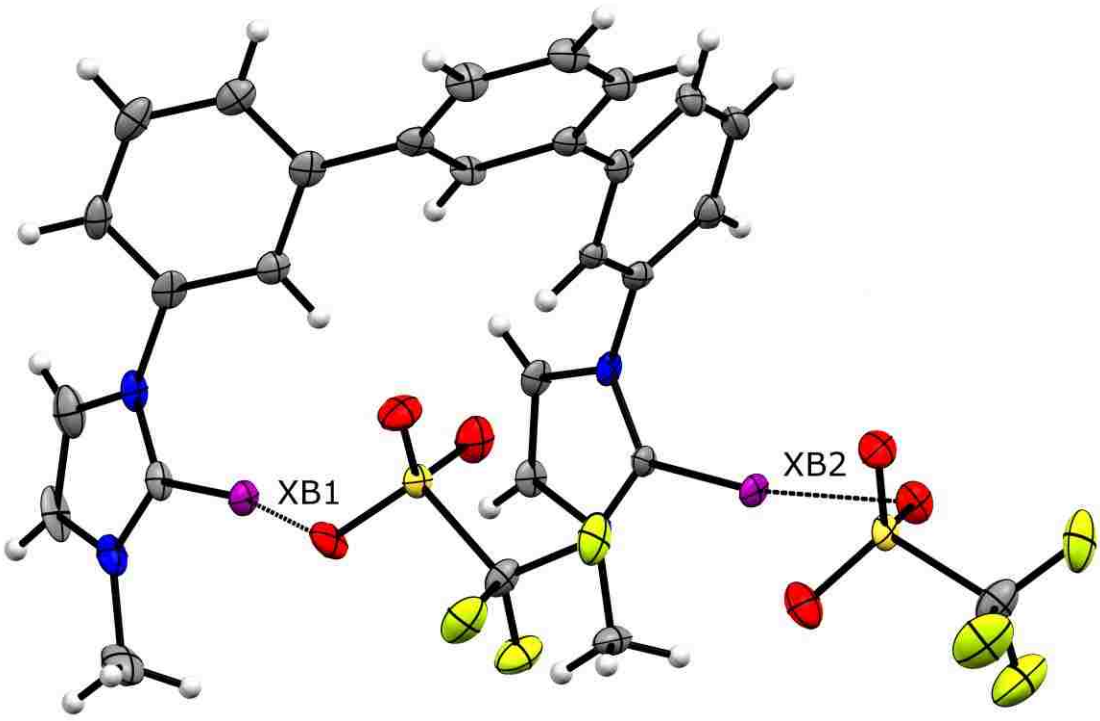

Figure 2.3 Crystal structure of **XB1b** showing XBs formed between the iodines of the imidazoliums and the triflate counteranions. Thermal ellipsoids are drawn at the 50 % probability level.

The comparison of crystal structures reveals interesting conformational characteristics about the XB host-guest complexes. The two receptors are arranged in remarkably similar orientations, despite the different substituents on the *meta*-terphenyl backbone, and the geometrically diverse counteranions/guests. In both **XB1b** (figure 2.3) and **XB1a·2I** (figure 2.4), the imidazoliums are orthogonal to the terminal rings of the *meta*-terphenyl backbone. In **XB1a·2I**, the average torsional angle between the imidazolium and the terminal phenyl ring is 72.25° (XB1: 74.9(5)° XB2: 69.6(5)°). In **XB1b**, the average torsional angle is 71.87° (XB1: 63.00(19)°, XB2: 80.74(19)°). The rings form a partially macrocyclic arrangement, with the iodoimidazoliums organized in a pre-convergent orientation. In figure 2.4, **XB1b** has two short contacts XB1 (2.822(5) Å,

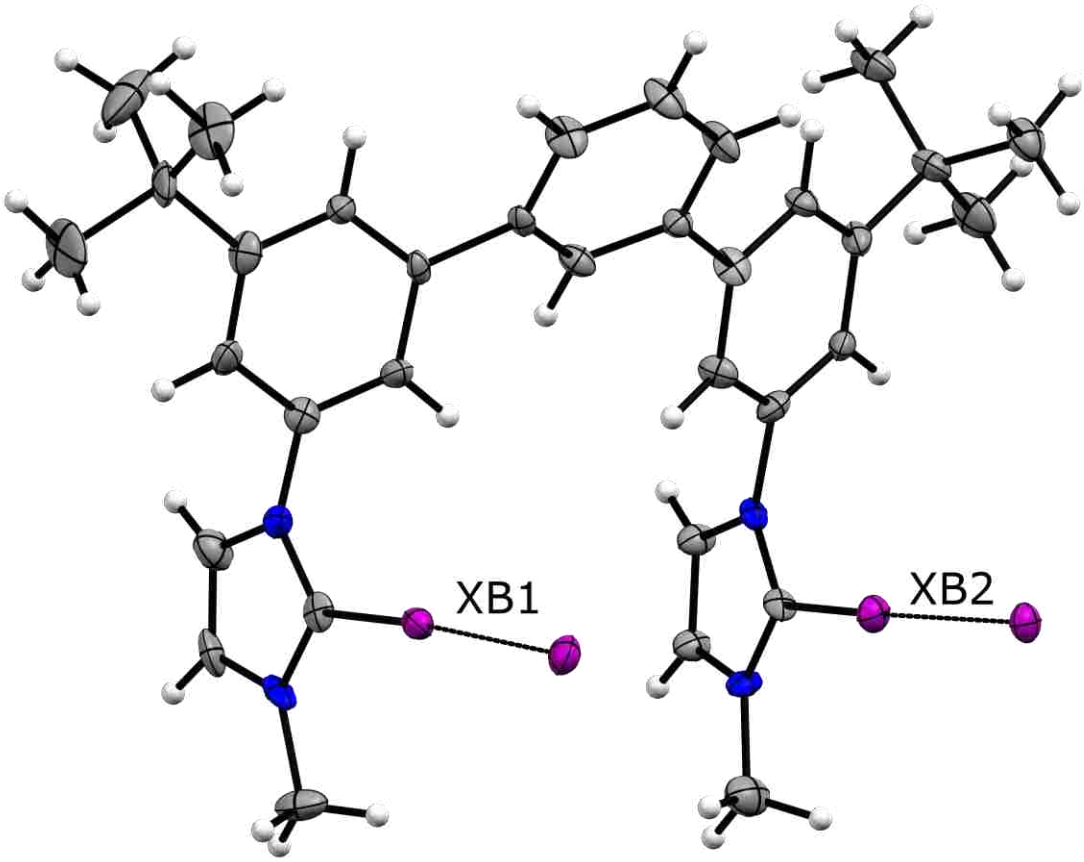

Figure 2.4 Crystal structure of **XB1a·2I** showing XBs formed between the iodines of the imidazoliums and the iodide counteranions. Thermal ellipsoids are drawn at the 50 % probability level.

80.2 % Σr_{VDW}, 169.92(15)°) and XB2 (2.831(5) Å, 80.0 % Σr_{VDW}, 171.98(17)°) that fall within the range of moderate to strong XBs. The same is true for **XB1a·2I**, figure 2.4, which also has two short contacts: XB1 (3.4063(14) Å, 83.5 % Σr_{VDW}, 175.1(3)°) and XB2 (3.3183(14) Å, 81.3 % Σr_{VDW}, 178.7(4)°). The distances are longer in the **XB1a·2I** crystal since the guests are iodides, and thus have a larger van der Waals radius (r_{VDW}) than the oxygens accepting the XBs in **XB1b**, figure 2.3.

The non-iodinated analogue **HB1** exhibits an alternative crystal packing compared to the XB receptors. Close examination of the crystal structure, figure 2.5,

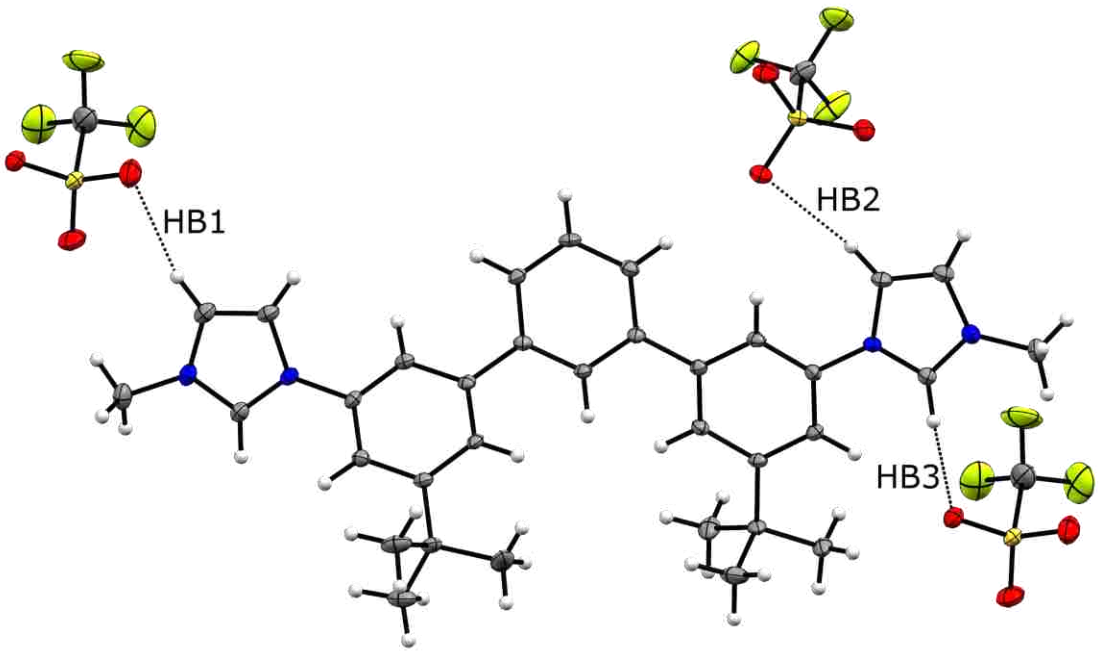

Figure 2.5 Crystal structure of **HB1**, demonstrating the splayed out, linear conformation and indiscriminate HBing. Thermal ellipsoids are drawn at the 50 % probability level.

shows how the triflate counteranions are dispersed around the host molecule, forming weak HBs. In addition to the lack of strong interactions, the receptor lacks any appreciable pre-convergent conformation. When the imidazole carbons are not substituted, it is more likely to become aligned coplanar with the bonded aromatic ring. When there are large groups in place (such as an iodine at the C2 position), the ring is likely to be more orthogonal due to steric hindrance. In figure 2.5, the average imidazole-arene torsional angle is 30.53° (HB1 side: 40.87(7)°, HB2 side: 20.19(7)°). This is over 40° closer to coplanarity than the iodinated receptors.

The crystal structure of **XB2b** (figure 2.6) shows a dimerization where the iodine on one imidazole donates a XB (3.8373(5) Å, 94.1 % Σr_{VDW}, 174.74(14)°) to the electron-rich belt of the iodine on the neighboring molecule's iodoimidazole (acceptor C-I···I

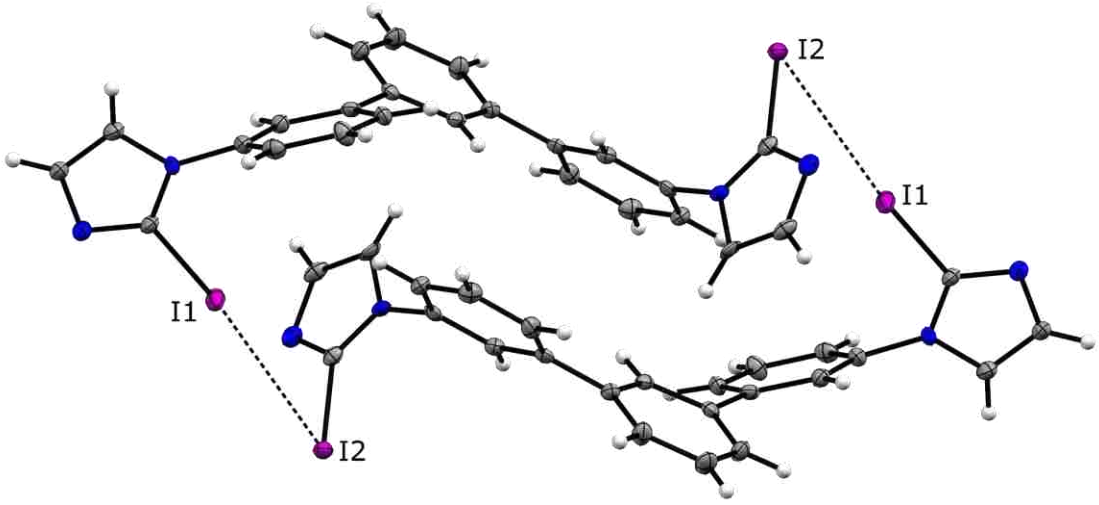

Figure 2.6 Crystal structure of **XB2b**. Thermal ellipsoids are drawn at the 50 % probability level.

angle: 64.35(10) Å). While the XBs in the unalkylated structure are weaker (since the donor-acceptor distance is only 94 % of the sum of the VDW radii), the iodoimidazole-arene torsional angle in the unalkylated receptor is also close to orthogonal (72.45(18)°). This demonstrates that a degree of preorganization may be imparted simply by using an iodinated structure over a protonated one.

2.5 Computations

The crystal structures provide valuable insight into the active conformation of the receptors. They show a large degree of pre-convergence in the solid-state. However, the solid-state structures do not necessarily show the low-energy solution phase conformation. While the scaffold was rationally designed to bind a guest in a bidentate fashion, the receptors exhibit multiple binding modes in solution. Additionally, while the bidentate orientation may appear to be a low energy conformation, other effects may be playing a significant role.

Computations were performed to compare the energies of the expected binding modes in the gas phase. Starting from the crystal structures, geometry optimizations were performed on receptors **XB1a** and **HB1**, in the presence of two chloride anions. The anions were arranged to favor an unbound, bidentate, or a bis-monodentate state upon geometry minimization (i.e., initially positioning the anions close to, or far from, the receptor). The calculations were performed at the B98 level of theory, using the 6-31+G(d,p) basis set for all non-halogen atoms, and LANL2DZ with effective core potential (ECP) for the iodines. The iodine atoms were further augmented with diffuse functions of p-symmetry and polarization functions of d-symmetry. This level of theory and basis set has been shown to correlate well with experimental XB studies.[61] In each conformation, chloride anions that were interacting with the iodine or hydrogen were appropriately linear (>169°). The results of the computation are shown in table 2.1. Expectedly, the bidentate association provides a greater stabilization in both the XBing and HBing system.

Table 2.1 Calculated gas-phase binding energies of **XB1a** and **HB1**

	Bidentate	**Monodentate**
Receptor·Guest	**ΔG (kcal·mol^{-1})**	**ΔG (kcal·mol^{-1})**
XB1a·2Cl$^-$	-23.66	-9.19
HB1·2Cl$^-$	-21.27	-14.83

2.6 Anion Titration Studies

The strength of association between the receptors and anions can provide valuable insight into the potential strength of the receptor as a catalyst. A receptor that

binds well to anions may also stabilize oxyanionic transition states (common in organic synthesis) if other factors such as active site availability are also favorable.

Receptor **XB1a**, **XB1c**, and **HB1** were chosen for the anion titration studies. Receptor **XB1a**, with two XB donors, is the best candidate for a XB catalyst using this scaffold. Receptor **XB1c** will also be studied to observe a mixed donor scaffold, with one HB and one XB donor. Finally, **HB1** will serve as the HB analogue to compare a structurally identical HBing receptor and XBing receptor.

The titrations were performed by observing changes in a measurable signal after sequential additions of a guest to a solution containing the receptor. In this study, NMR spectroscopy was chosen, since this technique can reveal more structural information about the interaction than UV-Vis, fluorescence, and ITC. Using NMR spectroscopy, the protons involved in guest binding can be determined by observing which proton resonances shift during the titration. Determination of the binding constants from these titrations is performed using HypNMR 2008:[98] software designed specifically for the determination of binding constants using NMR chemical shift data. The mathematical logic for the basis of this software can be found in an early guide by Hirose,[99] and in a more contemporary practical article by Thordarson.[100] However, the important points from the articles will be discussed. For a 1:1 association between a receptor (here referred to as host, H) and guest (G), the association constant (K_a) is shown in equation 2.1.

$$K_a = \frac{[HG]}{[H][G]} \tag{2.1}$$

Other terms that will be used in this explanation will be the total concentration of receptor/host, $[H]_0$, and the total concentration of guest $[G]_0$, which can be found in equations 2.2 and 2.3 respectively.

$$[H]_0 = [H] + [HG] \tag{2.2}$$

$$[G]_0 = [G] + [HG] \tag{2.3}$$

Titrations involving a guest being bound to a receptor purely by non-covalent interactions typically involves kinetics of "fast exchange": that is, the association and dissociation of the guest occurs faster than the NMR timescale (on average, tens of μs).[101] Because of this, distinct peaks for the free and bound receptors are not observed. Instead, upon the addition of guest to a solution containing the receptor, the spectrum will contain a single averaged peak between the expected signal for the free receptor, and the completely bound receptor. As the ratio of guest to receptor increases, the averaged peak moves closer to the resonance of the fully bound receptor. This averaged peak is the observed signal (δ) shown in equation 2.4, which also contains the signal of the free receptor (δ_H) and the signal of the complexed receptor (δ_{HG}). During these NMR titrations, it is important to always take a spectrum of the free receptor to obtain a δ_H value. Additionally, adding enough equivalents of guest to ensure that the dominant species in solution is HG allows a reasonable approximation of the δ_{HG} value.

$$[H]_0(\delta - \delta_H) = [HG](\delta_{HG} - \delta_H) \tag{2.4}$$

Since the signal of the free receptor and fully bound receptor remain constant, as does the concentration of receptor, by experimental design, the difference between the

observed signal and the free receptor is proportional to the concentration of the complex HG (equation 2.5).

$$(\delta - \delta_H) = \frac{[HG](\delta_{HG} - \delta_H)}{[H]_0} = [HG]c \quad (2.5)$$

Upon manipulation of equations 2.1, 2.2, and 2.3, one can obtain an expression for [HG] in which the only unknown is the association constant (equation 6).

$$[HG] = \frac{1}{2}\left(G_0 + H_0 + \frac{1}{K_a}\right) - \sqrt{\left(G_0 + H_0 + \frac{1}{K_a}\right)^2 + 4[H_0][G_0]} \quad (2.6)$$

Since a value for [HG] can be calculated from the knowns ($[G]_0$, $[H]_0$, and all δ values), the association can then be determined through an iterative process. A guess (based on understanding of the system, solvent used, etc.) is made for the value of K_a, and the resultant isotherm is fit to the observed shifts. The process is repeated until the isotherm converges with the data. While the initial guess is made by the experimenter, the subsequent iterations are performed by the software. For this reason, it is important to attempt to find convergence with multiple initial guesses. A binding isotherm is fit to the data (observed signal vs. $[G]_0/[H]_0$) based on the mathematical model. When the best fit is found (assuming the lineshape does indeed fit the data), the value for K_a is obtained.

In this study, a 1:2 association (equation 2.7) is present in addition to the 1:1 association. Similar reasoning (manipulation of equations 2.1, 2.2, 2.3, and 2.7) is used to obtain equations that relate the formation of the complex, HG_2, to the observed chemical signal. More details can be found in the Hirose and Thordarson reviews listed above.

$$K_2 = \frac{[HG_2]}{[G][HG]} \quad (2.7)$$

Trial titrations were performed with $CDCl_3$, and DCM-*d2*/$CDCl_3$ mixtures, however the resultant association constants were beyond the reliability of the spectrometer ($K_a > 10^6$). To combat this, acetonitrile-*d3* was chosen as a solvent for this study, since it is polar and will compete with the receptors. Observing significantly large association constants in a competitive solvent provides valuable information about potential solvent inhibition of the receptor, solvent inhibition of the guest, and subsequently, the ability of the receptor to remain in an active conformation enough to bind the guest. Each titration was performed in triplicate, beginning with zero equivalents of guest, and ending at five equivalents of guest. For each titration, the guest solution was made from an initial solution of receptor, to keep the host concentration constant throughout the titration Each titration contained between 18 and 24 points (spectra), to ensure enough data to create an isotherm that could be fit confidently to the model.

Upon incorporating a second association (1:2, H:G) into the model, the isotherm converged on the data with a better fit than a model that only contained a 1:1 association. This, along with the rational design of the receptor to be able to realistically adopt conformations that allow a 1:1 and 1:2 association, a solid-state example of 1:2 binding, and computational support for a 1:2 association being present, is evidence for a two-step association model for this system. The binding isotherms for the experiments performed here can be found in the Experimental Section. While the major association modes are likely to be 1:1 and 1:2 (H:G), additional associations need to be included in

the model before they can be ruled out. The poor isotherms that resulted from including a 2:1 (H:G) association in the model, and the lack of 2:1 association in the crystal structures, ruled out a significant contribution from a 2:1 association. Additionally, a 2:1 association would require four imidazoliums to crowd around a single monoatomic anion, which is unlikely due to Coulombic and steric repulsion. Conversely, the 1:1 and 1:2 model provided reasonable to excellent fits for the isotherms, supporting the hypothesis of that model being correct. Higher order associations (2:3, 3:2, 4:5, etc.) are unlikely due to the entropic penalty incurred upon forming large aggregates.

Table 2.2 Anion association constants for **XB1a**, **XB1c**, and **HB1**

Receptor	**Guest**	**Solvent**	**K_1**	**K_2**
XB1a	Cl^-	1 % D2O in CD_3CN	37,700	432
	Br^-	1 % D2O in CD_3CN	28,900	356
	I^-	1 % D2O in CD_3CN	12,990	455
	Br^-	0 % D2O in CD_3CN	236,000	2,380
	Br^-	5 % D2O in CD_3CN	3410	293
XB1c	Cl^-	1 % D2O in CD_3CN	5902	59.2
HB1	Cl^-	1 % D2O in CD_3CN	935	57.0
	Br^-	1 % D2O in CD_3CN	759	64.0
	I^-	1 % D2O in CD_3CN	624	47.3
	Br^-	0 % D2O in CD_3CN	11,000	425
	Br^-	5 % D2O in CD_3CN	229	18.4

Note: All mixed solvents are v/v. Each titration was performed in triplicate at 289 K to encourage intramolecular interactions, and discourage degradation of the receptor with iodide (observed at higher temperatures). All anions used were tetrabutylammonium salts, and the association constants K_1 and K_2 were calculated from the shifts of the imidazolium and methyl proton resonances. Errors are estimated to be 10 %.

The results of the titrations can be found in table 2.2. A few conclusions can be drawn from these data. First, the XBing receptor **XB1a** clearly has stronger associations to halides compared to its HBing analogue (with all K_1 values 24-40 times larger for the XBing receptor). Second, the strength of the **XB1a** associations follow the Hofmeister series. Chloride, the most charge dense halide studied, binds the strongest, followed by bromide and then iodide. This trend is also observed in the **HB1** association constants, indicating that the difference in binding is not due to size exclusion of the larger anions. The receptor with both a XB donor and a HB donor, **XB1c**, resulted in an intermediate association constant, demonstrating that the iodine plays an important role in binding for this system. Third, the XBing receptor shows a greater resistance to solvent inhibition. Increasing the water content from zero to 5 % decreases the association constants for both **XB1a** and **HB1**. This is not surprising, since the energy of hydration for chloride is so high. However, the average logarithm of the global association constant (logβ2, which can be found in the Experimental Section) for **XB1a** only decreases by 32 % (8.76 to 5.99), while the association constant for **HB1** decreases by 46 % (6.64 to 3.64) as the water content is increased. Therefore, scaffolds designed around XBs may produce organocatalysts that remain competitive in polar solvents or even water, while HBing organocatalysts are rendered inactive. This striking difference between the two interactions will lead to future designs based on XBing instead of HBing. These new XBing receptors are resistant to competitive solvents, and may be the key to designing receptors that remain active and selective in aqueous systems.

2.7 Conclusions

In this chapter, the synthesis, characterization, and anion binding properties of a XBing receptor were studied. A mixed system (XBing and HBing) analogue and HBing analogue were also prepared to further explore the effect of the XB, and to make comparisons to the more well-known HB. Crystal structures demonstrated more preorganization in the iodinated scaffold over the non-iodinated scaffold. Part of the preorganization may be due to the increased directionality of the XB over the HB. Anion titrations were also performed in solution. The results showed that not only does the XBing iodoimidazolium **XB1a** outperform its HBing counterpart **HB1**, it is also more resistant to increasing solvent polarity.

The increased strength and solvent resistance discovered in the anion titration study show that XB receptors may be competitive alternatives to HB receptors, especially in polar solvents. This study is one of the first examples of an isostructural comparison of XBs and HBs. While other comparison studies have shown polar solvent inhibition resistance between the two interactions, the non-covalent donors were on radically different scaffolds. Here, the advantages of using XBs over HBs are clear: Increased interaction strength will lead to better anion receptors and organocatalysts. The solvent resistance observed in the XB receptor lays the groundwork for the design of future receptors that can be used in competitive solvents. Beyond the benefits already listed for XBs, increasing the strength of a HB also increases its acidity, certain HBing receptors could be unsuitable in situations that are acid sensitive. A XBing

organocatalyst would not have that same issue, since the halogen will not be as readily removed as a proton, and may even be completely resistant to some Lewis bases.

Chapter 3

Hydrogen Bonding Host: Synthesis and Crystal Structures

3.1 Preface

The syntheses, characterization, diffraction quality recrystallizations, and computations in this chapter were performed by Nicholas Wageling. The crystallographic data were collected by Daniel A. Decato. The results have been accepted by *Supramolecular Chemistry*, and are in the process of being published.

3.2 Introduction

The increased receptor strength and solvent resistance of XBs was described in the previous chapter. Since the receptor was designed to explore the utility of XBing in organocatalysis, the results from that study led to intriguing thoughts regarding the transition states of reactions. While the crystal structure of **XB1a** demonstrates pre-convergence to favorably bind a guest in a bidentate fashion, the crystal structure of **HB1** shows enough conformational flexibility to adopt other binding modes.

Another XB receptor (**G1XB**) designed and synthesized by the Berryman group revealed an interesting guest binding geometry in the solid-state (figure 3.1).[102] A DMF solvate of **G1XB** highlights a bidentate XBing interaction to the carbonyl oxygen of DMF over the triflate counteranion. Crystal structures involving HBs to carbonyl oxygens show that the majority of HBs interact at the position of the lone pairs (i.e., 120° from the C=O bond, in the RC=O plane of the carbonyl).[103] However, XB donors may yet reveal catalyst binding modes that were previously ignored (or not explored).

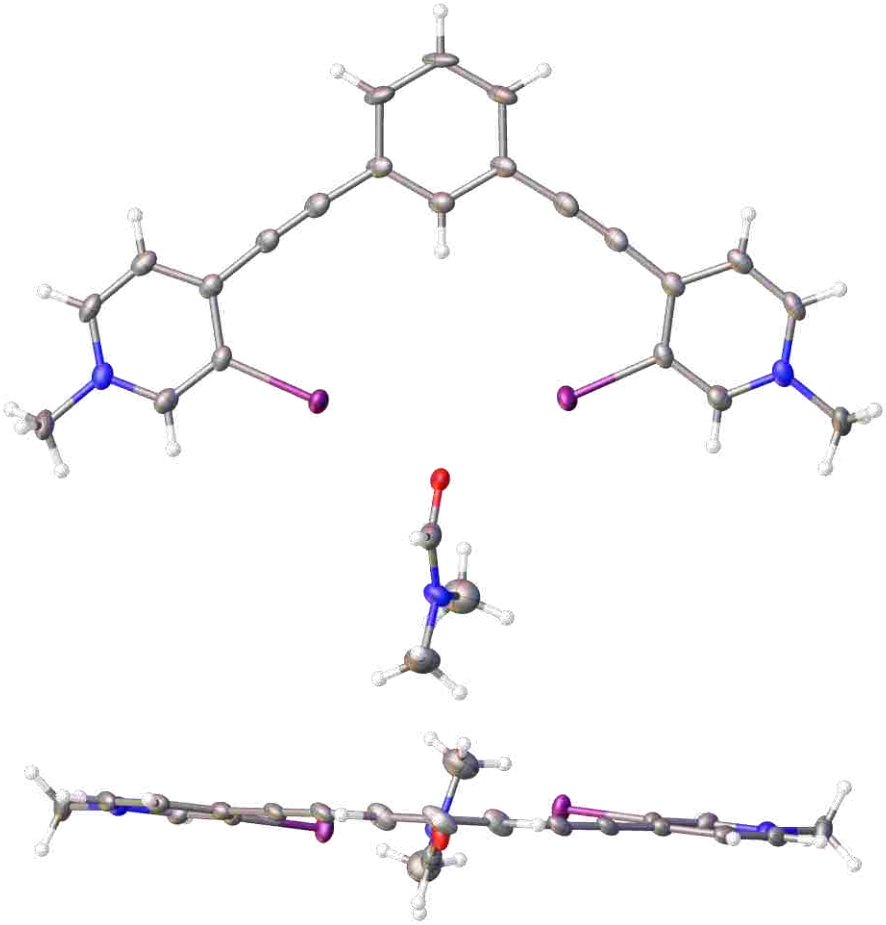

Figure 3.1 XB receptor G1XB binding DMF. Front view (top) and top view (bottom). Thermal ellipsoids are drawn at the 50 % probability level. CCDC 1520140.

Indeed, an alternative and unexplored binding mode for carbonyl organocatalysis is found in nature. Goodman and Simón[104] performed an analysis of oxyanion holes in biological enzymes catalogued in the Protein Databank (PDB). They also made a comparison to crystal structures of synthetic HBs being donated to carbonyls in the Cambridge Structural Database (CSD). What they found was that while synthetic HB donors interact with the lone pairs on carbonyl oxygens, biological HB donors in enzymes tend to bind carbonyl oxygens orthogonally to the lone pairs (figure

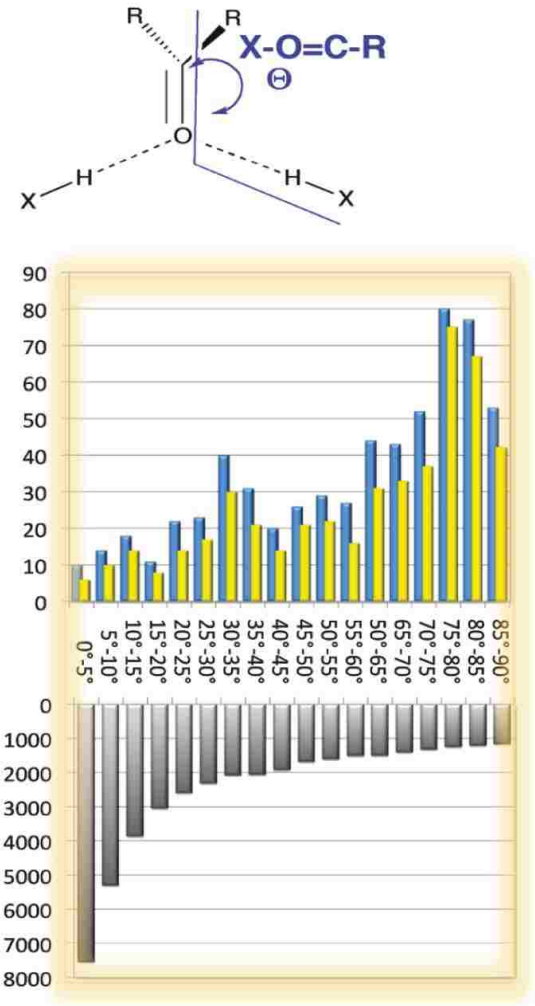

Figure 3.2 A comparison of PDB (top) and CSD (bottom) HB interactions with carbonyls. Reprinted with permission from L. Simón and J. M. Goodman *J. Org. Chem.* **2010**, 75, 1831-1840. Copyright © 2010, American Chemical Society.

3.2). This finding prompted small molecule solid-state investigations to obtain oxyanion hole-like geometry.

3.3 Design

Systematically modifying the active site of **XB1a** was not feasible due to the structural design of the system. The active conformation of **XB1a** does not place the iodines near any part of the scaffold that can be easily modified to “push” a guest into an orthogonal conformation. Additionally, the organocatalytic activity of the XB system

was untested. Because of this, any design based on **XB1a** would be unsuitable. Instead, an established organocatalyst motif that could be easily modified was chosen: a urea.

Ureas, can adopt various conformations. The active conformation is when the nitrogen protons are both in the "down, down" orientation (see figure 3.3). Early research,[105] supported by contemporary publications,[106,107] has shown that N,N'-diaryl ureas adopt a low energy conformation where the NH protons both point "down." This is due to a weak C-H HB from the aromatic ring to the oxygen. Exchanging the aromatic C-H HB for a stronger HB, such as one donated from an NH, or one that is charge enhanced, would further decrease the conformational variability in the structure. Both strategies can be employed by using a protonated 2-pyridinium as one of the arenes. As shown in figure 3.3, having a charged NH donor to the carbonyl oxygen will practically lock the pyridine ring in a conformation that directs the R group down beside the urea active site. Altering the size of the R group should direct the carbonyl guest into an orthogonal binding mode, similar to binding modes in the oxyanion hole of enzymes.

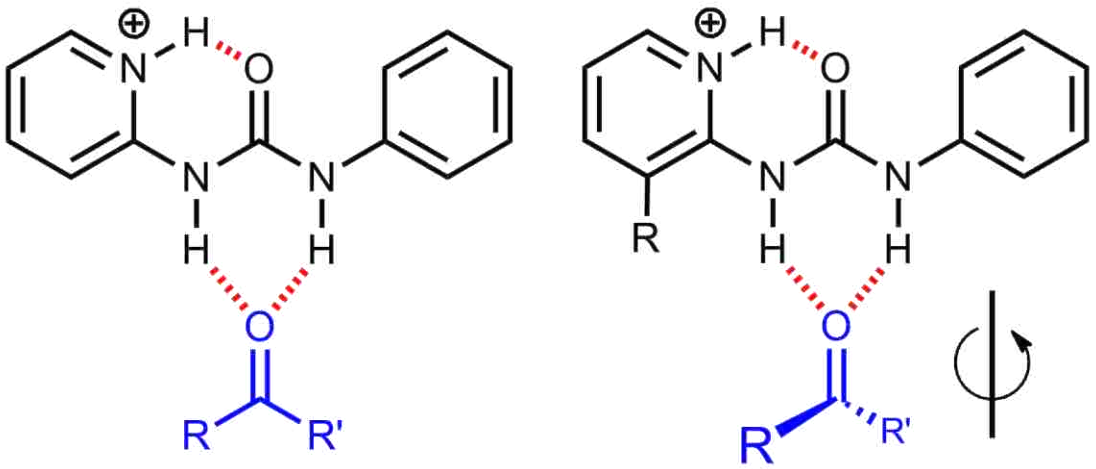

Figure 3.3 (2-pyridyl)urea without a bulky R group (left) and with a bulky R group (right).

3.4 Synthesis and Characterization of the Urea Catalysts

The urea hosts studied were synthesized through similar multistep paths (figure 3.4). The first step for each (2-pyridyl)urea was the nucleophilic addition of the appropriate 2-aiminopyridine to phenyl isocyanate, a common method for making asymmetric ureas. The reactions were carried out in DCM, under nitrogen for 24 hours. The yields of the free base ureas (**2a**, **2b**, **2c**) ranged from 69-93 %. The phenyl derivative starting material (2-amino-3-phenylpyridine, **3c**) was prohibitively expensive, and was synthesized via a Suzuki-Miyaura palladium mediated cross-coupling reaction[108] at an 81 % yield. The methyl and hydrogen derivatives of 2-aminopyridine were commercially available. Once the free-base ureas (**2a**, **2b**, **2c**) were synthesized, they were dissolved in methanol. Hydrogen chloride vapor was bubbled through each solution to protonate the

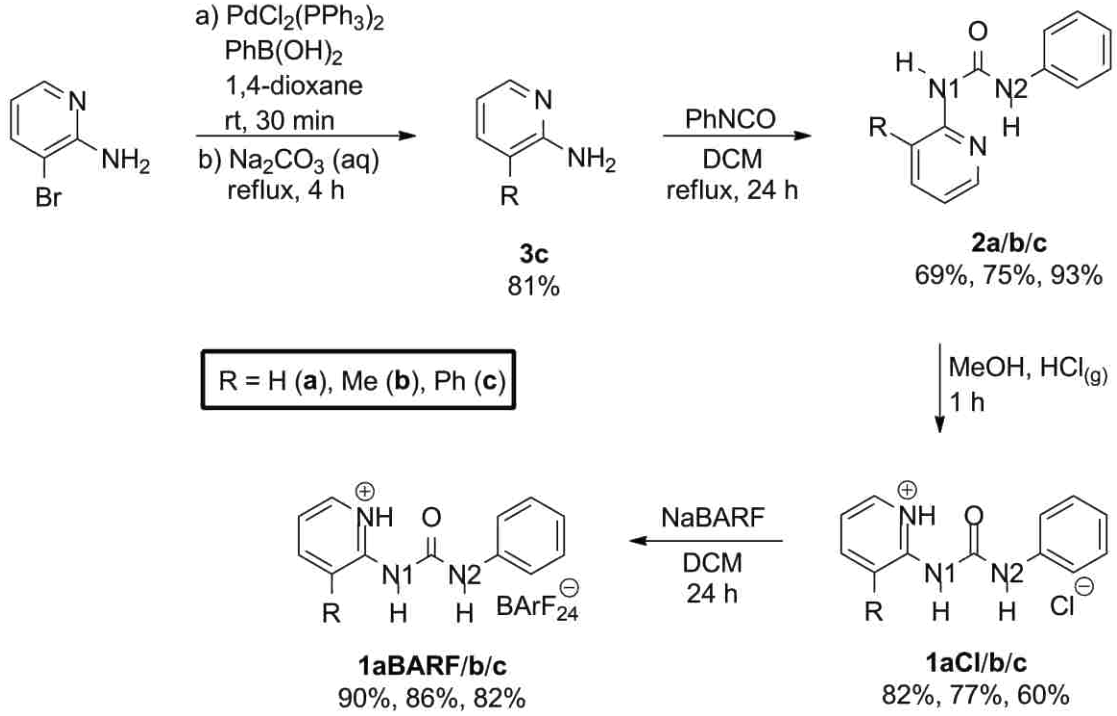

Figure 3.4 Synthetic scheme for the synthesis of the (2-pyridyl)ureas.

pyridine nitrogen, producing the hydrochloride salts of each urea (**1aCl**, **1bCl**, **1cCl**). Each urea was recrystallized from acetonitrile to produce large, clear, and colorless crystals that were separated from the supernatant by decanting it away, and rinsing the crystals with fresh acetonitrile. The crystals were dried on vacuum, crushed into a powder, and further dried on vacuum. The dried powders were each dissolved in dry DCM, and one equivalent of sodium tetrakis[3,5-bis(trifluoromethyl)phenyl]borate (NaBARF) was added to the solution. After stirring under nitrogen overnight, the fine precipitate was filtered, and the filtrate was concentrated on rotary evaporator. The residue was dried on vacuum, to give a brittle off-white foam. The foam was recrystallized from acetonitrile to give large, clear, and colorless crystals that were separated from the supernatant and rinsed with acetonitrile. The crystals were dried on vacuum, crushed into a powder, and dried on vacuum further. The resultant fine white powders of each protonated-urea BARF salt (**1aBARF**, **1bBARF**, **1cBARF**) were collected in 82-86 % yields.

At each step of the synthesis, the product was subjected to multiple methods of characterization experiments including: ^{1}H NMR spectroscopy, ^{13}C NMR spectroscopy, ^{19}F NMR spectroscopy, high-resolution mass spectrometry (ESI Q-TOF), and single crystal X-ray diffraction. The ^{1}H NMR spectra ($CDCl_3$) for the free-bases revealed the expected downfield shift of the N2 proton resonance due to the intramolecular hydrogen bond accepted by the pyridine nitrogen (conformation of **2a**/**b**/**c** shown in figure 3.5).[109,110] Upon protonation, the N2 proton signal shifts upfield (**1aCl**: 9.95 ppm, **1bCl**: 11.40 ppm, **1cCl**: 11.01 ppm), the N1 proton signal shifts downfield (**1aCl**: 13.52 ppm, **1bCl**: 11.86 ppm, **1cCl**: 11.94 ppm), and a broad signal appears at > 15 ppm from the pyridinium N-H

proton (**1a·Cl**: 15.10 ppm, **1b·Cl**: 15.65 ppm, **1c·Cl**: 15.86 ppm). This signal is also present in the BARF salt ^{1}H NMR spectra (CD_3CN), although it appears slightly further upfield (**1aBARF**: 14.46 ppm, **1bBARF**: 14.64 ppm, **1cBARF**: 14.94 ppm).

3.5 Crystal Structures

Diffraction quality crystals were grown at each step of the synthesis. Single crystal X-ray diffraction data was obtained for **2a**, **2b**, **2c**, **1aCl**, **1bCl**, **1aBARF**, and

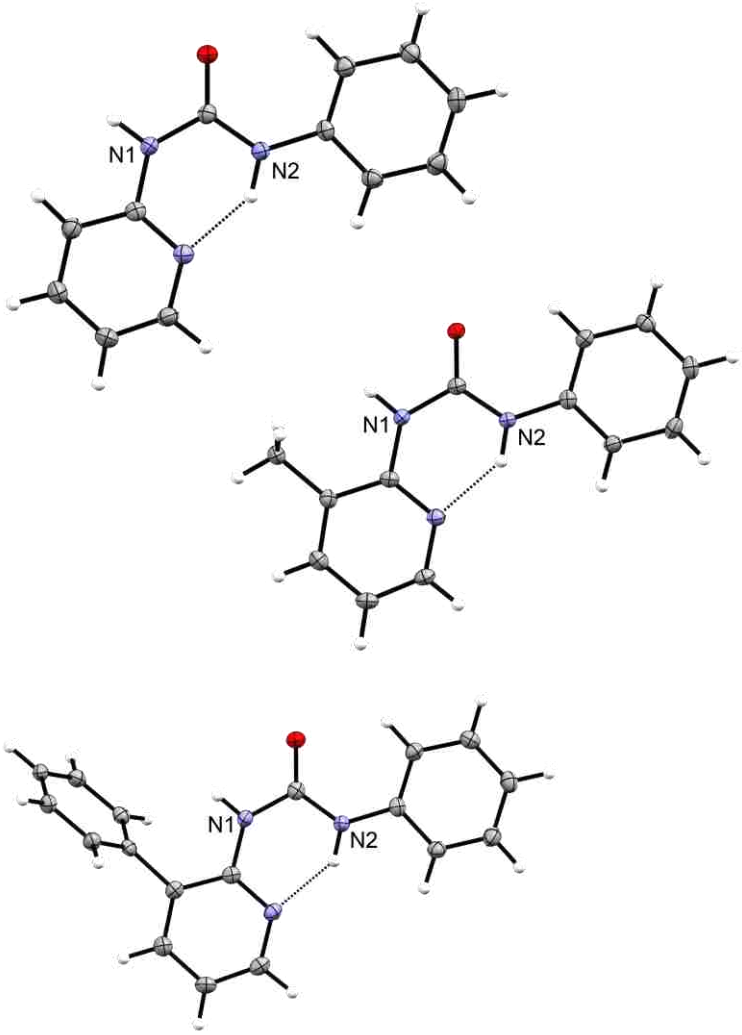

Figure 3.5 Free base (2-pyridyl)ureas **2a**, **2b**, and **2c** (top to bottom). Thermal ellipsoids are drawn at the 50 % probability level.

1cBARF (as a co-crystal with *trans*-β-nitrostyrene). Additionally, the free bases were protonated with trifluoroacetic acid (TFA), and diffraction data was obtained for each urea (the samples will be referred to as **1aTFA**, **1bTFA**, and **1cTFA**, following the same substitution scheme as in figure 3.4).

In the past, (2-pyridyl)ureas have been reported as adopting an "up, down" geometry in the solid-state.[111,112] The "up, down" conformation was also observed for these ureas, as shown in figure 3.5. The intramolecular HBs in these structures are all very similar, with an average distance of 1.90(3) Å, and an average angle of 141(3)°. The angle is not ideal, but the short distance is indicative of a strong HB. This demonstrates that the identity of the substituent in the 3-position does not play a large role in the conformation of the urea.

Upon protonation, the conformation rearranges to the "down, down" conformation, as observed in the chloride salts of **1aCl** and **1bCl**. These structures (in addition to providing additional evidence of protonation) demonstrate the binding preference of the urea-anion complex (figure 3.6). Interestingly, the anion does not charge-pair with the pyridinium (most likely due to the charge delocalization), but

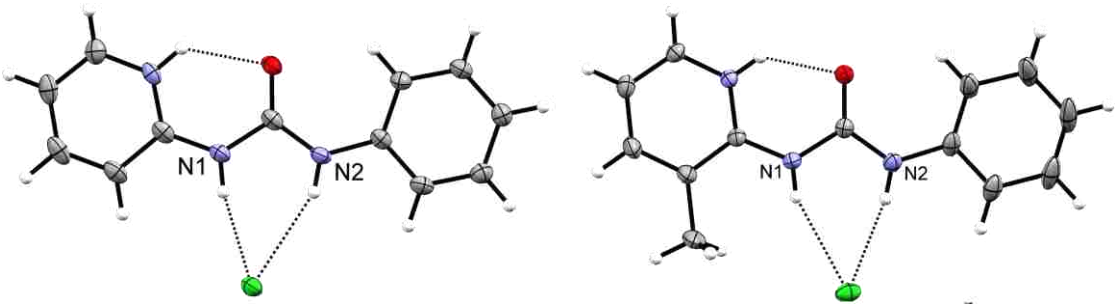

Figure 3.6 Crystal structures of **1aCl** (left) and **1bCl** (right). Thermal ellipsoids are drawn at the 50 % probability level.

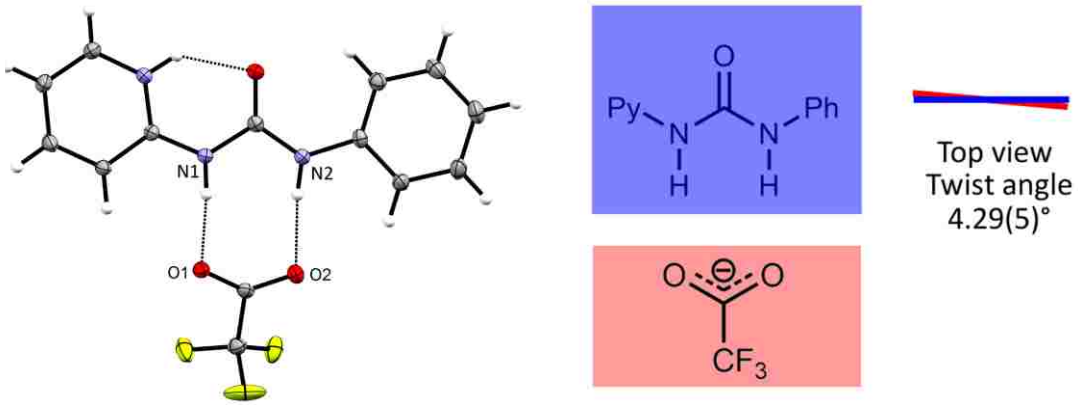

Figure 3.7 Crystal structure of **1aTFA** with twist angle. Thermal ellipsoids are drawn at the 50 % probability level.

accepts HBs from the urea NH protons (**1aCl** ∠N1H···Cl 2.21(3) Å, 167(2)°; ∠N2H···Cl 2.56(3)Å, 155(2)°; **1bCl** ∠N1H···Cl 2.48(3) Å, 156(2)°; ∠N2H···Cl 2.28(3)Å, 170.0(18)°)

The binding preferences were further explored by protonating the ureas with TFA. Trifluoroacetate (TFA^-) is a polyatomic anion, it is more charge diffuse, and can illuminate alternative binding modes (specifically those that mimic enzymatic oxyanion holes). The crystal structures of the protonated urea TFA^- salts show that the anion binds to the urea NH protons instead of the charged pyridinium ring. Additionally, the binding mode of TFA^- is different for each of the ureas, dependent on the substituent at the 3-position. The hydrogen derivative (**1aTFA**, figure 3.7) binds in the conventional fashion,[111] with two monodentate HBs from the urea to each oxygen of the TFA^- (∠N1H···O1 1.833(16) Å, 170.9(19)°; ∠N2H···O2 1.970(16) Å, 167.9(17)°). The O-C-O plane of the TFA^- is only 4.29(5)° away from planarity relative to the N-C-N plane of the urea. **1aTFA** is the only salt in the series that binds in this bis-monodentate fashion.

The methyl derivative (**1bTFA**) donates two HBs from the urea nitrogen protons to a single oxygen on the TFA^- (∠N1H···O 2.014(19) Å, 151.3(17)°; ∠N2H···O 1.851(19) Å,

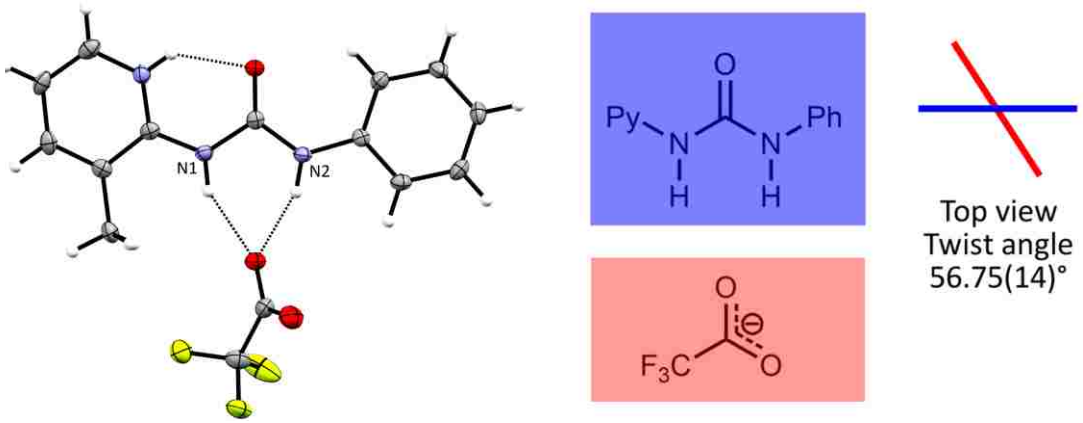

Figure 3.8 Crystal structure of **1bTFA** with twist angle. Thermal ellipsoids are drawn at the 50 % probability level.

160.7(17)°). As shown in figure 3.8, the anion is twisted away from coplanarity with the N-C-N plane of the urea by 56.75(14)°. The average HB distance and angle for **1bTFA** (1.933(27) Å, 156.0(24)°) is less favorable than for **1aTFA** (1.902(23) Å, 169.4(25)°).

The phenyl derivative (**1cTFA**) crystal structure (figure 3.9) shows an association that is twisted almost perpendicular (84.88(17)°). As expected, the TFA^- is unable to move close enough to the active protons of the urea to ideally interact with them (∠N1H···O 2.207(14) Å, 152.2(19)°; ∠N2H···O 2.033(19) Å, 161.2(18)°). To compare, the

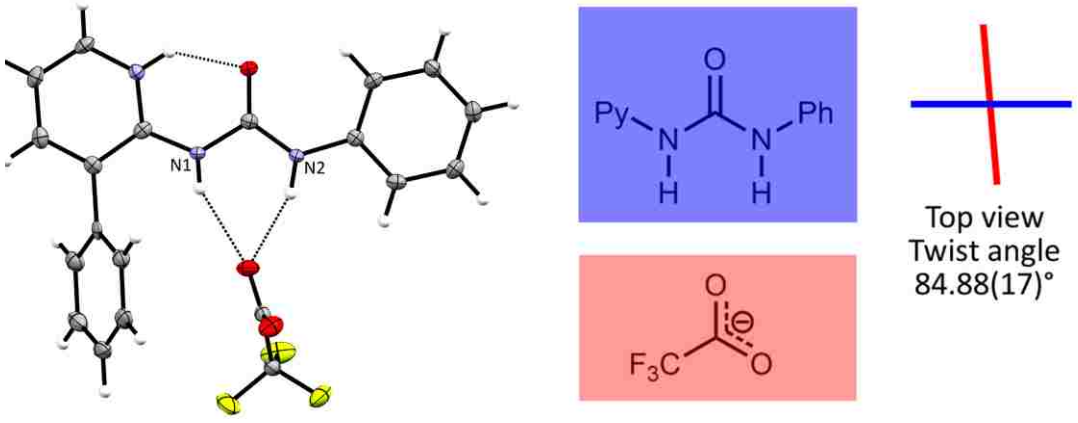

Figure 3.9 Crystal structure of **1cTFA** with twist angle. Thermal ellipsoids are drawn at the 50 % probability level.

average distances and angle here are 2.120(24) Å, and 156.7(26)°, even less ideal HBing geometry than in the **1bTFA** crystal structure.

To further probe the solid-state properties of these ureas, diffraction quality

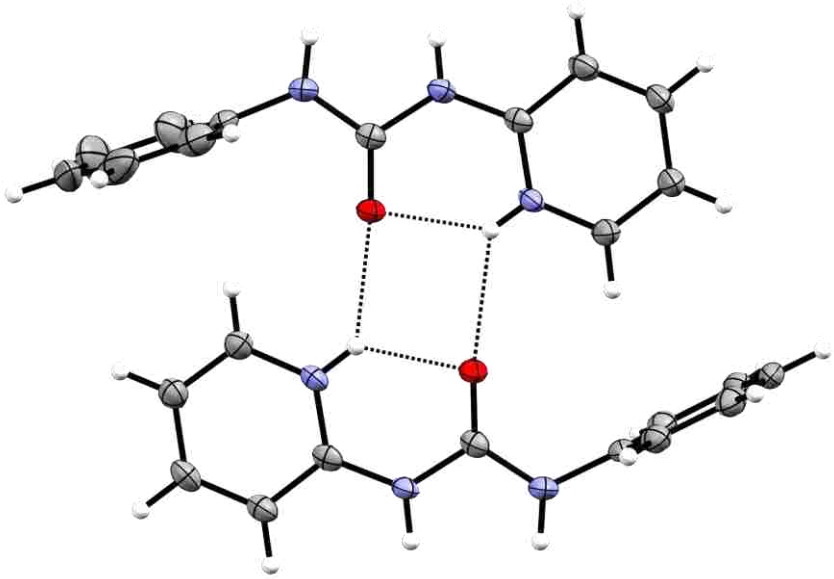

Figure 3.10 Crystal structure of **1aBARF.** Anions omitted for clarity. Thermal ellipsoids are drawn at the 50 % probability level.

crystals of **1aBARF** were studied by single crystal X-ray diffraction. The $BARF^-$ anion should negligibly interact with the urea, since it is one of the most charge diffuse anions known. Indeed, what is observed is a dimerization of the ureas in an antiparallel head-to-head fashion (figure 3.10). This helps demonstrate that the active conformation of the urea is independent of guest presence in the active site. In the past, *ortho*-substituted ureas/thioureas were thought to be catalytically inactive due to the high loss of entropy upon binding a carbonyl guest compared to their unsubstituted (or *meta*/*para* substituted) analogues.[26] Many of the thiourea scaffolds rely on neutral rings with C-H HB donors to a sulfur (thiocarbonyl) acceptor. Therefore, they rely on the symmetry of a *para*- or 3,5-substitution pattern to leave two *ortho* protons available for

HBing to the sulfur. This is compared to only one HB that would be available upon an *ortho* (or zero HBs for di-*ortho)* substitution. In the work presented here, the HB donor is stronger (N_{Py}-H vs C-H) and the HB acceptor is better (O=C vs. S=C). Therefore, the barrier to rotation should be higher than a neutral thiourea system with weaker HBs.

3.6 Conclusions

Here, a set of (2-pyridyl)ureas were synthesized with a systematically increasing steric group at the 3-position. Crystal structures demonstrated that the protonation state of the pyridyl group dictates the urea conformation. Solution and solid-state data shows that the neutral urea adopts an "up, down," and inactive, conformation. In contrast, the protonated ureas are preorganized in the "down, down" conformation enabling guests to preferentially interact with the urea NH protons over the pyridinium proton. Additionally, the crystal structure of **1aBARF** demonstrates that the preorganization of the urea is due to the intramolecular HB from the pyridinium to the oxygen, and not from guest binding. The crystal structures of the TFA salts show that increasing steric hindrance at the 3-position dictates guest binding. As steric hindrance increases, the urea-TFA^- geometry approaches orthogonality, similar to enzyme oxyanion holes.

Chapter 4

Hydrogen Bonding Catalyst Screens

4.1 Preface

The HB catalysis screens and computations in this chapter were performed by Nicholas Wageling, and the XB catalysis screens were performed by George Neuhaus. A portion of the work in the chapter has been accepted by *Supramolecular Chemistry*, and is in the process of being published.

4.2 Introduction

Of the numerous scaffolds one can use for HB based catalysis, ureas and thioureas are pervasive in the literature. Urea catalysis began with the work of Curran,[23] inspired by the observation made by Kelly[36] that biphenylenediols accelerate certain Diels-Alder reactions. From there, the field of (thio)urea catalysis grew. Schreiner,[25,26] Mattson,[113] Kass[114] (and others) pushed the limits of (thio)urea activity by augmenting the strength of the (thio)urea NH protons. Other groups decided to forego the optimization of activity for improved (and impressive) enantioselectivity. Jacobsen,[21] Rawal,[115] Connon[116] (and others) are some of the more active researchers in those studies.

This chapter will focus on work performed in an attempt to improve catalyst activity. The previous chapter described results that show how steric hindrance can affect guest binding in urea receptors. Those results, paired with the observations made by Goodman and Simón[117] regarding orthogonal carbonyl binding in biological oxyanion holes, guided the choice of reactions to screen for catalysis. Here, the question being

asked is whether orthogonal guest binding in small molecule organocatalysts will show increased acceleration over their coplanar counterparts.

4.3 Kinetics data

To emulate the guests from Goodman's study, carbonyls were chosen as the primary guests for the reactions screened. The ureas described in this work had already shown differential binding modes in the solid-state, with **1cTFA** showing orthogonal binding to TFA^-, a geometrically similar guest to a carbonyl. In an attempt at biomimicry, 23 reactions were screened that contained carbonyls with roles as electrophilic sites (table 4.1). During the screens, the active ureas (**1aBARF**, **1bBARF**, and **1cBARF**) were added in 50-100 mol% to search for activity. The reactions were monitored by ^1H NMR spectroscopy, comparing the integrations of resonances associated with the starting material to those associated with the product. While some of the screened reactions were accelerated by the active ureas, there was not an appreciable difference in urea activity based on substitution.

Of the reactions screened, the 1,4-additions of pyrrolidine into α,β-unsaturated carbonyls were revealing (figure 4.1) . A series of alkyl acrylates were screened, and the

Table 4.1 General table of reactions screened

Reaction Types	Electrophiles	Nucleophiles
1,2-addition	Carbonyl	Thiol
1,4-addition	α,β-unsaturated carbonyl	Hydroxyl
Cycloaddition	Nitroso	Amine
		Silyl enol ether
		Enamine (indole)

reactions that were accelerated over the control were insensitive to the size of the alkoxy group.

Acrylamide was also screened with the acrylate esters, and an accelerated reaction was observed there as well. However, none of the alkyl methacrylates (α-methylated) showed any rate acceleration. This is likely due to the inability of the ester to bind the urea active site in a coplanar orientation. If an addition into a methacrylate could be accelerated by a urea in an orthogonal binding mode, it would likely proceed faster for methacrylates over acrylates due to the cooperative effect of the methyl group on the α carbon. Since this is not observed, it is likely that these ureas cannot activate carbonyls when they are bound orthogonally.

Additional reactions were screened to further explore the possibility of a difference in activity based on guest geometry. The early literature on urea

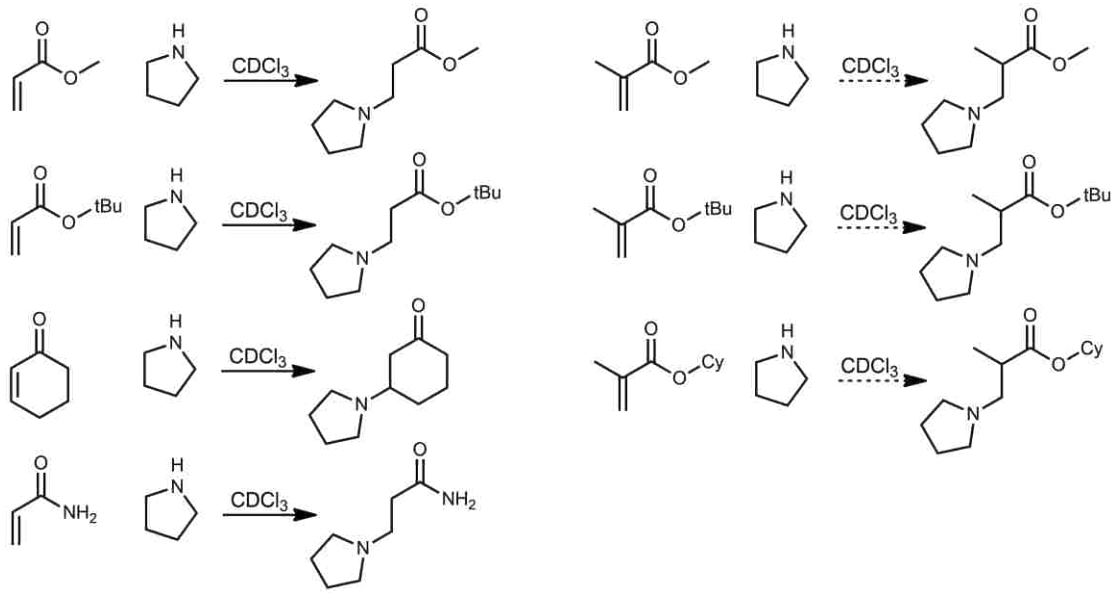

Figure 4.1 1,4-additions of pyrrolidine into acrylates and methacrylates. Reactions were screened with ureas **1aBARF**, **1bBARF**, and **1cBARF**. Solid arrows represent catalyzed reactions, dashed arrows represent no acceleration over control reactions.

organocatalysts focused on their ability to HB to nitro groups, and many screens include the addition reaction between indole and *trans*-β-nitrostyrene. This reaction is often included as a benchmark for proving catalytic performance in ureas and thioureas. In this work, *N*-methylindole and *trans*-β-nitrostyrene were chosen as reactants, and each urea was added at 6 mol% catalyst loading. With no additive, or with a simple Brønsted acid,[118] the reaction will convert only a negligible amount of starting material (< 1 %) over five hours.

The difference between the ureas' activities for this reaction was pronounced. The triplicate results from the reaction screen are shown in figure 4.2. The greatest increase in reaction rate was observed in the reactions that had **1aBARF** as an additive.

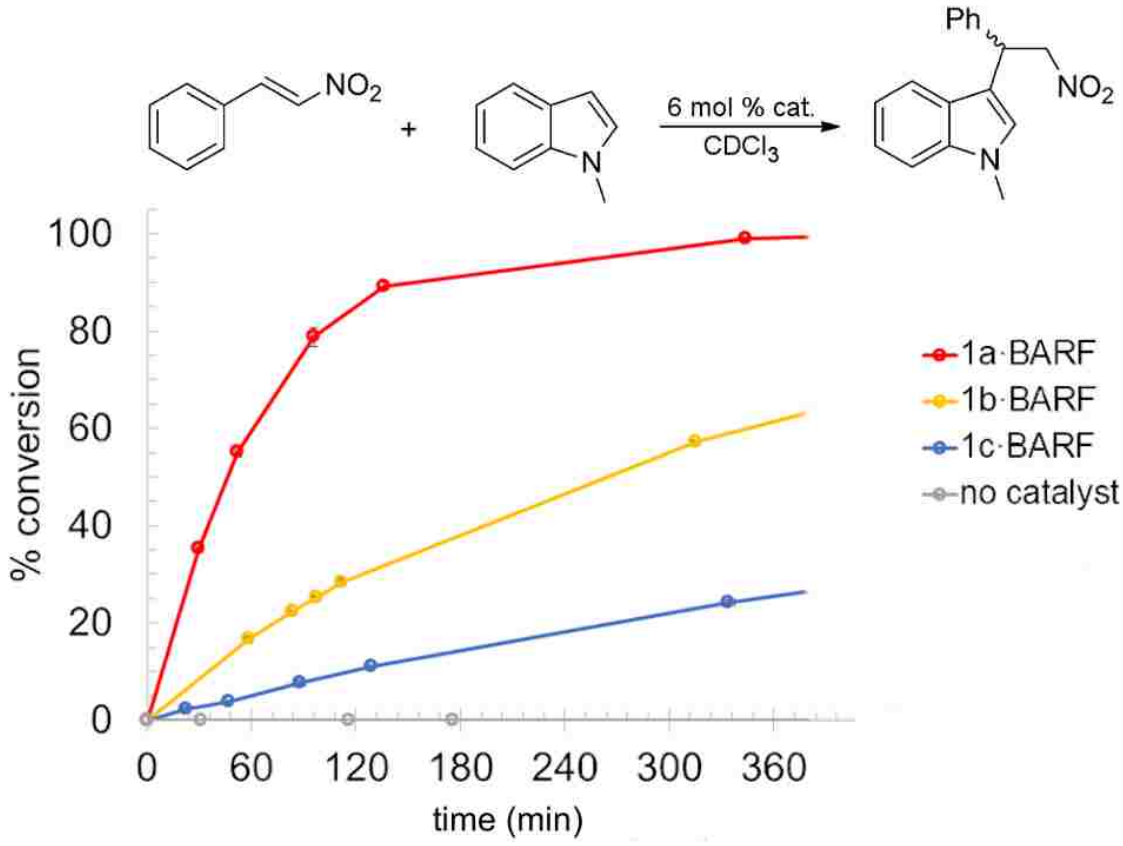

Figure 4.2 Graph of the % conversion vs. time for the reaction of *N*-methylindole and *trans*-β-nitrostyrene catalyzed by **1aBARF**, **1bBARF** and **1cBARF**.

By two hours, the reaction had reached approximately 89 % conversion. In comparison, by the same amount of time elapsed, the reactions with **1bBARF** and **1cBARF** had only reached 28 and 11 % conversion respectively. As one can see, the difference in reaction rates correlates with the size of the substituent in the 3-position of the pyridine on the urea.

While nitro groups are geometrically similar to carboxylates, the steric groups may influence binding in unexpected ways. Often, a nitro group will accept a hydrogen bond with each oxygen from a urea receptor in a coplanar arrangement. The more

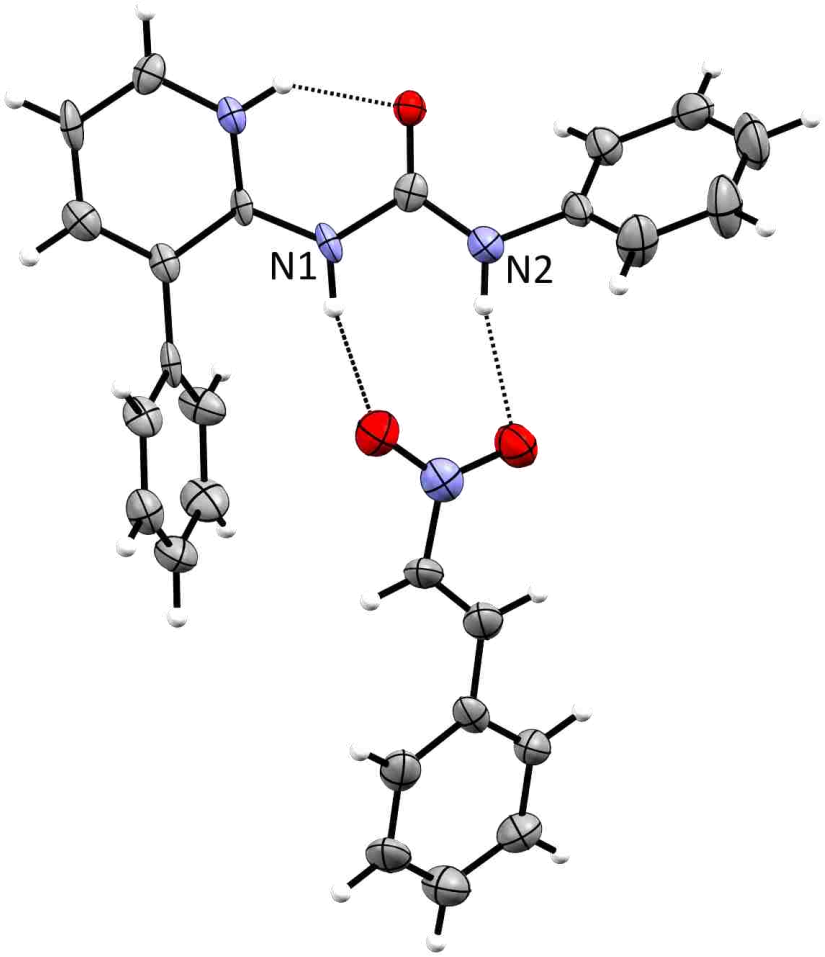

Figure 4.3 Co-crystal structure of **1cBARF** and *trans*-β-nitrostyrene. Thermal ellipsoids are drawn at the 50 % probability level.

sterically encumbered ureas may disrupt that typical interaction. Again, X-ray diffraction was employed to explore the binding geometry of guests in the active site of the ureas. Despite numerous recrystallization attempts, only the phenyl derivative was successfully crystallized (figure 4.3). A co-crystal was grown from a 1:1 solution of **1cBARF** and *trans*-β-nitrostyrene in chloroform. Despite the ubiquity of *trans*-β-nitrostyrene in urea organocatalysis, this is the first example of a co-crystal containing the reactant, and only one of three co-crystals containing ureas binding nitro groups.

The crystal structure reveals multiple notable features about the interaction (note: There are two sets of urea:guest complexes in the unit cell. However, since the binding geometry between them is so similar, only one of the interactions will be shown for clarity, and any values described will be averages from the two complexes). First, the binding mode is bis-monodentate, unlike the crystal structure of **1cTFA** (figure 3.9), which is bidentate. Second, like the other crystal structures involving the **1c** urea scaffold, the guest is primarily interacting with the urea NH protons over the pyridinium NH proton. Third, a qualitative observation of the crystal structure clearly shows that the interaction between the nitro group and the urea is not ideal: non-linear HBs are typically weaker. The *trans*-β-nitrostyrene is twisted out of planarity with the urea by 21.53(27)°. An ideal interaction would have a torsional angle of 0°. Since unfavorable HBs will decrease the activity of a catalyst, the non-ideal HBs formed in this crystal structure may explain the lower activity of **1cBARF** as compared to its less sterically hindered counterparts.

4.4 Computations

While the largest noticeable difference between ureas is the size of the substituent in the 3-position of the pyridine ring, there are other variables to consider. Changing substituents on the ring will affect the acidity of the N_{Py}-H proton. If the acidity of the N_{Py}-H proton increases, it will form a stronger HB to the urea oxygen and increase the acidity of the urea NH protons. This, in turn, will increase the activity of the urea in question. To properly probe the effect of sterics on the system, it is necessary to generate ureas with the smallest difference in acidities, while still maintaining a significant change in bulk near the active site.

The substituents chosen do not have strong electron donating or withdrawing properties, so the acidity difference between ureas should be small. The acidity of the urea NH protons cannot be determined while the ureas are in their active (i.e., protonated) state. The proton at the pyridine nitrogen is far more acidic than a urea NH proton, and would be removed first, deactivating the urea. Therefore, computations were used to determine the acidity of the N1 and N2 protons on each of the ureas.

The geometry for each urea was minimized using molecular mechanics (MM) simulations. The structures were then further minimized using a quantum mechanical (QM) model, followed by frequency calculations to ensure a global minimum. At this point the single point energies for the structures could be calculated. The MM minimizations were performed in Avogadro, an open source molecular modeling software.[119] The QM minimizations (geometry and frequency) and the single point energy calculations were performed in the Gaussian 09 suite (details can be found in the

experimental section). The QM geometry/frequency calculations were performed at the B3LYP/6-31G(d) level of theory, and the single point energies were calculated at the 6-31++G(d,p) level of theory. All calculations were performed in the gas phase, without a solvation model.

To calculate the energy of the deprotonated structure (at the N1 or N2 urea nitrogens), the proton was removed in GaussView 5 (the editing software in the Gaussian 09 suite) and a negative charge was applied to the deprotonated nitrogen. Typically, the absolute energy of systems studied using DFT can only be compared when they contain the same atoms. However, since the only atom was removed was a proton, the electronics of the system remained the same. This way, the energy of the urea with and without a proton at the N1 or N2 nitrogen could be compared while still in the active state (i.e., protonated at the pyridine nitrogen).

The results of these computations are listed in table 4.2. The fully protonated structures are labeled **1a**, **1b**, and **1c**. The structures deprotonated at the N1 nitrogen are labeled **1aZWIT1**, **1bZWIT1**, **1cZWIT1**, and the structures deprotonated at the N2 nitrogen are labeled **1aZWIT2**, **1bZWIT2**, **1cZWIT2**. The output energy is in Hartrees and was converted to $kJ \cdot mol^{-1}$ to compare to known values. From the resultant proton affinities, one can see that the range of affinities for N1 is 22.82 $kJ \cdot mol^{-1}$. For N2 the range of affinities is 18.48 $kJ \cdot mol^{-1}$. This proton affinity range can be compared to another system of structurally similar compounds, ammonia and methylamine. The difference in gas phase proton affinity for ammonia and methyl amine is 47.7 $kJ \cdot mol^{-1}$ (aqueous pK_as for ammonia[120] and methylamine[121] are 9.2 and 10.6 respectively). This

data suggests that the difference in acidity between the ureas is not large enough to account for the difference in activity. Additionally, the proton affinities show that, computationally, **1cBARF** has the most acidic N1 proton, which should result in higher activity.

Table 4.2 Single point energy calculations and proton affinities of ureas **1a**, **1b** and **1c**

Urea	Energy (Hartrees)	Energy (kJ·mol^{-1})	Proton Affinity (kJ·mol^{-1})
1a	-703.8429562	-1847938.032	–
1b	-743.1676565	-1951184.94	–
1c	-934.9191327	-2454627.991	–
1aZWIT1	-703.4441584	-1846890.989	1047.042584
1bZWIT1	-742.767136	-1950133.375	1051.565398
1cZWIT1	-934.5116432	-2453558.129	1069.862701
1aZWIT2	-703.4148491	-1846814.038	1123.994035
1bZWIT2	-742.7378111	-1950056.382	1128.557856
1cZWIT2	-934.4839854	-2453485.513	1142.478166

4.5 Conclusions

In this chapter, ureas with systematically increasing bulk proximal to the active site were explored as organocatalysts. A study by Goodman and Simón revealed that enzymes with oxyanion holes tend to bind carbonyls orthogonally. Crystal structures of the ureas studied here demonstrated that they bind carboxylate guests with various degrees of orthogonally, depending on the amount of steric hindrance introduced. Numerous reactions were chosen to screen the catalytic ability of the ureas. Carbonyls, and α,β-unsaturated carbonyls were initially screened as electrophilic guests, but the reactions that were accelerated did not show a significant catalytic difference between the three ureas. Successfully catalyzed reactions between pyrrolidine and acrylates, and unsuccessfully catalyzed reactions between pyrrolidine and methacrylates were

indicative of the inability of these ureas to catalyze reactions while orthogonally binding a guest. Reactions without carbonyl active sites were also explored. The addition reaction between *N*-methylindole and *trans*-β-nitrostyrene resulted in different degrees of catalysis for each urea added.

Chapter 5

Conclusions and Future Work

The work performed here was done to improve and expand the chemists' understanding of small molecule active sites. This work began with the exploration of a poorly understood interaction: the XB. Being a highly directional, attractive, non-covalent interaction, it holds high promise as a substitute or compliment to HBing systems. A bidentate receptor was designed, synthesized, and its anion binding properties were determined as a benchmark for the potential of XBs in the active site.

Crystal structures of the scaffold were obtained, showing that the iodinated receptor **XB1a** arranges itself in a more preconvergent conformation, compared to the splayed-out non-iodinated receptor **HB1**. This preconvergent conformation is important when designing receptors that retain enough conformational flexibility to allow guest binding but are rigid enough to reduce the entropic penalty upon binding.

The NMR titrations with halides revealed that the XBing analogue **XB1a** outperformed the HBing analogue **HB1**. Not only are the association constants for **XB1a** 24-40 times larger than those for **HB1**, depending on the anion, but they are also more resistant to the addition of water: a desirable feature in an anion receptor or organocatalyst. This is the first example of a comparison of the solvent effects on isostructural XBing and HBing scaffolds. This research will usher in a new generation of XB based catalysts that will show even more solvent resistance, higher binding strengths, and better preconvergence.

The results of the anion binding study piqued interest in other peculiarities regarding active sites that stabilize negative charges. Inspired by the PDB/CSD analysis performed by Simón and Goodman,[117] it was hypothesized that an orthogonal binding mode may be a better approach to activating carbonyls. The **XB1a** scaffold is too conformationally flexible to test this hypothesis, and the synthetic challenge of modifying it appropriately precluded it as a viable test molecule.

Instead, a set of (2-pyridyl)ureas were synthesized to observe the effect of orthogonal binding. The literature contains many examples of ureas that are active as organocatalysts. Additionally, the conformation of the urea can be rigidified through an intramolecular HB. By semi-locking the conformation of the urea, peripheral carbons of the molecule could be substituted to sterically block the active site by systematically increasing amounts.

Crystal structures of the ureas with various anions showed that the active conformation of the ureas is independent of the HB accepting strength of the anion present. The anions also have limited interaction with the cationic pyridinium-NH of the active ureas, favoring the NH protons of the urea. Crystals structures containing TFA^- show that systematically increasing steric bulk around the active site not only changes the binding mode from bis-monodentate to bidentate, but also twists the guest so that the torsional angle approaches orthogonality.

The ureas were added to test reactions to observe their effect on the kinetics. The reactions were monitored by ^1H NMR spectroscopy, and conversions were measured by comparing starting material and product proton integrations. Of the

reactions that were accelerated, none showed an appreciable difference in activity between the three ureas tested. One set of reactions (the addition of pyrrolidine into α,β-unsaturated carbonyls) showed activity for acryloyls, but not for methacryloyls. This is likely because the methyl of the methacryloyls prevents coplanar binding of the carbonyl. Therefore, the reaction does not proceed when the substrate is pushed orthogonally for these small molecule receptors.

The system used here is much simpler than the proteins studied by Goodman and Simón. Proteins rarely rely on a single interaction to catalyze a reaction. They have other factors to consider, such as artificially high local concentration in the active site, secondary stabilizing interactions, and mechanical manipulation of the substrate through protein conformational change. The ureas studied here only incorporated a single unique feature from biology in their design. Future studies on active site geometry (figure 5.1) should include an exploration into thioureas (for increased NH acidity/stronger NH HB donation) and guanidiniums (covalently fixing the conformation of the receptor). Additionally, symmetrical ureas could be explored, where there is a 2-pyridinium on either side of the urea. Symmetrical ureas were attempted in this study,

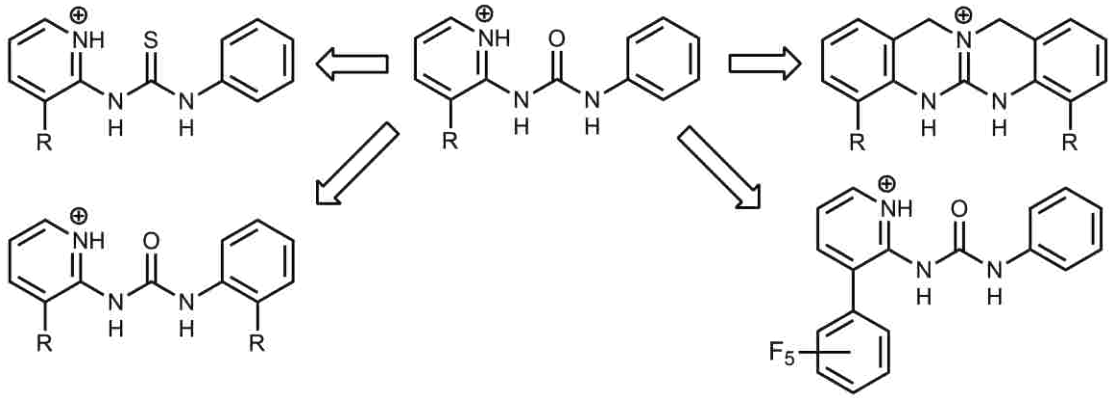

Figure 5.1 Potential structural changes to the urea model

but were abandoned due to the low solubility expected from a dicationic, organic molecule. During the attempted synthesis, the dicationic species was found to be too Brønsted acidic, and would likely lose its active conformation after deprotonation.

The remaining mysteries of organocatalysis are not few in number. Incorporating XBs into catalysts is already a reality, but more diverse systems need to be explored, and current systems need to be improved. The XB scaffold could benefit from additional conformational rigidity and more secondary interactions (such as HBs or anion-arene interactions) to improve its chances of acting as an organocatalyst. Future work on the ureas could guide the design of the XB organocatalyst. By affixing a larger variety of R groups to the 3-position of the pyridine, secondary interactions with the guest, or even interactions with a second guest, could guide organocatalyst development closer to a competitive, robust, and enzyme-like activator.

Experimental Section

General Experimental

All reagents were obtained from Acros Organics, Oakwood Chemical, Alfa Aesar, or EMD Millipore and were used without further purification unless otherwise noted. The sodium tetrakis[3,5-bis(trifluoromethyl)phenyl]borate used in this study was synthesized using the Bergman method[122] and correctly matched the reported ^{1}H, ^{13}C, and ^{19}F NMR resonances. The synthesis of **3c** was adapted from a previously reported procedure.[108] The synthesis of the ureas (**2a**, **2b**, **2c**) was adapted from a previously reported procedure,[123] as was the anion metathesis procedure to generate the BARF salts **1aBARF**, **1bBARF**, and **1cBARF**.[124] Column chromatography was performed using normal phase silica gel (230–400 mesh, SiliaFlash® P60, SiliCycle). Thin layer chromatography was performed using normal phase silica gel, glass backed plates (0.25 mm, F-254, SiliCycle) and observed under UV light. Activated Fisher Grade 514 molecular sieves were used when anhydrous solvents were required. Standard Schlenk and air-free techniques were employed where needed. Melting points were obtained from a MEL-TEMP capillary melting point apparatus. High-resolution masses for new compounds were obtained using an Agilent 6520 Accurate-Mass Q-TOF LC/MS. X-ray crystallographic data were measured on a Bruker D8 Venture. Nuclear magnetic resonance (NMR) spectra were recorded on a VNMRS Varian 500 MHz, Bruker Avance 400 MHz, or Agilent DD2 400 MHz spectrometer. Chemical shifts are reported in parts per million (ppm) from high to low frequency. All proton (^{1}H) resonances are reported to

the nearest 0.01 ppm using the residual solvent peak as the internal reference ($CHCl_3$ = 7.26 ppm, MeCN = 1.94 ppm). The multiplicity of the signals is designated as: s = singlet, d = doublet, t = triplet, q = quartet, m = multiplet, or some combination thereof. Coupling constants (*J*) are reported in to the nearest 0.1 Hertz (Hz). All proton decoupled carbon resonances ($^{13}C\{^1H\}$) are reported to the nearest 0.01 ppm and are labeled relative to the center resonance of the residual solvent as the internal reference ($CDCl_3$ = 77.16 ppm, MeCN-d3 = 118.26 ppm). All ^{13}C NMR signals are singlets unless stated otherwise. For the ^{19}F NMR spectra, hexafluorobenzene (C_6F_6 = -164.9 ppm) was used as an internal standard, and was isolated from the sample in a sealed capillary tube.

Halogen Bonding Scaffold

General procedure for N-arylation of imidazole

Salicylaldoxime (Saldox, 0.2 equiv), imidazole (1.2 equiv), Cs_2CO_3 (2.0 equiv), and Cu_2O (0.1 equiv) were added to an oven dried Schlenk tube under an inert atmosphere (dry N_2). A sparged solution of 1-bromo-3-(*tert*-butyl)-5-iodobenzene (**5**) (prepared by a known procedure,[125] or 1- bromo-3-iodobenzene (commercially available) (1 equiv, 0.8 M in total reaction mixture) dissolved in dry acetonitrile was then added to the Schlenk tube using a cannula and the clear reaction mixture with Cu_2O and Cs_2CO_3 suspension was raised to 50 °C in an oil bath and left to stir for 25 h. The solution was then allowed to cool to rt before diluting with DCM and filtering through diatomaceous earth. The product was then purified by flash column chromatography using normal phase silica,

and/or by vacuum distillation at 1 Torr (bp listed for individual compounds where needed).

General procedure for Suzuki–Miyaura cross-coupling

$PdCl_2(PPh_3)_2$ (0.1 equiv), and 1,3-phenylenediboronic acid (0.5 equiv) were added to a Schlenk flask under an inert atmosphere (dry N_2). Sparged solutions of 1-bromo-3-iodobenzene, **5**, **4**, or **4a** in DMF (1 equiv, 0.1 M in total reaction mixture) and TBAF (1 M in THF, 7.8 equiv) were then added to the Schlenk flask with a cannula. The yellow mixture was then heated to 90 °C in an oil bath. The reaction turned black after 10 min, and was allowed to stir at 90 °C under N_2 overnight. After cooling to rt, the volatiles were removed by rotary evaporator leaving a black oil that was dissolved in DCM and filtered through diatomaceous earth. The filtrate was concentrated on rotary evaporator and the resultant black oil was purified by flash column chromatography on normal phase silica.

General procedure for iodination

3 or **3a** (1 equiv) was dissolved in dry THF and sparged with dry N_2 before cooling to −50 °C. To the slightly yellow mixture, *n*-BuLi (2.5 M in hexanes, 2.5 equiv) was added dropwise, and was allowed to stir at –50 °C for 30 min. A sparged solution of I_2 (0.76 M in THF, 2.3 equiv) was added to the solution dropwise, turning the solution red. The reaction mixture was allowed to warm to rt over 2 h and allowed to stir for an additional 22 h under N_2. The solvent was then removed and the concentrate was dissolved in DCM, washed with saturated aqueous sodium thiosulfate, followed by DI water and finally brine. The organic layer was dried over anhydrous $MgSO_4$, filtered and

concentrated. The product was purified by flash column chromatography on normal phase silica.

General procedure for methylation

XB2a, **XB2b**, **XB2c**, **3**, or **3a** (1 equiv) was dissolved in dry DCM and sparged with dry N_2. MeOTf (4 equiv) was then added dropwise to the solution, and it was allowed to stir under N_2 overnight. The product was filtered and purified by recrystallisation (details included in compound syntheses below).

General procedure for anion titrations

Stock solutions of **XB1a**, **XB1c**, and **HB1** were prepared in the given solvent. Aliquots (0.500 mL) from each stock solution were transferred via gas-tight syringe into three separate NMR tubes sealed with rubber septa. The stock solutions were then used to make host/guest solutions corresponding to their experiment number. After obtaining free-host spectra of **XB1a**, **XB1c**, and **HB1**, aliquots of corresponding guest solution (containing **XB1a**, **XB1c**, or **HB1** and TBA+X– at specified concentrations) were added to their respective NMR tubes. A spectrum was obtained after each addition. A constant host concentration was maintained, while TBA^+X^- concentrations in the NMR tube gradually increased throughout the titration. HypNMR[98] 2008 was used to fit the binding isotherms for multiple signals (**XB1a**: Ha, Hb, and Hc; **XB1c**: Ha, Hb, Hc, Hd, He, Hf, and Hg; **HB1**: Ha, Hb, Hc, and Hd) simultaneously.

Syntheses and characterization

1-(3-bromo-5-(tert-butyl)phenyl)-1H-imidazole Prepared from **5** by following the general procedure for *N*-arylation. Yellow oil: 85.7% yield; eluent conditions

1.5% (v/v) NH_4OH (14.8 M, aq.) 3:2 hexanes:EtOAc; ^1H NMR (500 MHz, $CDCl_3$) δ 7.83 (s, 1H), 7.52 (t, *J* = 1.6 Hz, 1H), 7.37 (t, *J* = 1.9 Hz, 1H), 7.31 (t, *J* = 1.7 Hz, 1H), 7.26 (s, 1H), 7.21 (s, 1H), 1.35 (s, 9H). $^{13}C\{^1H\}$ NMR (125 MHz, $CDCl_3$) δ 155.39, 138.22, 135.60, 130.60, 127.93, 123.10, 121.96, 118.28, 117.64, 35.17, 31.07. HRMS (ESI-TOF) *m*/*z*: 279.0491 $(M + 1H)^+$ 50%, 281.0472 $(M + 2 + 1H)^+$ 50%, $C_{13}H_{16}BrN_2^+$ (calc. 279.049, 281.047).

1-(3-bromophenyl)-1H-imidazole Prepared from 1-bromo-3-iodoimidazole by following the general procedure for *N*-arylation. Yellow oil: 84% yield; bp: 190–200 °C, ~1 Torr. ^1H NMR (500 MHz, $CDCl_3$) δ = 7.86 (s, 1H), 7.56 (t, *J* = 2.0 Hz, 1H), 7.51–7.49 (m, 1H), 7.37–7.32 (m, 2H), 7.27 (s, 1H), 7.22 (s, 1H). $^{13}C\{^1H\}$ NMR (125 MHz, $CDCl_3$) δ = 138.5, 135.6, 131.3, 130.9, 130.7, 124.7, 123.5, 120.1, 118.2. HRMS (ESITOF) *m*/*z*: 222.9865 $(M + 1H)^+$ 50%, 224.9845 $(M + 2 + 1H)^+$ 50%, $C_9H_8BrN_2^+$ (calc. 222.986, 224.984).

1,1′-(5,5″-di-tert-butyl-[1,1′:3′,1″-terphenyl]-3,3″-diyl)bis(1H-imidazole) Prepared from **4** by following the general procedure for Suzuki–Miyaura cross-coupling. White solid: 60% yield; eluent conditions 0.25% (v/v) MeOH, 1.5% (v/v) NH_4OH (14.8 M, aq.) in EtOAc; mp: 207–210 °C. ^1H NMR (400 MHz, DMSO-*d6*) δ 8.39 (d, *J* = 1.4 Hz, 2H), 8.06 (t, *J* = 1.8 Hz, 1H), 7.90 (t, *J* = 1.3 Hz, 2H), 7.82–7.76 (m, 4H), 7.68 (t, *J* = 1.5 Hz, 2H), 7.64–7.59 (m, 3H), 7.12 (d, *J* = 1.3 Hz, 2H), 1.41 (s, 18H). $^{13}C\{^1H\}$ NMR (100 MHz, DMSO-*d6*) δ 153.50, 141.81, 140.71, 137.43, 135.91, 129.70, 129.46, 126.83, 126.26, 122.60, 118.46, 116.80, 116.73, 34.98, 31.05. HRMS (ESI-TOF) *m*/*z*: 238.1465 $(M + 2H)^{2+}$, $C_{32}H_{36}N_4^{2+}$ (calc. 238.146).

3,3″-di(1H-imidazol-1-yl)-1,1′:3′,1″-terphenyl Prepared from **4a** by following the general procedure for Suzuki–Miyaura cross-coupling. Yellow oil: 78% yield; eluent conditions 2.5% (v/v) MeOH, 1.5% (v/v) NH_4OH (14.8 M, aq.) in EtOAc. ^1H NMR (400 MHz, $CDCl_3$) δ = 7.95 (s, 2H), 7.81 (t, *J* = 2.5 Hz, 1H), 7.66–7.64 (m, 6H), 7.62–7.57 (m, 3H), 7.42 (dt, *J* = 9.5 Hz, 2.0 Hz, 2H), 7.36 (s, 2H), 7.25 (s, 2H). $^{13}C\{^1H\}$ NMR (100 MHz, $CDCl_3$) δ = 143.1, 140.9, 138.1, 135.8, 130.62, 130.58, 129.9, 127.1, 126.6, 126.3, 120.8, 120.6, 118.5. HRMS (ESI-TOF) *m*/*z*: 363.1604 (M + 1H)+ $C_{24}H_{19}N_4^+$ (calc. 363.160)

1,1′-(5,5″-di-tert-butyl-[1,1′:3′,1″-terphenyl]-3,3″-diyl)bis(2-iodo-1H-imidazole) Prepared from **3** by following the general procedure for iodination. White solid: 58% yield; eluent conditions 1.5% (v/v) NH_4OH (14.8 M, aq.) 3:2 hexanes:EtOAc (note: product degrades on normal phase silica); mp: 157 °C (decomposition). ^1H NMR (500 MHz, CD_3CN) δ 8.01 (t, *J* = 1.6 Hz, 1H), 7.89 (t, *J* = 1.6 Hz, 2H), 7.76 (dd, *J* = 7.7, 1.7 Hz, 2H), 7.64–7.59 (m, 3H), 7.50 (t, *J* = 1.8 Hz, 2H), 7.45 (d, *J* = 1.2 Hz, 2H), 7.16 (d, *J* = 1.1 Hz, 2H), 1.42 (s, 18H). $^{13}C\{^1H\}$ NMR (125 MHz, CD_3CN) δ 154.48, 142.53, 141.73, 139.81, 133.31, 130.70, 127.88, 127.10, 126.24, 125.64, 124.34, 123.66, 91.53, 35.94, 31.42. HRMS (ESI-TOF) *m*/*z*: 364.0431 $(M + 2H)^{2+}$, $C_{32}H_{34}I_2N_4^{2+}$ (calc. 364.043).

3,3″-bis(2-iodo-1H-imidazol-1-yl)-1,1′:3′,1″-terphenyl Prepared from **3a** by following the general procedure for iodination. White solid: 52% yield; eluent conditions 1.5% (v/v) NH_4OH (14.8 M, aq.) 1:1 hexanes:acetone. ^1H NMR (500 MHz, CD_2Cl_2) δ = 7.89 (s, 1H), 7.81 (d, *J* = 7.8 Hz, 2H), 7.70–7.67 (m, 4H), 7.63–7.59 (m, 3H), 7.39 (d, *J* = 7.9 Hz, 2H), 7.32 (d, *J* = 1.3 Hz, 2H), 7.19 (d, *J* = 1.2 Hz, 2H). $^{13}C\{^1H\}$ NMR (100 MHz, $CDCl_3$) δ = 142.43, 140.56, 139.11, 133.22, 130.05, 129.93, 127.97, 127.09, 126.25, 125.84, 125.75,

124.93, 90.42 HRMS (ESI-TOF) *m*/*z*: 307.9805 $(M + 2H)^{2+}$ $C_{24}H_{18}I_2N_4^{2+}$ (calc. 307.980).

1-(3",5-di-tert-butyl-5"-(1H-imidazol-1-yl)-[1,1':3',1"-terphenyl]-3-yl)-2-iodo-1H-imidazole Prepared from **3** by following the general iodination procedure (monoiodination occurs as a side product in the iodination step). White solid: 17% yield; eluent conditions 1.5% (v/v) NH_4OH (14.8 M, aq.) 2:3 hexanes:EtOAc; mp: 140 °C (decomposition). ^{1}H NMR (400 MHz, CD_3CN) δ 8.05 (s, 1H), 8.03 (t, *J* = 1.7 Hz, 1H), 7.89 (t, *J* = 1.7 Hz, 1H), 7.79–7.74 (m, 3H), 7.69 (t, *J* = 1.8 Hz, 1H), 7.64–7.57 (m, 3H), 7.55 (t, *J* = 1.9 Hz, 1H), 7.50 (t, *J* = 1.8 Hz, 1H), 7.46 (d, *J* = 1.3 Hz, 1H), 7.16 (d, *J* = 1.3 Hz, 1H), 7.13 (s, 1H), 1.43 (s, 18H). ^{13}C{^{1}H} NMR (125 MHz, CD_3CN) δ 155.03, 154.42, 143.10, 142.56, 142.04, 141.66, 139.75, 138.81, 133.28, 130.58, 127.96, 127.82, 127.18, 126.22, 125.65, 124.31, 124.22, 123.65, 91.54, 35.91, 31.39, 31.36. HRMS (ESI-TOF) *m*/*z*: 301.0948 $(M + 2H)^{2+}$, $C_{32}H_{35}IN_4^{2+}$ (calc. 301.095).

1,1'-(5,5"-di-tert-butyl-[1,1':3',1"-terphenyl]-3,3"-diyl)bis(2-iodo-3-methyl-1H-imidazol-3-ium) trifluoromethanesulfonate Prepared from **XB2a** by following the general procedure for methylation. White solid: 72% yield; Recrystallized from $CHCl_3$; mp: 218 °C (decomposition). ^{1}H NMR (500 MHz, CD_3CN) δ 8.03 (t, *J* = 1.6 Hz, 2H), 7.99 (t, *J* = 1.6 Hz, 1H), 7.83 (d, *J* = 2.1 Hz, 2H), 7.77 (dd, *J* = 7.6, 1.9 Hz, 4H), 7.68–7.63 (m, 3H), 7.55 (t, *J* = 1.8 Hz, 2H), 3.93 (s, 6H), 1.44 (s, 18H). ^{13}C{^{1}H} NMR (100 MHz, CD_3CN) δ 155.40, 143.17, 141.21, 138.31, 130.97, 128.27, 127.73, 127.68, 127.57, 127.04, 124.16, 123.45, 121.99 (q, *J* = 318 Hz), 101.78, 40.76, 36.12, 31.32. ^{19}F NMR (376 MHz, CD_3CN) δ –79.70. HRMS (ESI-TOF) *m*/*z*: 378.0587 M^{2+}, $C_{34}H_{38}I_2N_4^{2+}$ (calc. 378.059, triflate anions omitted).

1,1′-([1,1′:3′,1″-terphenyl]-3,3″-diyl) bis(2-iodo-3-methyl-1H-imidazol-3-ium) trifluoromethanesulfonate Prepared from **XB2b** by following the general procedure for methylation. White solid: 86% yield; filtered from reaction and rinsed with DCM to give product. ^{1}H NMR (400 MHz, CD_3CN) δ 8.26 (s, 2H), 8.16–8.11 (m, 7H), 7.87–7.81 (m, 4H), 7.73–7.66 (m, 3H), 4.13 (s, 6H) $^{13}C\{^{1}H\}$ NMR (125 MHz, CD_3CN) δ 143.29, 140.63, 138.42, 131.65, 131.10, 130.68, 128.13, 127.78, 127.57, 126.84, 126.65, 126.33, 123.28, 120.73, 101.78, 40.73 (note: the peaks at 123.28 and 120.73 are from 19F coupling to the triflate carbon. The carbon peak should split into a quartet, but only the two inside peaks are observed, as the two outside peaks are below the noise) ^{19}F NMR (470 MHz, CD_3CN) δ 79.68 HRMS (ESITOF) *m*/*z*: 321.9961 M^{2+}, $C_{26}H_{22}I_2N_4^{2+}$ (calc. 321.996, triflate anions omitted)

1-(3″,5-di-tert-butyl-5″-(3-methyl-1H-imidazol-3-ium-1-yl)-[1,1′:3′,1″-terphenyl]-3-yl)-2-iodo-3-methyl-1H-imidazol-3-ium) trifluoromethanesulfonate Prepared from **XB2c** by following the general procedure for methylation. White solid: 86% yield; recrystallized from 1:9 hexanes:$CHCl_3$; mp 146 °C (decomposition). ^{1}H NMR (500 MHz, CD_3CN) δ 9.00 (s, 1H), 8.04 (t, *J* = 1.6 Hz, 1H), 8.02 (t, *J* = 1.5 Hz, 1H), 7.96 (t, *J* = 1.6 Hz, 1H), 7.88 (t, *J* = 1.9 Hz, 1H), 7.84 (d, *J* = 2.1 Hz, 1H), 7.81–7.75 (m, 4H), 7.68–7.64 (m, 2H), 7.63 (t, *J* = 1.9 Hz, 1H), 7.56 (t, *J* = 1.8 Hz, 2H), 3.96 (s, 3H), 3.93 (s, 3H), 1.44 (d, *J* = 2.9 Hz, 18H). $^{13}C\{^{1}H\}$ NMR (125 MHz, CD_3CN) δ 155.77, 155.37, 143.48, 143.19, 141.33, 141.12, 138.20, 136.48, 136.47, 136.25, 130.89, 128.36, 128.26, 127.75, 127.69, 127.58, 127.15, 127.03, 125.18, 124.13, 123.39, 122.70, 119.74, 119.48, 101.70, 40.75, 37.20,

36.12, 36.10, 31.26, 31.24. ^{19}F NMR (376 MHz, CD3CN) δ -79.69. HRMS (ESI-TOF) *m*/*z*: 315.1095 M^{2+}, $C_{34}H_{39}IN_4^{2+}$ (calc. 315.110, triflate anions omitted).

1,1′-(5,5″-di-tert-butyl-[1,1′:3′,1″-terphenyl]-3,3″-diyl)bis(3-methyl-1H-imidazol-3-ium) Trifluoromethanesulfonate Prepared from **3** using the general procedure for methylation. White solid: 96% yield; recrystallized from 1:3 hexanes: $CHCl_3$; mp: 203 °C (decomposition). ^{1}H NMR (400 MHz, CD_2Cl_2) δ 9.56 (s, 2H), 8.11 (s, 1H), 8.00–7.98 (t, 2H), 7.88 (s, 2H), 7.75–7.69 (m, 4H), 7.65–7.61 (t, 1H), 7.46 (t, *J* = 1.6 Hz, 2H), 7.45–7.42 (t, 2H), 4.12 (s, 6H), 1.44 (s, 18H). ^{13}C{^{1}H} NMR (125 MHz, CD_2Cl_2) δ 155.36, 143.56, 140.84, 136.82, 135.67, 130.10, 127.62, 127.15, 126.88, 124.51, 122.08, 119.40, 118.59, 54.00, 37.30, 35.82, 31.47. ^{19}F NMR (376 MHz, CD_2Cl_2) δ -81.36. HRMS (ESI-TOF) *m*/*z*: 252.1621 M^{2+}, $C_{34}H_{40}N_4^{2+}$ (calc. 252.162, triflate anions omitted)

Spectra

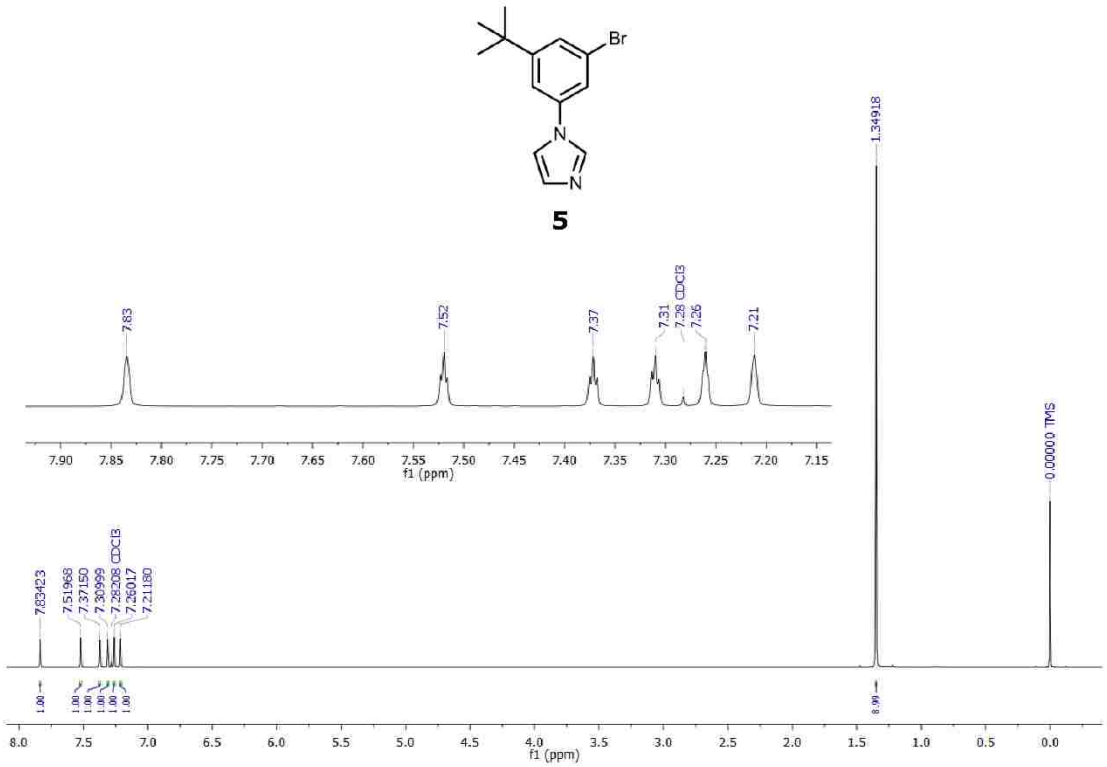
Br
N
N
5
7.83
7.52
7.37
7.31
7.28 CDCl3
7.26
7.21
1.34918
0.00000 TMS
7.83423
7.51968
7.37150
7.30999
7.29208 CDCl3
7.26017
7.21180
f1 (ppm)

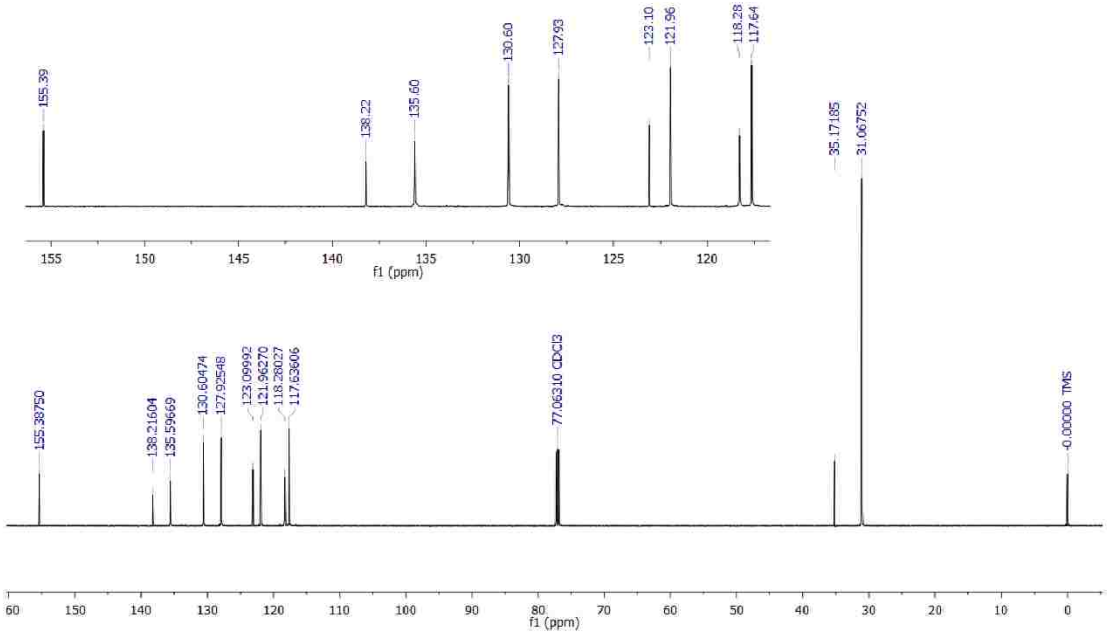
155.39
138.22
135.60
130.60
127.93
123.10
121.96
118.28
117.64
35.17185
31.06752
155.38750
138.21604
135.59669
130.60474
127.92548
123.09992
121.96270
118.28027
117.63606
77.06310 CDCl3
0.00000 TMS
f1 (ppm)

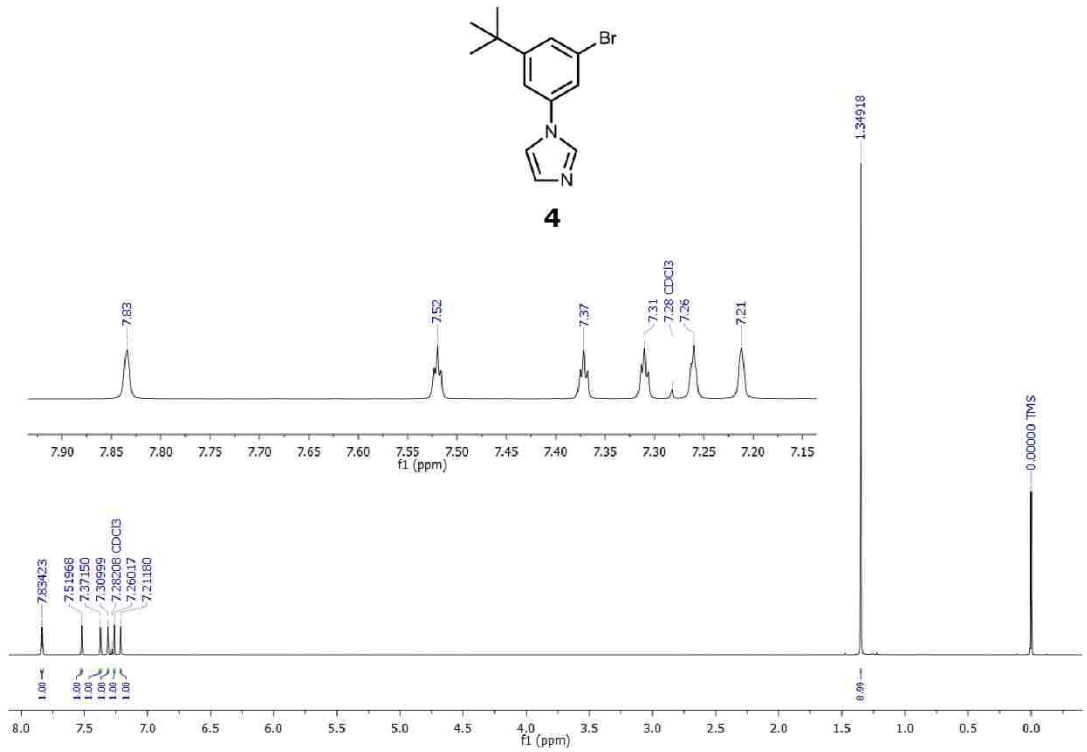
Br
N
N
4
7.83
7.52
7.37
7.31
7.28 CDCl3
7.26
7.21
1.34918
0.00000 TMS
7.83423
7.51968
7.37150
7.30999
7.28206 CDCl3
7.26017
7.21180
f1 (ppm)

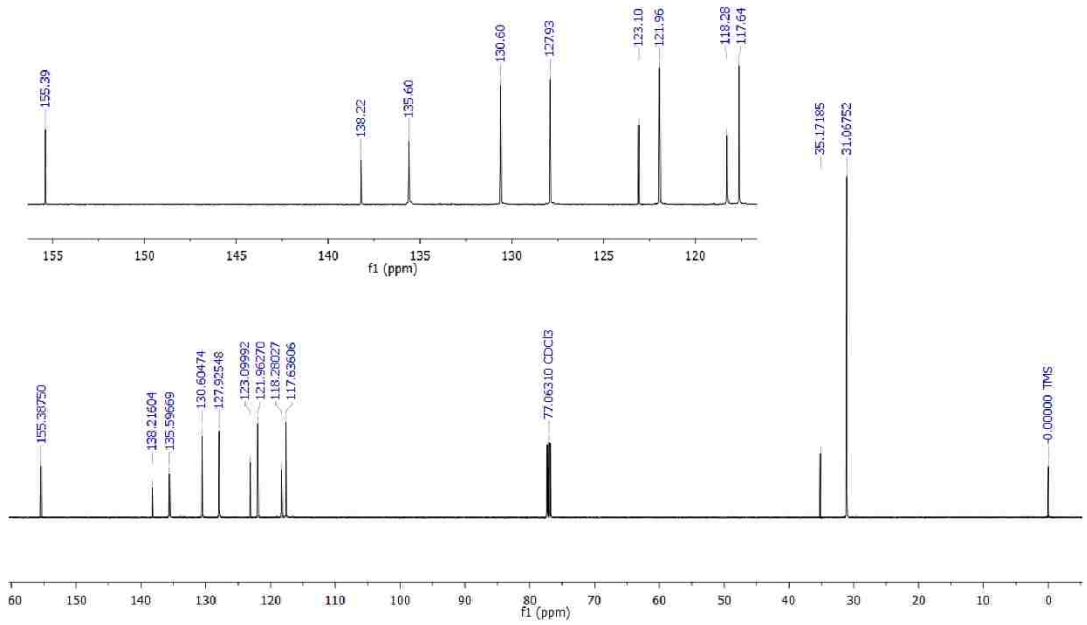
155.39
138.22
135.60
130.60
127.93
123.10
121.96
118.28
117.64
35.17185
31.06752
155.38750
138.21504
135.59669
130.60474
127.92548
123.09992
121.96270
118.28027
117.63606
77.06310 CDCl3
0.00000 TMS
f1 (ppm)

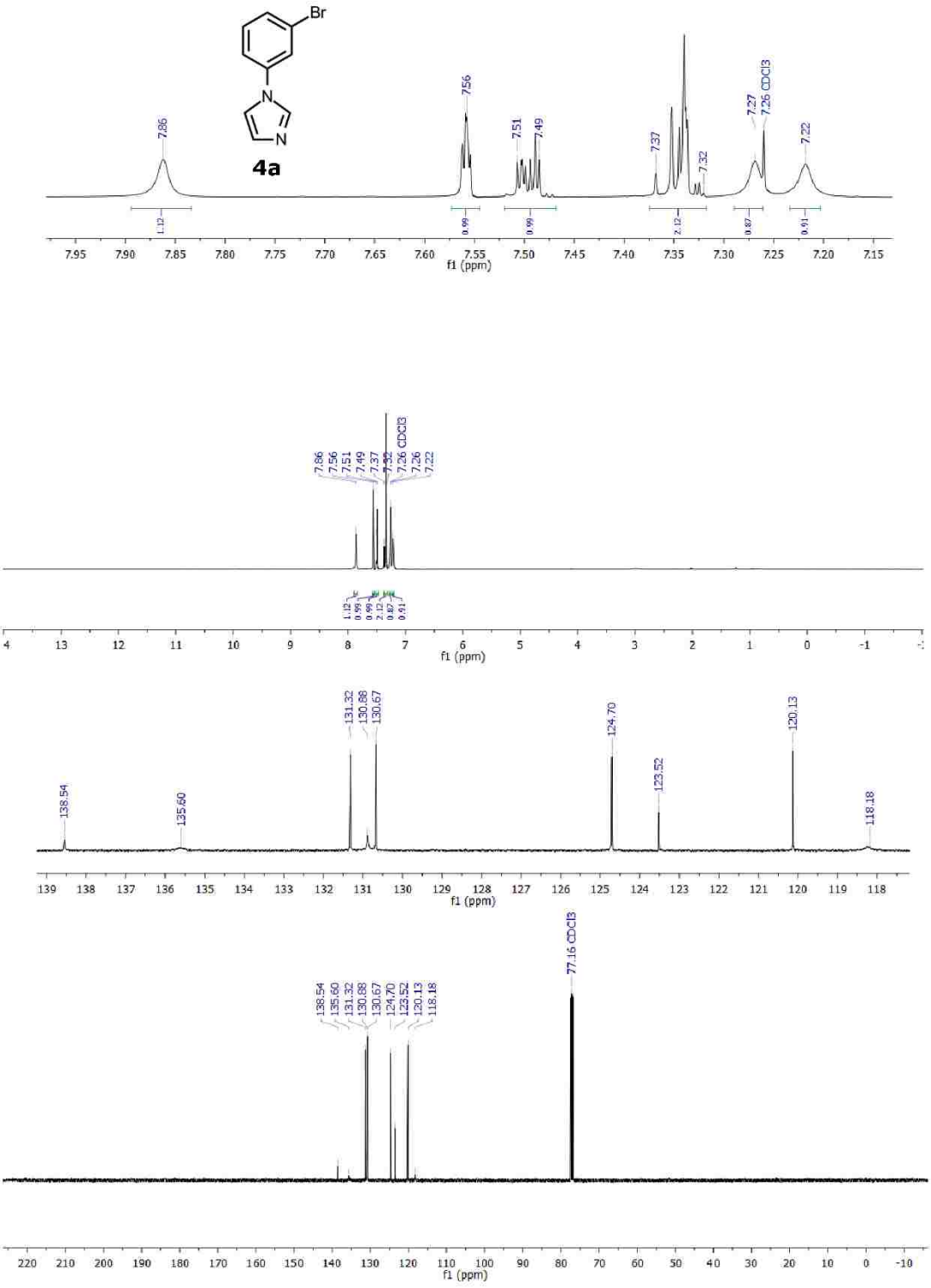
Br
N
N
4a
7.86
7.56
7.51
7.49
7.37
7.32
7.27
7.26 CDCl3
7.22
f1 (ppm)
138.54
135.60
131.32
130.88
130.67
124.70
123.52
120.13
118.18
77.16 CDCl3

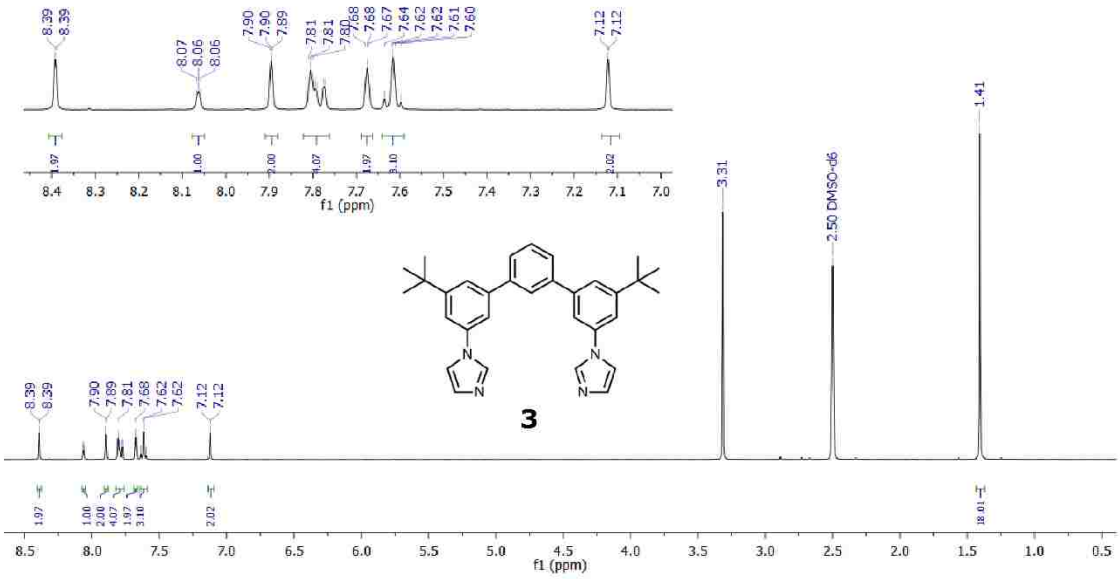
8.39
8.39
8.07
8.06
8.06
7.90
7.90
7.89
7.81
7.81
7.80
7.68
7.68
7.67
7.64
7.62
7.62
7.61
7.60
7.12
7.12
f1 (ppm)
3.31
2.50 DMSO-d6
1.41
3
f1 (ppm)

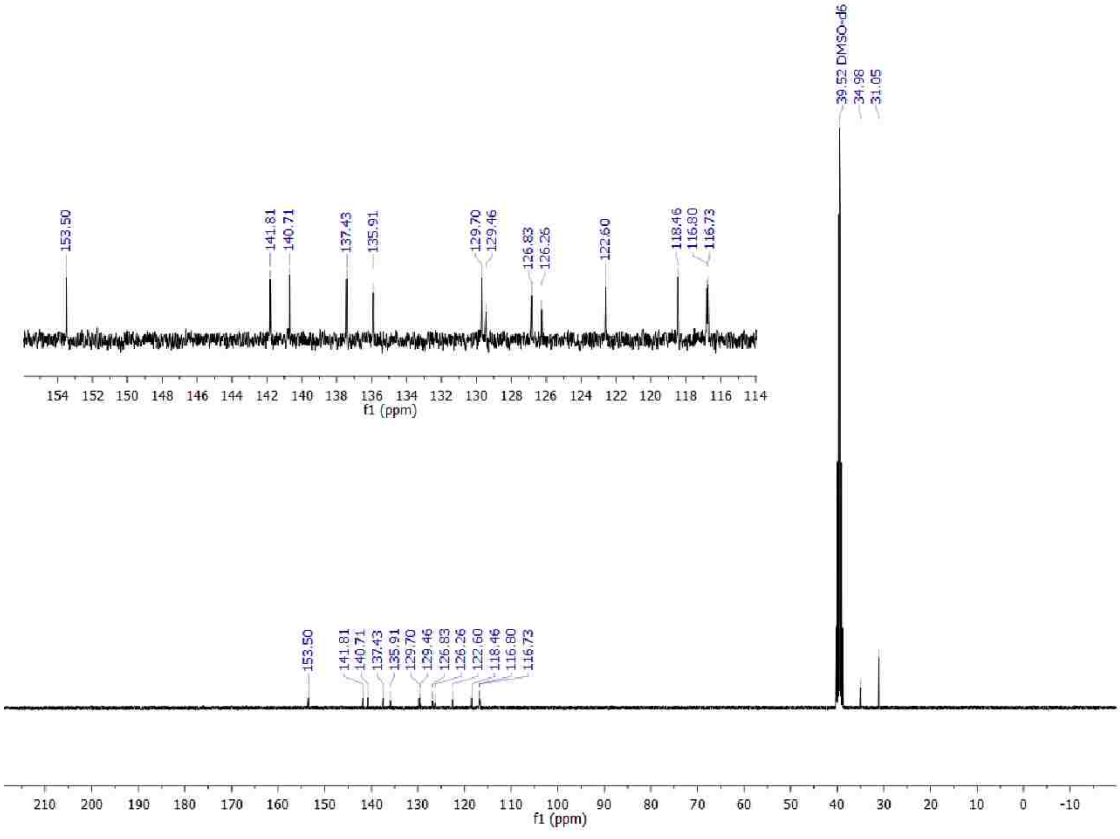
39.52 DMSO-d6
34.98
31.05
153.50
141.81
140.71
137.43
135.91
129.70
129.46
126.83
126.26
122.60
118.46
116.80
116.73
f1 (ppm)
f1 (ppm)

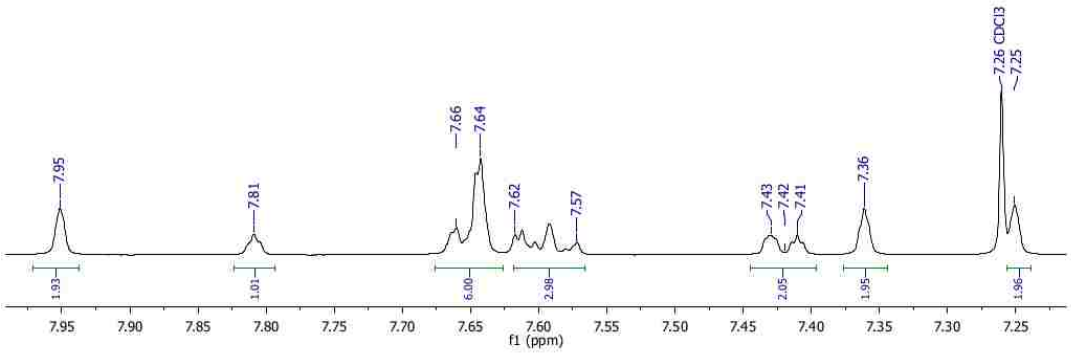
7.95
7.81
7.66
7.64
7.62
7.57
7.43
7.42
7.41
7.36
7.26 CDCl3
7.25
1.93
1.01
6.00
2.98
2.05
1.95
1.96
f1 (ppm)

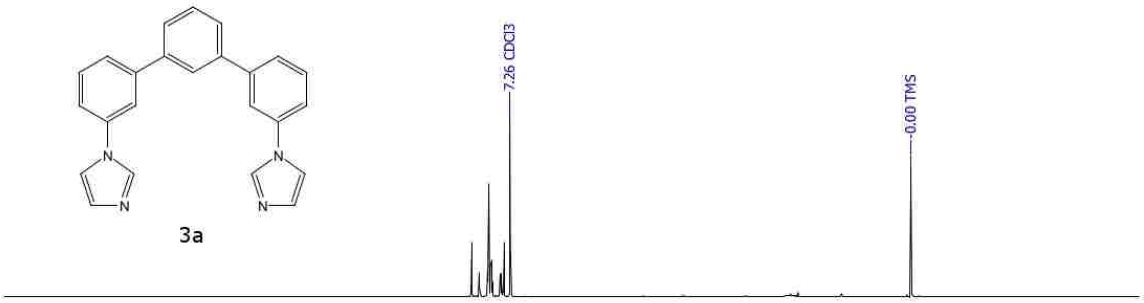
7.26 CDCl3
0.00 TMS
f1 (ppm)

3a

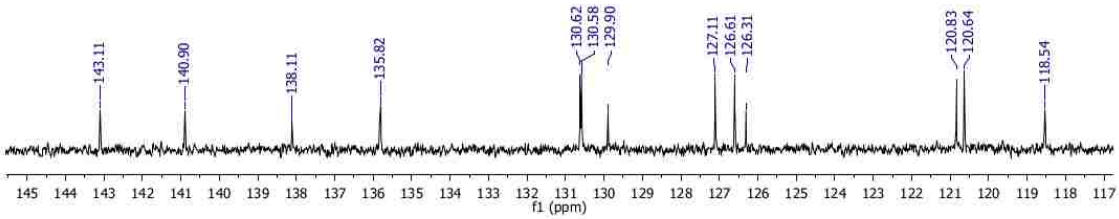
143.11
140.90
138.11
135.82
130.62
130.58
129.90
127.11
126.61
126.31
120.83
120.64
118.54
f1 (ppm)

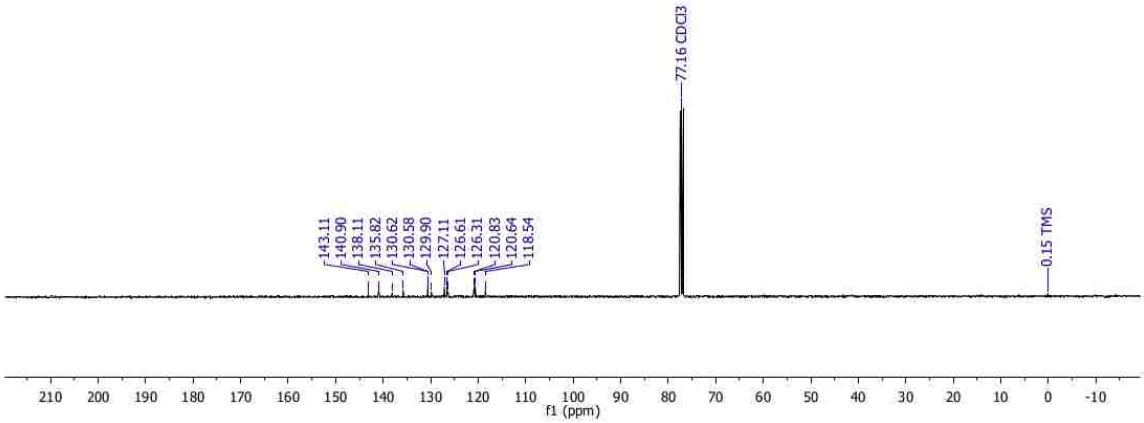
77.16 CDCl3
143.11
140.90
138.11
135.82
130.62
130.58
129.90
127.11
126.61
126.31
120.83
120.64
118.54
0.15 TMS
f1 (ppm)

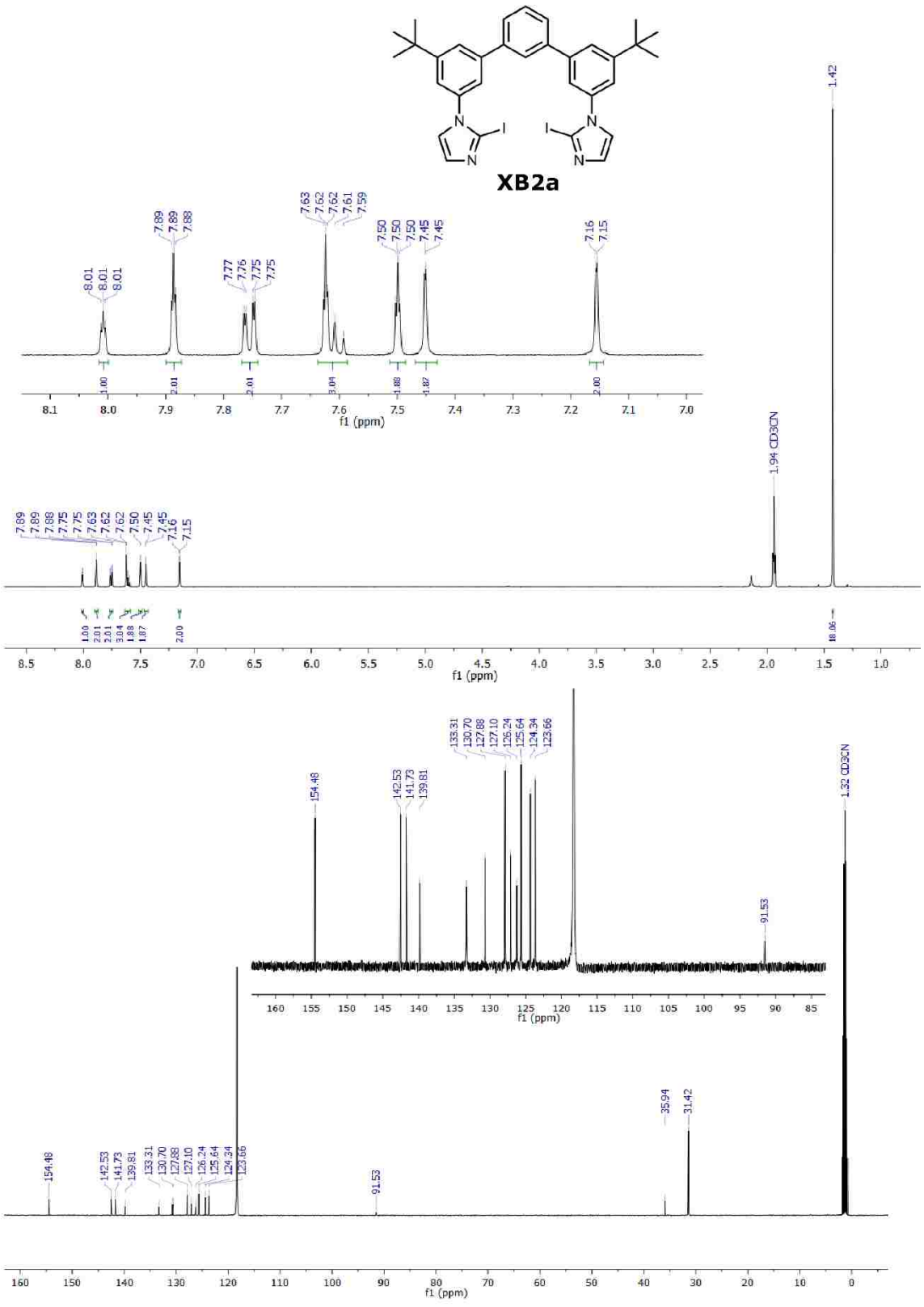
XB2a
f1 (ppm)
CD3CN

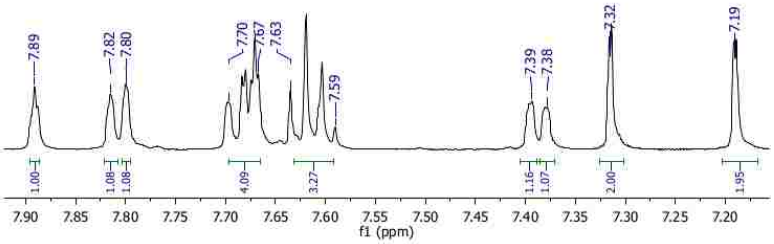
7.89
7.82
7.80
7.70
7.67
7.63
7.59
7.39
7.38
7.32
7.19
1.00
1.08
1.08
4.09
3.27
1.16
1.07
2.00
1.95
7.90 7.85 7.80 7.75 7.70 7.65 7.60 7.55 7.50 7.45 7.40 7.35 7.30 7.25 7.20
f1 (ppm)

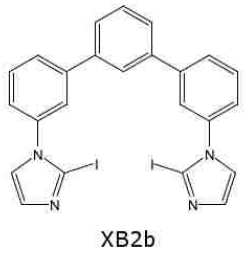

XB2b

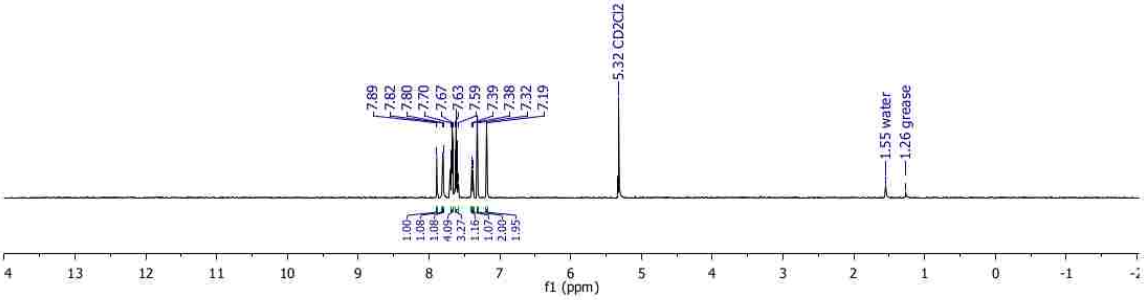
7.89
7.82
7.80
7.70
7.67
7.63
7.59
7.39
7.38
7.32
7.19
5.32 CD2Cl2
1.55 water
1.26 grease
1.00
1.08
1.08
4.09
3.27
1.16
1.07
2.00
1.95
4 13 12 11 10 9 8 7 6 5 4 3 2 1 0 -1
f1 (ppm)

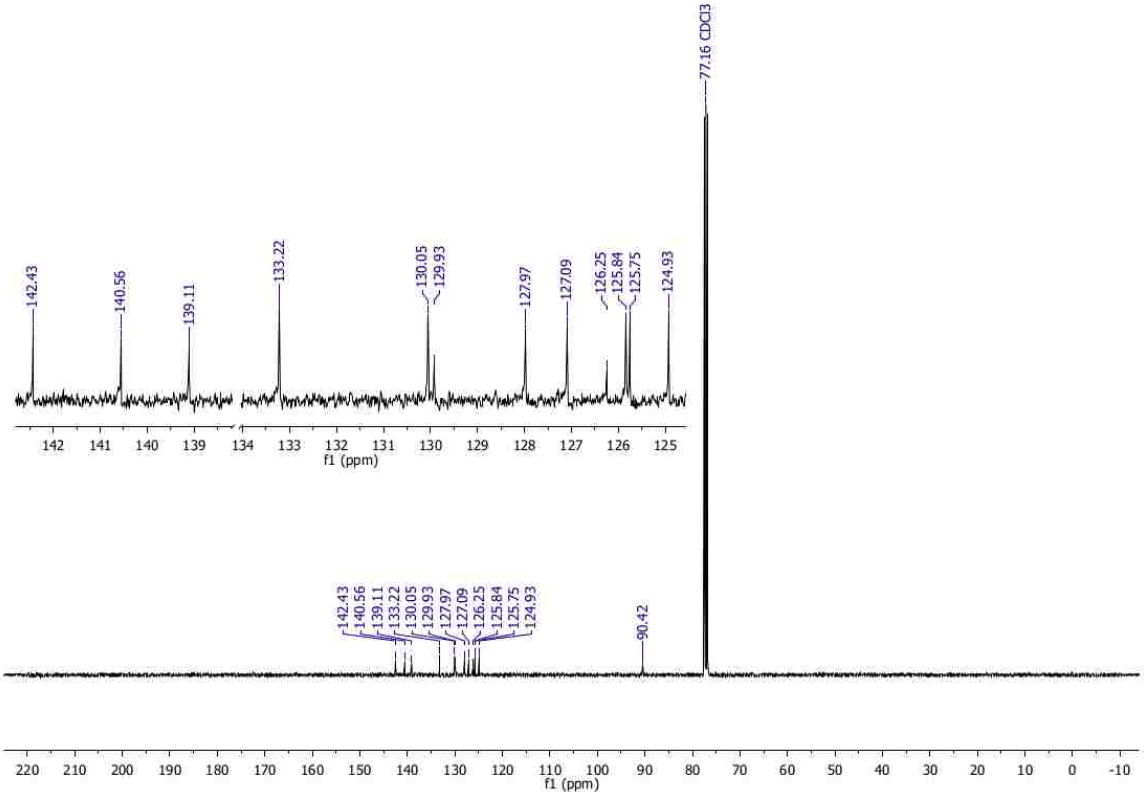
77.16 CDCl3
142.43
140.56
139.11
133.22
130.05
129.93
127.97
127.09
126.25
125.84
125.75
124.93
90.42
142 141 140 139 134 133 132 131 130 129 128 127 126 125
f1 (ppm)
220 210 200 190 180 170 160 150 140 130 120 110 100 90 80 70 60 50 40 30 20 10 0 -10
f1 (ppm)

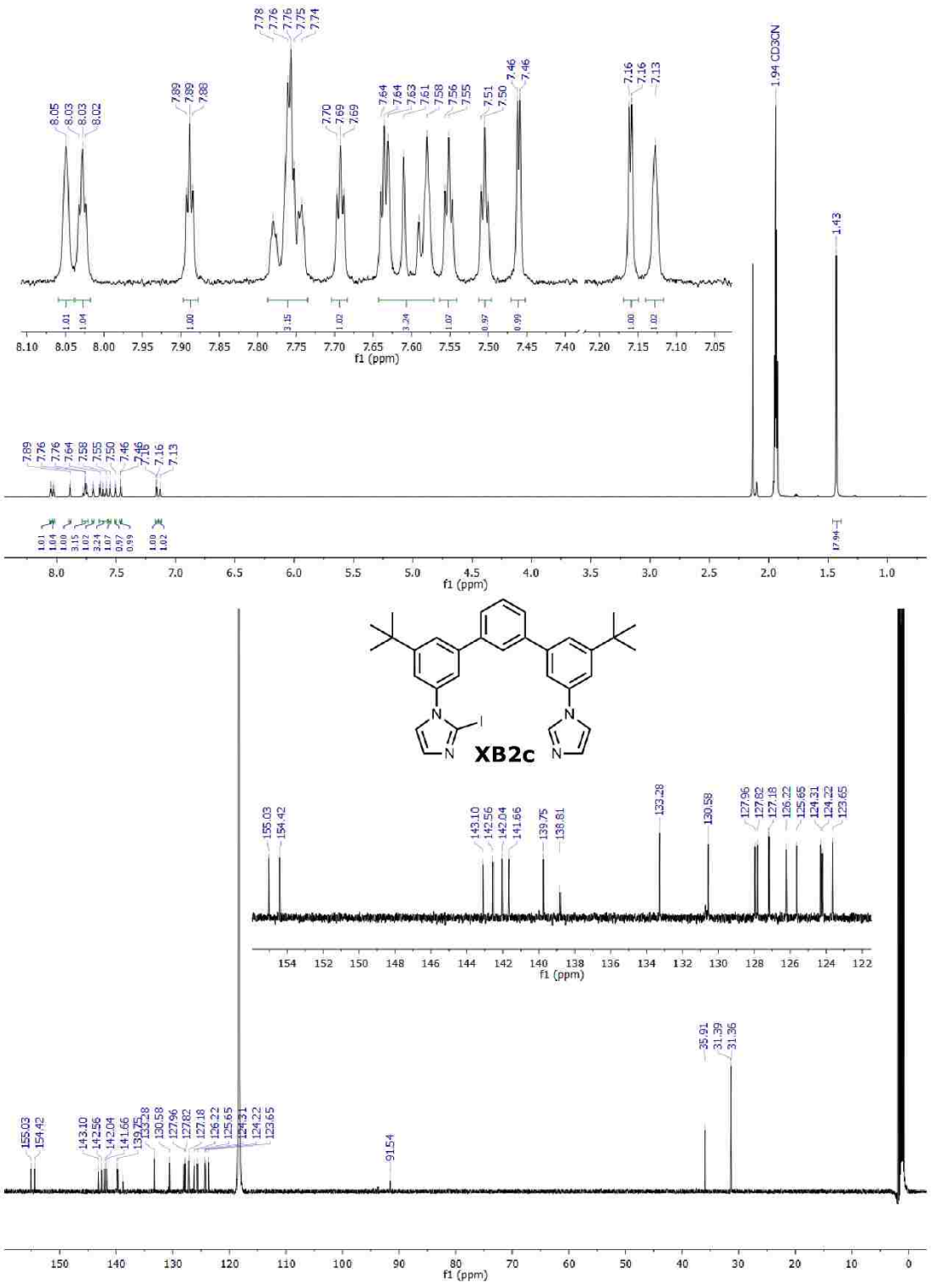
XB2c

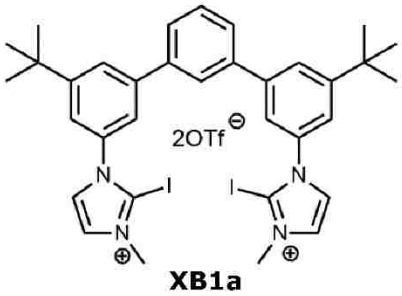
2OTf
N
I
N
⊕

XB1a

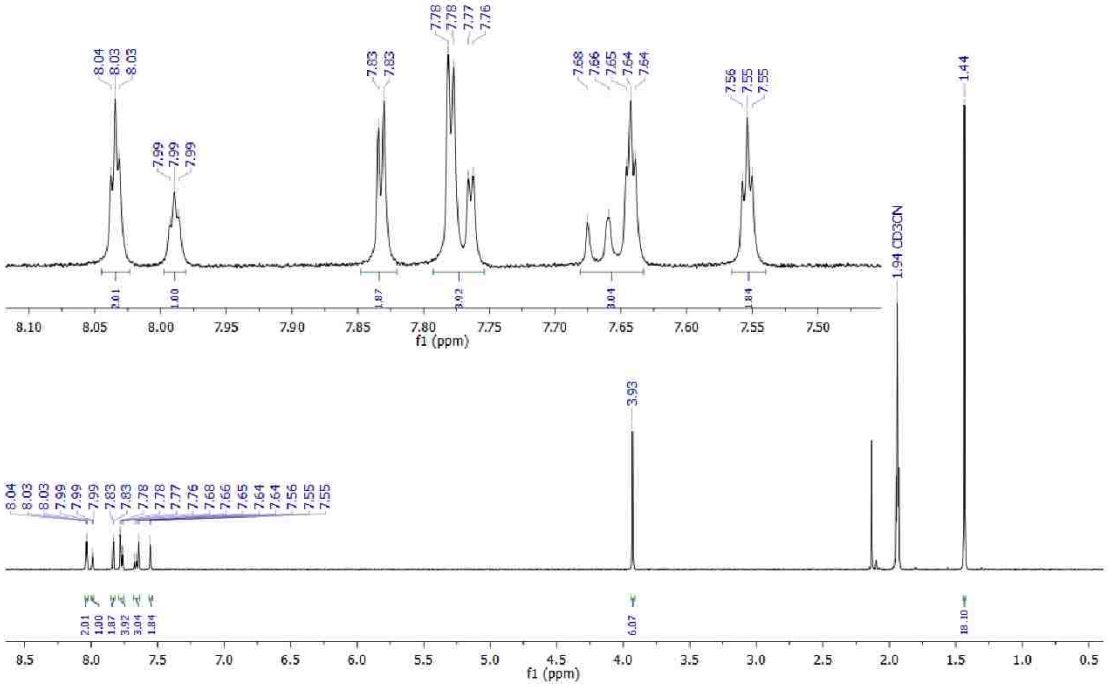
8.04
8.03
8.03
7.99
7.99
7.99
7.83
7.83
7.78
7.78
7.77
7.76
7.68
7.66
7.65
7.64
7.64
7.56
7.55
7.55
1.94 CD3CN
1.44
3.93
f1 (ppm)

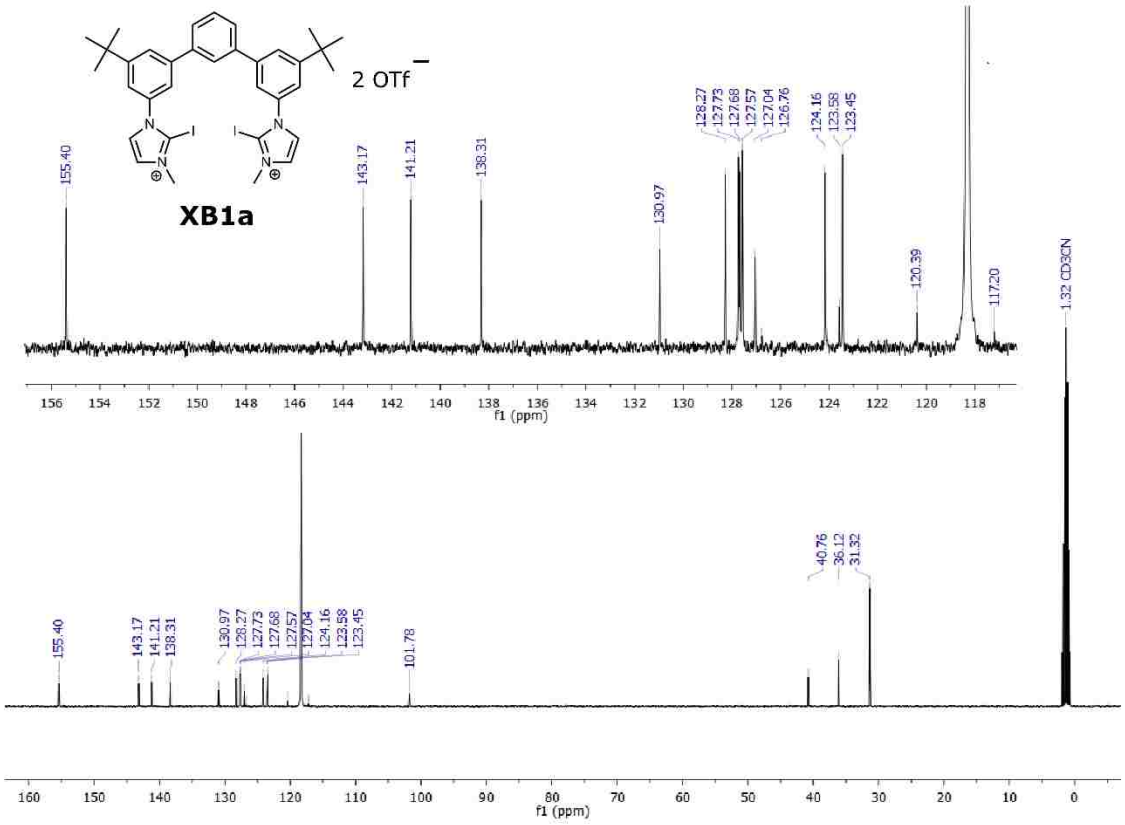
2 OTf
XB1a
155.40
143.17
141.21
138.31
130.97
128.27
127.73
127.68
127.57
127.04
126.76
124.16
123.58
123.45
120.39
117.20
1.32 CD3CN
f1 (ppm)

155.40
143.17
141.21
138.31
130.97
128.27
127.73
127.68
127.57
127.04
124.16
123.58
123.45
101.78
40.76
36.12
31.32
f1 (ppm)

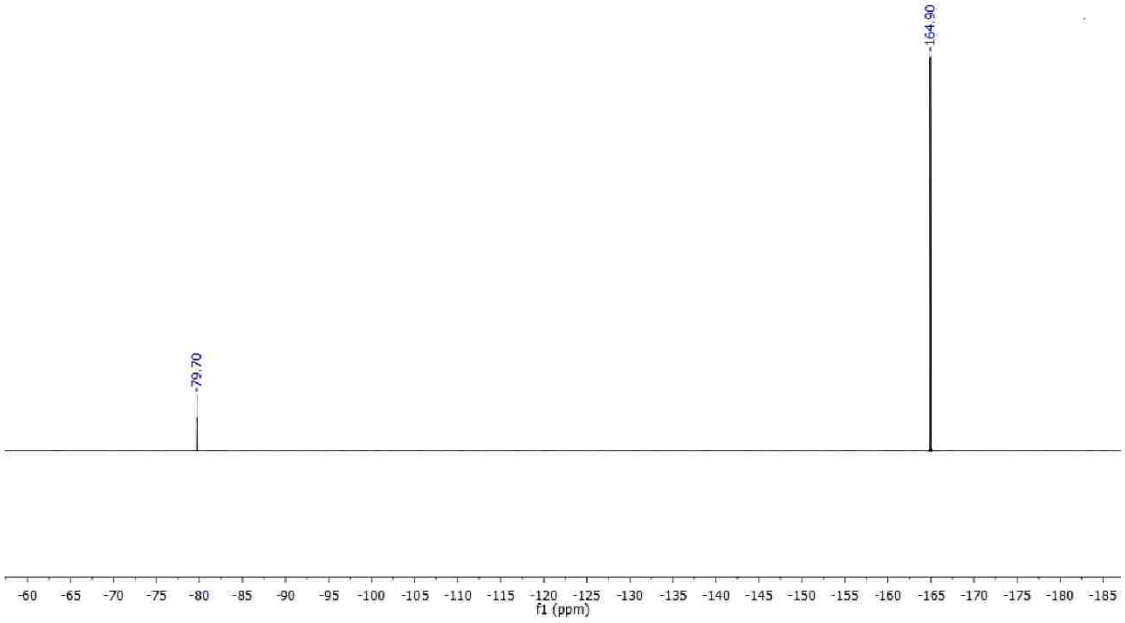
-164.90
-79.70
f1 (ppm)

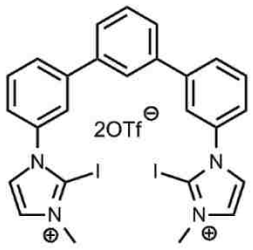
2OTf
N
I
N
⊕

XB1b

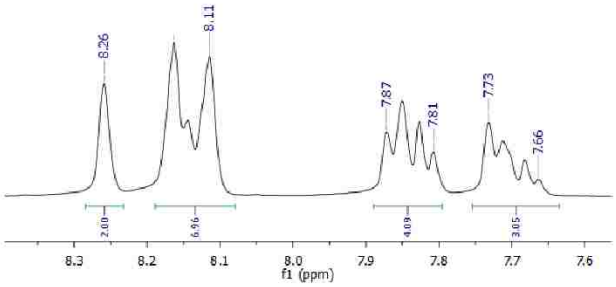
8.26
8.11
7.87
7.81
7.73
7.66
2.00
6.96
4.09
3.05
8.3
8.2
8.1
8.0
7.9
7.8
7.7
7.6
f1 (ppm)

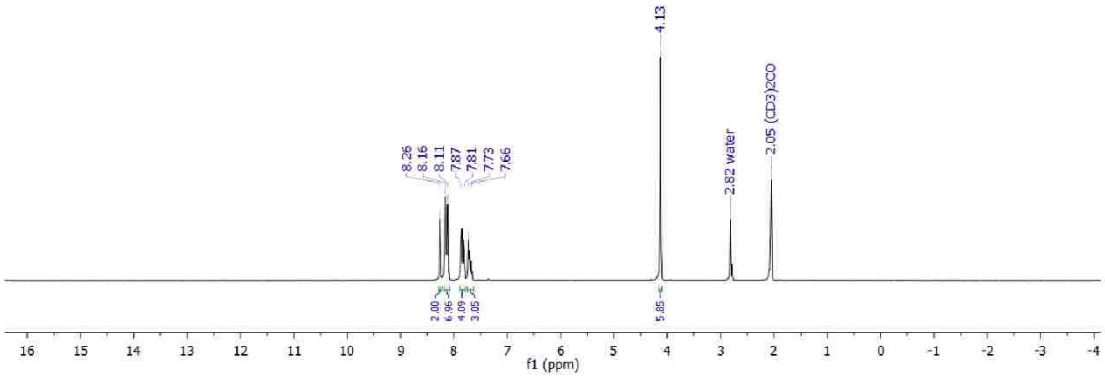
4.13
2.82 water
2.05 (CD3)2CO
8.26
8.16
8.11
7.87
7.81
7.73
7.66
2.00
6.96
4.09
3.05
5.85
16
15
14
13
12
11
10
9
8
7
6
5
4
3
2
1
0
-1
-2
-3
-4
f1 (ppm)

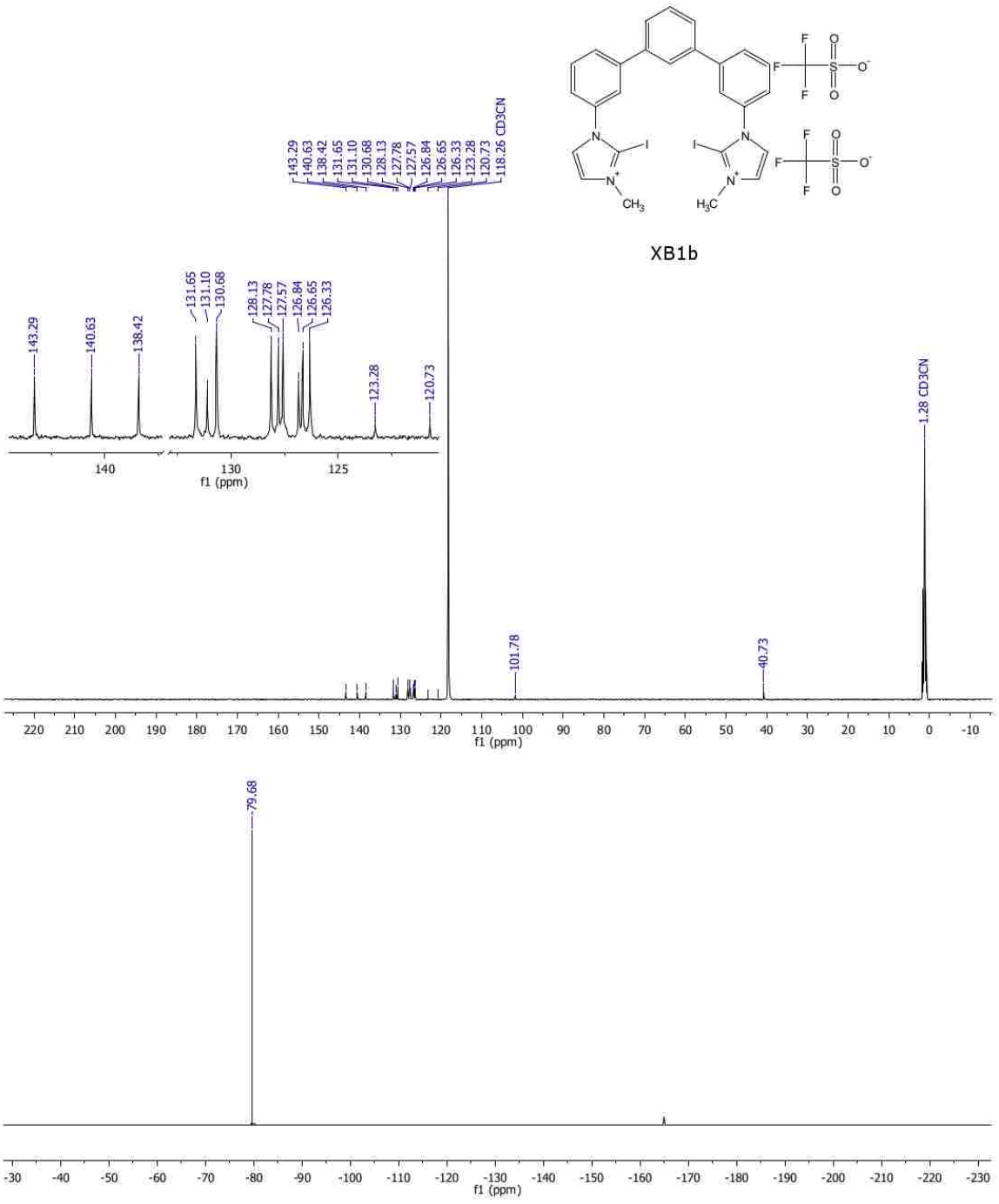
XB1b
143.29
140.63
138.42
131.65
131.10
130.68
128.13
127.78
127.57
126.84
126.65
126.33
123.28
120.73
118.26 CD3CN
101.78
40.73
1.28 CD3CN
f1 (ppm)
-79.68
f1 (ppm)

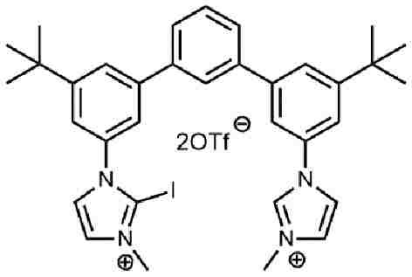

XB1c

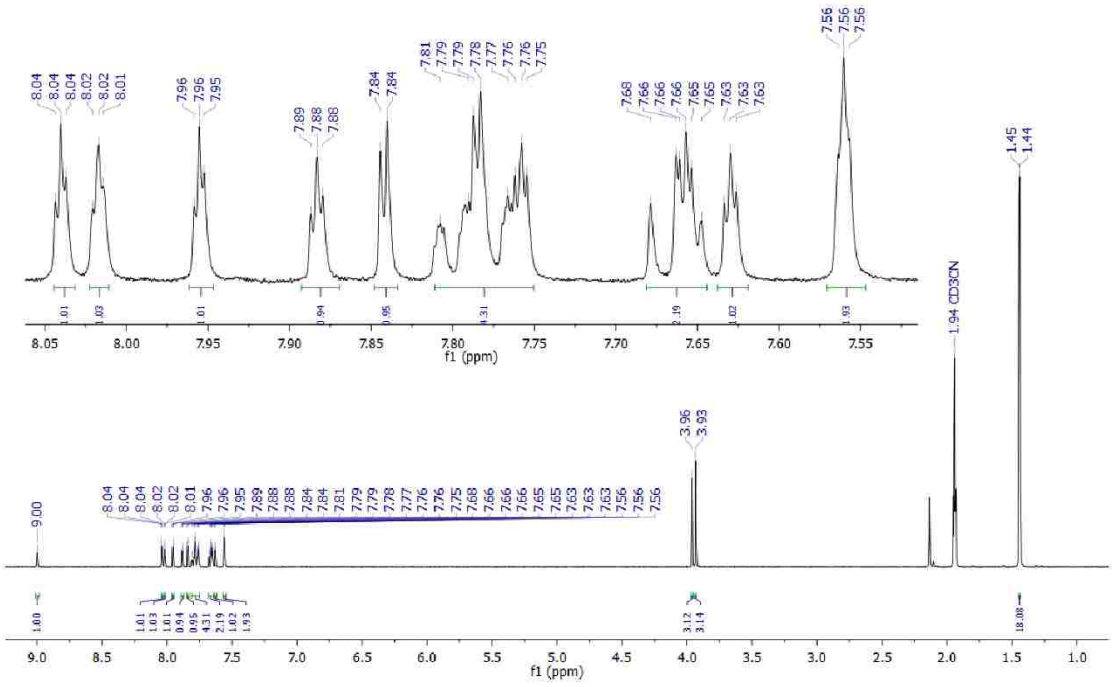

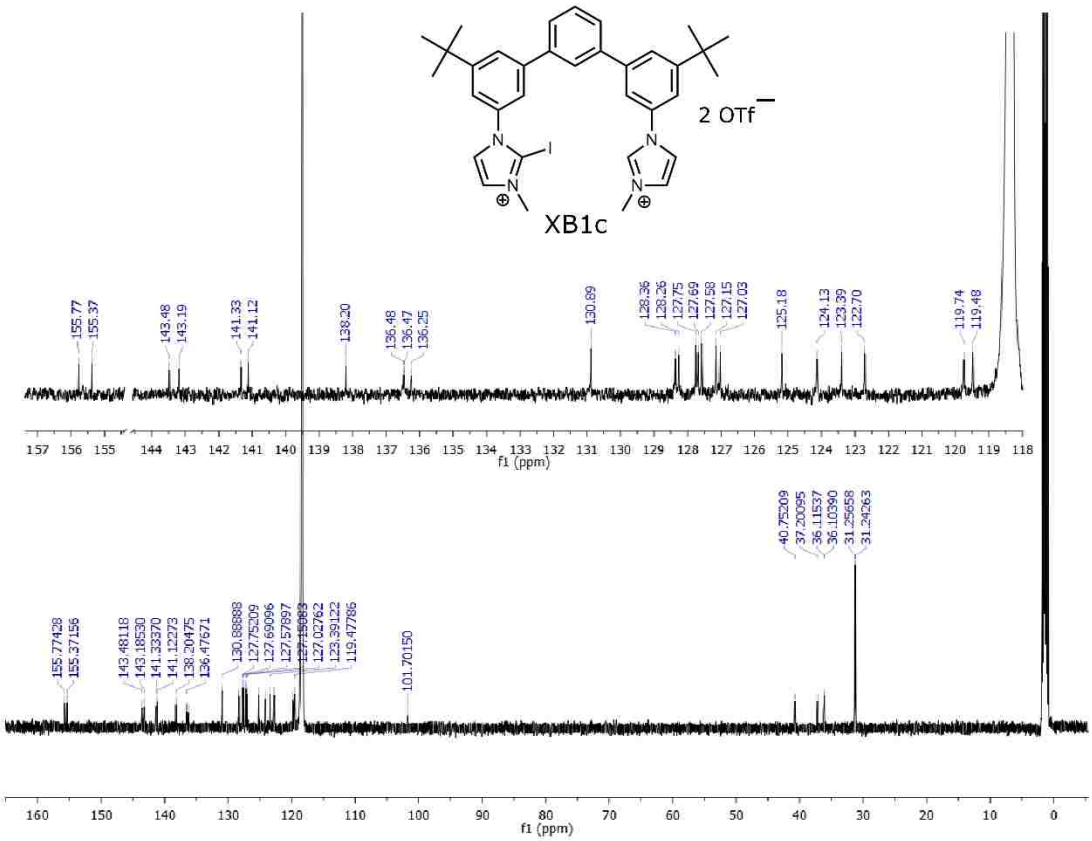
2 OTf
XB1c
155.77
155.37
143.48
143.19
141.33
141.12
138.20
136.48
136.47
136.25
130.89
128.36
128.26
127.75
127.69
127.58
127.15
127.03
125.18
124.13
123.39
122.70
119.74
119.48
f1 (ppm)
40.75209
37.20095
36.11537
36.10390
31.25658
31.24263
155.77428
155.37156
143.48118
143.18530
141.33370
141.12273
138.20475
136.47671
130.88888
127.75209
127.69096
127.57697
127.15983
127.02762
123.39122
119.47786
101.70150
f1 (ppm)

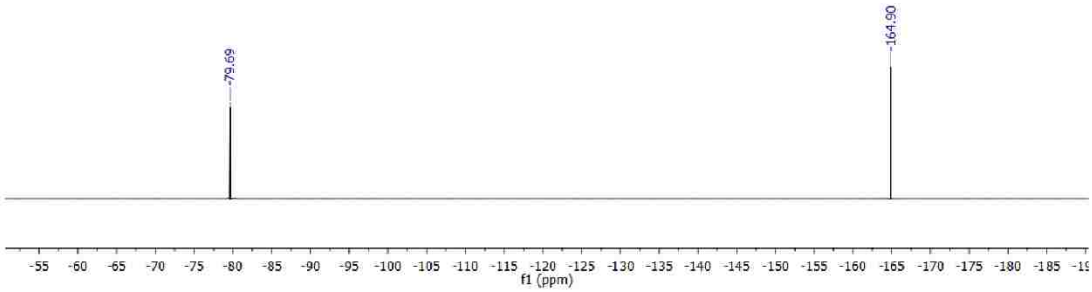
79.69
164.90
f1 (ppm)

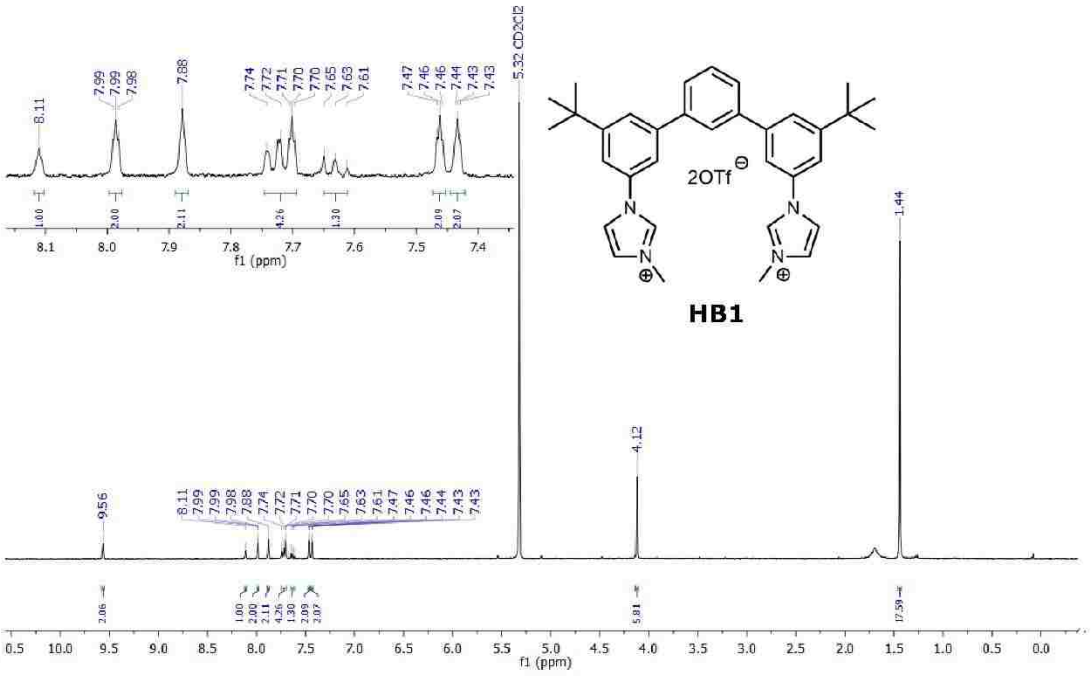
8.11
7.99
7.99
7.98
7.88
7.74
7.72
7.71
7.70
7.70
7.65
7.63
7.61
7.47
7.46
7.46
7.44
7.43
7.43
5.32 CD2Cl2
1.00
2.00
2.11
4.26
1.30
2.09
2.07
8.1
8.0
7.9
7.8
7.7
7.6
7.5
7.4
f1 (ppm)
2OTf⊖
HB1
1.44
4.12
9.56
2.06
5.81
17.59
0.5
10.0
9.5
9.0
8.5
8.0
7.5
7.0
6.5
6.0
5.5
5.0
4.5
4.0
3.5
3.0
2.5
2.0
1.5
1.0
0.5
0.0
f1 (ppm)

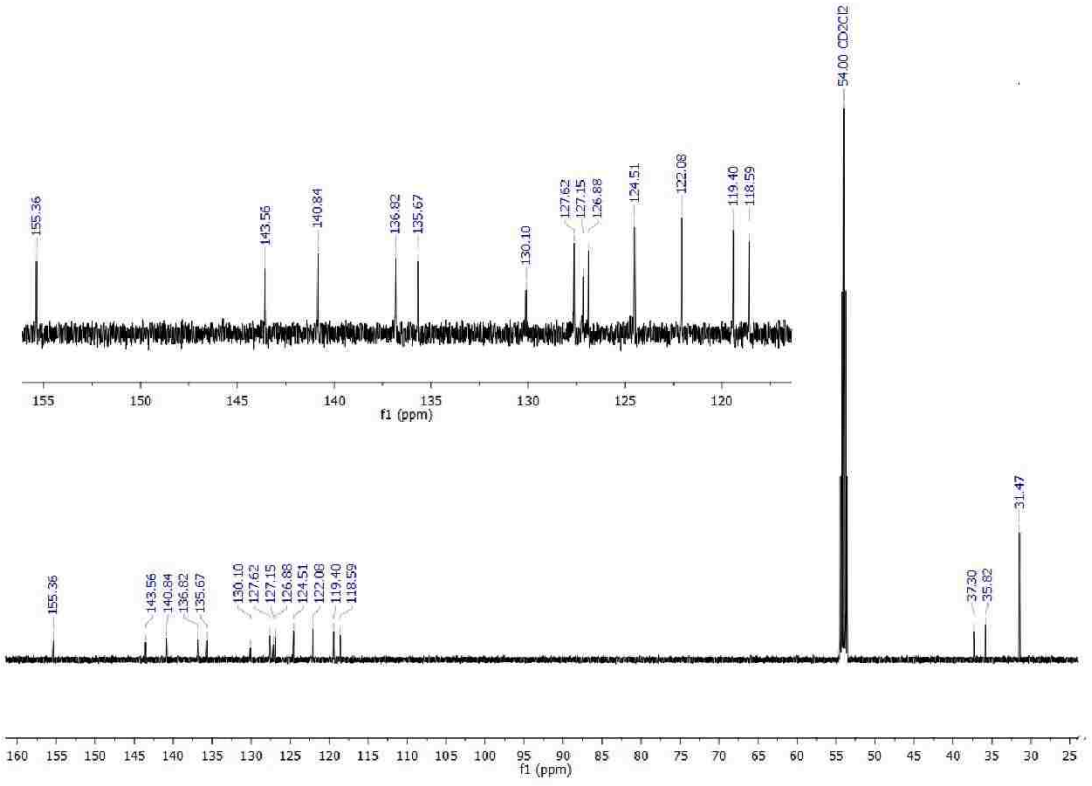
54.00 CD2Cl2
155.36
143.56
140.84
136.82
135.67
130.10
127.62
127.15
126.88
124.51
122.08
119.40
118.59
155
150
145
140
135
130
125
120
f1 (ppm)
31.47
37.30
35.82
160
155
150
145
140
135
130
125
120
115
110
105
100
95
90
85
80
75
70
65
60
55
50
45
40
35
30
25
f1 (ppm)

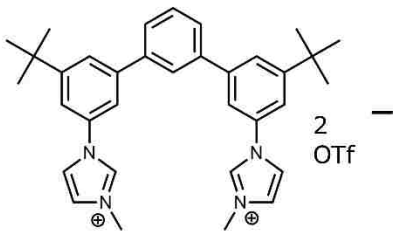
2
OTf

HB1

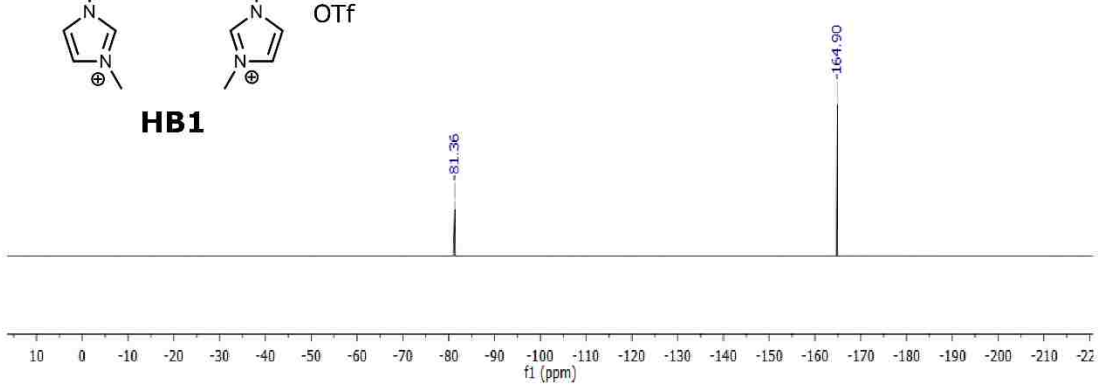
-81.36
-164.90
10 0 -10 -20 -30 -40 -50 -60 -70 -80 -90 -100 -110 -120 -130 -140 -150 -160 -170 -180 -190 -200 -210 -22
f1 (ppm)

Computations

All DFT calculations were performed using the Gaussian 09 suite.[126] We performed geometry optimizations at the B98 level, using the 6-31+G(d,p) basis set for non-halogen atoms C, O, N, H, and LANL2DZ with effective core potential (ECP) for halogens I and Cl. For the Iodine atoms, this was augmented with diffuse functions of p-symmetry and polarization functions of d-symmetry downloaded from the EMSL Basis Set Exchange. This method takes into account the large polarizability of the covalently bonded Iodines on the receptor, and accurately models the "σ-hole". We did not perform an exhaustive conformation search, but instead modeled in accordance with the bidentate conformation for all geometry optimizations.

Anion Binding data

All experiments were performed on a Varian Drive Direct 500 MHz NMR Spectrometer. TBA^+X^- (X=Halide) salts, **XB1a**, **XB1c**, and **HB1** were dried under vacuum and stored in a desiccator. Stock solutions of **XB1a**, **XB1c**, and **HB1** were prepared in 1%D_2O:CD_3CN. 0.500 mL aliquots from each stock solution were syringed into three separate NMR tubes with screw caps and septa. The stock solutions were then used to make three guest solutions corresponding to experiment number. After obtaining free-host spectra of **XB1a**, **XB1c**, and **HB1** aliquots of corresponding guest solution (containing **XB1a**, **XB1c**, or **HB1** and TBA^+X^- at specified concentrations) were added to their respective NMR tubes. Spectra were obtained after each addition (20x). A constant host concentration was maintained, while TBA^+X^- concentrations gradually increased

throughout the titration (see data below). Intuitions of stoichiometric displacement led to the stepwise anion exchange model:

$$H + G \rightleftharpoons HG \qquad K_1 = \frac{[HG]}{[H][G]}$$

$$HG + G \rightleftharpoons HG_2 \qquad K_2 = \frac{[HG_2]}{[HG][G]}$$

A simple 1:1 model, dimerization, and higher order binding were ruled out due to the emergence of an obvious pattern in residuals, unrealistic assigned shifts, poor convergence, and/or larger standard deviations. HypNMR 2008 was used to refine the isothermal fits of multiple signals (**XB1a**: H_a, H_b, and H_c; **XB1c**: H_a, H_b, H_c, H_d, H_e, H_f, and H_g; **HB1**: H_a, H_b, H_c, and H_d) simultaneously.

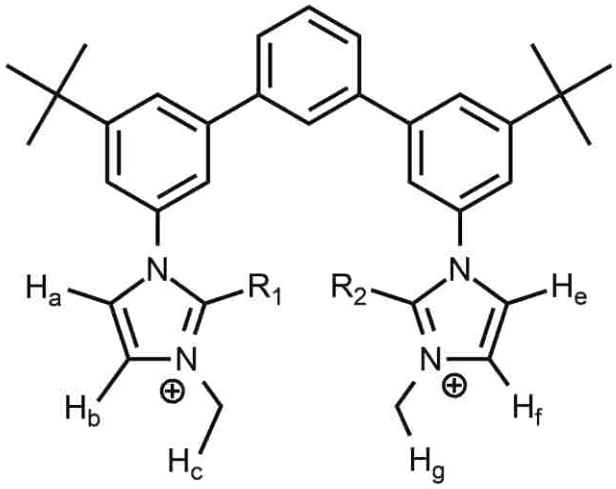

XB1a $R_1=R_2=I$, $H_a=H_e$, $H_b=H_f$, $H_c=H_g$
XB1c $R_1=I$, $R_2=H_d$
HB1 $R_1=R_2=H_d$, $H_a=H_e$, $H_b=H_f$, $H_c=H_g$

Calculated fits for titrations

(Receptor-guest-experiment number)

0% D_2O, CD_3CN

XB1a-Br-Exp1

Point	[X-]	[R]	peak (ppm)	peak (ppm)	peak (ppm)
1	0	0.001517105	7.83587	7.78191	3.92553
2	0.000352137	0.001517105	7.80968	7.75313	3.93075
3	0.000684341	0.001517105	7.78482	7.72577	3.9358
4	0.000895557	0.001517105	7.7689	7.70824	3.93883
5	0.001099093	0.001517105	7.75423	7.69172	3.94154
6	0.001295359	0.001517105	7.74118	-	3.94384
7	0.001484739	0.001517105	7.7312	7.66472	3.94515
8	0.001667589	0.001517105	7.72467	7.65572	3.94526
9	0.00184424	0.001517105	7.72072	7.64918	3.94476
10	0.002015004	0.001517105	7.71802	7.64395	3.94411
11	0.002180168	0.001517105	7.71601	7.63956	3.94323
12	0.002570319	0.001517105	7.71225	7.63127	3.9415
13	0.002930914	0.001517105	7.71026	7.62513	3.94024
14	0.003575922	0.001517105	7.7075	7.61703	3.93835
15	0.00413606	0.001517105	7.7064	7.61276	3.93734
16	0.004627045	0.001517105	7.70575	7.61004	3.93668
17	0.005447152	0.001517105	7.70548	7.60765	3.93593
18	0.006104862	0.001517105	7.70564	7.60664	3.93558
19	0.006644066	0.001517105	7.7058	7.60608	3.93527
20	0.00764516	0.001517105	7.70665	7.60611	3.935

	model	raw value	std. dev.	final value
log β1	RG	5.3575	0.1009	5.4(1)
log β2	RG_2	8.7592	0.1252	8.8(1)

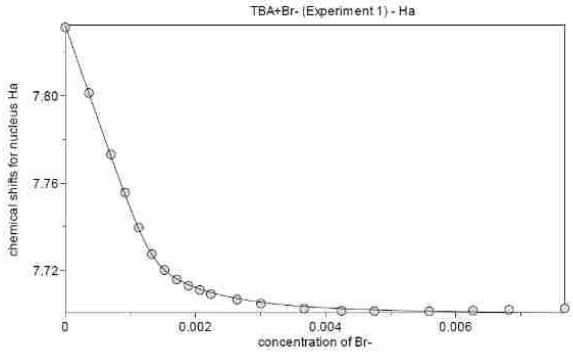
TBA+Br- (Experiment 1) - Ha
chemical shifts for nucleus Ha
7.80
7.76
7.72
0
0.002
0.004
0.006
concentration of Br-

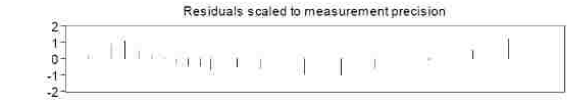
Residuals scaled to measurement precision
2
1
0
-1
-2

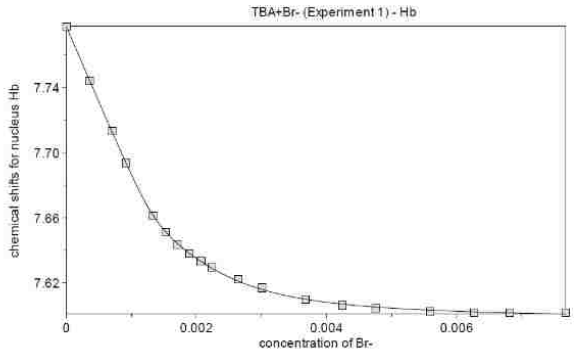
TBA+Br- (Experiment 1) - Hb
chemical shifts for nucleus Hb
7.74
7.70
7.66
7.62
0
0.002
0.004
0.006
concentration of Br-

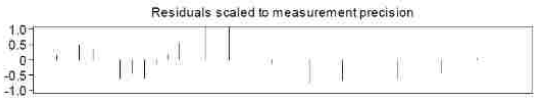
Residuals scaled to measurement precision
1.0
0.5
0
-0.5
-1.0

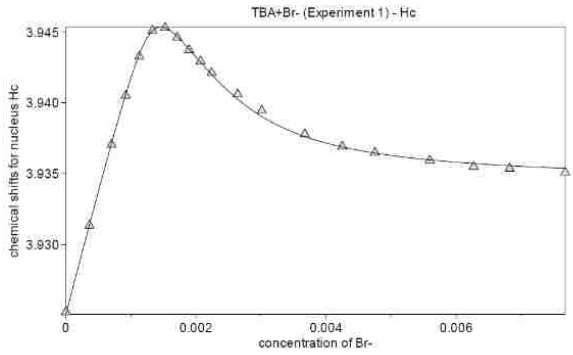
TBA+Br- (Experiment 1) - Hc
chemical shifts for nucleus Hc
3.945
3.940
3.935
3.930
0
0.002
0.004
0.006
concentration of Br-

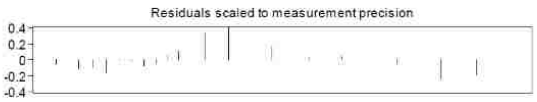
Residuals scaled to measurement precision
0.4
0.2
0
-0.2
-0.4

XB1a-Br-Exp2

Point	[X-]	[R]	peak (ppm)	peak (ppm)	peak (ppm)
1	0	0.001517105	7.83576	7.7817	3.92538
2	0.000352137	0.001517105	7.80983	7.75338	3.93094
3	0.000684341	0.001517105	7.7851	7.72605	3.93564
4	0.000895557	0.001517105	7.76968	7.70895	3.93867
5	0.001099093	0.001517105	7.75517	7.69282	3.94138
6	0.001295359	0.001517105	7.74216	-	3.94364
7	0.001484739	0.001517105	7.73218	7.66604	3.94501
8	0.001667589	0.001517105	7.72556	7.65699	3.94523
9	0.00184424	0.001517105	7.72161	7.65063	3.94487
10	0.002015004	0.001517105	7.7188	7.64537	3.94415
11	0.002180168	0.001517105	7.71669	7.64109	3.94341
12	0.002570319	0.001517105	7.71334	7.63308	3.94196
13	0.002930914	0.001517105	7.71109	7.62705	3.94054
14	0.003575922	0.001517105	7.70795	7.61854	3.93864
15	0.00413606	0.001517105	7.7067	7.61404	3.93756
16	0.004627045	0.001517105	7.70589	7.61102	3.93688
17	0.005447152	0.001517105	7.70538	7.60805	3.93598
18	0.006104862	0.001517105	7.70544	7.60675	3.93554
19	0.006644066	0.001517105	7.70574	7.60625	3.93524
20	0.00764516	0.001517105	7.70642	7.60605	3.93513

	model	raw value	std. dev.	final value
log β1	RG	5.4199	0.075	5.42(7)
log β2	RG_2	8.8302	0.0962	8.83(1)

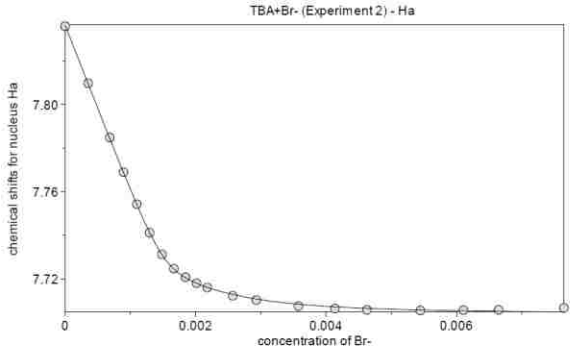
TBA+Br- (Experiment 2) - Ha
chemical shifts for nucleus Ha
7.80
7.76
7.72
0
0.002
0.004
0.006
concentration of Br-

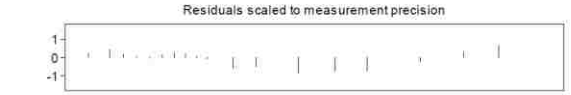
Residuals scaled to measurement precision
1
0
-1

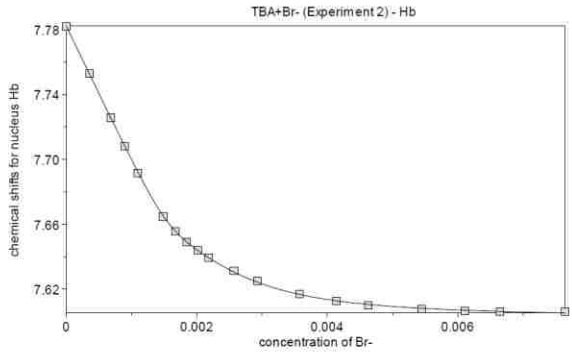
TBA+Br- (Experiment 2) - Hb
chemical shifts for nucleus Hb
7.78
7.74
7.70
7.66
7.62
0
0.002
0.004
0.006
concentration of Br-

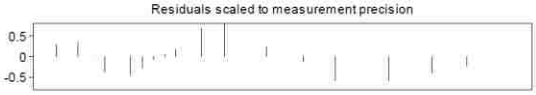
Residuals scaled to measurement precision
0.5
0
-0.5

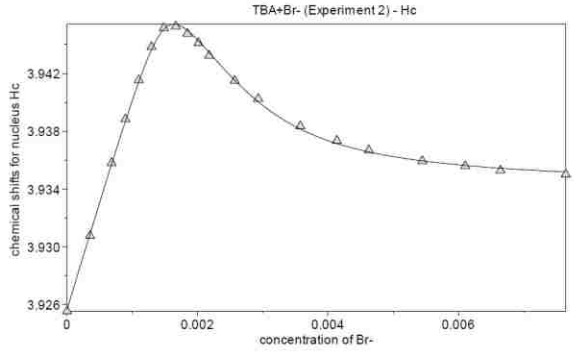
TBA+Br- (Experiment 2) - Hc
chemical shifts for nucleus Hc
3.942
3.938
3.934
3.930
3.926
0
0.002
0.004
0.006
concentration of Br-

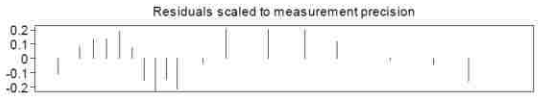
Residuals scaled to measurement precision
0.2
0.1
0
-0.1
-0.2

XB1a-Br-Exp3

Point	[X-]	[R]	peak (ppm)	peak (ppm)	peak (ppm)
1	0	0.001327467	7.83117	7.77714	3.92523
2	0.000361403	0.001327467	7.8012	7.74407	3.93133
3	0.00070235	0.001327467	7.77311	7.71313	3.93704
4	0.000919124	0.001327467	7.75565	7.69371	3.94049
5	0.001128016	0.001327467	7.73958	-	3.94325
6	0.001329448	0.001327467	7.72745	7.66095	3.94508
7	0.001523812	0.001327467	7.72018	7.6509	3.94527
8	0.001711473	0.001327467	7.71584	7.64331	3.94458
9	0.001892773	0.001327467	7.71305	7.63784	3.94371
10	0.00206803	0.001327467	7.71106	7.63324	3.94291
11	0.002237541	0.001327467	7.70924	7.62943	3.9421
12	0.002637959	0.001327467	7.70668	7.62208	3.94058
13	0.003008044	0.001327467	7.70482	7.61686	3.93943
14	0.003670025	0.001327467	7.70254	7.60974	3.93777
15	0.004244904	0.001327467	7.70153	7.60606	3.93689
16	0.004748809	0.001327467	7.7014	7.60438	3.93647
17	0.005590498	0.001327467	7.70129	7.6025	3.93591
18	0.006265516	0.001327467	7.70159	7.60171	3.93547
19	0.006818909	0.001327467	7.70204	7.60155	3.93536
20	0.007672233	0.001327467	7.70264	7.60163	3.93507

	model	raw value	std. dev.	final value
log β1	RG	5.3366	0.076	5.34(8)
log β2	RG_2	8.6478	0.0963	8.65(1)

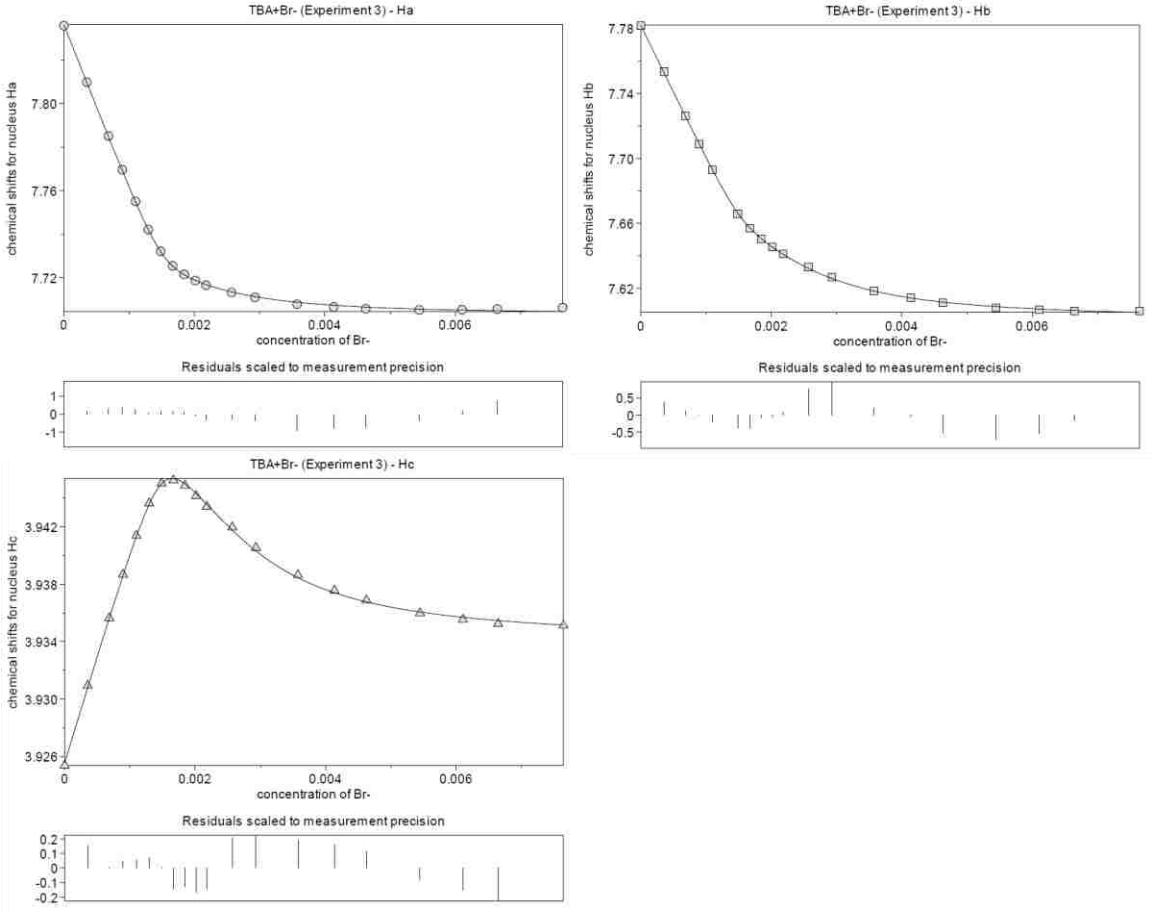
TBA+Br- (Experiment 3) - Ha
chemical shifts for nucleus Ha
7.80
7.76
7.72
0
0.002
0.004
0.006
concentration of Br-
Residuals scaled to measurement precision
1
0
-1
TBA+Br- (Experiment 3) - Hb
chemical shifts for nucleus Hb
7.78
7.74
7.70
7.66
7.62
0
0.002
0.004
0.006
concentration of Br-
Residuals scaled to measurement precision
0.5
0
-0.5
TBA+Br- (Experiment 3) - Hc
chemical shifts for nucleus Hc
3.942
3.938
3.934
3.930
3.926
0
0.002
0.004
0.006
concentration of Br-
Residuals scaled to measurement precision
0.2
0.1
0
-0.1
-0.2

HB1-Br-Exp1

Point	[X-]	[R]	peak (ppm)	peak (ppm)	peak (ppm)	peak (ppm)
1	0	0.001807034	8.98203	7.8861	7.75809	3.95317
2	0.000562462	0.001807034	9.22641	7.91848	7.82969	3.96294
3	0.001103291	0.001807034	9.46808	7.9515	7.90072	3.97185
4	0.001623712	0.001807034	9.6587	7.97877	7.95708	3.97997
5	0.002124857	0.001807034	9.80335	7.99826	7.99826	3.98496
6	0.00260778	0.001807034	9.91153	8.01452	8.02978	3.98922
7	0.003073455	0.001807034	9.99787	8.02798	8.05465	3.99257
8	0.00352279	0.001807034	10.06602	8.03857	8.07419	3.99547
9	0.003956631	0.001807034	10.11964	8.04724	8.0893	3.9976
10	0.004375766	0.001807034	10.16591	8.05582	8.10346	4.00024
11	0.004780929	0.001807034	10.20303	8.06192	8.11309	4.00128
12	0.005172809	0.001807034	10.23472	8.06749	8.12203	4.00282
13	0.005552047	0.001807034	10.26171	8.07244	8.12956	4.00404
14	0.005919246	0.001807034	10.28578	8.07726	8.13607	4.00507
15	0.00627497	0.001807034	10.306	8.08142	8.14189	4.00622
16	0.006619748	0.001807034	10.32459	8.08548	8.14716	4.00739
17	0.006954079	0.001807034	10.34102	8.08814	8.15108	4.00722
18	0.007437001	0.001807034	10.36242	8.09368	8.15782	4.00948
19	0.008048471	0.001807034	10.386	8.09832	8.16375	4.0099
20	0.008625733	0.001807034	10.40733	8.10329	8.1696	4.01116

	model	raw value	std. dev.	final value
log β1	RG	4.0673	0.03	4.07(6)
log β2	RG_2	6.6532	0.0711	6.65(7)

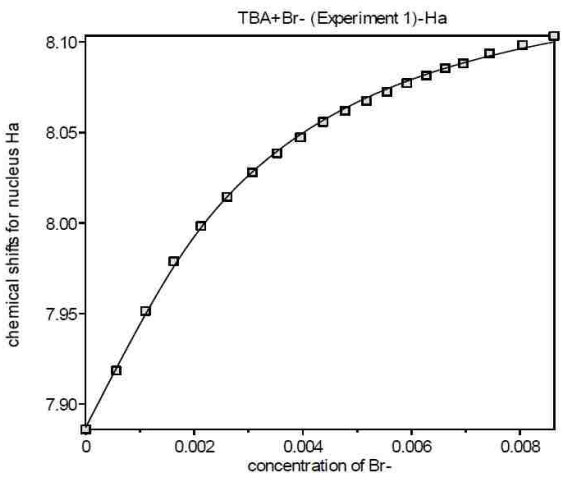
TBA+Br- (Experiment 1)-Ha
chemical shifts for nucleus Ha
8.10
8.05
8.00
7.95
7.90
0
0.002
0.004
0.006
0.008
concentration of Br-

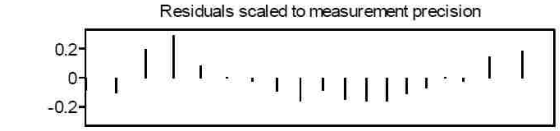
Residuals scaled to measurement precision
0.2
0
-0.2

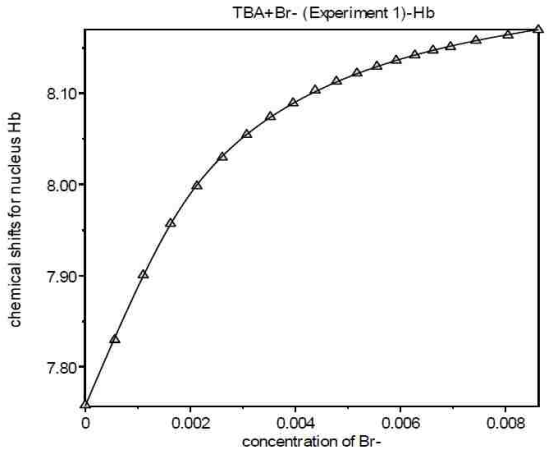
TBA+Br- (Experiment 1)-Hb
chemical shifts for nucleus Hb
8.10
8.00
7.90
7.80
0
0.002
0.004
0.006
0.008
concentration of Br-

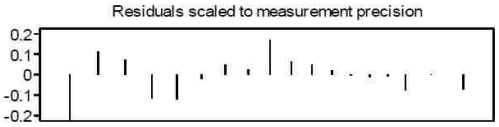
Residuals scaled to measurement precision
0.2
0.1
0
-0.1
-0.2

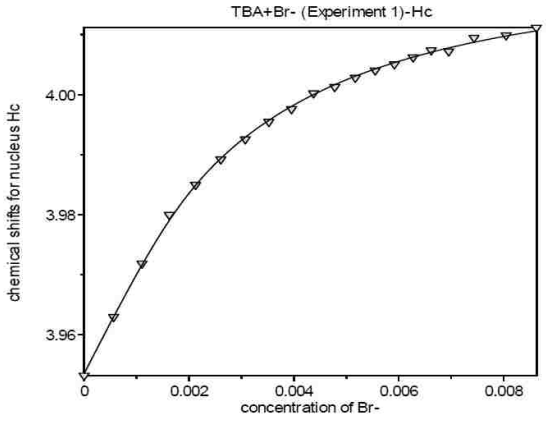
TBA+Br- (Experiment 1)-Hc
chemical shifts for nucleus Hc
4.00
3.98
3.96
0
0.002
0.004
0.006
0.008
concentration of Br-

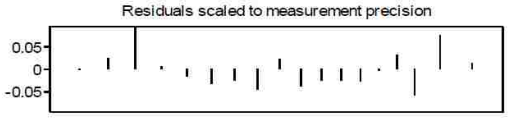
Residuals scaled to measurement precision
0.05
0
-0.05

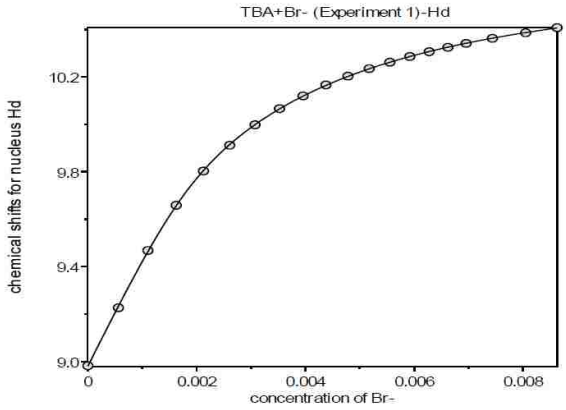
TBA+Br- (Experiment 1)-Hd
chemical shifts for nucleus Hd
10.2
9.8
9.4
9.0
0
0.002
0.004
0.006
0.008
concentration of Br-

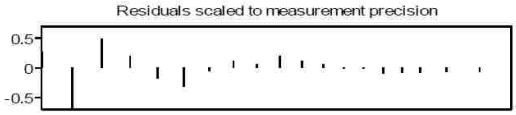
Residuals scaled to measurement precision
0.5
0
-0.5

HB1-Br-Exp2

Point	[X-]	[R]	peak (ppm)	peak (ppm)	peak (ppm)	peak (ppm)
1	0	0.001290739	8.98223	7.88581	7.75743	3.95364
2	0.000470899	0.001290739	9.27267	7.92566	7.84338	3.9648
3	0.000923686	0.001290739	9.52314	7.95925	7.91555	3.97399
4	0.001359387	0.001290739	9.7064	7.98405	7.96858	3.97987
5	0.00177895	0.001290739	9.84228	8.00431	8.00763	3.98526
6	0.002183257	0.001290739	9.94494	8.01938	8.03866	3.9897
7	0.002573125	0.001290739	10.0255	8.03104	8.06129	3.99263
8	0.002949313	0.001290739	10.08805	8.04107	8.07921	3.99527
9	0.003312528	0.001290739	10.13768	8.04967	8.09382	3.99777
10	0.003663432	0.001290739	10.17892	8.05655	8.10504	3.99931
11	0.004002639	0.001290739	10.21376	8.0625	8.11488	4.00085
12	0.004330724	0.001290739	10.24244	8.06797	8.12359	4.00239
13	0.004648225	0.001290739	10.26771	8.07254	8.13037	4.00347
14	0.004955648	0.001290739	10.28962	8.07669	8.13592	4.0045
15	0.005253463	0.001290739	10.30837	8.08058	8.14149	4.00553
16	0.005542115	0.001290739	10.32332	8.08375	8.14592	4.00649
17	0.00582202	0.001290739	10.3391	8.08705	8.15052	4.00747
18	0.006093569	0.001290739	10.35254	8.0901	8.15404	4.00812
19	0.006613055	0.001290739	10.37609	8.09518	8.16046	4.00902
20	0.007221544	0.001290739	10.3999	8.10062	8.1669	4.01023

	model	raw value	std. dev.	final value
log β1	RG	4.081	0.0072	4.081(7)
log β2	RG_2	6.6532	fixed	6.6532

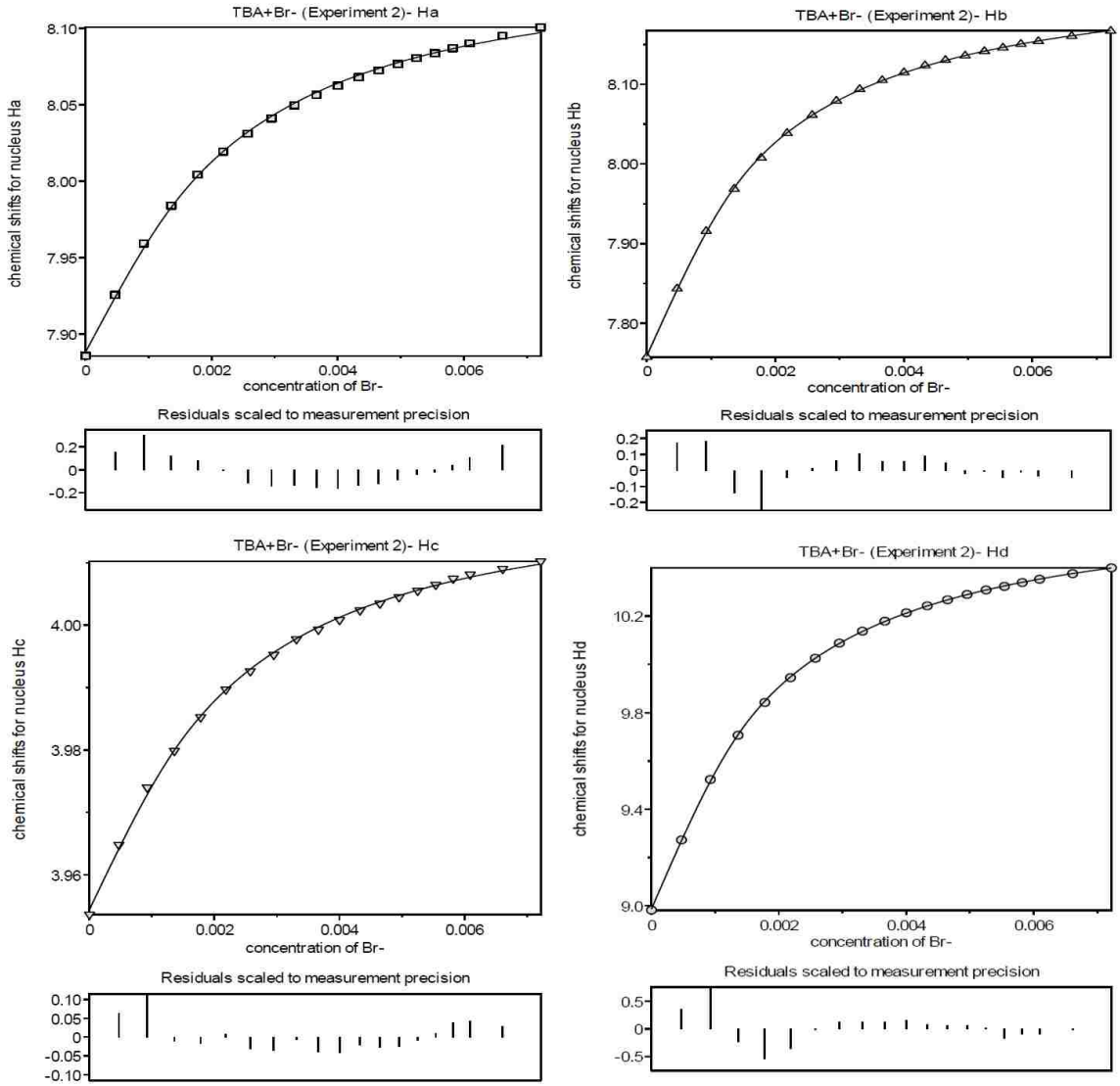
TBA+Br- (Experiment 2)- Ha
chemical shifts for nucleus Ha
8.10
8.05
8.00
7.95
7.90
0
0.002
0.004
0.006
concentration of Br-
Residuals scaled to measurement precision
0.2
0
-0.2
TBA+Br- (Experiment 2)- Hb
chemical shifts for nucleus Hb
8.10
8.00
7.90
7.80
0
0.002
0.004
0.006
concentration of Br-
Residuals scaled to measurement precision
0.2
0.1
0
-0.1
-0.2
TBA+Br- (Experiment 2)- Hc
chemical shifts for nucleus Hc
4.00
3.98
3.96
0
0.002
0.004
0.006
concentration of Br-
Residuals scaled to measurement precision
0.10
0.05
0
-0.05
-0.10
TBA+Br- (Experiment 2)- Hd
chemical shifts for nucleus Hd
10.2
9.8
9.4
9.0
0
0.002
0.004
0.006
concentration of Br-
Residuals scaled to measurement precision
0.5
0
-0.5

HB1-Br-Exp3

Point	[X-]	[R]	peak (ppm)	peak (ppm)	peak (ppm)	peak (ppm)
1	0	0.001548886	8.98786	7.88681	7.75873	3.9543
2	0.000483979	0.001548886	9.21589	7.91766	7.82651	3.96276
3	0.000949344	0.001548886	9.44527	7.94849	7.8947	3.97226
4	0.001397147	0.001548886	9.6285	7.97462	7.94511	3.97841
5	0.001828366	0.001548886	9.76988	7.9947	7.9914	3.98395
6	0.002243903	0.001548886	9.8802	8.011	8.02085	3.98829
7	0.0026446	0.001548886	9.96688	8.02334	8.04502	3.99074
8	0.003031238	0.001548886	10.03756	8.0351	8.06612	3.99463
9	0.003404543	0.001548886	10.0933	8.04329	8.08128	3.99604
10	0.003765194	0.001548886	10.13939	8.05102	8.09475	3.99817
11	0.004113823	0.001548886	10.17805	8.05755	8.10546	3.99967
12	0.004451022	0.001548886	10.21145	8.0637	8.11493	4.00133
13	0.004777343	0.001548886	10.23918	8.06871	8.1229	4.0026
14	0.005093305	0.001548886	10.26395	8.07349	8.12991	4.0038
15	0.005399393	0.001548886	10.28537	8.07744	8.13592	4.00479
16	0.005696063	0.001548886	10.30443	8.08106	8.14082	4.00561
17	0.005983742	0.001548886	10.3213	8.0848	8.14528	4.0065
18	0.006262835	0.001548886	10.33649	8.08785	8.14962	4.00726
19	0.006796751	0.001548886	10.36063	8.09316	8.15651	4.00865
20	0.007422142	0.001548886	10.38736	8.09888	8.1639	4.01022

	model	raw value	std. dev.	final value
log β1	RG	3.9706	0.008	3.971(8)
log β2	RG_2	6.6208	fixed	6.6208

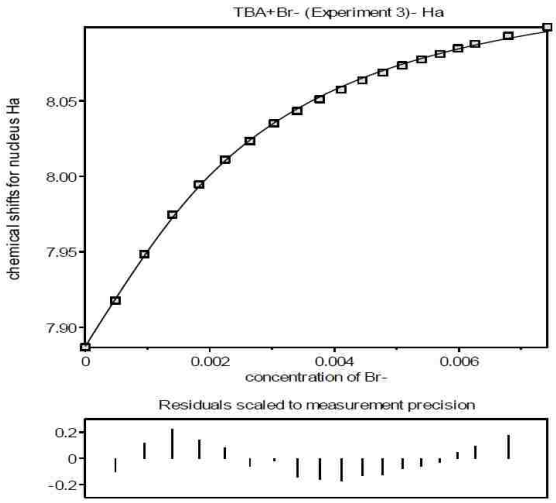
TBA+Br- (Experiment 3)- Ha
chemical shifts for nucleus Ha
8.05
8.00
7.95
7.90
0
0.002
0.004
0.006
concentration of Br-

Residuals scaled to measurement precision
0.2
0
-0.2

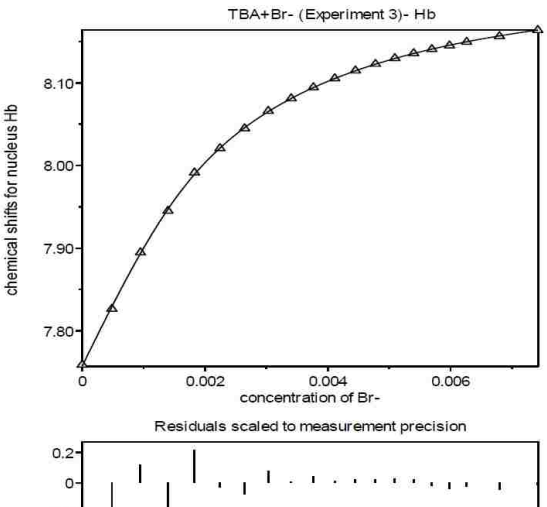
TBA+Br- (Experiment 3)- Hb
chemical shifts for nucleus Hb
8.10
8.00
7.90
7.80
0
0.002
0.004
0.006
concentration of Br-

Residuals scaled to measurement precision
0.2
0
-0.2

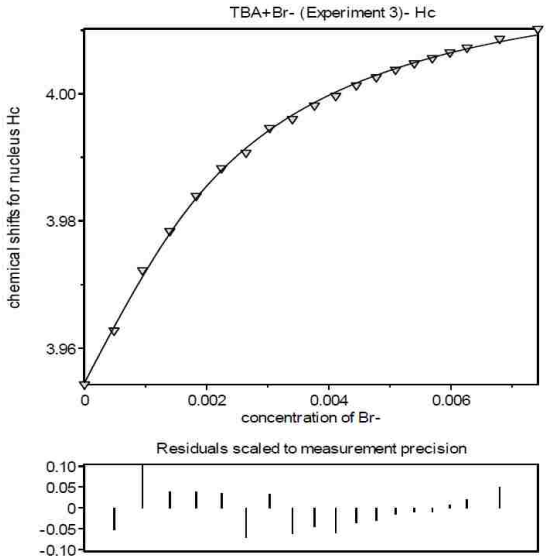
TBA+Br- (Experiment 3)- Hc
chemical shifts for nucleus Hc
4.00
3.98
3.96
0
0.002
0.004
0.006
concentration of Br-

Residuals scaled to measurement precision
0.10
0.05
0
-0.05
-0.10

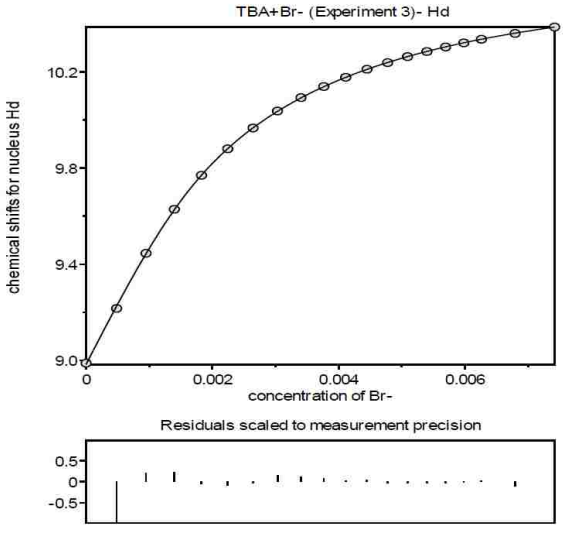
TBA+Br- (Experiment 3)- Hd
chemical shifts for nucleus Hd
10.2
9.8
9.4
9.0
0
0.002
0.004
0.006
concentration of Br-

Residuals scaled to measurement precision
0.5
0
-0.5

1% D_2O CD_3CN

XB1a-Cl-Exp1

Point	[X-]	[R]	peak (ppm)	peak (ppm)	peak (ppm)
1	0.00000E+00	1.47272E-03	7.83319	7.78344	3.92424
2	3.98243E-04	1.47272E-03	7.80342	7.75053	3.92968
3	7.73943E-04	1.47272E-03	7.77598	7.72018	3.93462
4	1.01282E-03	1.47272E-03	7.75997	7.70251	3.93752
5	1.24300E-03	1.47272E-03	7.74609	7.68682	3.93986
6	1.46496E-03	1.47272E-03	7.73576	7.67492	3.94137
7	1.67914E-03	1.47272E-03	7.72971	-	3.94233
8	1.88593E-03	1.47272E-03	7.72644	7.66332	3.94268
9	2.08571E-03	1.47272E-03	7.72456	7.66044	3.94268
10	2.27883E-03	1.47272E-03	7.72353	7.65846	3.94253
11	2.46562E-03	1.47272E-03	7.72285	7.65702	3.94239
12	2.90686E-03	1.47272E-03	7.72181	7.6542	3.94185
13	3.31467E-03	1.47272E-03	7.72133	7.65228	3.94133
14	4.04413E-03	1.47272E-03	7.72112	7.64993	3.94067
15	4.67761E-03	1.47272E-03	7.72105	7.64807	3.93988
16	5.23288E-03	1.47272E-03	7.72113	7.64708	3.9394
17	6.16036E-03	1.47272E-03	7.72151	7.64604	3.93879
18	6.90419E-03	1.47272E-03	7.72184	7.64545	3.93834
19	7.51399E-03	1.47272E-03	7.72205	7.64489	3.93782
20	8.02300E-03	1.47272E-03	7.72231	7.64484	3.93771

	model	raw value	std. dev.	final value
log β1	RG	4.5634	0.0267	4.56(2)
log β2	RG_2	7.1685	0.0676	7.17(7)

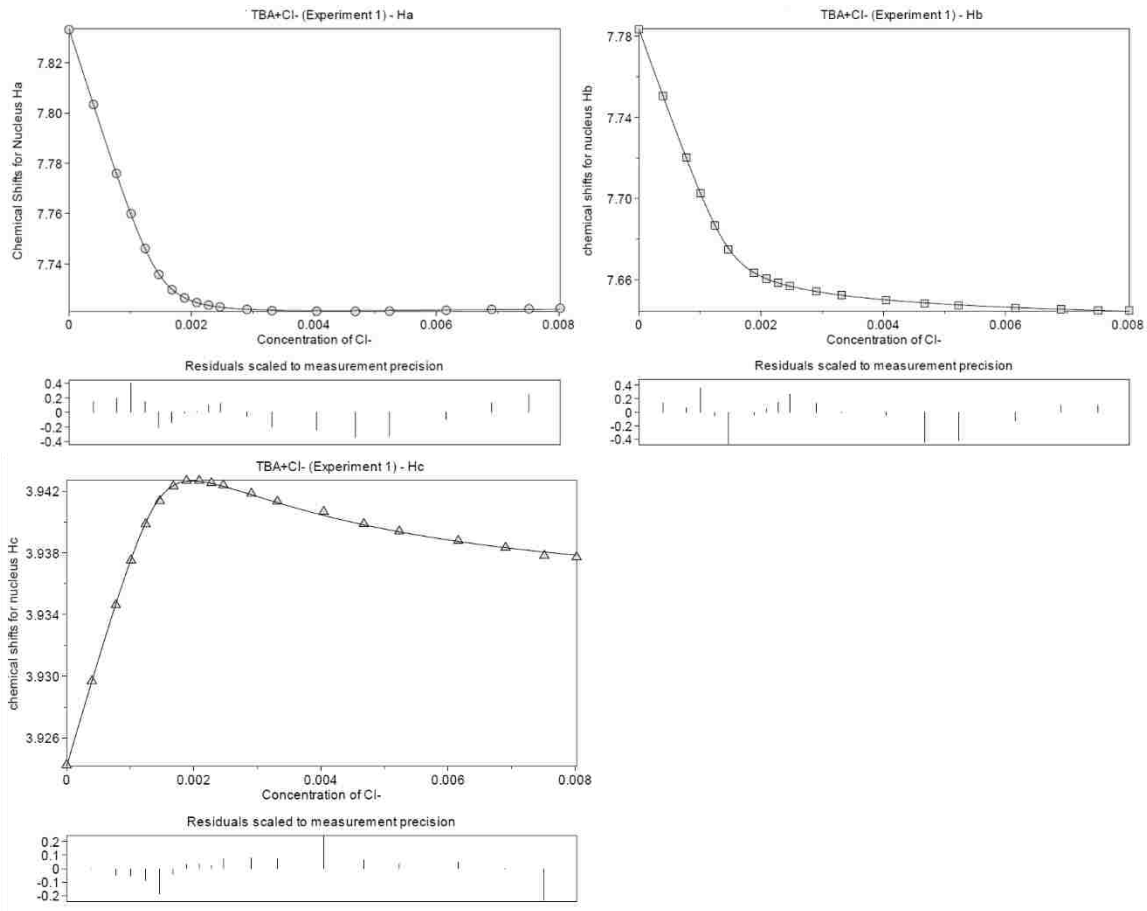
TBA+Cl- (Experiment 1) - Ha
Chemical Shifts for Nucleus Ha
7.82
7.80
7.78
7.76
7.74
0
0.002
0.004
0.006
0.008
Concentration of Cl-
Residuals scaled to measurement precision
0.4
0.2
0
-0.2
-0.4
TBA+Cl- (Experiment 1) - Hb
chemical shifts for nucleus Hb
7.78
7.74
7.70
7.66
0
0.002
0.004
0.006
0.008
Concentration of Cl-
Residuals scaled to measurement precision
0.4
0.2
0
-0.2
-0.4
TBA+Cl- (Experiment 1) - Hc
chemical shifts for nucleus Hc
3.942
3.938
3.934
3.930
3.926
0
0.002
0.004
0.006
0.008
Concentration of Cl-
Residuals scaled to measurement precision
0.2
0.1
0
-0.1
-0.2

XB1a-Cl-Exp2

Point	[X-]	[R]	peak (ppm)	peak (ppm)	peak (ppm)
1	0	0.001472722	7.83311	7.78338	3.92425
2	0.000398243	0.001472722	7.80347	7.75057	3.92962
3	0.000773943	0.001472722	7.77708	7.72135	3.93445
4	0.001012815	0.001472722	7.76042	7.70284	3.93733
5	0.001243	0.001472722	7.7462	7.68701	3.9399
6	0.001464964	0.001472722	7.73554	7.67471	3.94168
7	0.00167914	0.001472722	7.72934	-	3.94253
8	0.001885931	0.001472722	7.7261	7.66293	3.94274
9	0.002085712	0.001472722	7.7243	7.66	3.94265
10	0.002278833	0.001472722	7.72327	7.65804	3.94249
11	0.002465623	0.001472722	7.72261	7.65654	3.94228
12	0.002906858	0.001472722	7.72167	7.65379	3.94169
13	0.003314667	0.001472722	7.72122	7.65187	3.94117
14	0.004044127	0.001472722	7.72101	7.64949	3.94046
15	0.004677605	0.001472722	7.7212	7.64813	3.93996
16	0.005232876	0.001472722	7.72118	7.64693	3.93929
17	0.006160362	0.001472722	7.72168	7.64602	3.93879
18	0.006904188	0.001472722	7.72187	7.6452	3.93814
19	0.007513991	0.001472722	7.72209	7.64488	3.93781
20	0.008023	0.001472722	7.72232	7.64467	3.93752

	model	raw value	std. dev.	final value
log β1	RG	4.5982	0.0286	4.6(3)
log β2	RG_2	7.2571	0.0506	7.26(5)

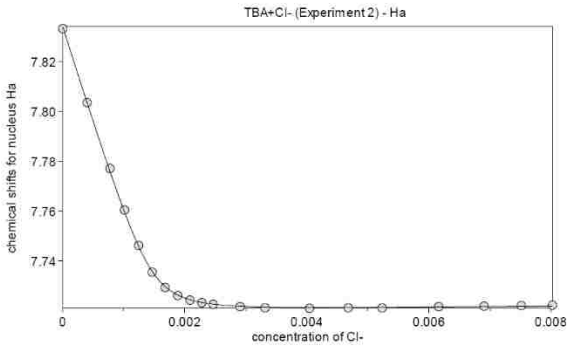
TBA+Cl- (Experiment 2) - Ha
chemical shifts for nucleus Ha
7.82
7.80
7.78
7.76
7.74
0
0.002
0.004
0.006
0.008
concentration of Cl-

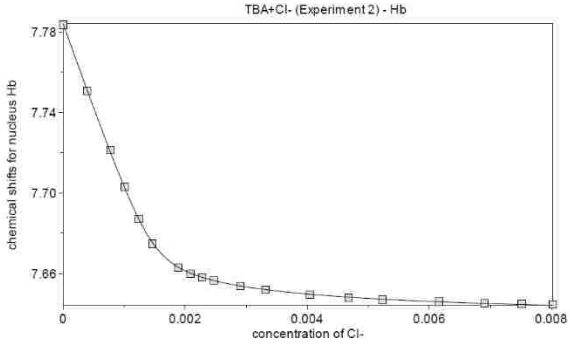
TBA+Cl- (Experiment 2) - Hb
chemical shifts for nucleus Hb
7.78
7.74
7.70
7.66
0
0.002
0.004
0.006
0.008
concentration of Cl-

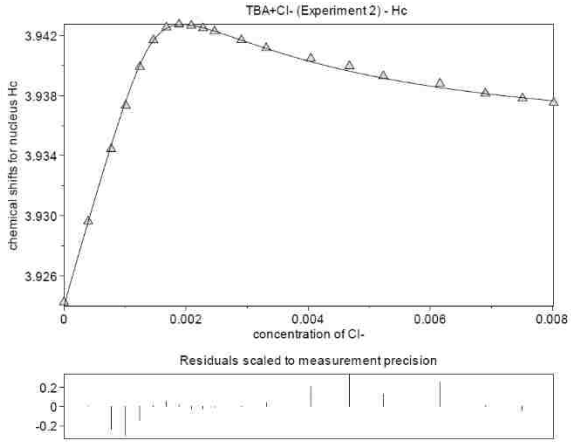
TBA+Cl- (Experiment 2) - Hc
chemical shifts for nucleus Hc
3.942
3.938
3.934
3.930
3.926
0
0.002
0.004
0.006
0.008
concentration of Cl-

Residuals scaled to measurement precision
0.2
0
-0.2

XB1a-Cl-Exp3

Point	[X-]	[R]	peak (ppm)	peak (ppm)	peak (ppm)
1	0	0.001472722	7.83309	7.78336	3.92416
2	0.000398243	0.001472722	7.80379	7.75081	3.92959
3	0.000773943	0.001472722	7.77649	7.72098	3.93449
4	0.001012815	0.001472722	7.76033	7.70314	3.93776
5	0.001243	0.001472722	7.74639	7.68719	3.93998
6	0.001464964	0.001472722	7.73621	7.67556	3.94168
7	0.00167914	0.001472722	7.7299	-	3.94253
8	0.001885931	0.001472722	7.72647	7.66335	3.94268
9	0.002085712	0.001472722	7.72475	7.6608	3.94289
10	0.002278833	0.001472722	7.72349	7.65844	3.94249
11	0.002465623	0.001472722	7.7229	7.65712	3.94247
12	0.002906858	0.001472722	7.72189	7.65436	3.94196
13	0.003314667	0.001472722	7.72134	7.65226	3.94129
14	0.004044127	0.001472722	7.72116	7.65	3.94079
15	0.004677605	0.001472722	7.721	7.64824	3.93993
16	0.005232876	0.001472722	7.72103	7.64705	3.9393
17	0.006160362	0.001472722	7.72143	7.64605	3.93875
18	0.006904188	0.001472722	7.72169	7.64532	3.93825
19	0.007513991	0.001472722	7.72203	7.64515	3.938
20	0.008023	0.001472722	7.72224	7.64483	3.93768

	model	raw value	std. dev.	final value
log β1	RG	4.5677	0.0212	4.57(2)
log β2	RG_2	7.2098	0.0377	7.21(4)

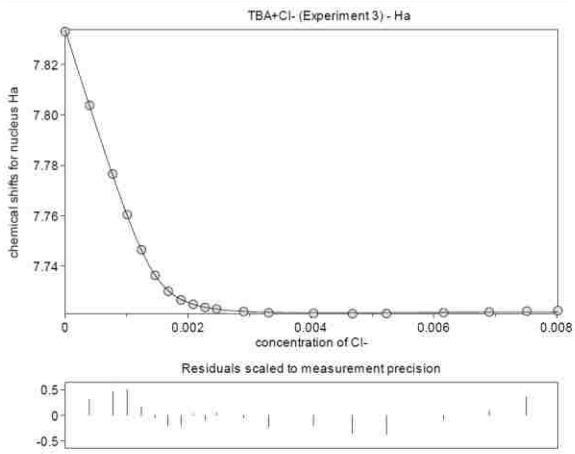
TBA+Cl- (Experiment 3) - Ha
chemical shifts for nucleus Ha
7.82
7.80
7.78
7.76
7.74
0
0.002
0.004
0.006
0.008
concentration of Cl-

Residuals scaled to measurement precision
0.5
0
-0.5

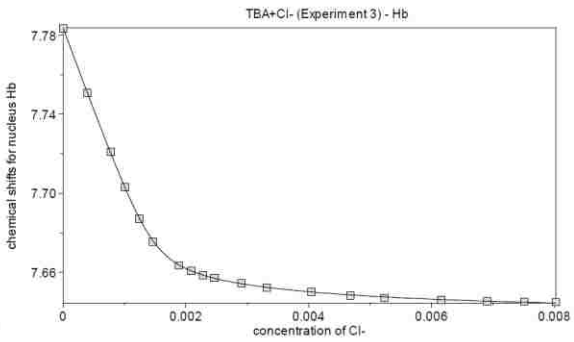
TBA+Cl- (Experiment 3) - Hb
chemical shifts for nucleus Hb
7.78
7.74
7.70
7.66
0
0.002
0.004
0.006
0.008
concentration of Cl-

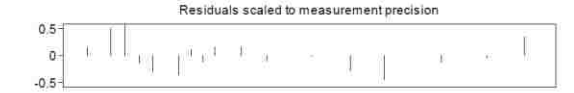
Residuals scaled to measurement precision
0.5
0
-0.5

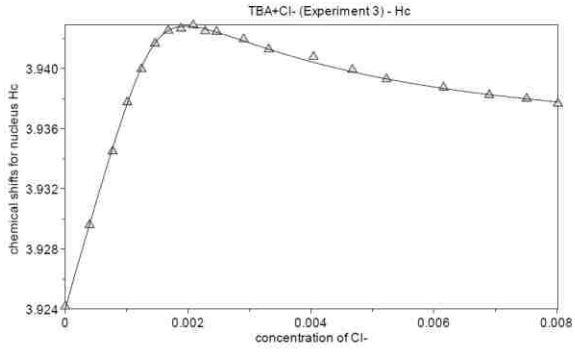
TBA+Cl- (Experiment 3) - Hc
chemical shifts for nucleus Hc
3.940
3.936
3.932
3.928
3.924
0
0.002
0.004
0.006
0.008
concentration of Cl-

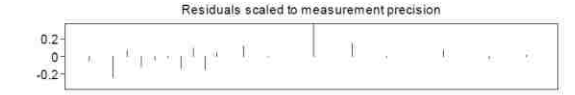
Residuals scaled to measurement precision
0.2
0
-0.2

XB1a-Br-Exp1

Point	[X-]	[R]	peak (ppm)	peak (ppm)	peak (ppm)
1	0.00000E+00	1.47500E-03	7.83357	7.78432	3.92675
2	3.40000E-04	1.47500E-03	7.80816	7.7556	3.9312
3	6.61000E-04	1.47500E-03	7.7846	7.72901	3.93523
4	8.65000E-04	1.47500E-03	7.77021	7.71275	3.9376
5	1.06100E-03	1.47500E-03	7.75762	7.69817	3.93973
6	1.25100E-03	1.47500E-03	7.74693	7.68574	3.94127
7	1.43300E-03	1.47500E-03	7.73917	-	3.94232
8	1.61000E-03	1.47500E-03	7.73375	7.66969	3.94273
9	1.78000E-03	1.47500E-03	7.73033	7.66498	3.94303
10	1.94500E-03	1.47500E-03	7.72783	7.66138	3.94301
11	2.10500E-03	1.47500E-03	7.72588	7.65837	3.94289
12	2.48100E-03	1.47500E-03	7.72258	7.65294	3.94247
13	2.83000E-03	1.47500E-03	7.72053	7.64922	3.94211
14	3.45200E-03	1.47500E-03	7.71777	7.64377	3.94128
15	3.99300E-03	1.47500E-03	-	7.64027	3.94082
16	4.46700E-03	1.47500E-03	-	7.63792	3.94051
17	5.25900E-03	1.47500E-03	-	7.63487	3.93996
18	5.89400E-03	1.47500E-03	7.71296	7.6332	3.93973
19	6.84900E-03	1.47500E-03	7.71208	7.63106	3.93927
20	7.53300E-03	1.47500E-03	7.7119	7.63034	3.93916

	model	raw value	std. dev.	final value
log β1	RG	4.4924	0.0741	4.49(7)
log β2	RG_2	7.0013	0.1483	7.0(1)

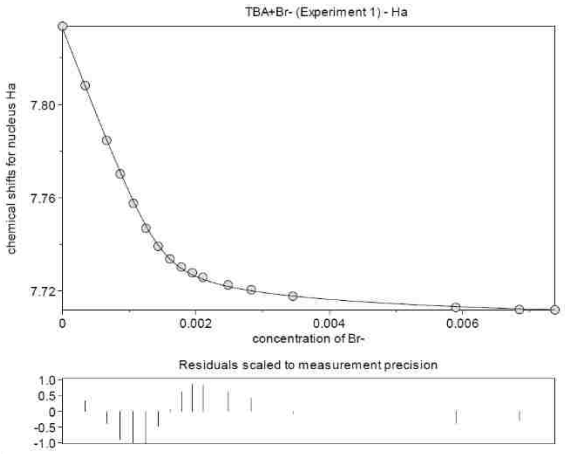
TBA+Br- (Experiment 1) - Ha
chemical shifts for nucleus Ha
7.80
7.76
7.72
0
0.002
0.004
0.006
concentration of Br-

Residuals scaled to measurement precision
1.0
0.5
0
-0.5
-1.0

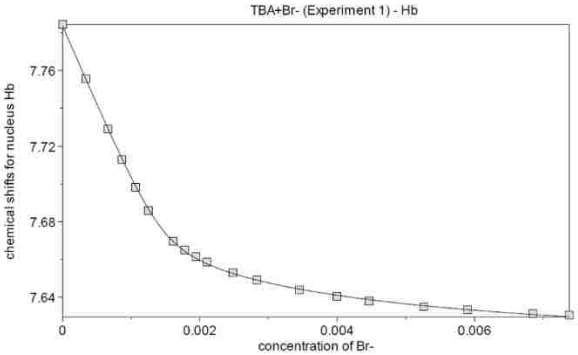
TBA+Br- (Experiment 1) - Hb
chemical shifts for nucleus Hb
7.76
7.72
7.68
7.64
0
0.002
0.004
0.006
concentration of Br-

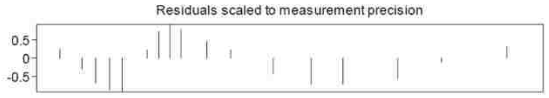
Residuals scaled to measurement precision
0.5
0
-0.5

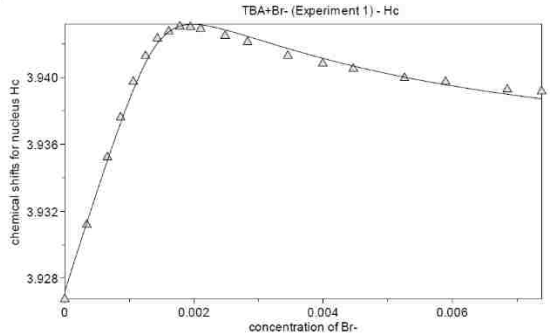
TBA+Br- (Experiment 1) - Hc
chemical shifts for nucleus Hc
3.940
3.936
3.932
3.928
0
0.002
0.004
0.006
concentration of Br-

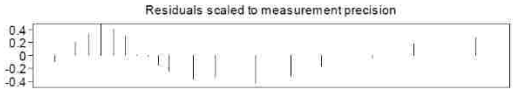
Residuals scaled to measurement precision
0.4
0.2
0
-0.2
-0.4

XB1a-Br-Exp2

Point	[X-]	[R]	peak (ppm)	peak (ppm)	peak (ppm)
1	0.00000E+00	1.47500E-03	7.83341	7.78408	3.92665
2	3.40000E-04	1.47500E-03	7.80747	7.75475	3.93117
3	6.61000E-04	1.47500E-03	7.7838	7.72816	3.93537
4	8.65000E-04	1.47500E-03	7.76945	7.71188	3.9378
5	1.06100E-03	1.47500E-03	7.75697	7.69742	3.93981
6	1.25100E-03	1.47500E-03	7.74695	7.68574	3.94139
7	1.43300E-03	1.47500E-03	7.73921	-	3.94238
8	1.61000E-03	1.47500E-03	7.734	7.66995	3.94284
9	1.78000E-03	1.47500E-03	7.73041	7.66513	3.94304
10	1.94500E-03	1.47500E-03	7.72792	7.66145	3.94304
11	2.10500E-03	1.47500E-03	7.7259	7.65836	3.94291
12	2.48100E-03	1.47500E-03	7.7227	7.65299	3.94268
13	2.83000E-03	1.47500E-03	7.72036	7.64898	3.94208
14	3.45200E-03	1.47500E-03	7.71761	7.64357	3.94135
15	3.99300E-03	1.47500E-03	7.71599	7.64026	3.94089
16	4.46700E-03	1.47500E-03	7.71496	7.63774	3.94051
17	5.25900E-03	1.47500E-03	-	7.63486	3.93989
18	5.89400E-03	1.47500E-03	7.71281	7.63295	3.93963
19	6.84900E-03	1.47500E-03	7.71181	7.63075	3.93904
20	7.53300E-03	1.47500E-03	7.71183	7.63034	3.9391

	model	raw value	std. dev.	final value
log β1	RG	4.4522	0.0589	4.45(6)
log β2	RG_2	6.9654	0.095	6.97(9)

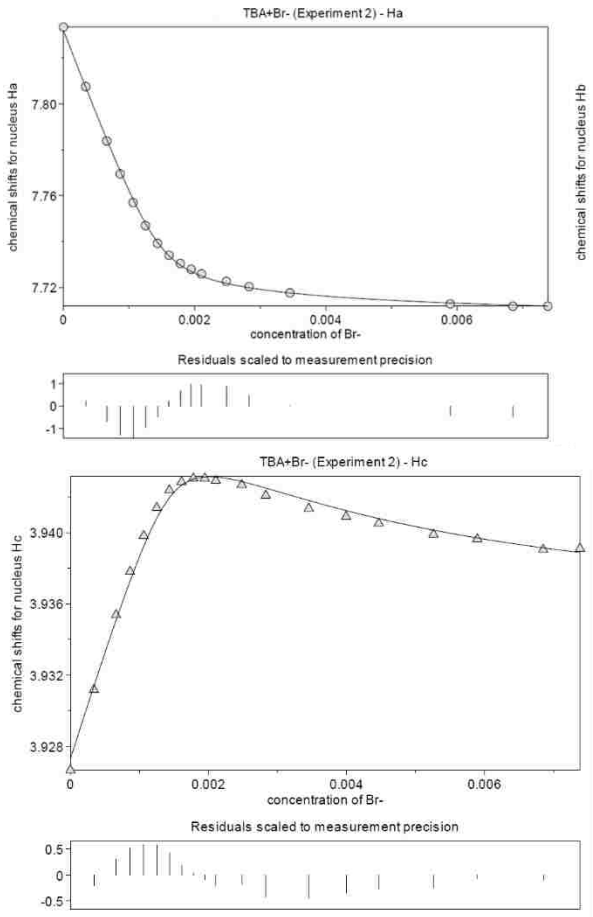
TBA+Br- (Experiment 2) - Ha
chemical shifts for nucleus Ha
7.80
7.76
7.72
0
0.002
0.004
0.006
concentration of Br-
Residuals scaled to measurement precision
1
0
-1

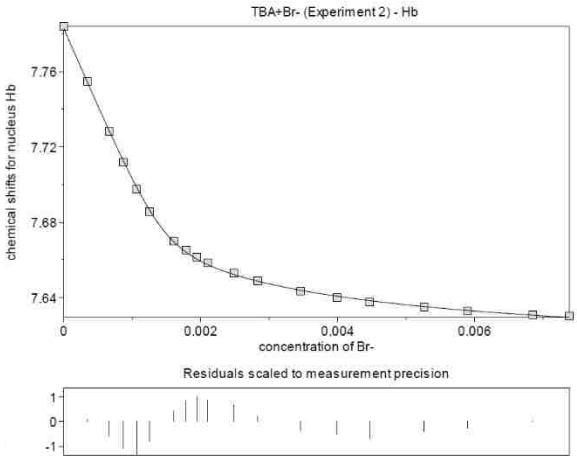
TBA+Br- (Experiment 2) - Hb
chemical shifts for nucleus Hb
7.76
7.72
7.68
7.64
0
0.002
0.004
0.006
concentration of Br-
Residuals scaled to measurement precision
1
0
-1

TBA+Br- (Experiment 2) - Hc
chemical shifts for nucleus Hc
3.940
3.936
3.932
3.928
0
0.002
0.004
0.006
concentration of Br-
Residuals scaled to measurement precision
0.5
0
-0.5

XB1a-Br-Exp3

Point	[X-]	[R]	peak (ppm)	peak (ppm)	peak (ppm)
1	0.00000E+00	1.47496E-03	7.83347	7.78413	3.92664
2	3.39964E-04	1.47496E-03	7.80823	7.75563	3.93114
3	6.60685E-04	1.47496E-03	7.78463	7.72896	3.93527
4	8.64600E-04	1.47496E-03	7.77031	7.71279	3.93767
5	1.06110E-03	1.47496E-03	7.75796	7.69854	3.93973
6	1.25058E-03	1.47496E-03	7.74729	7.68613	3.94135
7	1.43342E-03	1.47496E-03	7.73935	-	3.94239
8	1.60995E-03	1.47496E-03	7.73387	7.66984	3.94292
9	1.78049E-03	1.47496E-03	7.73022	7.66487	3.94297
10	1.94535E-03	1.47496E-03	7.7277	7.66111	3.94303
11	2.10481E-03	1.47496E-03	7.72574	7.65808	3.94288
12	2.48147E-03	1.47496E-03	7.72245	7.65266	3.9426
13	2.82960E-03	1.47496E-03	7.72032	7.64892	3.94208
14	3.45231E-03	1.47496E-03	7.71765	7.64367	3.94134
15	3.99309E-03	1.47496E-03	-	7.64028	3.94082
16	4.46710E-03	1.47496E-03	7.71491	7.63785	3.94046
17	5.25886E-03	1.47496E-03	7.71358	7.6347	3.93988
18	5.89383E-03	1.47496E-03	7.71281	7.63297	3.93963
19	6.84892E-03	1.47496E-03	7.71194	7.63093	3.93916
20	7.53306E-03	1.47496E-03	7.71203	7.63072	3.93944

	model	raw value	std. dev.	final value
log β1	RG	4.4962	0.0657	4.5(7)
log β2	RG_2	7.068	0.1275	7.1(1)

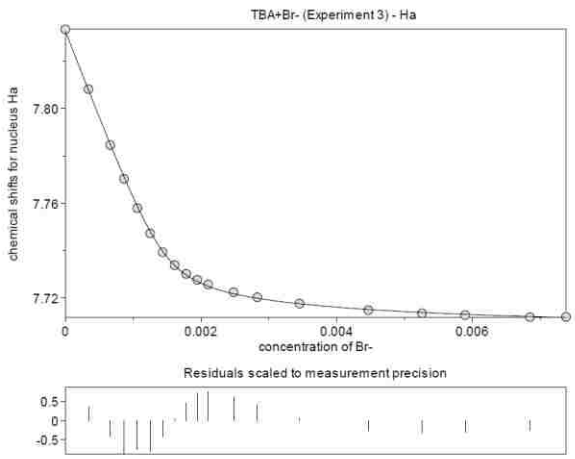
TBA+Br- (Experiment 3) - Ha
chemical shifts for nucleus Ha
7.80
7.76
7.72
0
0.002
0.004
0.006
concentration of Br-

Residuals scaled to measurement precision
0.5
0
-0.5

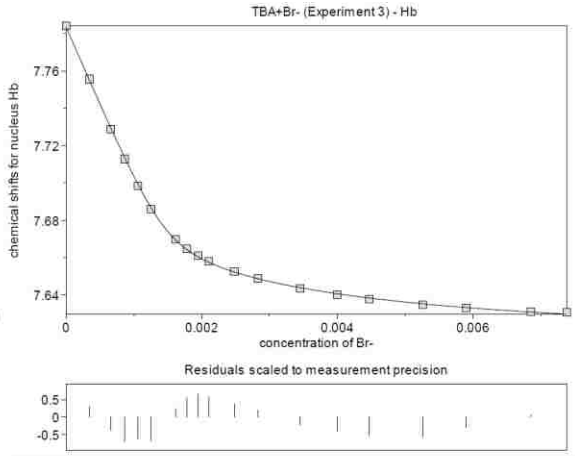
TBA+Br- (Experiment 3) - Hb
chemical shifts for nucleus Hb
7.76
7.72
7.68
7.64
0
0.002
0.004
0.006
concentration of Br-

Residuals scaled to measurement precision
0.5
0
-0.5

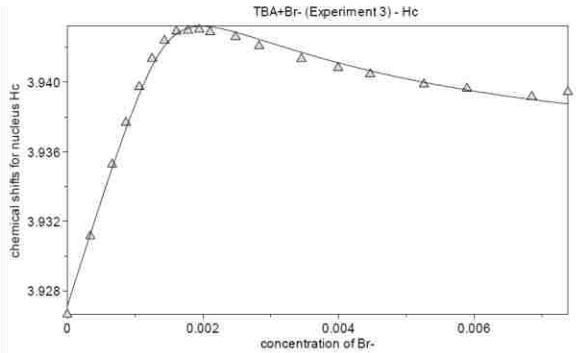
TBA+Br- (Experiment 3) - Hc
chemical shifts for nucleus Hc
3.940
3.936
3.932
3.928
0
0.002
0.004
0.006
concentration of Br-

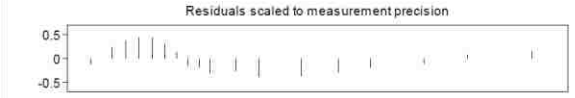
Residuals scaled to measurement precision
0.5
0
-0.5

XB1a-I-Exp1

Point	[X-]	[R]	peak (ppm)	peak (ppm)	peak (ppm)
1	0	0.001231233	7.83261	7.78264	3.92411
2	0.000345703	0.001231233	7.80416	7.74929	3.92764
3	0.000665798	0.001231233	7.77976	7.72038	3.93096
4	0.00096303	0.001231233	7.76005	7.69677	3.93282
5	0.001239762	0.001231233	7.74591	7.67964	3.93394
6	0.001498046	0.001231233	7.73639	7.66751	3.93469
7	0.001739667	0.001231233	7.72973	7.65886	3.93507
8	0.001966186	0.001231233	7.72463	7.65195	3.93521
9	0.002178976	0.001231233	7.72073	7.64668	3.93539
10	0.00237925	0.001231233	7.71761	7.64241	3.93562
11	0.002568079	0.001231233	7.71498	7.63863	3.93567
12	0.002996092	0.001231233	7.71023	7.63201	3.93609
13	0.003370604	0.001231233	7.70675	7.6265	3.93588
14	0.003701055	0.001231233	7.70438	7.62312	3.93618
15	0.004257605	0.001231233	7.70095	7.61783	3.93638
16	0.004708145	0.001231233	7.69868	7.61436	3.93633
17	0.005392966	0.001231233	7.69658	7.61103	3.93662
18	0.005888871	0.001231233	7.69541	7.60905	3.93681
19	0.006264557	0.001231233	7.69477	7.60806	3.93693
20	0.006683591	0.001231233	7.69415	7.60714	3.93697

	model	raw value	std. dev.	final value
log β1	RG	4.109	0.0794	4.11(8)
log β2	RG_2	6.7844	0.1217	6.8(1)

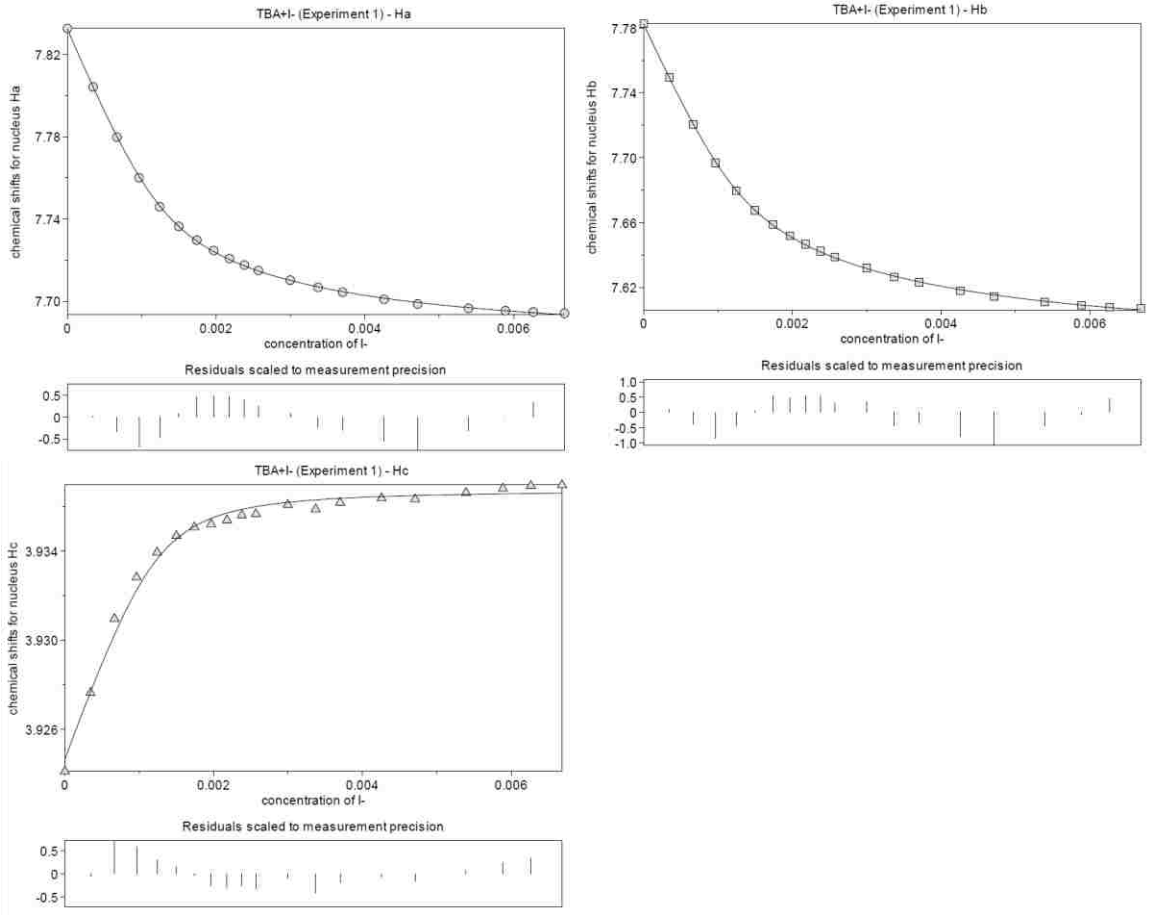
TBA+I- (Experiment 1) - Ha
chemical shifts for nucleus Ha
7.82
7.78
7.74
7.70
0
0.002
0.004
0.006
concentration of I-
Residuals scaled to measurement precision
0.5
0
-0.5
TBA+I- (Experiment 1) - Hb
chemical shifts for nucleus Hb
7.78
7.74
7.70
7.66
7.62
0
0.002
0.004
0.006
concentration of I-
Residuals scaled to measurement precision
1.0
0.5
0
-0.5
-1.0
TBA+I- (Experiment 1) - Hc
chemical shifts for nucleus Hc
3.934
3.930
3.926
0
0.002
0.004
0.006
concentration of I-
Residuals scaled to measurement precision
0.5
0
-0.5

XB1a-I-Exp2

Point	[X-]	[R]	peak (ppm)	peak (ppm)	peak (ppm)
1	0	0.001231233	7.83258	7.78265	3.92408
2	0.000345703	0.001231233	7.8046	7.74979	3.92764
3	0.000665798	0.001231233	7.78058	7.72141	3.93052
4	0.00096303	0.001231233	7.76129	7.69837	3.93256
5	0.001239762	0.001231233	7.74731	7.68125	3.93386
6	0.001498046	0.001231233	7.73762	7.66906	3.93464
7	0.001739667	0.001231233	7.73086	7.66022	3.93495
8	0.001966186	0.001231233	7.72571	7.65344	3.93519
9	0.002178976	0.001231233	7.72182	7.6482	3.93535
10	0.00237925	0.001231233	7.71862	7.64379	3.93546
11	0.002568079	0.001231233	7.71611	7.64022	3.93562
12	0.002996092	0.001231233	7.71387	7.63704	3.93569
13	0.003370604	0.001231233	7.70965	7.63094	3.93586
14	0.003701055	0.001231233	7.70663	7.62647	3.93596
15	0.004257605	0.001231233	7.70251	7.62029	3.93618
16	0.004708145	0.001231233	7.70005	7.61647	3.93632
17	0.005392966	0.001231233	7.69721	7.61212	3.93651
18	0.005888871	0.001231233	7.69589	7.60985	3.9367
19	0.006264557	0.001231233	7.69496	7.60836	3.93675
20	0.006683591	0.001231233	7.6942	7.60711	3.93681

	model	raw value	std. dev.	final value
log β1	RG	4.0961	0.0572	4.1(6)
log β2	RG_2	6.7366	0.088	6.74(9)

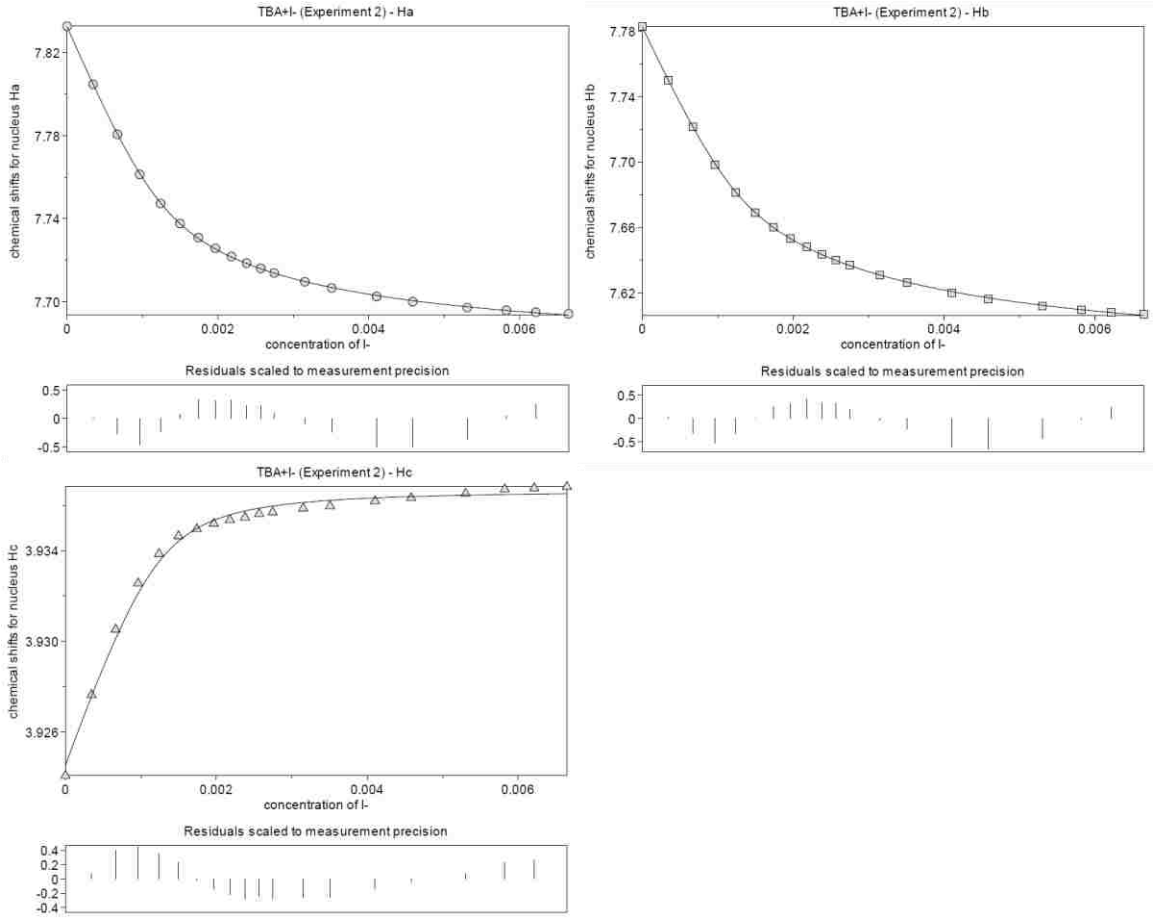
TBA+I- (Experiment 2) - Ha
chemical shifts for nucleus Ha
7.82
7.78
7.74
7.70
0
0.002
0.004
0.006
concentration of I-
Residuals scaled to measurement precision
0.5
0
-0.5
TBA+I- (Experiment 2) - Hb
chemical shifts for nucleus Hb
7.78
7.74
7.70
7.66
7.62
0
0.002
0.004
0.006
concentration of I-
Residuals scaled to measurement precision
0.5
0
-0.5
TBA+I- (Experiment 2) - Hc
chemical shifts for nucleus Hc
3.934
3.930
3.926
0
0.002
0.004
0.006
concentration of I-
Residuals scaled to measurement precision
0.4
0.2
0
-0.2
-0.4

XB1a-I-Exp3

Point	[X-]	[R]	peak (ppm)	peak (ppm)	peak (ppm)
1	0	0.001231233	7.83258	7.7826	3.92412
2	0.000345703	0.001231233	7.80478	7.74999	3.92772
3	0.000665798	0.001231233	7.78066	7.72137	3.93042
4	0.00096303	0.001231233	7.76133	7.69835	3.93222
5	0.001239762	0.001231233	7.74734	7.68122	3.93382
6	0.001498046	0.001231233	7.7375	7.66886	3.93452
7	0.001739667	0.001231233	7.73081	7.66025	3.93486
8	0.001966186	0.001231233	7.7257	7.65345	3.93517
9	0.002178976	0.001231233	7.72182	7.64819	3.93537
10	0.00237925	0.001231233	7.71859	7.64379	3.93539
11	0.002568079	0.001231233	7.71612	7.64033	3.93564
12	0.002996092	0.001231233	7.71151	7.63345	3.93601
13	0.003370604	0.001231233	7.70783	7.6282	3.93597
14	0.003701055	0.001231233	7.70539	7.62473	3.93617
15	0.004257605	0.001231233	7.70175	7.61914	3.93625
16	0.004708145	0.001231233	7.69952	7.61566	3.93623
17	0.005392966	0.001231233	7.697	7.61182	3.9364
18	0.005888871	0.001231233	7.69579	7.60972	3.93662
19	0.006264557	0.001231233	7.69496	7.60833	3.93665
20	0.006683591	0.001231233	7.69438	7.60735	3.93679

	model	raw value	std. dev.	final value
log β1	RG	4.1347	0.0575	4.13(6)
log β2	RG_2	6.7921	0.0864	6.79(9)

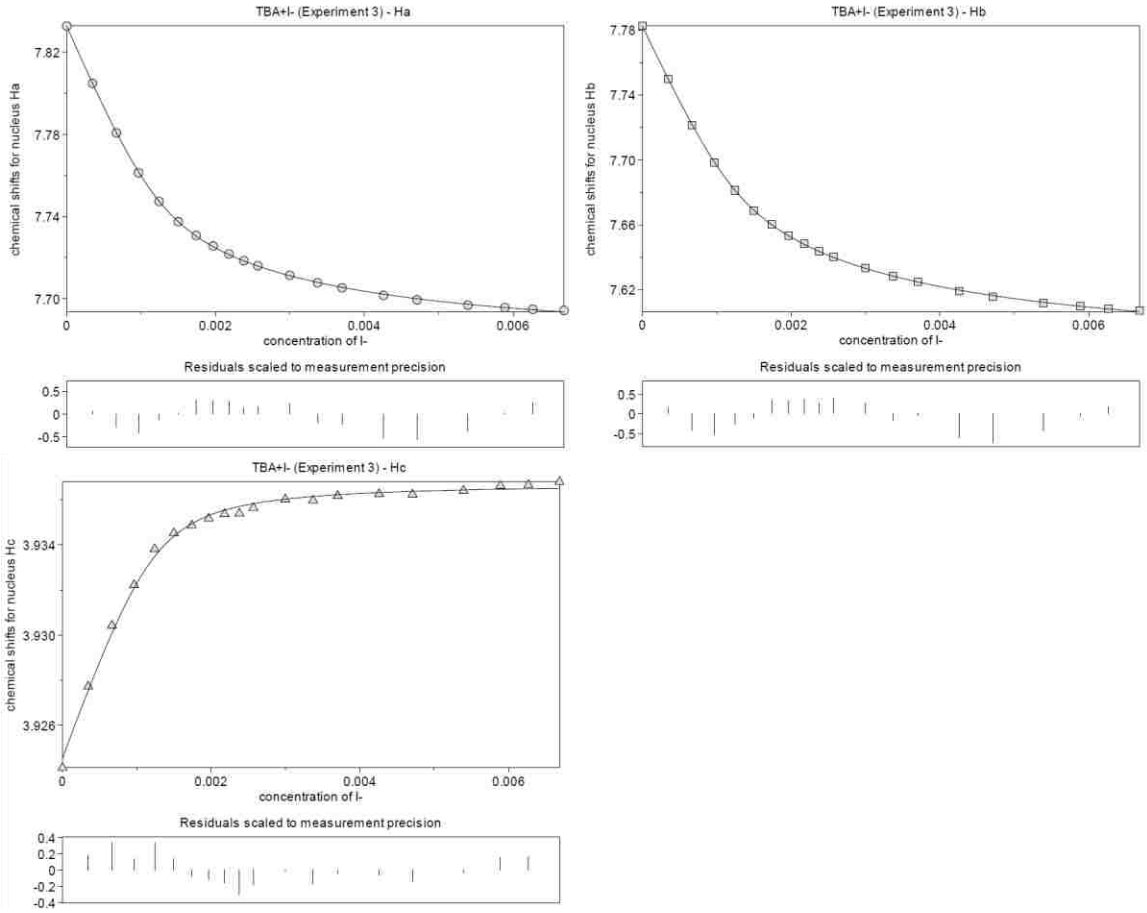
TBA+I- (Experiment 3) - Ha
chemical shifts for nucleus Ha
7.82
7.78
7.74
7.70
0
0.002
0.004
0.006
concentration of I-
Residuals scaled to measurement precision
0.5
0
-0.5
TBA+I- (Experiment 3) - Hb
chemical shifts for nucleus Hb
7.78
7.74
7.70
7.66
7.62
0
0.002
0.004
0.006
concentration of I-
Residuals scaled to measurement precision
0.5
0
-0.5
TBA+I- (Experiment 3) - Hc
chemical shifts for nucleus Hc
3.934
3.930
3.926
0
0.002
0.004
0.006
concentration of I-
Residuals scaled to measurement precision
0.4
0.2
0
-0.2
-0.4

XB1c-Cl-Exp1

Point	[X-]	[R]	peak (ppm)	peak (ppm)	peak (ppm)	peak (ppm)	peak (ppm)	peak (ppm)	peak (ppm)
1	0	0.001466182	9.00261	7.88516	7.83685	7.7846	7.64575	3.9504	3.92499
2	0.000422696	0.001466182	9.10515	7.89178	7.80365	7.74103	7.65931	3.95435	3.92337
3	0.000821466	0.001466182	9.19357	7.8975	7.77574	7.70358	7.67102	3.95782	3.92204
4	0.001075005	0.001466182	9.24452	7.90088	7.76136	-	-	3.9598	3.92142
5	0.001319325	0.001466182	9.28495	7.90364	7.75023	7.66839	7.68287	3.96136	3.9209
6	0.001554918	0.001466182	9.3189	7.90599	7.74257	7.65709	7.68734	3.9631	3.92068
7	0.001782245	0.001466182	9.34586	7.90808	7.73724	7.64857	7.69079	3.96418	3.92046
8	0.002001734	0.001466182	9.36821	7.90982	7.73392	7.6428	7.69357	3.96512	3.92036
9	0.002213782	0.001466182	9.38762	7.9115	7.73201	7.63851	7.69645	3.96607	3.92028
10	0.002418762	0.001466182	9.40409	7.91277	7.73104	7.6356	7.69838	3.96715	3.9204
11	0.002617021	0.001466182	9.41798	7.91401	7.7306	7.63327	7.70006	3.96771	3.92037
12	0.003085349	0.001466182	9.44727	7.91676	7.73113	7.63011	7.7037	3.96949	3.92059
13	0.003518199	0.001466182	9.47015	7.91906	7.73275	7.62899	7.70659	3.97075	3.92077
14	0.00429245	0.001466182	9.50815	7.9228	7.73692	7.62828	7.71113	3.97279	3.92117
15	0.004964826	0.001466182	9.53487	7.92556	7.74095	-	7.71433	3.97455	3.92151
16	0.005554193	0.001466182	9.55748	7.92817	7.74477	7.62912	7.71726	3.97581	3.92181
17	0.00653863	0.001466182	9.59465	-	7.75141	7.63152	7.72182	3.97818	3.92239
18	0.007328129	0.001466182	9.62112	-	7.75661	-	7.72494	3.97974	3.9228
19	0.00851564	0.001466182	9.65646	7.93922	7.76389	-	7.72936	3.98189	3.92339
20	0.009438245	0.001466182	9.68061	7.94246	7.76898	-	7.73228	3.98343	3.92383

	model	raw value	std. dev.	final value
log β1	RG	3.7687	0.0073	3.769(7)
log β2	RG_2	5.4855	0.0155	5.49(2)

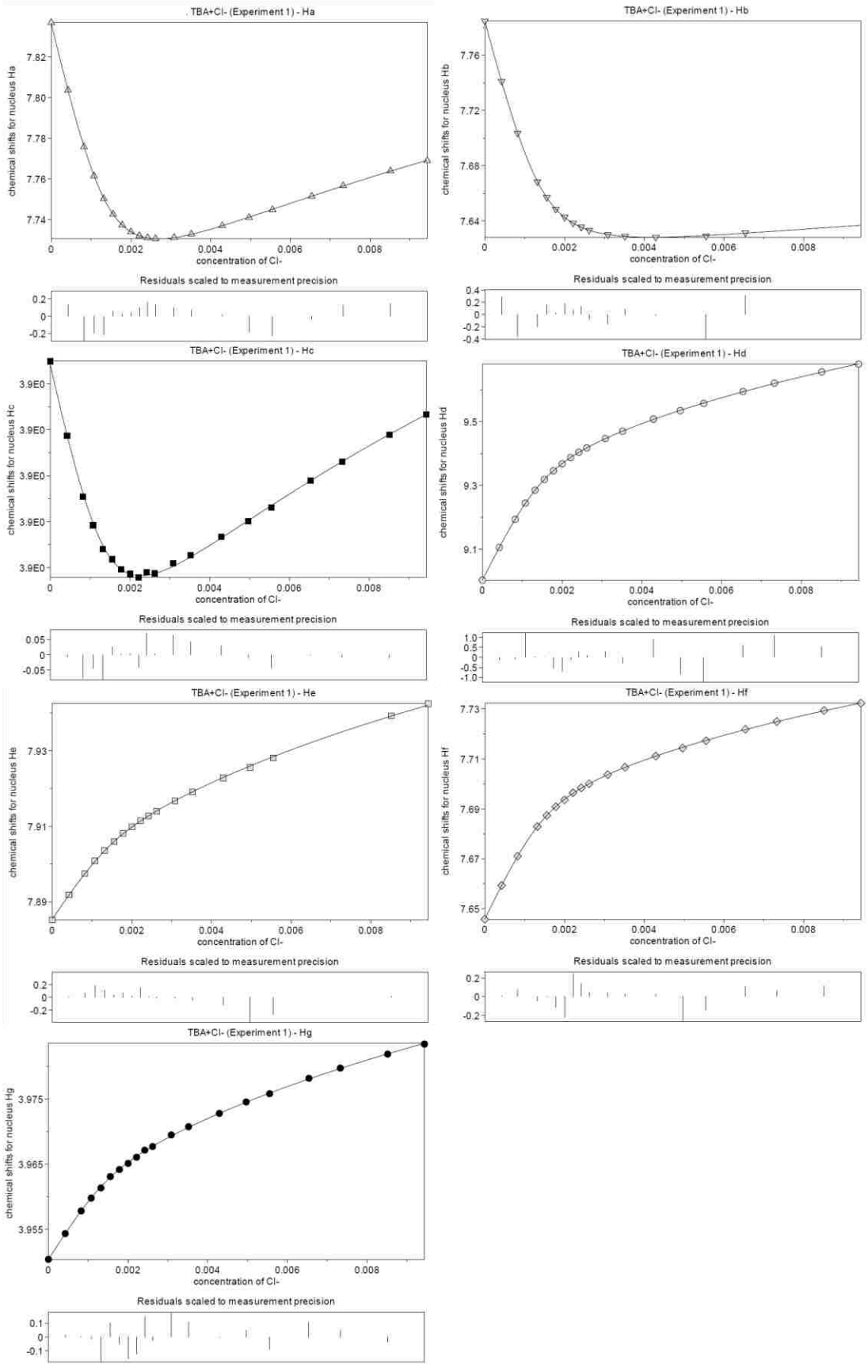
TBA+Cl- (Experiment 1) - Ha
chemical shifts for nucleus Ha
concentration of Cl-
Residuals scaled to measurement precision
TBA+Cl- (Experiment 1) - Hb
chemical shifts for nucleus Hb
concentration of Cl-
Residuals scaled to measurement precision
TBA+Cl- (Experiment 1) - Hc
chemical shifts for nucleus Hc
concentration of Cl-
Residuals scaled to measurement precision
TBA+Cl- (Experiment 1) - Hd
chemical shifts for nucleus Hd
concentration of Cl-
Residuals scaled to measurement precision
TBA+Cl- (Experiment 1) - He
chemical shifts for nucleus He
concentration of Cl-
Residuals scaled to measurement precision
TBA+Cl- (Experiment 1) - Hf
chemical shifts for nucleus Hf
concentration of Cl-
Residuals scaled to measurement precision
TBA+Cl- (Experiment 1) - Hg
chemical shifts for nucleus Hg
concentration of Cl-
Residuals scaled to measurement precision

XB1c-Cl-Exp2

Point	[X-]	[R]	peak (ppm)	peak (ppm)	peak (ppm)	peak (ppm)	peak (ppm)	peak (ppm)	peak (ppm)
1	0	0.001466182	9.00376	7.88512	7.83662	7.78443	7.64577	3.95065	3.925
2	0.000422696	0.001466182	9.1047	7.89164	7.80335	7.74043	7.65915	3.95436	3.9233
3	0.000821466	0.001466182	9.19269	7.89737	7.77586	7.70386	7.67083	3.95778	3.92203
4	0.001075005	0.001466182	9.24282	7.90062	7.76151	-	-	3.95979	3.92139
5	0.001319325	0.001466182	9.28651	7.90373	7.75012	7.66824	7.68298	3.96151	3.92094
6	0.001554918	0.001466182	9.3206	7.90596	7.74226	7.6567	7.68732	3.96314	3.92062
7	0.001782245	0.001466182	9.34742	7.90814	7.73692	7.64808	7.69085	3.96409	3.9204
8	0.002001734	0.001466182	9.37028	7.90992	7.73357	7.64218	7.69373	3.96521	3.92029
9	0.002213782	0.001466182	9.39002	7.91168	7.73178	7.63797	7.69641	3.96607	3.92029
10	0.002418762	0.001466182	9.4082	7.91307	7.73087	7.63484	7.69856	3.96697	3.92028
11	0.002617021	0.001466182	9.42189	7.91425	7.73062	7.63273	7.70069	3.96799	3.92037
12	0.003085349	0.001466182	9.4531	7.91719	7.73134	7.62965	7.70435	3.96967	3.92055
13	0.003518199	0.001466182	9.47654	7.91943	7.73319	-	7.70722	3.97098	3.92076
14	0.00429245	0.001466182	9.51545	7.92366	7.73798	7.62851	7.71213	3.97333	3.92127
15	0.004964826	0.001466182	9.54481	7.92672	7.7425	7.62896	7.71562	3.97512	3.92166
16	0.005554193	0.001466182	9.56813	7.92939	7.74651	7.62975	7.71845	3.97626	3.92193
17	0.00653863	0.001466182	9.60403	7.93362	7.75328	7.63205	7.72301	3.9787	3.92255
18	0.007328129	0.001466182	9.62904	7.93631	7.75835	-	7.72614	3.98038	3.92302
19	0.00851564	0.001466182	9.66464	7.94056	7.76562	-	7.73037	3.98249	3.92355
20	0.009438245	0.001466182	9.68798	7.94339	7.7706	7.63797	7.73297	3.98373	3.9239

	model	raw value	std. dev.	final value
log β1	RG	3.768	0.0065	3.768(7)
log β2	RG_2	5.6174	0.0122	5.62(1)

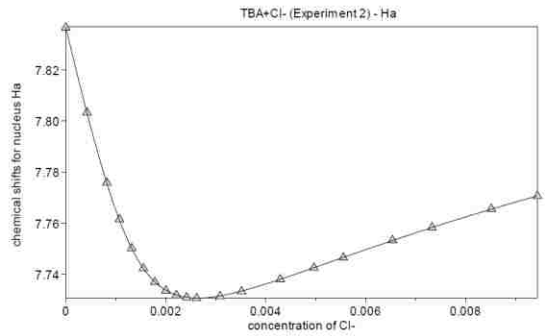
TBA+Cl- (Experiment 2) - Ha
chemical shifts for nucleus Ha
7.82
7.80
7.78
7.76
7.74
0
0.002
0.004
0.006
0.008
concentration of Cl-

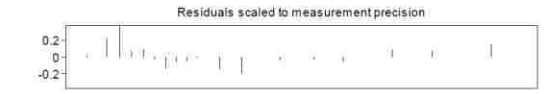
Residuals scaled to measurement precision
0.2
0
-0.2

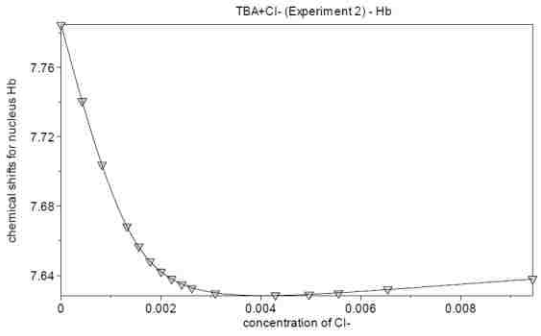
TBA+Cl- (Experiment 2) - Hb
chemical shifts for nucleus Hb
7.76
7.72
7.68
7.64
0
0.002
0.004
0.006
0.008
concentration of Cl-

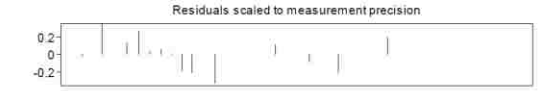
Residuals scaled to measurement precision
0.2
0
-0.2

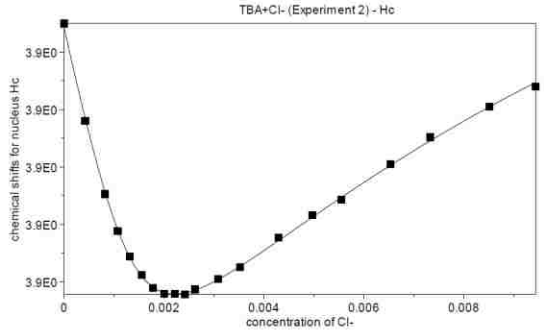
TBA+Cl- (Experiment 2) - Hc
chemical shifts for nucleus Hc
3.9E0
3.9E0
3.9E0
3.9E0
3.9E0
0
0.002
0.004
0.006
0.008
concentration of Cl-

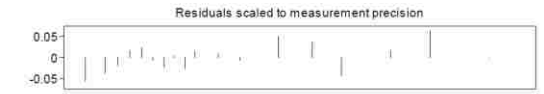
Residuals scaled to measurement precision
0.05
0
-0.05

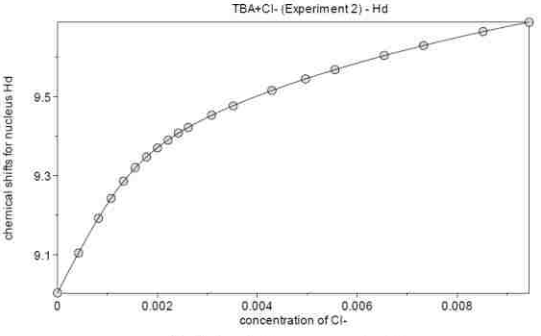
TBA+Cl- (Experiment 2) - Hd
chemical shifts for nucleus Hd
9.5
9.3
9.1
0
0.002
0.004
0.006
0.008
concentration of Cl-

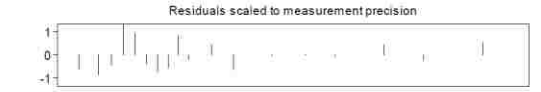
Residuals scaled to measurement precision
1
0
-1

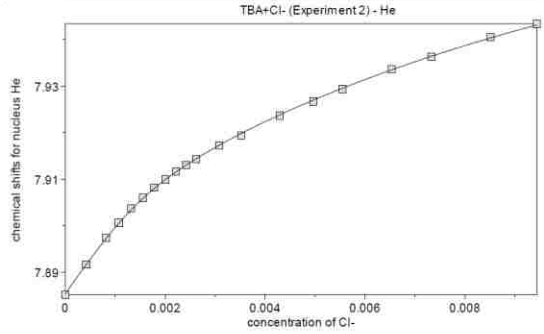
TBA+Cl- (Experiment 2) - He
chemical shifts for nucleus He
7.93
7.91
7.89
0
0.002
0.004
0.006
0.008
concentration of Cl-

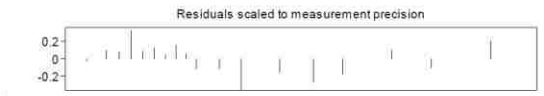
Residuals scaled to measurement precision
0.2
0
-0.2

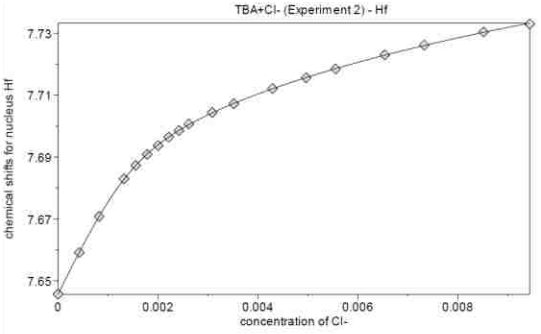
TBA+Cl- (Experiment 2) - Hf
chemical shifts for nucleus Hf
7.73
7.71
7.69
7.67
7.65
0
0.002
0.004
0.006
0.008
concentration of Cl-

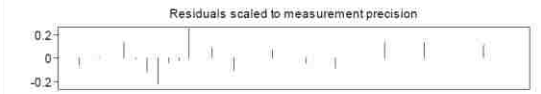
Residuals scaled to measurement precision
0.2
0
-0.2

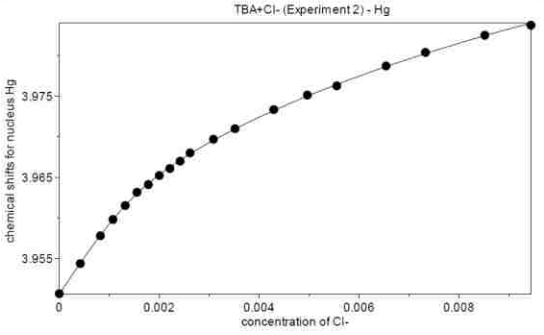
TBA+Cl- (Experiment 2) - Hg
chemical shifts for nucleus Hg
3.975
3.965
3.955
0
0.002
0.004
0.006
0.008
concentration of Cl-

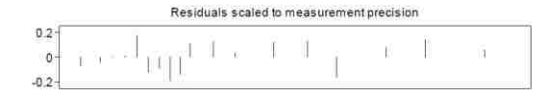
Residuals scaled to measurement precision
0.2
0
-0.2

XB1c-Cl-Exp3

Point	[X-]	[R]	peak (ppm)	peak (ppm)	peak (ppm)	peak (ppm)	peak (ppm)	peak (ppm)	peak (ppm)
1	0	0.001466182	9.00247	7.88507	7.83677	7.78464	7.64565	3.95071	3.92503
2	0.000422696	0.001466182	9.10468	7.89169	7.80351	7.74078	7.65925	3.95434	3.92338
3	0.000821466	0.001466182	9.19493	7.8976	7.7757	7.70359	7.6709	3.95797	3.92208
4	0.001075005	0.001466182	9.24348	7.90069	7.76131	7.68378	-	3.95978	3.9214
5	0.001319325	0.001466182	9.28519	7.9037	7.75038	7.66855	7.683	3.96163	3.92101
6	0.001554918	0.001466182	9.31995	7.90609	7.7425	7.65689	7.68758	3.96324	3.9207
7	0.001782245	0.001466182	9.34615	7.90818	7.73729	7.64855	7.69099	3.96432	3.92048
8	0.002001734	0.001466182	9.36847	7.90979	7.73408	7.64297	7.69388	3.96525	3.92042
9	0.002213782	0.001466182	9.38765	7.91141	7.73215	7.63869	7.6963	3.96625	3.92035
10	0.002418762	0.001466182	9.4034	7.91276	7.73105	7.63581	7.69835	3.96713	3.92041
11	0.002617021	0.001466182	9.41692	7.91389	7.73065	7.6335	7.69997	3.96782	3.9204
12	0.003085349	0.001466182	9.44615	7.9168	7.73121	7.63035	7.70386	3.96936	3.92054
13	0.003518199	0.001466182	9.47099	7.91897	7.73278	7.62912	7.70674	3.97077	3.92081
14	0.00429245	0.001466182	9.50682	7.92275	7.73689	7.6282	7.71109	3.97268	3.9211
15	0.004964826	0.001466182	9.53616	7.92577	7.74105	7.62867	7.7145	3.97449	3.9215
16	0.005554193	0.001466182	9.55906	7.92859	7.74502	7.62941	7.71769	3.97616	3.92193
17	0.00653863	0.001466182	9.59413	-	7.75143	7.63144	7.72179	3.97801	3.92237
18	0.007328129	0.001466182	9.62011	-	7.7565	-	7.72487	3.9797	3.92278
19	0.00851564	0.001466182	9.65531	-	7.76384	7.63541	7.72917	3.98184	3.92338
20	0.009438245	0.001466182	9.67944	7.94258	7.76886	7.63739	7.73228	3.98341	3.92381

	model	raw value	std. dev.	final value
log β1	RG	3.7764	0.0063	3.776(6)
log β2	RG_2	5.5163	0.0132	5.52(1)

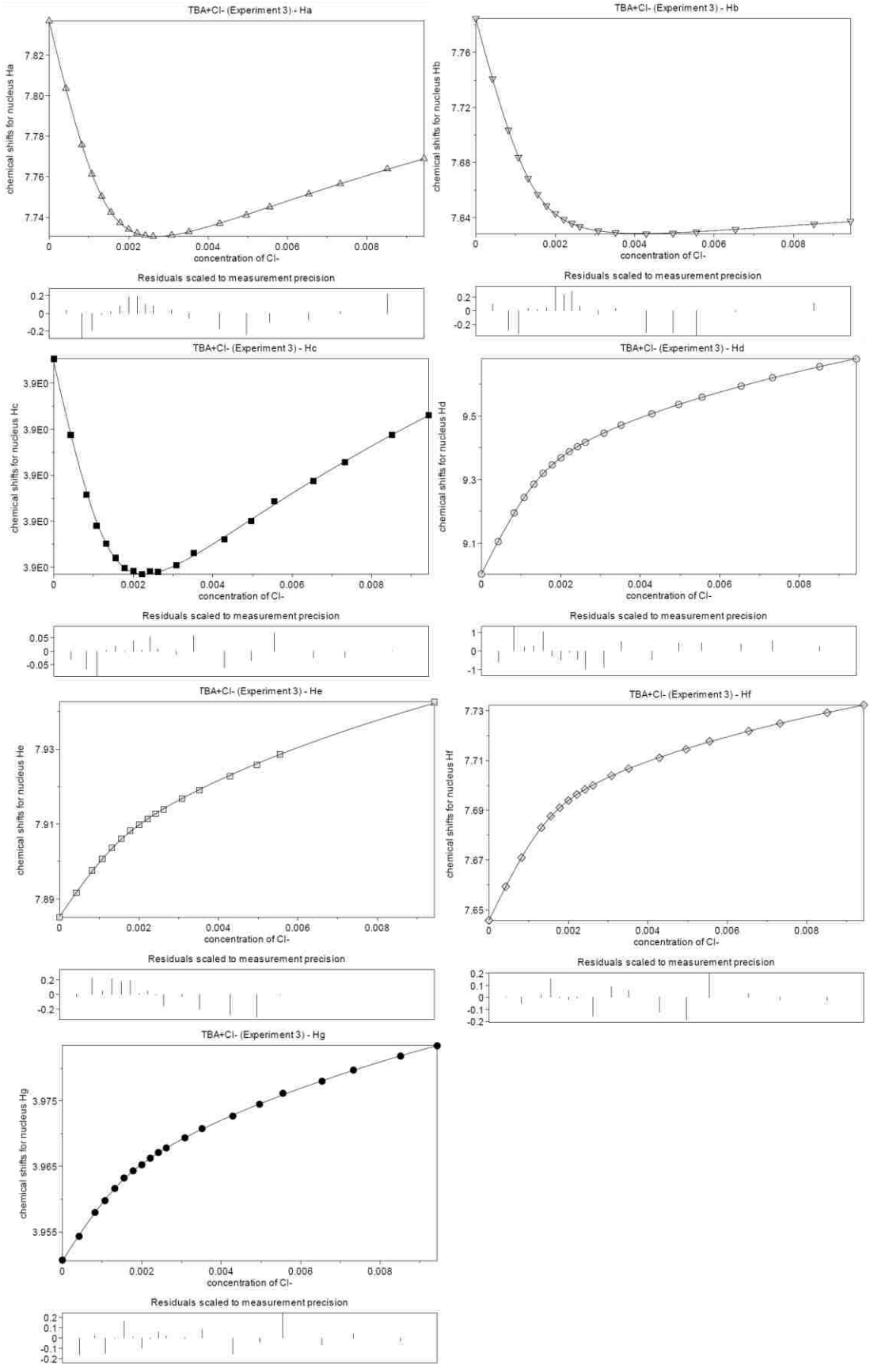
TBA+Cl- (Experiment 3) - Ha
chemical shifts for nucleus Ha
concentration of Cl-
Residuals scaled to measurement precision
TBA+Cl- (Experiment 3) - Hb
chemical shifts for nucleus Hb
concentration of Cl-
Residuals scaled to measurement precision
TBA+Cl- (Experiment 3) - Hc
chemical shifts for nucleus Hc
concentration of Cl-
Residuals scaled to measurement precision
TBA+Cl- (Experiment 3) - Hd
chemical shifts for nucleus Hd
concentration of Cl-
Residuals scaled to measurement precision
TBA+Cl- (Experiment 3) - He
chemical shifts for nucleus He
concentration of Cl-
Residuals scaled to measurement precision
TBA+Cl- (Experiment 3) - Hf
chemical shifts for nucleus Hf
concentration of Cl-
Residuals scaled to measurement precision
TBA+Cl- (Experiment 3) - Hg
chemical shifts for nucleus Hg
concentration of Cl-
Residuals scaled to measurement precision

HB1-Cl-Exp1

Point	[X-]	[R]	peak (ppm)	peak (ppm)	peak (ppm)	peak (ppm)
1	0	0.00197	9.01016	7.89112	7.75719	3.95278
2	0.000613803	0.00197	9.30008	7.93131	7.8395	3.96286
3	0.001203999	0.00197	9.52116	7.96301	7.90308	3.97148
4	0.001771923	0.00197	9.69677	7.98864	7.9542	3.97865
5	0.002318813	0.00197	9.8336	8.00876	7.99354	3.98415
6	0.002845816	0.00197	9.93652	8.02371	8.02371	3.98867
7	0.003353997	0.00197	10.01331	8.03551	8.04499	3.99143
8	0.003844347	0.00197	10.07958	8.04597	8.06436	3.99435
9	0.004317789	0.00197	10.13688	8.05531	8.08109	3.9969
10	0.004775182	0.00197	10.18209	8.06284	8.09432	3.99911
11	0.005217329	0.00197	10.22206	8.06948	8.10576	4.00098
12	0.005644979	0.00197	10.25486	8.07537	8.11556	4.00278
13	0.006847744	0.00197	10.32717	8.08846	8.13629	4.00615
14	0.007942799	0.00197	10.37953	8.09913	8.15115	4.00886
15	0.008943992	0.00197	10.41772	8.10607	8.16232	4.01081
16	0.010434657	0.00197	10.46494	8.11691	8.17591	4.01375
17	0.01173899	0.00197	10.50073	8.12618	8.18675	4.01708
18	0.013912877	0.00197	10.54212	8.13671	8.19817	4.01857

	model	raw value	std. dev.	final value
log β1	RG	2.9423	0.0816	2.94(8)
log β2	RG_2	4.769	0.2752	4.8(3)

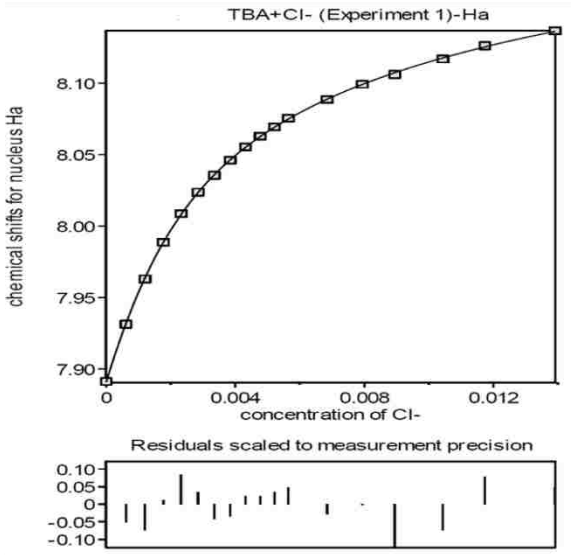
TBA+Cl- (Experiment 1)-Ha
chemical shifts for nucleus Ha
8.10
8.05
8.00
7.95
7.90
0
0.004
0.008
0.012
concentration of Cl-
Residuals scaled to measurement precision
0.10
0.05
0
-0.05
-0.10

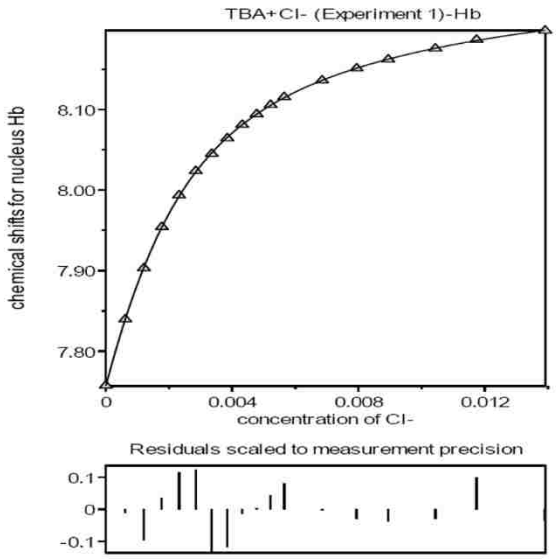
TBA+Cl- (Experiment 1)-Hb
chemical shifts for nucleus Hb
8.10
8.00
7.90
7.80
0
0.004
0.008
0.012
concentration of Cl-
Residuals scaled to measurement precision
0.1
0
-0.1

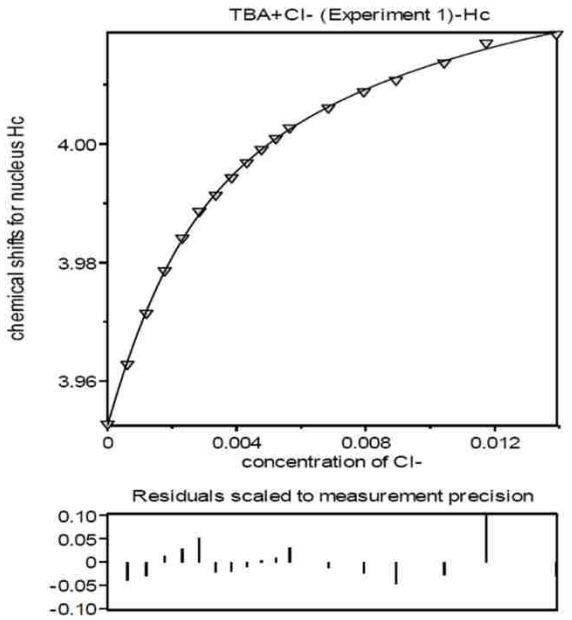
TBA+Cl- (Experiment 1)-Hc
chemical shifts for nucleus Hc
4.00
3.98
3.96
0
0.004
0.008
0.012
concentration of Cl-
Residuals scaled to measurement precision
0.10
0.05
0
-0.05
-0.10

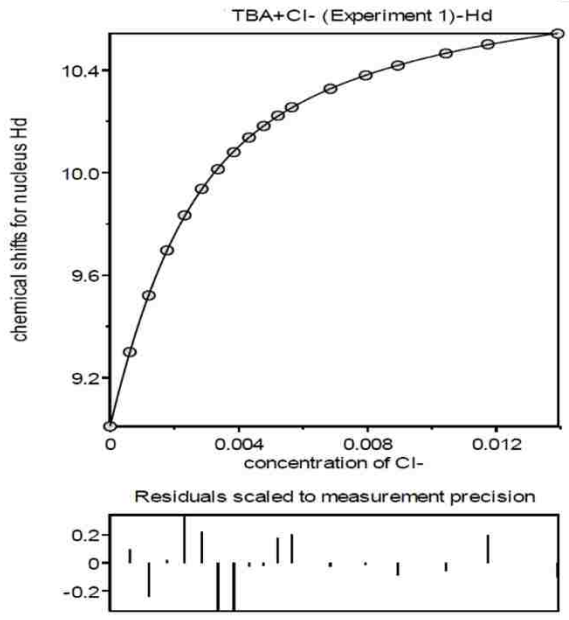
TBA+Cl- (Experiment 1)-Hd
chemical shifts for nucleus Hd
10.4
10.0
9.6
9.2
0
0.004
0.008
0.012
concentration of Cl-
Residuals scaled to measurement precision
0.2
0
-0.2

HB1-Cl-Exp2

Point	[X-]	[R]	peak (ppm)	peak (ppm)	peak (ppm)	peak (ppm)
1	0	0.00197	9.0095	7.89084	7.75714	3.95334
2	0.000613803	0.00197	9.29129	7.93041	7.8377	3.96297
3	0.001203999	0.00197	9.5099	7.96139	7.90054	3.97148
4	0.001771923	0.00197	9.68657	7.98705	7.95229	3.97883
5	0.002318813	0.00197	9.8165	8.00571	7.98917	3.98388
6	0.002845816	0.00197	9.92137	8.02078	8.02078	3.98816
7	0.003353997	0.00197	10.00657	8.03418	8.04413	3.99172
8	0.003844347	0.00197	10.07381	8.04465	8.06374	3.99471
9	0.004317789	0.00197	10.13168	8.05372	8.08059	3.99739
10	0.004775182	0.00197	10.17851	8.06162	8.09398	3.99929
11	0.005217329	0.00197	10.21708	8.06834	8.10523	4.00128
12	0.005644979	0.00197	10.25205	8.07425	8.11518	4.00276
13	0.006847744	0.00197	10.32819	8.08799	8.1372	4.00651
14	0.007942799	0.00197	10.38256	8.09867	8.15257	4.00921
15	0.008943992	0.00197	10.42063	8.1067	8.16373	4.01136
16	0.010434657	0.00197	10.46846	8.1178	8.17766	4.01431
17	0.01173899	0.00197	10.50075	8.1253	8.18706	4.0165
18	0.013912877	0.00197	10.5449	8.13719	8.19938	4.01897

	model	raw value	std. dev.	final value
log β1	RG	2.9108	0.0492	2.91(5)
log β2	RG_2	4.2868	0.4263	4.3(4)

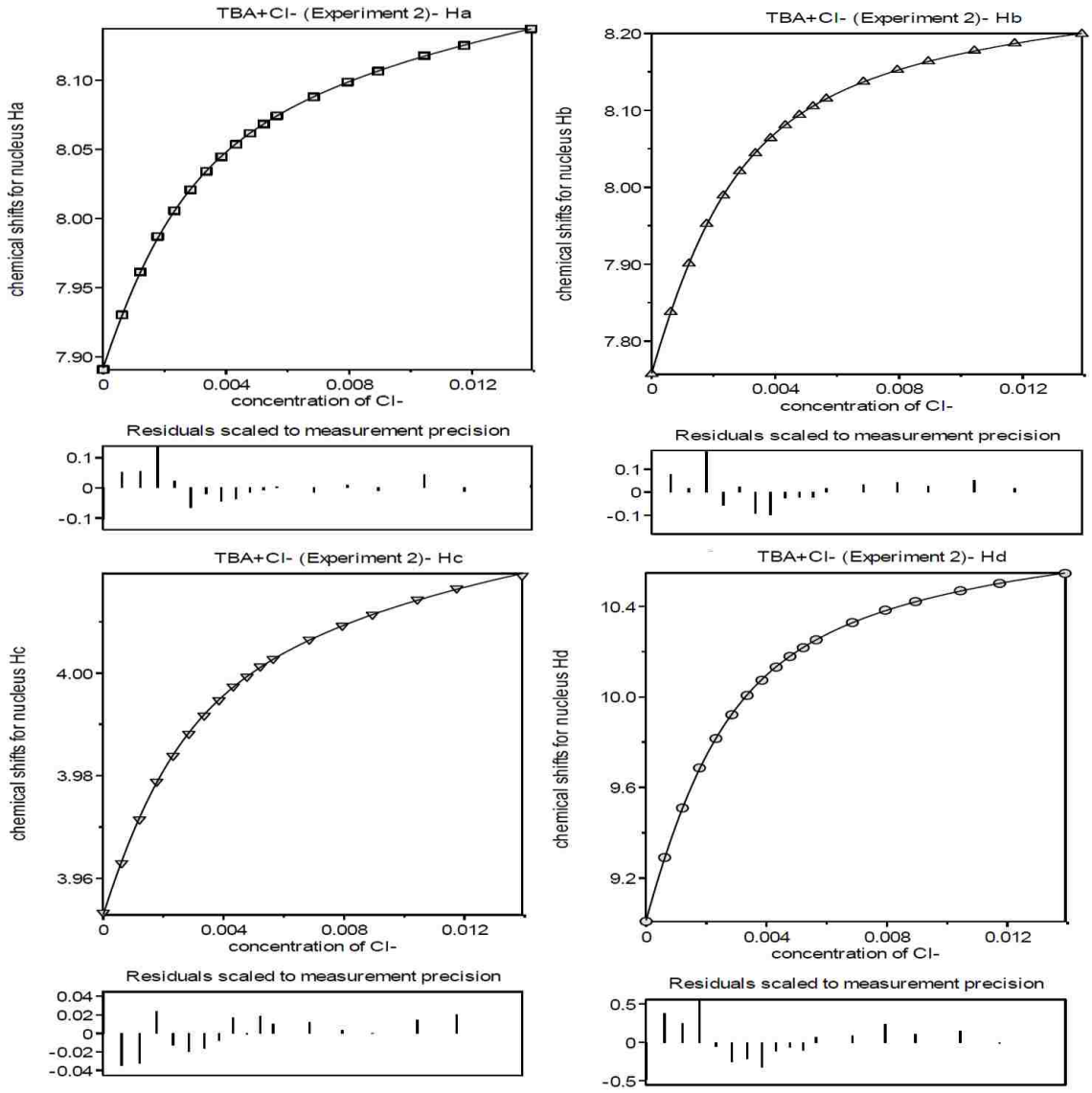
TBA+Cl- (Experiment 2)- Ha
chemical shifts for nucleus Ha
8.10
8.05
8.00
7.95
7.90
0
0.004
0.008
0.012
concentration of Cl-
Residuals scaled to measurement precision
0.1
0
-0.1
TBA+Cl- (Experiment 2)- Hb
chemical shifts for nucleus Hb
8.20
8.10
8.00
7.90
7.80
0
0.004
0.008
0.012
concentration of Cl-
Residuals scaled to measurement precision
0.1
0
-0.1
TBA+Cl- (Experiment 2)- Hc
chemical shifts for nucleus Hc
4.00
3.98
3.96
0
0.004
0.008
0.012
concentration of Cl-
Residuals scaled to measurement precision
0.04
0.02
0
-0.02
-0.04
TBA+Cl- (Experiment 2)- Hd
chemical shifts for nucleus Hd
10.4
10.0
9.6
9.2
0
0.004
0.008
0.012
concentration of Cl-
Residuals scaled to measurement precision
0.5
0
-0.5

HB1-Cl-Exp3

Point	[X-]	[R]	peak (ppm)	peak (ppm)	peak (ppm)	peak (ppm)
1	0	0.00197	9.00907	7.89033	7.7566	3.9528
2	0.000613803	0.00197	9.28728	7.93014	7.83675	3.96293
3	0.001203999	0.00197	9.51593	7.96217	7.90221	3.97163
4	0.001771923	0.00197	9.6934	7.9875	7.95393	3.97888
5	0.002318813	0.00197	9.82585	8.00698	7.992	3.98423
6	0.002845816	0.00197	9.931	8.0226	8.0226	3.98859
7	0.003353997	0.00197	10.01878	8.0362	8.04747	3.99233
8	0.003844347	0.00197	10.08872	8.0473	8.06783	3.99538
9	0.004317789	0.00197	10.14698	8.05666	8.08483	3.99796
10	0.004775182	0.00197	10.19402	8.06431	8.0986	4.00029
11	0.005217329	0.00197	10.23036	8.07065	8.10901	4.00198
12	0.005644979	0.00197	10.26159	8.07615	8.11814	4.00339
13	0.006847744	0.00197	10.3336	8.08932	8.13879	4.0068
14	0.007942799	0.00197	10.38499	8.09979	8.15378	4.00955
15	0.008943992	0.00197	10.4243	8.10775	8.16477	4.01161
16	0.010434657	0.00197	10.46924	8.11776	8.1777	4.01442
17	0.01173899	0.00197	10.50291	8.1264	8.18753	4.0165
18	0.013912877	0.00197	10.54665	8.13817	8.1999	4.01954

	model	raw value	std. dev.	final value
log β1	RG	2.9882	0.0053	2.988(5)
log β2	RG_2	4.686725	fixed	4.6867

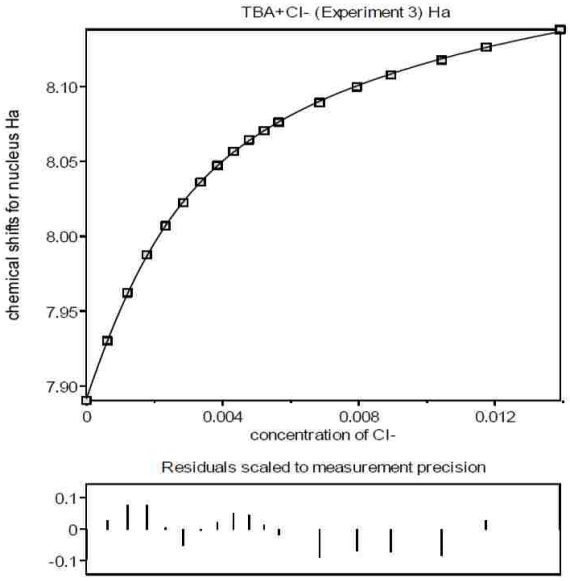
TBA+Cl- (Experiment 3) Ha
chemical shifts for nucleus Ha
8.10
8.05
8.00
7.95
7.90
0
0.004
0.008
0.012
concentration of Cl-
Residuals scaled to measurement precision
0.1
0
-0.1

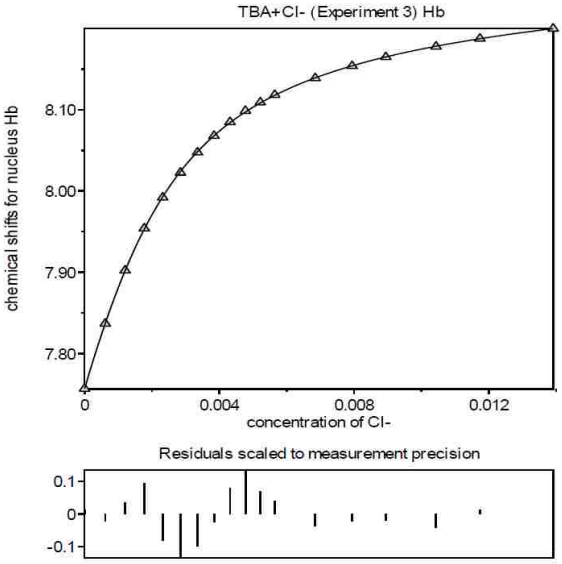
TBA+Cl- (Experiment 3) Hb
chemical shifts for nucleus Hb
8.10
8.00
7.90
7.80
0
0.004
0.008
0.012
concentration of Cl-
Residuals scaled to measurement precision
0.1
0
-0.1

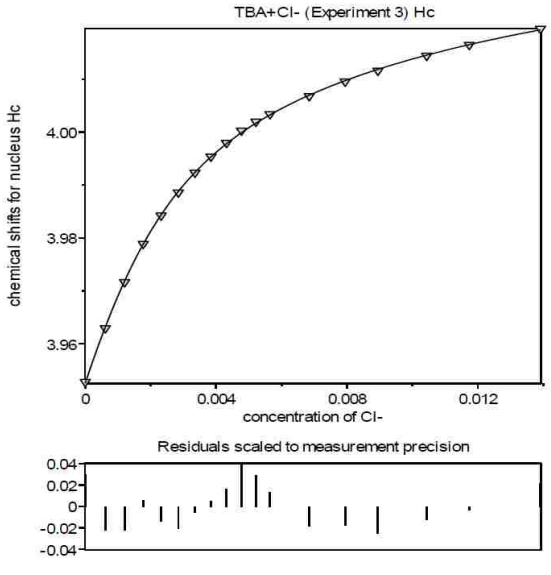
TBA+Cl- (Experiment 3) Hc
chemical shifts for nucleus Hc
4.00
3.98
3.96
0
0.004
0.008
0.012
concentration of Cl-
Residuals scaled to measurement precision
0.04
0.02
0
-0.02
-0.04

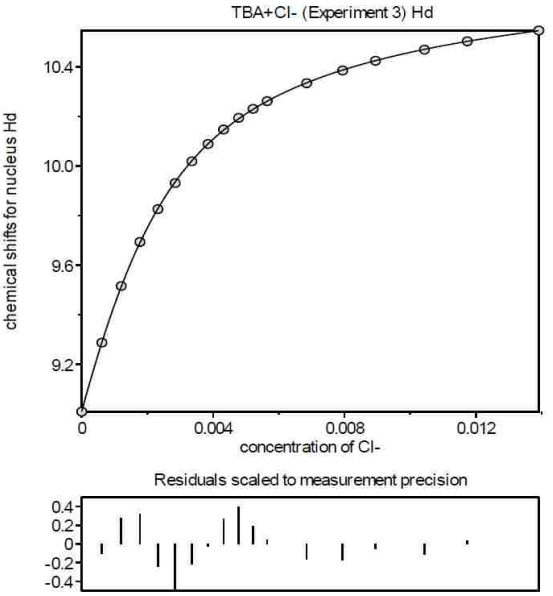
TBA+Cl- (Experiment 3) Hd
chemical shifts for nucleus Hd
10.4
10.0
9.6
9.2
0
0.004
0.008
0.012
concentration of Cl-
Residuals scaled to measurement precision
0.4
0.2
0
-0.2
-0.4

HB1-Br-Exp1

Point	[X-]	[R]	peak (ppm)	peak (ppm)	peak (ppm)	peak (ppm)
1	0	0.0019929	9.01618	7.89221	7.75911	3.95881
2	0.000598107	0.0019929	9.18951	7.91691	7.81053	3.96615
3	0.001173209	0.0019929	9.32182	7.9361	7.857	3.97225
4	0.00172661	0.0019929	9.43127	7.95209	7.89225	3.97706
5	0.002259514	0.0019929	9.5208	7.96528	7.92058	3.98108
6	0.00277304	0.0019929	9.59213	7.9756	7.94028	3.9834
7	0.003268226	0.0019929	9.65272	7.98467	7.96263	3.98624
8	0.003746037	0.0019929	9.70323	7.99246	7.97878	3.98864
9	0.004207371	0.0019929	9.74734	7.99928	7.99282	3.9908
10	0.004653067	0.0019929	9.78395	8.0047	8.0047	3.9926
11	0.005083907	0.0019929	9.81632	8.01412	8.01056	3.99417
12	0.005500621	0.0019929	9.84473	8.01503	8.02326	3.99595
13	0.006672628	0.0019929	9.91211	8.02728	8.04512	4.00031
14	0.007739679	0.0019929	9.9589	8.03467	8.05939	4.00206
15	0.008715269	0.0019929	9.99562	8.04136	8.07044	4.00362
16	0.010167814	0.0019929	10.03919	8.05075	8.08533	4.00725
17	0.01143879	0.0019929	10.0738	8.05717	8.0956	4.00968
18	0.013557085	0.0019929	10.11599	8.06551	8.10714	4.01116
19	0.015977993	0.0019929	10.15517	8.07504	8.12012	4.01506
20	0.018302065	0.0019929	10.18695	8.08245	8.12871	4.01602

	model	raw value	std. dev.	final value
log β1	RG	2.778	0.0597	2.78(6)
log β2	RG_2	4.3111	0.2795	4.3(3)

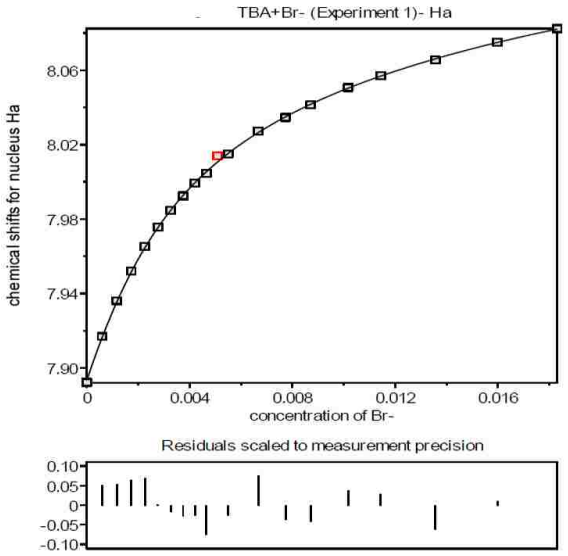
TBA+Br- (Experiment 1)- Ha
chemical shifts for nucleus Ha
8.06
8.02
7.98
7.94
7.90
0
0.004
0.008
0.012
0.016
concentration of Br-
Residuals scaled to measurement precision
0.10
0.05
0
-0.05
-0.10

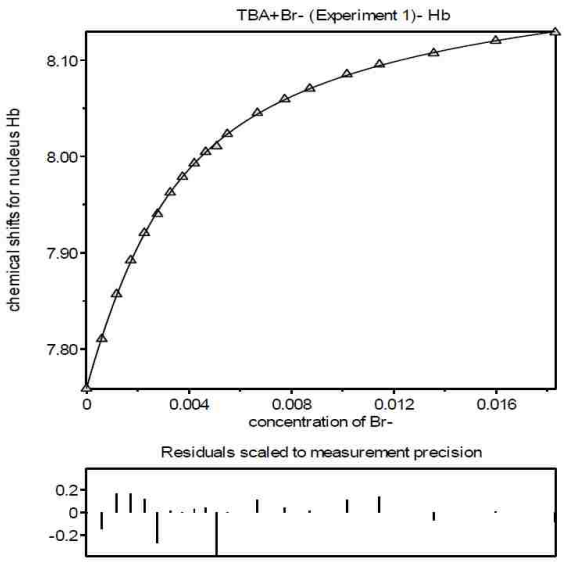
TBA+Br- (Experiment 1)- Hb
chemical shifts for nucleus Hb
8.10
8.00
7.90
7.80
0
0.004
0.008
0.012
0.016
concentration of Br-
Residuals scaled to measurement precision
0.2
0
-0.2

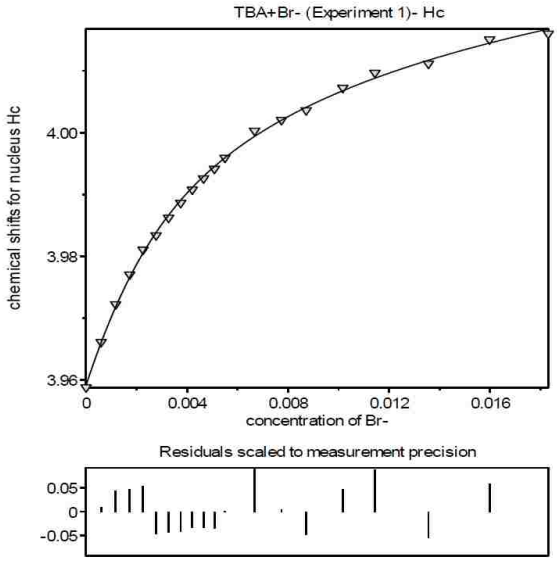
TBA+Br- (Experiment 1)- Hc
chemical shifts for nucleus Hc
4.00
3.98
3.96
0
0.004
0.008
0.012
0.016
concentration of Br-
Residuals scaled to measurement precision
0.05
0
-0.05

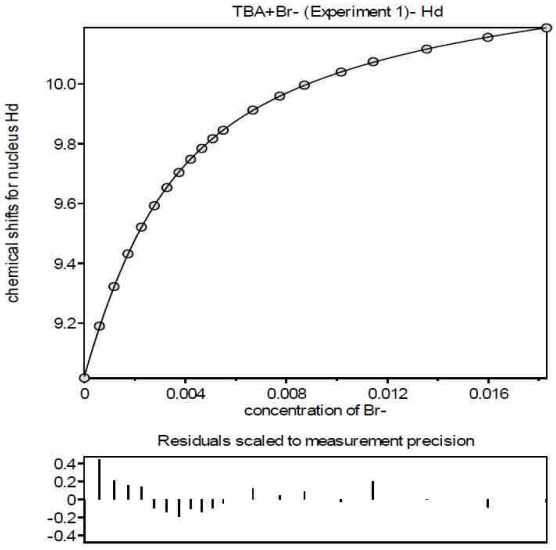
TBA+Br- (Experiment 1)- Hd
chemical shifts for nucleus Hd
10.0
9.8
9.6
9.4
9.2
0
0.004
0.008
0.012
0.016
concentration of Br-
Residuals scaled to measurement precision
0.4
0.2
0
-0.2
-0.4

HB1-Br-Exp2

Point	[X-]	[R]	peak (ppm)	peak (ppm)	peak (ppm)	peak (ppm)
1	0.00000E+00	1.99290E-03	9.01857	7.89232	7.75962	3.95889
2	5.98107E-04	1.99290E-03	9.1846	7.91547	7.81221	3.96505
3	1.17321E-03	1.99290E-03	9.31846	7.93529	7.85574	3.97189
4	1.72661E-03	1.99290E-03	9.42806	7.94666	7.89082	3.97674
5	2.25951E-03	1.99290E-03	9.51423	7.96369	7.91786	3.97988
6	2.77304E-03	1.99290E-03	9.58767	7.9753	7.94386	3.98414
7	3.26823E-03	1.99290E-03	9.64892	7.9845	7.96205	3.98713
8	3.74604E-03	1.99290E-03	9.69891	7.99174	7.97709	3.98835
9	4.20737E-03	1.99290E-03	9.74214	7.99829	7.99129	3.99075
10	4.65307E-03	1.99290E-03	9.77906	8.00412	8.00412	3.9923
11	5.08391E-03	1.99290E-03	9.81196	8.01027	8.0138	3.99501
12	5.50062E-03	1.99290E-03	9.84003	8.01541	8.02223	3.99643
13	6.67263E-03	1.99290E-03	9.90763	8.02649	8.04409	4.00014
14	7.73968E-03	1.99290E-03	9.95538	8.03406	8.05831	4.00191
15	8.71527E-03	1.99290E-03	9.9917	8.04085	8.06957	4.00373
16	1.01678E-02	1.99290E-03	10.04074	8.05073	8.08544	4.00772
17	1.14388E-02	1.99290E-03	10.07408	8.05745	8.09568	4.00981
18	1.35571E-02	1.99290E-03	10.11935	8.06629	8.10848	4.01152
19	1.59780E-02	1.99290E-03	10.16141	8.0763	8.12181	4.01568
20	1.83021E-02	1.99290E-03	10.19184	8.0801	8.13063	4.01625

	model	raw value	std. dev.	final value
log β1	RG	2.8815	0.0603	4.88(6)
log β2	RG_2	4.6647	0.1611	4.7(2)

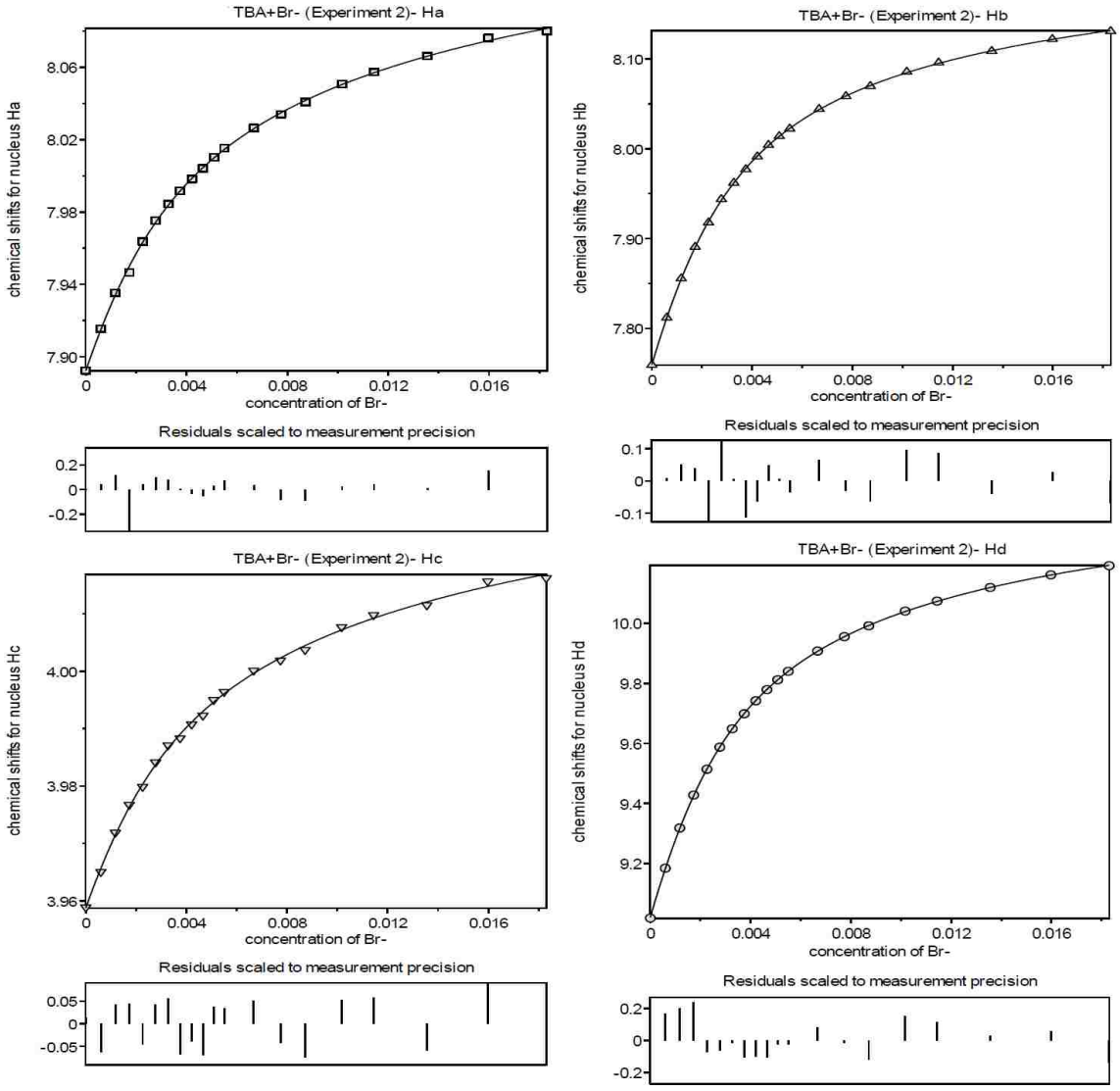
TBA+Br- (Experiment 2)- Ha
chemical shifts for nucleus Ha
8.06
8.02
7.98
7.94
7.90
0
0.004
0.008
0.012
0.016
concentration of Br-
Residuals scaled to measurement precision
0.2
0
-0.2
TBA+Br- (Experiment 2)- Hb
chemical shifts for nucleus Hb
8.10
8.00
7.90
7.80
0
0.004
0.008
0.012
0.016
concentration of Br-
Residuals scaled to measurement precision
0.1
0
-0.1
TBA+Br- (Experiment 2)- Hc
chemical shifts for nucleus Hc
4.00
3.98
3.96
0
0.004
0.008
0.012
0.016
concentration of Br-
Residuals scaled to measurement precision
0.05
0
-0.05
TBA+Br- (Experiment 2)- Hd
chemical shifts for nucleus Hd
10.0
9.8
9.6
9.4
9.2
0
0.004
0.008
0.012
0.016
concentration of Br-
Residuals scaled to measurement precision
0.2
0
-0.2

HB1-Br-Exp3

Point	[X-]	[R]	peak (ppm)	peak (ppm)	peak (ppm)	peak (ppm)
1	0.00000E+00	0.0019929	9.02121	7.89308	7.7599	3.95868
2	5.98107E-04	0.0019929	9.18413	7.91648	7.81267	3.96618
3	1.17321E-03	0.0019929	9.31783	7.93511	7.85528	3.97135
4	1.72661E-03	0.0019929	9.42573	7.95124	7.89029	3.97708
5	2.25951E-03	0.0019929	9.51372	7.96407	7.91782	3.98005
6	2.77304E-03	0.0019929	9.58719	7.97525	7.94362	3.98368
7	3.26823E-03	0.0019929	9.64717	7.98407	7.96092	3.98646
8	3.74604E-03	0.0019929	9.69636	7.99168	7.97648	3.98852
9	4.20737E-03	0.0019929	9.74252	7.99973	7.99563	3.99211
10	4.65307E-03	0.0019929	9.77909	8.00567	8.00567	3.9935
11	5.08391E-03	0.0019929	9.80902	8.00945	8.01266	3.9944
12	5.50062E-03	0.0019929	9.83679	8.01441	8.02077	3.9956
13	6.67263E-03	0.0019929	9.90459	8.02543	8.04246	3.99919
14	7.73968E-03	0.0019929	9.95555	8.03435	8.05829	4.00202
15	8.71527E-03	0.0019929	9.99178	8.04107	8.06954	4.00396
16	1.01678E-02	0.0019929	10.03723	8.04957	8.08399	4.00676
17	1.14388E-02	0.0019929	10.0692	8.05602	8.09338	4.00852
18	1.35571E-02	0.0019929	10.1152	8.06601	8.10769	4.01241
19	0.015977993	0.0019929	10.15439	8.07418	8.11922	4.01409
20	0.018302065	0.0019929	10.17884	8.0775	8.12317	4.01491

	model	raw value	std. dev.	final value
log β1	RG	2.8688	0.0875	2.87(9)
log β2	RG_2	4.7094	0.2247	4.7(2)

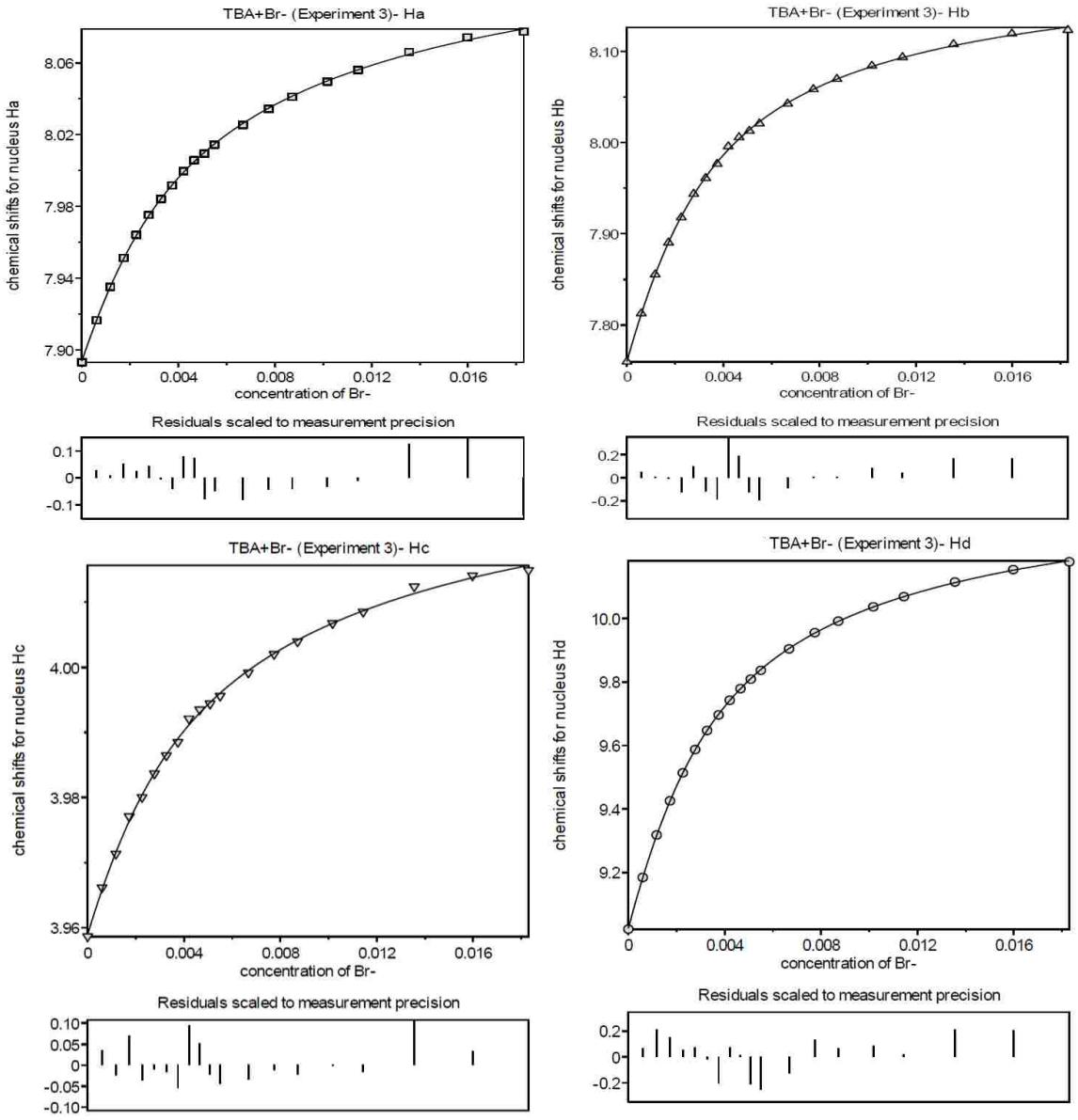
TBA+Br- (Experiment 3)- Ha
chemical shifts for nucleus Ha
8.06
8.02
7.98
7.94
7.90
0
0.004
0.008
0.012
0.016
concentration of Br-
Residuals scaled to measurement precision
0.1
0
-0.1
TBA+Br- (Experiment 3)- Hb
chemical shifts for nucleus Hb
8.10
8.00
7.90
7.80
0
0.004
0.008
0.012
0.016
concentration of Br-
Residuals scaled to measurement precision
0.2
0
-0.2
TBA+Br- (Experiment 3)- Hc
chemical shifts for nucleus Hc
4.00
3.98
3.96
0
0.004
0.008
0.012
0.016
concentration of Br-
Residuals scaled to measurement precision
0.10
0.05
0
-0.05
-0.10
TBA+Br- (Experiment 3)- Hd
chemical shifts for nucleus Hd
10.0
9.8
9.6
9.4
9.2
0
0.004
0.008
0.012
0.016
concentration of Br-
Residuals scaled to measurement precision
0.2
0
-0.2

HB1-I-Exp1

Point	[X-]	[R]	peak (ppm)	peak (ppm)
1	0.00000E+00	1.99000E-03	9.00938	3.9524
2	5.94547E-04	1.99000E-03	9.0702	3.95716
3	1.16623E-03	1.99000E-03	9.12153	3.95941
4	1.71633E-03	1.99000E-03	9.16257	3.96204
5	2.24607E-03	1.99000E-03	9.19806	3.96429
6	2.75654E-03	1.99000E-03	9.22829	3.96648
7	3.24878E-03	1.99000E-03	9.25447	3.96803
8	3.72374E-03	1.99000E-03	9.27738	3.96951
9	4.18233E-03	1.99000E-03	9.2979	3.97096
10	4.62537E-03	1.99000E-03	9.31674	3.9722
11	5.05365E-03	1.99000E-03	9.33309	3.97331
12	5.46788E-03	1.99000E-03	9.34855	3.97432
13	6.63292E-03	1.99000E-03	9.3886	3.97715
14	7.69362E-03	1.99000E-03	9.41956	3.9795
15	8.66340E-03	1.99000E-03	9.44397	3.98108
16	1.01073E-02	1.99000E-03	9.47634	3.98339
17	1.13707E-02	1.99000E-03	9.50043	3.98522
18	1.34764E-02	1.99000E-03	9.53691	3.98794
19	1.58829E-02	1.99000E-03	9.56956	3.9905
20	1.81931E-02	1.99000E-03	9.59912	3.99288

	model	raw value	std. dev.	final value
log β1	RG	2.7985	0.011	2.8(1)
log β2	RG_2	4.4695	fixed	4.4695

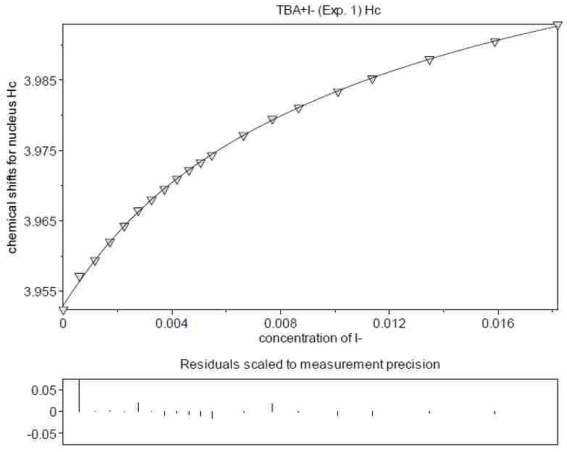

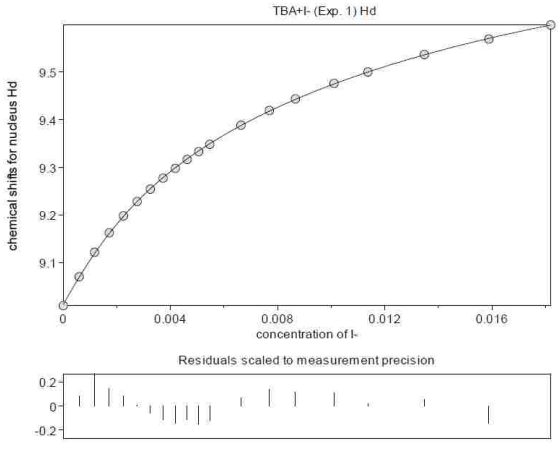

HB1-I-Exp2

Point	[X-]	[R]	peak (ppm)	peak (ppm)	peak (ppm)
1	0	0.00199	9.00899	7.89029	7.75716
2	0.000594547	0.00199	9.06783	7.89857	7.78205
3	0.001166227	0.00199	9.11878	7.90548	7.80658
4	0.001716334	0.00199	9.15848	7.90966	7.8197
5	0.002246067	0.00199	9.19374	7.91445	7.83442
6	0.002756536	0.00199	9.22491	7.91877	7.84785
7	0.003248775	0.00199	9.25081	7.92211	7.85838
8	0.003723742	0.00199	9.27394	7.92537	7.86782
9	0.004182331	0.00199	9.29495	7.92801	7.87632
10	0.004625374	0.00199	9.31392	7.93077	7.88433
11	0.00505365	0.00199	9.33046	7.93309	7.89119
12	0.005467884	0.00199	9.34542	7.93512	7.89738
13	0.006632916	0.00199	9.38426	7.94159	7.91309
14	0.007693616	0.00199	9.4136	7.94125	7.92537
15	0.0086634	0.00199	9.43841	7.94807	7.9381
16	0.0101073	0.00199	9.47061	7.94858	7.94417
17	0.011370712	0.00199	9.49516	7.95688	7.95688
18	0.0134764	0.00199	9.53005	7.96171	7.97129
19	0.0158829	0.00199	9.56638	7.96722	7.98491
20	0.01819314	0.00199	9.59384	7.97145	7.99551

	model	raw value	std. dev.	final value
log β1	RG	2.7865	0.004	2.787(4)
log β2	RG_2	4.452	0.0147	4.45(1)

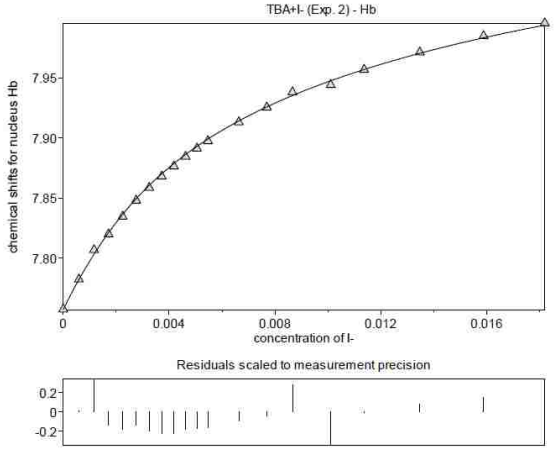
TBA+I- (Exp. 2) - Hb
chemical shifts for nucleus Hb
7.95
7.90
7.85
7.80
0
0.004
0.008
0.012
0.016
concentration of I-
Residuals scaled to measurement precision
0.2
0
-0.2

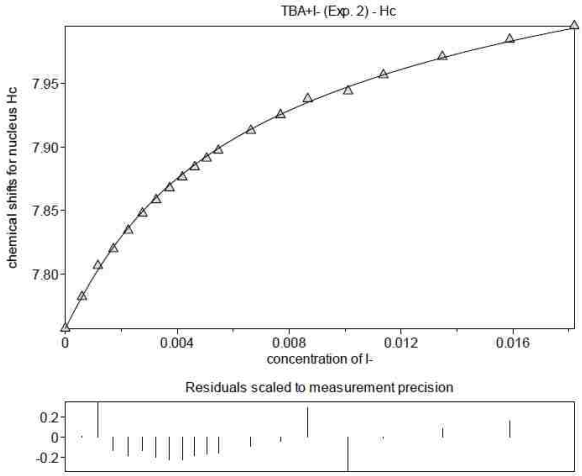
TBA+I- (Exp. 2) - Hc
chemical shifts for nucleus Hc
7.95
7.90
7.85
7.80
0
0.004
0.008
0.012
0.016
concentration of I-
Residuals scaled to measurement precision
0.2
0
-0.2

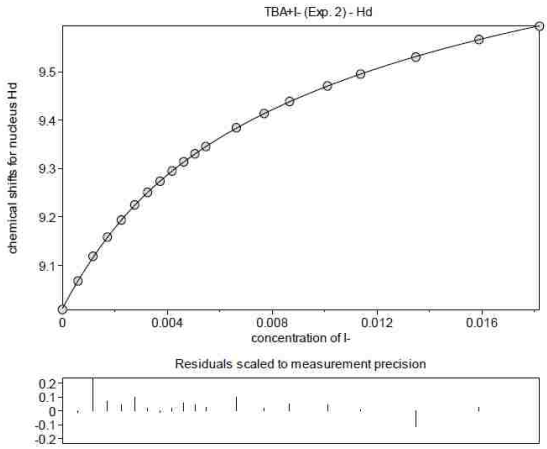
TBA+I- (Exp. 2) - Hd
chemical shifts for nucleus Hd
9.5
9.4
9.3
9.2
9.1
0
0.004
0.008
0.012
0.016
concentration of I-
Residuals scaled to measurement precision
0.2
0.1
0
-0.1
-0.2

HB1-I-Exp3

Point	[X-]	[R]	peak (ppm)	peak (ppm)	peak (ppm)
1	0.00000E+00	1.99000E-03	9.00944	7.89047	3.95253
2	5.94547E-04	1.99000E-03	9.069	7.89886	3.95701
3	1.16623E-03	1.99000E-03	9.11802	7.90443	3.95919
4	1.71633E-03	1.99000E-03	9.15948	7.90993	3.96186
5	2.24607E-03	1.99000E-03	9.19492	7.91458	3.96407
6	2.75654E-03	1.99000E-03	9.2231	7.91828	3.96606
7	3.24878E-03	1.99000E-03	9.24996	7.92221	3.96771
8	3.72374E-03	1.99000E-03	9.27469	7.92608	3.97051
9	4.18233E-03	1.99000E-03	9.29401	7.92799	3.97071
10	4.62537E-03	1.99000E-03	9.31389	7.93151	3.97299
11	5.05365E-03	1.99000E-03	9.33109	7.9338	3.97413
12	5.46788E-03	1.99000E-03	9.34499	7.9352	3.97427
13	6.63292E-03	1.99000E-03	9.38334	7.9418	3.97692
14	7.69362E-03	1.99000E-03	9.41403	7.94447	3.979
15	8.66340E-03	1.99000E-03	9.43845	7.94818	3.98068
16	1.01073E-02	1.99000E-03	9.47068	7.95236	3.98307
17	1.13707E-02	1.99000E-03	9.49556	7.95697	3.98487
18	1.34764E-02	1.99000E-03	9.53067	7.96181	3.98748
19	1.58829E-02	1.99000E-03	9.56513	7.96712	3.99017
20	1.81931E-02	1.99000E-03	9.5927	7.97138	3.99276

	model	raw value	std. dev.	final value
log β1	RG	2.7199	0.1277	2.7(1)
log β2	RG_2	4.3477	0.2585	4.3(3)

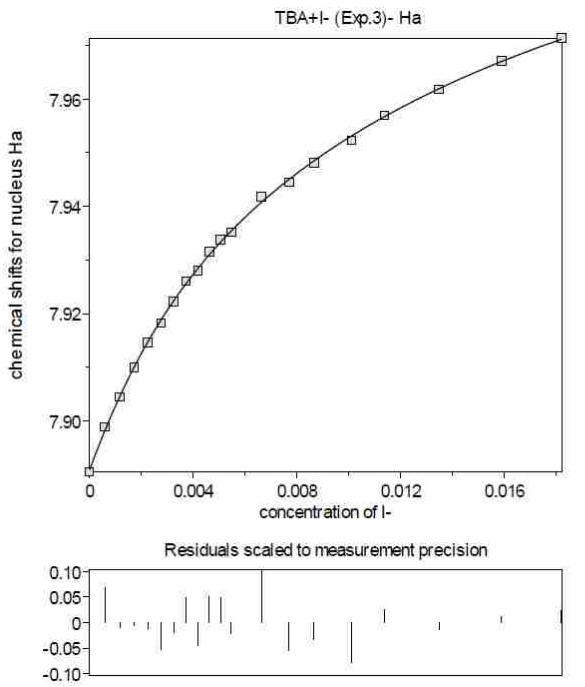
TBA+I- (Exp.3)- Ha
chemical shifts for nucleus Ha
7.96
7.94
7.92
7.90
0
0.004
0.008
0.012
0.016
concentration of I-
Residuals scaled to measurement precision
0.10
0.05
0
-0.05
-0.10

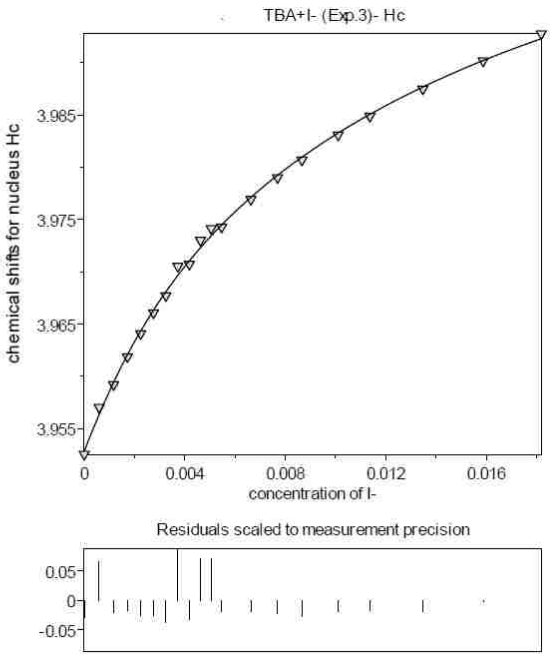
TBA+I- (Exp.3)- Hc
chemical shifts for nucleus Hc
3.985
3.975
3.965
3.955
0
0.004
0.008
0.012
0.016
concentration of I-
Residuals scaled to measurement precision
0.05
0
-0.05

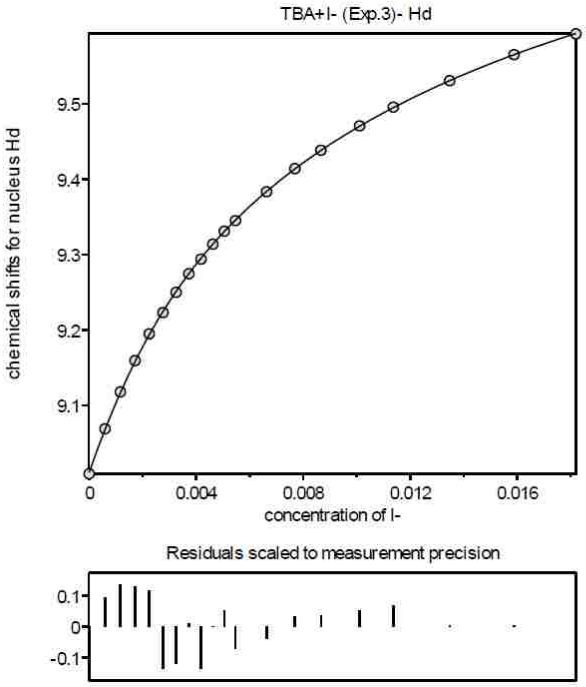
TBA+I- (Exp.3)- Hd
chemical shifts for nucleus Hd
9.5
9.4
9.3
9.2
9.1
0
0.004
0.008
0.012
0.016
concentration of I-
Residuals scaled to measurement precision
0.1
0
-0.1

5% D_2O CD_3CN

XB1a-Br-Exp1

Point	[X-]	[R]	peak (ppm)	peak (ppm)	peak (ppm)
1	0	0.001453893	7.83414	7.79988	3.91904
2	0.000361403	0.001453893	7.8192	7.78246	3.92149
3	0.00070235	0.001453893	7.80659	7.76794	3.92336
4	0.000919124	0.001453893	7.79943	7.75953	3.92451
5	0.001128016	0.001453893	7.79318	7.75216	3.92547
6	0.001329448	0.001453893	7.78771	7.74579	3.92625
7	0.001523812	0.001453893	7.7833	7.74067	3.92705
8	0.001711473	0.001453893	7.77925	7.73601	3.9276
9	0.001892773	0.001453893	7.77576	7.73194	3.928
10	0.00206803	0.001453893	7.77294	7.72868	3.92849
11	0.002237541	0.001453893	7.77038	7.72574	3.92881
12	0.002637959	0.001453893	7.76559	7.72006	3.92958
13	0.003008044	0.001453893	7.76206	7.716	3.93008
14	0.003670025	0.001453893	7.75688	7.7102	3.93078
15	0.004244904	0.001453893	7.75382	7.70675	3.93126
16	0.004748809	0.001453893	7.75173	7.70436	3.93137
17	0.005590498	0.001453893	7.74927	7.7017	3.93175
18	0.006265516	0.001453893	7.74762	7.69987	3.93189
19	0.006818909	0.001453893	7.74648	7.69867	3.93186
20	0.007672233	0.001453893	7.74505	7.69676	3.93217

	model	raw value	std. dev.	final value
log β1	RG	3.5751	0.0277	3.58(3)
log β2	RG_2	6.138	0.0473	6.14(5)

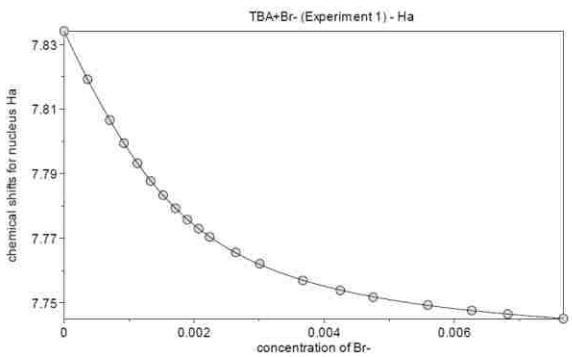
TBA+Br- (Experiment 1) - Ha
chemical shifts for nucleus Ha
7.83
7.81
7.79
7.77
7.75
0
0.002
0.004
0.006
concentration of Br-

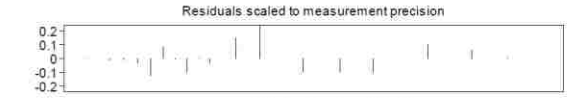
Residuals scaled to measurement precision
0.2
0.1
0
-0.1
-0.2

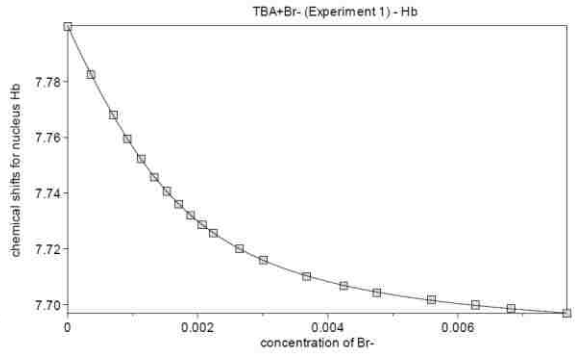
TBA+Br- (Experiment 1) - Hb
chemical shifts for nucleus Hb
7.78
7.76
7.74
7.72
7.70
0
0.002
0.004
0.006
concentration of Br-

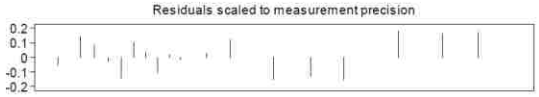
Residuals scaled to measurement precision
0.2
0.1
0
-0.1
-0.2

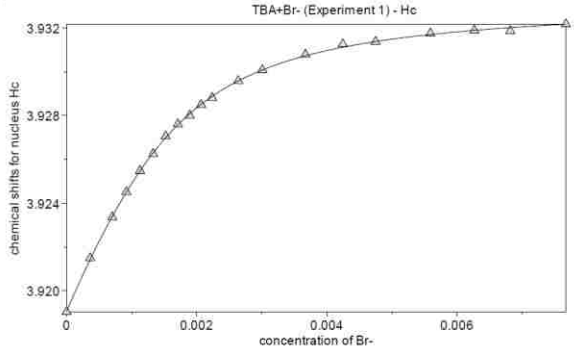
TBA+Br- (Experiment 1) - Hc
chemical shifts for nucleus Hc
3.932
3.928
3.924
3.920
0
0.002
0.004
0.006
concentration of Br-

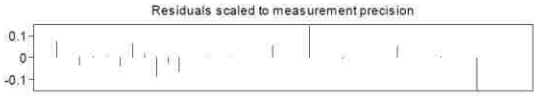
Residuals scaled to measurement precision
0.1
0
-0.1

XB1a-Br-Exp2

Point	[X-]	[R]	peak (ppm)	peak (ppm)	peak (ppm)
1	0	0.001643531	7.83861	7.80424	3.91917
2	0.00035677	0.001643531	7.82343	7.78657	3.92163
3	0.000693345	0.001643531	7.81083	7.77173	3.92355
4	0.000907341	0.001643531	7.80348	7.76323	3.92465
5	0.001113555	0.001643531	7.7971	7.75595	3.92561
6	0.001312404	0.001643531	7.79148	7.74934	3.9265
7	0.001504275	0.001643531	7.78669	7.74376	3.92719
8	0.001689531	0.001643531	7.78242	7.73875	3.92785
9	0.001868507	0.001643531	7.77896	7.7346	3.92828
10	0.002041517	0.001643531	7.77593	7.731	3.92877
11	0.002208854	0.001643531	7.77303	7.72792	3.92911
12	0.002604139	0.001643531	7.76778	7.72198	3.92988
13	0.002969479	0.001643531	7.76429	7.71783	3.9304
14	0.003622973	0.001643531	7.75934	7.71208	3.93109
15	0.004190482	0.001643531	7.75642	7.70904	3.93164
16	0.004687927	0.001643531	7.75438	7.70661	3.93171
17	0.005518825	0.001643531	7.75195	7.70396	3.93194
18	0.006185189	0.001643531	7.75053	7.70242	3.93212
19	0.006731488	0.001643531	7.7496	7.70143	3.93223
20	0.007745755	0.001643531	7.74836	-	3.93245

	model	raw value	std. dev.	final value
log β1	RG	3.4761	0.0219	3.48(2)
log β2	RG_2	5.8656	0.0536	5.87(5)

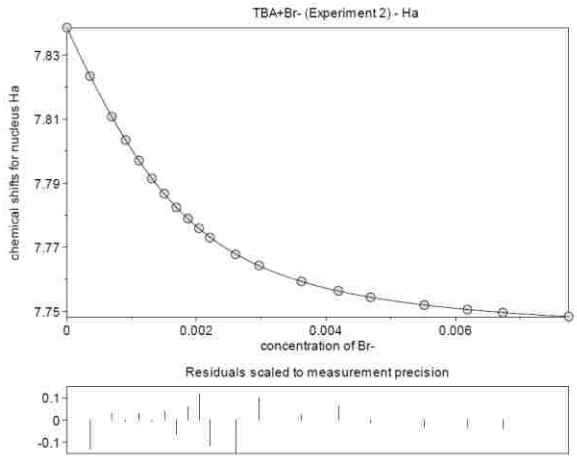
TBA+Br- (Experiment 2) - Ha
chemical shifts for nucleus Ha
7.83
7.81
7.79
7.77
7.75
0
0.002
0.004
0.006
concentration of Br-

Residuals scaled to measurement precision
0.1
0
-0.1

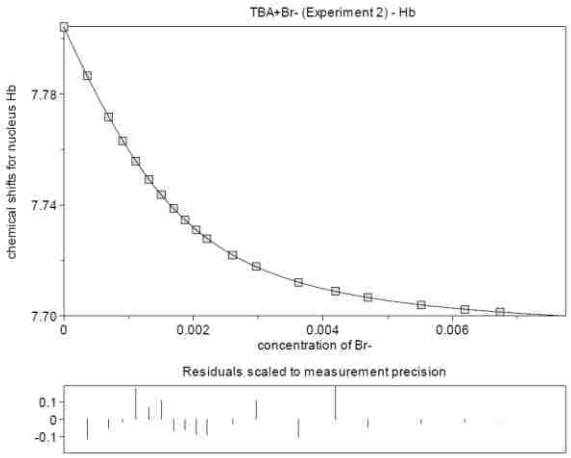
TBA+Br- (Experiment 2) - Hb
chemical shifts for nucleus Hb
7.78
7.74
7.70
0
0.002
0.004
0.006
concentration of Br-

Residuals scaled to measurement precision
0.1
0
-0.1

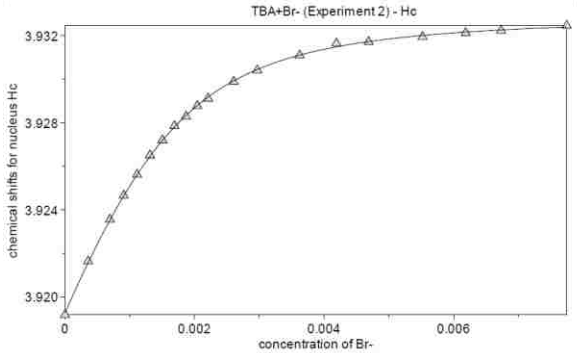
TBA+Br- (Experiment 2) - Hc
chemical shifts for nucleus Hc
3.932
3.928
3.924
3.920
0
0.002
0.004
0.006
concentration of Br-

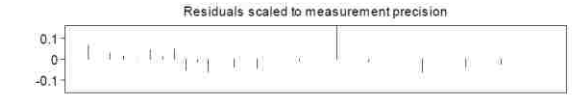
Residuals scaled to measurement precision
0.1
0
-0.1

XB1a-Br-Exp3

Point	[X-]	[R]	peak (ppm)	peak (ppm)	peak (ppm)
1	0	0.001643531	7.83859	7.80425	3.91918
2	0.00035677	0.001643531	7.8234	7.78646	3.92148
3	0.000693345	0.001643531	7.81042	7.77132	3.92345
4	0.000907341	0.001643531	7.80292	7.76258	3.92463
5	0.001113555	0.001643531	7.79637	7.75503	3.92566
6	0.001312404	0.001643531	7.79061	7.74836	3.92639
7	0.001504275	0.001643531	7.78581	7.74268	3.92728
8	0.001689531	0.001643531	7.78154	7.7378	3.92783
9	0.001868507	0.001643531	7.77811	7.73373	3.92847
10	0.002041517	0.001643531	7.77488	7.72999	3.92907
11	0.002208854	0.001643531	7.77205	7.72674	3.92934
12	0.002604139	0.001643531	7.76702	7.72095	3.93006
13	0.002969479	0.001643531	7.76366	7.71691	3.93054
14	0.003622973	0.001643531	7.75883	7.71151	3.93116
15	0.004190482	0.001643531	7.756	7.7084	3.93149
16	0.004687927	0.001643531	7.75406	7.70619	3.93168
17	0.005518825	0.001643531	7.75177	7.70379	3.93196
18	0.006185189	0.001643531	7.75052	7.70236	3.9321
19	0.006731488	0.001643531	7.74954	7.70138	3.93223
20	0.007745755	0.001643531	7.74835	-	3.93246

	model	raw value	std. dev.	final value
log β1	RG	3.5424	0.0201	3.54(2)
log β2	RG_2	5.9711	0.0477	5.97(5)

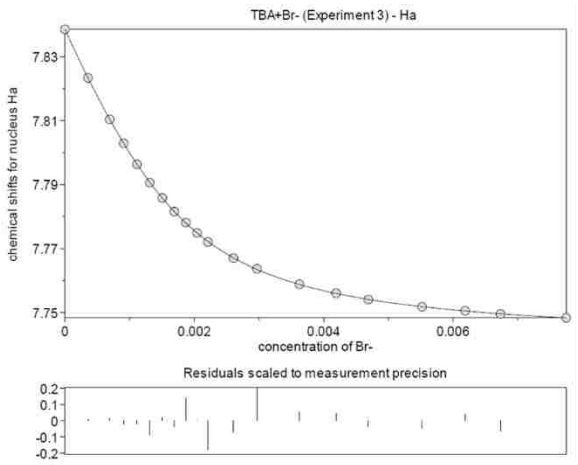
TBA+Br- (Experiment 3) - Ha
chemical shifts for nucleus Ha
7.83
7.81
7.79
7.77
7.75
0
0.002
0.004
0.006
concentration of Br-
Residuals scaled to measurement precision
0.2
0.1
0
-0.1
-0.2

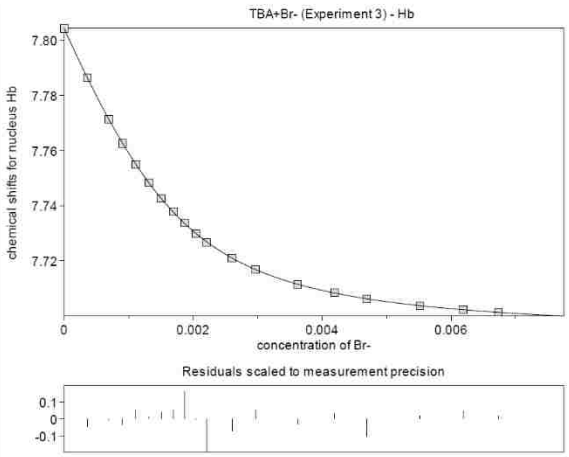
TBA+Br- (Experiment 3) - Hb
chemical shifts for nucleus Hb
7.80
7.78
7.76
7.74
7.72
0
0.002
0.004
0.006
concentration of Br-
Residuals scaled to measurement precision
0.1
0
-0.1

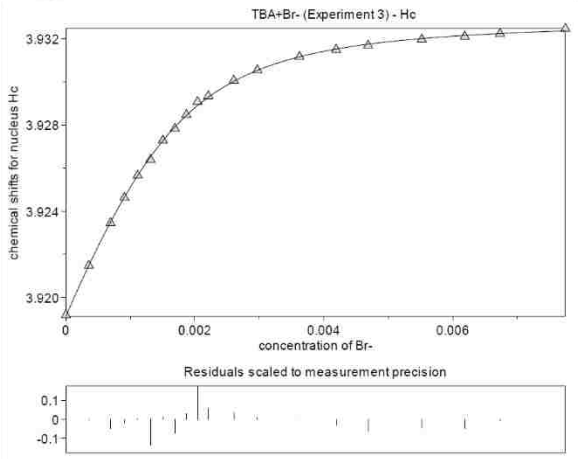
TBA+Br- (Experiment 3) - Hc
chemical shifts for nucleus Hc
3.932
3.928
3.924
3.920
0
0.002
0.004
0.006
concentration of Br-
Residuals scaled to measurement precision
0.1
0
-0.1

HB1-Br-Exp1

Point	[X-]	[R]	peak (ppm)	peak (ppm)
1	0	0.001807034	9.07959	7.75171
2	0.000588623	0.001807034	9.11551	7.76505
3	0.001154607	0.001807034	9.14662	7.77709
4	0.001699233	0.001807034	9.17378	7.78655
5	0.002223688	0.001807034	9.19717	7.79597
6	0.002729072	0.001807034	9.21833	7.80323
7	0.003216406	0.001807034	9.23761	7.81094
8	0.003686641	0.001807034	9.25419	7.81629
9	0.004140661	0.001807034	9.27092	7.82207
10	0.00457929	0.001807034	9.28558	7.82792
11	0.005003298	0.001807034	9.29713	7.8322
12	0.005413405	0.001807034	9.3095	7.83673
13	0.005810282	0.001807034	9.32007	7.84167
14	0.00619456	0.001807034	9.33163	7.84487
15	0.006566829	0.001807034	9.3402	7.84814
16	0.006927644	0.001807034	9.34898	7.85169
17	0.007277525	0.001807034	9.35709	7.85502
18	0.007782908	0.001807034	9.3686	7.85966
19	0.008422819	0.001807034	9.38203	7.86475
20	0.00902693	0.001807034	9.39361	7.8686
21	0.009598164	0.001807034	9.40672	7.8734
22	0.010139134	0.001807034	9.41521	7.87661
23	0.010776335	0.001807034	9.4271	7.88071
24	0.011373957	0.001807034	9.4371	7.88508

	model	raw value	std. dev.	final value
log β1	RG	2.3647	0.0254	2.36(3)
log β2	RG_2	3.6741	fixed	3.6741

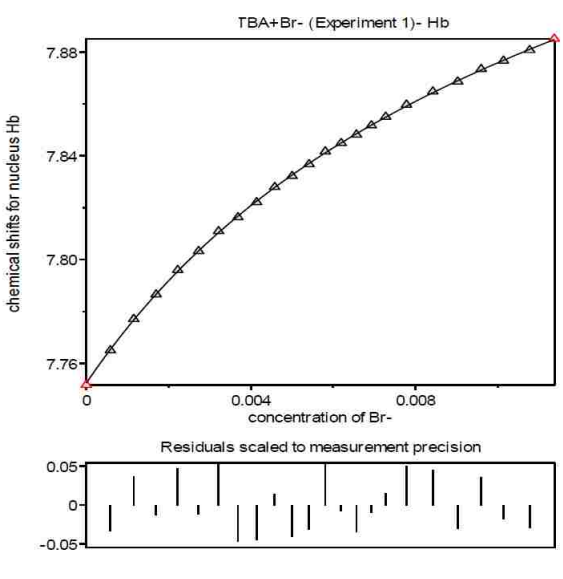
TBA+Br- (Experiment 1)- Hb
chemical shifts for nucleus Hb
7.88
7.84
7.80
7.76
0
0.004
0.008
concentration of Br-
Residuals scaled to measurement precision
0.05
0
-0.05

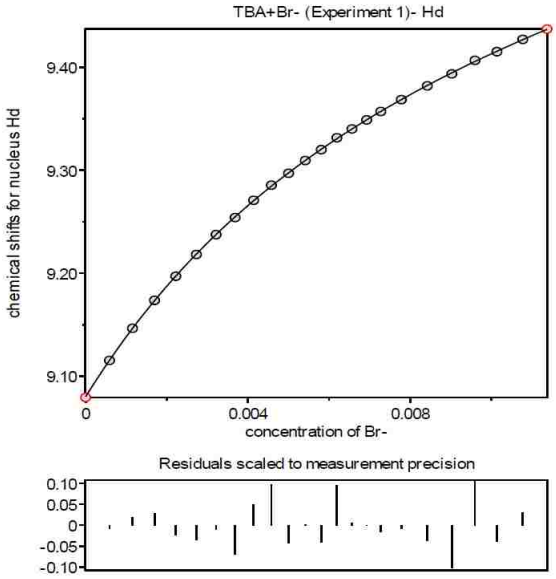
TBA+Br- (Experiment 1)- Hd
chemical shifts for nucleus Hd
9.40
9.30
9.20
9.10
0
0.004
0.008
concentration of Br-
Residuals scaled to measurement precision
0.10
0.05
0
-0.05
-0.10

HB1-Br-Exp2

Point	[X-]	[R]	peak (ppm)	peak (ppm)	peak (ppm)
1	0	0.001548886	9.07679	7.75144	3.94806
2	0.000483979	0.001548886	9.10887	7.76236	3.94899
3	0.000949344	0.001548886	9.13668	7.7726	3.95106
4	0.001397147	0.001548886	9.15996	7.78217	3.95294
5	0.001828366	0.001548886	9.18422	7.79033	3.95502
6	0.002243903	0.001548886	-	-	-
7	0.0026446	0.001548886	9.21855	7.80314	3.95711
8	0.003031238	0.001548886	9.23597	7.80939	3.95805
9	0.003404543	0.001548886	9.24867	7.81438	3.95863
10	0.003765194	0.001548886	9.26318	7.82007	3.96033
11	0.004113823	0.001548886	9.27528	7.82456	3.96102
12	0.004451022	0.001548886	9.28642	7.82892	3.96232
13	0.004777343	0.001548886	9.29732	7.83276	3.96292
14	0.005093305	0.001548886	9.30623	7.83623	3.96374
15	0.005399393	0.001548886	9.31494	7.83949	3.96432
16	0.005696063	0.001548886	9.32315	7.84255	3.96501
17	0.005983742	0.001548886	9.33131	7.84537	3.96567
18	0.006262835	0.001548886	9.33856	7.84847	3.9662
19	0.006796751	0.001548886	9.35202	7.85315	3.96708
20	0.007422142	0.001548886	9.36667	7.85851	3.96824

	model	raw value	std. dev.	final value
log β1	RG	2.3659	0.0387	2.37(4)
log β2	RG_2	3.6371	fixed	3.6371

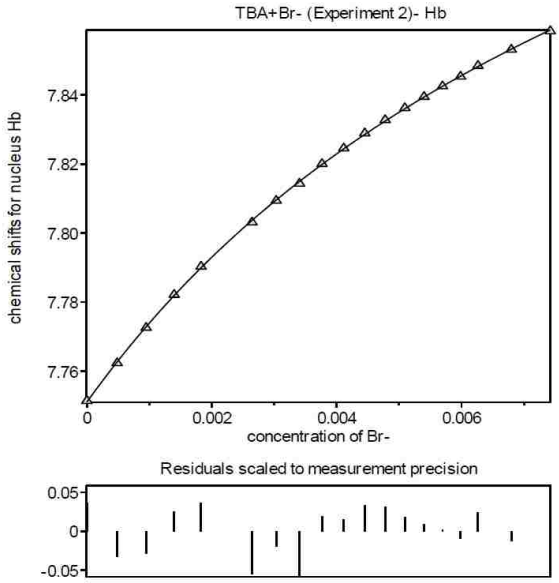
TBA+Br- (Experiment 2)- Hb
chemical shifts for nucleus Hb
7.84
7.82
7.80
7.78
7.76
0
0.002
0.004
0.006
concentration of Br-
Residuals scaled to measurement precision
0.05
0
-0.05

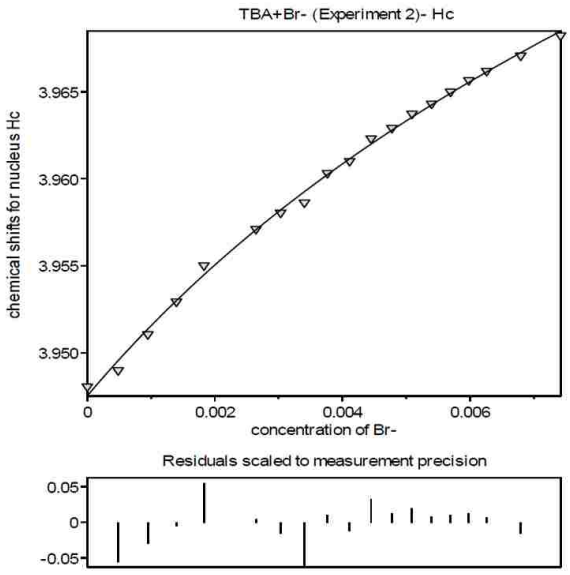
TBA+Br- (Experiment 2)- Hc
chemical shifts for nucleus Hc
3.965
3.960
3.955
3.950
0
0.002
0.004
0.006
concentration of Br-
Residuals scaled to measurement precision
0.05
0
-0.05

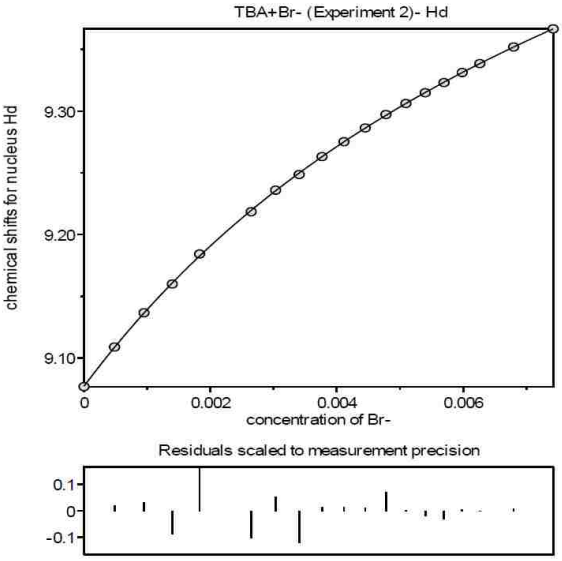
TBA+Br- (Experiment 2)- Hd
chemical shifts for nucleus Hd
9.30
9.20
9.10
0
0.002
0.004
0.006
concentration of Br-
Residuals scaled to measurement precision
0.1
0
-0.1

HB1-Br-Exp3

Point	[X-]	[R]	peak (ppm)	peak (ppm)	peak (ppm)	peak (ppm)
1	0	0.00167796	9.07789	7.89913	7.75033	3.94705
2	0.00051014	0.00167796	9.10984	7.90485	7.76216	3.94985
3	0.00100066	0.00167796	9.13869	7.9104	7.77353	3.95221
4	0.001472669	0.00167796	9.16194	7.91399	7.78199	3.95323
5	0.001927196	0.00167796	9.18545	7.919	7.79167	3.95601
6	0.002365196	0.00167796	9.20347	7.92151	7.79741	3.95599
7	0.002787552	0.00167796	9.222	7.92473	7.80435	3.95733
8	0.003195089	0.00167796	-	-	-	-
9	0.003588572	0.00167796	9.25256	7.9307	7.81592	3.95955
10	0.003968718	0.00167796	9.26693	7.93284	7.82142	3.96059
11	0.004336192	0.00167796	9.27935	7.93492	7.82615	3.96181
12	0.004691617	0.00167796	9.29033	7.93745	7.8303	3.9626
13	0.005035578	0.00167796	9.30124	7.93908	7.83439	3.96352
14	0.005368618	0.00167796	9.31139	7.94107	7.83802	3.96423
15	0.005691252	0.00167796	9.32032	7.94269	7.84151	3.96487
16	0.006003958	0.00167796	9.32871	7.94426	7.84467	3.96558
17	0.006307188	0.00167796	9.3372	7.9459	7.84771	3.96612
18	0.006601367	0.00167796	9.34471	7.94713	7.85077	3.96706
19	0.007164143	0.00167796	9.35742	7.94971	7.85539	3.96775
20	0.007823339	0.00167796	9.37347	7.95241	7.86185	3.97002

	model	raw value	std. dev.	final value
log β1	RG	2.3481	0.0339	2.35(3)
log β2	RG_2	3.6229	fixed	3.6229

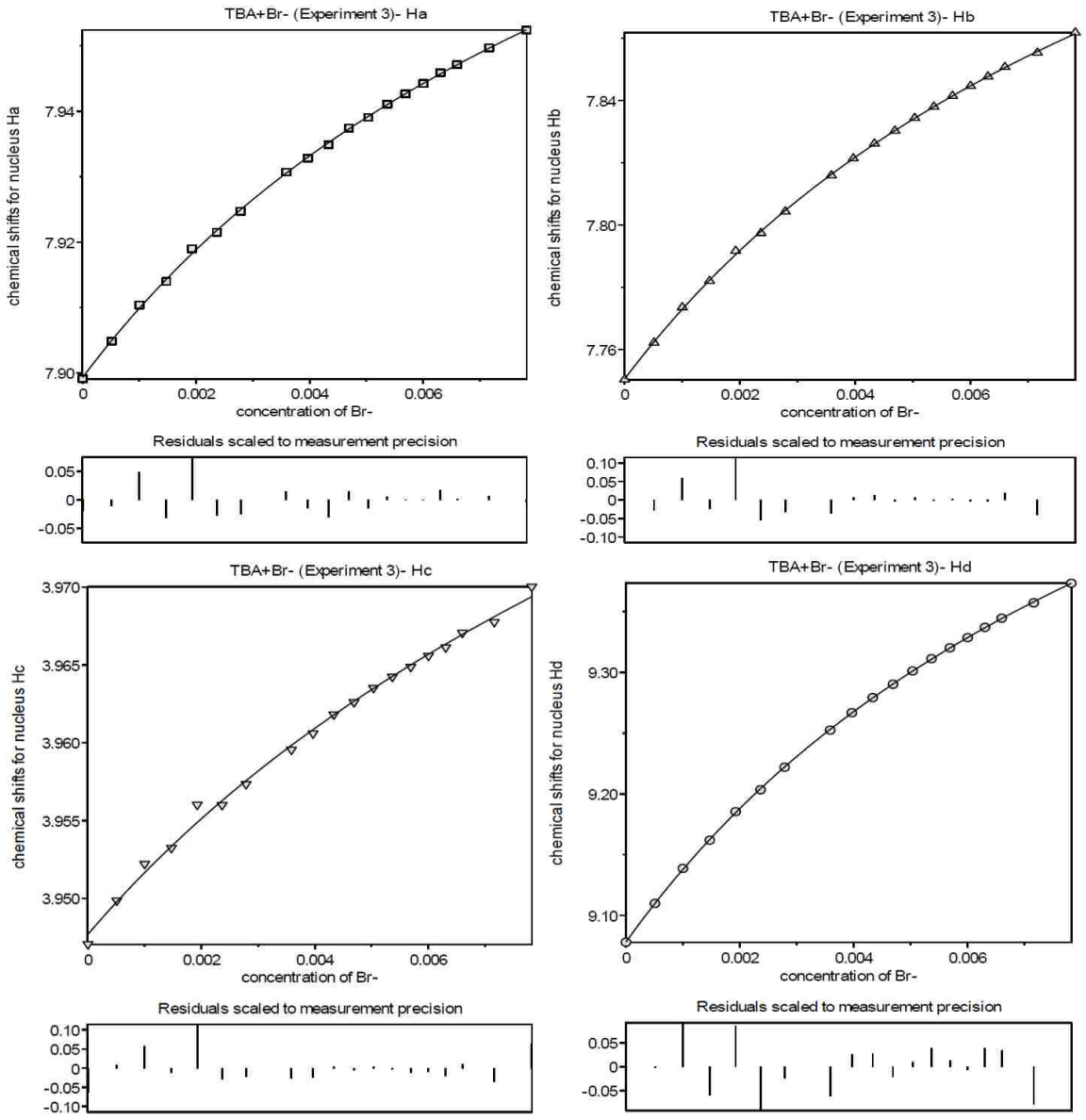
TBA+Br- (Experiment 3)- Ha
chemical shifts for nucleus Ha
7.94
7.92
7.90
0
0.002
0.004
0.006
concentration of Br-
Residuals scaled to measurement precision
0.05
0
-0.05
TBA+Br- (Experiment 3)- Hb
chemical shifts for nucleus Hb
7.84
7.80
7.76
0
0.002
0.004
0.006
concentration of Br-
Residuals scaled to measurement precision
0.10
0.05
0
-0.05
-0.10
TBA+Br- (Experiment 3)- Hc
chemical shifts for nucleus Hc
3.970
3.965
3.960
3.955
3.950
0
0.002
0.004
0.006
concentration of Br-
Residuals scaled to measurement precision
0.10
0.05
0
-0.05
-0.10
TBA+Br- (Experiment 3)- Hd
chemical shifts for nucleus Hd
9.30
9.20
9.10
0
0.002
0.004
0.006
concentration of Br-
Residuals scaled to measurement precision
0.05
0
-0.05

***General crystallographic information for* XB1a·2I, XB1b, and XB2b, and HB1**

XB1a·2I – CCDC 1407398

X-ray diffraction data for **XB1a·2I** were collected at 100K on a Bruker D8 Venture using CuKα (λ = 1.54178) radiation. Data have been corrected for absorption using SADABS[1] area detector absorption correction program. Using Olex2[2], the structure was solved with the ShelXT structure solution program using Direct Methods and refined with the ShelXL refinement package using least squares minimization. All non-hydrogen atoms were refined with anisotropic thermal parameters. Hydrogen atoms were refined in calculated positions in a ridged group model with isotropic thermal parameters U(H) = 1.2Ueq (C) for all C(H) groups and U(H)=1.5Ueq (C) for all C(H,H,H) groups. Fourteen additional acetonitrile molecules per unit cell are highly disordered and were treated by SQUEEZE.[3] The correction of the X-ray data by SQUEEZE, 297 electrons per unit cell, is close to the required value for fourteen acetonitrile molecules in the unit cell, 308 electrons per unit cell. Partial degradation of **XB1a·2I** has been observed in solution when in the presence of iodide and is present in the solid-state. Attempts to collect a data set without the partial degradation product have been unsuccessful. The decomposition is limited to one imidazolium and is not present throughout the entire crystal as examination of the difference map reveals an undeniable presence of both the intact imidazolium and residual electron density corresponding to the unknown

[1] G. M. Sheldrick, SADABS: Area Detector Absorption Correction; University of Göttingen: Göttingen, Germany, 2001.
[2] Dolomanov, O.V.; Bourhis, L.J.; Gildea, R.J.; Howard, J.A.K.; Puschmann, H., OLEX2: A complete structure solution, refinement and analysis program (2009). J. Appl. Cryst., 42, 339-341.
[3] P. Van der Sluis, A. L. Spek, Acta Crys. A, 1990, A46, 194-201.

degraded product. The presented structure models the intact imidazolium, and disregards the decomposition product as its identity eludes us, resulting in a large residual electron density peak that resides 0.800 Å from C33 of the imidazolium. Additionally, to model the intact imidazolium the coordinates of C33, nearest the large residual electron density from the degradation, were fixed. Calculations and refinement of structures were carried out using APEX,[4] SHELXTL,[5] Olex, and Platon.[6]

Crystallographic Data for **XB1a·2I**: C36H41I4N5, M =1051.34, monoclinic, space group *P*21/c, a = 26.008(3), b = 27.034(3), c = 12.7014(12), β = 99.978(2), V = 8795.2(15), Z = 8, T = 100 K, μ(MoKα) = 2.861 mm-1, ρcalcd =1.588 g ml-1, 2Θmax = 50.872, 97788 reflections collected, 16195 unique (Rint = 0.0678, Rsigma = 0.0503), R1 = 0.0910 (I > 2σ(I)), wR2 = 0.2147 (all data).

XB1b – CCDC 1407399

X-ray diffraction data for **XB1b** were collected at 100 K on a Bruker D8 Venture using MoKα-radiation (λ=0.71073 Å) radiation. Data have been corrected for absorption using SADABS area detector absorption correction program. Using Olex2, the structure was solved with the ShelXT structure solution program using Direct Methods and refined with the ShelXL refinement package using least squares minimization. All non-hydrogen atoms were refined with anisotropic thermal parameters. Hydrogen atoms were placed in calculated positions using a ridged group model with isotropic thermal parameters.

[4] Bruker (2007). APEX2. Bruker AXS Inc., Madison, Wisconsin, USA.
[5] Sheldrick, G. M. A short history of SHELX (2008). Acta Cryst. A64, 112-122.
[6] Spek, A. L. (2009). Acta Cryst. D65, 148-155

Calculations and refinement of structures were carried out using APEX, SHELXTL, and Olex2 software.

Crystallographic Data for **XB1b** C28H22F6I2N4O6S2,M = 942.41, triclinic, space group P-1, a = 10.2943(6), b = 12.7728(8), c = 13.5306(8), α = 108.062(2), β = 93.633(2), γ = 101.697(2), V = 1641.01(17), Z = 2, T = 100 K, μ(MoKα) = 2.126 mm-1, , ρcalcd = 1.907 g ml-1, 2Θmax = 61.19, 51469 reflections collected, 10096 unique (Rint = 0.0402, Rsigma = 0.0320), R1 = 0.0343 (I > 2σ(I)), wR2 = 0.0802 (all data).

HB1 – CCDC 1407397

X-ray diffraction data for **HB1** were collected at 100 K on a Bruker D8 Venture using MoKα-radiation (λ=0.71073 Å) radiation. Data have been corrected for absorption using SADABS area detector absorption correction program. Using Olex2, the structure was solved with the ShelXT structure solution program using Direct Methods and refined with the ShelXL refinement package using least squares minimization. All non-hydrogen atoms were refined with anisotropic thermal parameters. Hydrogen atoms can be found from the residual density maps but were finally placed in calculated positions using a ridged group model with isotropic thermal parameters. Hydrogen atoms contributing to hydrogen bonding were located and refined using isotropic thermal parameters. Calculations and refinement of structures were carried out using APEX, SHELXTL, and Olex2 software.

Crystallographic Data for **HB1** C40H48F6N4O7S2, M =874.94, triclinic, space group P-1, a = 9.8222(7), b = 13.8891(10), c = 16.2284(12), α = 92.339(2), β = 94.211(2), γ = S156

109.170(2), V = 2080.5(3), Z = 2, T = 100 K, μ(MoKα) = 0.208 mm-1, ρcalcd =1.397 g ml-1, 2Θmax = 56.564, 77593 reflections collected, 10151 unique (Rint = 0.0452, Rsigma = 0.0296), R1 = 0.0460 (I > 2σ(I)), wR2 = 0.1190 (all data).

Urea Project

Syntheses

3-phenylpyridin-2-amine (3c) A 100 mL Schlenk flask was charged with 3-bromopyridin-2-amine (1.000 g, 1.0 equiv, 5.78 mmol), phenylboronic acid (0.775 g, 1.1 equiv, 6.36 mmol), $PdCl_2(PPh_3)_2$ (0.244 g,0.06 equiv, 0.347 mmol) and nitrogen sparged 1,4-dioxane (35 mL). The solution was stirred for 30 min at rt under N_2, after which Na_2CO_3 (19.1 mL, 1 $M_{(aq)}$, 3.3 equiv, 19.1 mmol) was added, a condensing column was affixed to the flask, and the solution was brought to reflux. The solution was stirred at reflux for 4 h, allowed to cool to rt, and concentrated under reduced pressure. The green/black residue was redissolved in EtOAc, washed with DI H_2O, and dried with brine. The EtOAc was separated, dried with anhydrous $MgSO_4$, and concentrated under reduced pressure to give a maroon/black residue. The crude material was purified by normal phase flash chromatography (R_f = 0.14 [fluoresces blue under 256 nm], 1:1 hexanes:EtOAc) to give 0.79 g (81%)of **3c** as a beige powder (mp 105 °C). ^{1}H NMR (400 MHz, $CDCl_3$) δ 8.08 (dd, *J* = 5.2, 1.5 Hz, 1H), 7.48-7.42 (m, 4H), 7.40-7.35 (m, 2H), 6.75 (dd, *J* = 7.7, 5.1 Hz, 1H), 4.56 (s, br, 2H). $^{13}C\{^1H\}$ NMR (101 MHz, $CDCl_3$) δ 156.00, 147.46, 138.26, 137.96, 129.21, 128.82, 127.90, 121.99, 114.64. HRMS-QTOF: calcd for $C_{11}H_{10}N_2$ $(M + H)^+$ 171.092, found 171.091.

1-phenyl-3-(pyridin-2-yl)urea (2a) A 250 mL round bottom flask was charged with 2-aminopyridine (4.000 g, 1.0 equiv, 42.5 mmol), phenylisocyanate (5.08 g, 1.1 equiv, 46.7 mmol) and anhydrous DCM (100 mL). A condensing column was affixed and the solution was stirred at reflux for 1 hour under N_2 (a white precipitate formed after minutes). The

solution was cooled to rt, and then -20 °C. The chilled solution was filtered, and the solid was washed with cold DCM. The product was dried on vacuum to yield 9.07 g (66%) of a white fluffy solid (mp 189 °C). ^{1}H NMR (400 MHz, $CDCl_3$) δ 11.79 (s, 1H), 8.27 (d, *J* = 4.3 Hz, 1H), 8.09 (s, 1H), 7.67-7.60 (m, 3H), 7.35 (t, *J* = 7.7 Hz, 2H), 7.09 (t, *J* = 7.4 Hz, 1H), 6.95 (t, *J* = 5.9 Hz, 1H), 6.83 (d, *J* = 8.2 Hz, 1H). ^{13}C{^{1}H} NMR (101 MHz, $CDCl_3$) δ 153.86, 153.25, 146.10, 138.78, 138.74, 129.07, 123.55, 120.42, 117.34, 112.41. HRMS-QTOF: calcd for $C_{12}H_{11}N_3O$ $(M + H)^+$ 214.097, found 214.095.

1-(3-methylpyridin-2-yl)-3-phenylurea (2b) A 50 mL round bottom flask was charged with 2-amino-3-methylpyridine (1.00 mL, 9.92 mmol), phenylisocyanate (1.08 mL, 9.92 mmol) and anhydrous DCM (20 mL). A condensing column was affixed and the solution was stirred at reflux under N_2 for 24 h. The solution was concentrated under reduced pressure, and the residue was rinsed with benzene. The rinsed material was placed on vacuum to give 2.25 g (85%) of white needles (mp 170 °C). ^{1}H NMR (400 MHz, $CDCl_3$) δ 12.14 (s, 1H), 8.14 (d, *J* = 4.9 Hz, 1H), 7.61 (d, *J* = 8.0 Hz, 2H), 7.48 (d, *J* = 7.3 Hz, 1H), 7.34 (t, *J* = 7.7 Hz, 2H), 7.09 (t, *J* = 7.5 Hz, 2H), 6.89 (dd, *J* = 7.2, 5.2 Hz, 1H), 6.79 (s, br, 1H), 2.27 (s, 3H). ^{13}C{^{1}H} NMR (101 MHz, $CDCl_3$) δ 152.90, 151.41, 143.71, 139.39, 138.67, 129.04, 123.54, 120.42, 119.25, 117.34, 17.10. HRMS-QTOF: calcd for $C_{13}H_{13}N_3O$ $(M + H)^+$ 228.113, found 228.112.

1-phenyl-3-(3-phenylpyridin-2-yl)urea (2c) A 50 mL round bottom flask was charged with **3c** (0.764 g, 1.0 equiv, 4.49 mmol), phenylisocyanate (0.536 mL, 1.1 equiv, 4.93 mmol), and DCM (20 mL). A condensing column was affixed, and the solution was stirred at reflux, under N_2, for 24 h. The solution was concentrated under reduced pressure to a

clear yellow oil, and the crude material was purified via normal phase flash chromatography (R_f = 0.28, DCM) to give 1.213 g (93%) of white powder (mp 132 °C). ^{1}H NMR (400 MHz, $CDCl_3$) δ 12.06 (s, 1H), 8.29 (d, *J* = 5.0 Hz, 1H), 7.60 (d, *J* = 8.1 Hz, 2H) 7.56-7.44 (m, 4H), 7.39 (d, *J* = 7.0 Hz, 2H), 7.34 (t, *J* = 7.7 Hz, 2H), 7.10-7.01 (m, 3H). $^{13}C\{^1H\}$ NMR (101 MHz, $CDCl_3$) δ 152.52, 150.09, 145.18, 139.30, 138.64, 135.64, 129.84, 129.13, 129.08, 129.05, 125.15, 123.55, 120.39, 117.38. HRMS-QTOF: calcd for $C_{18}H_{15}N_3O$ $(M + H)^+$ 290.129, found 290.130.

2-(3-phenylureido)pyridin-1-ium chloride (1a·Cl) A 250 mL Schlenk tube was charged with **2a** (1.000 g, 4.69 mmol) and 140 mL MeOH. A glass tube with a fritted end was used to bubble HCl vapor through the solution for 2 h. The solution was then concentrated under reduced pressure and the white powder was dissolved in a minimal amount of boiling MeCN. The solution was allowed to cool and partially evaporate overnight. The solution was decanted, and the clear colorless crystals were washed with cold MeCN. They were crushed and dried on vacuum to give 0.973 g (82%) of white powder (mp 160 °C). ^{1}H NMR (400 MHz, $CDCl_3$) δ 15.13 (s, br, 1H), 13.51 (s, 1H), 9.94 (s, 1H), 8.06 (d, *J* = 5.9 Hz, 1H), 8.02 (d, *J* = 8.1 Hz, 1H), 7.68 (d, *J* = 8.4 Hz, 1H), 7.51 (d, *J* = 8.0 HZ, 2H), 7.31 (t, *J* = 7.8 Hz, 2H), 7.19 (t, *J* = 6.9 Hz, 1H), 7.13 (t, *J* = 7.8 Hz, 1H). $^{13}C\{^1H\}$ NMR (101 MHz $CDCl_3$) δ 153.60, 150.13, 145.11, 136.65, 136.32, 129.09, 124.78, 120.54, 117.41, 116.22. HRMS-QTOF: calcd for $C_{12}H_{12}N_3O^+$ $(M – Cl)^+$ 214.097, found 214.101.

3-methyl-2-(3-phenylureido)pyridin-1-ium chloride (1b·Cl) A 250 mL Schlenk tube was charged with **2b** (1.482 g, 6.52 mmol) and 50 mL MeOH. A glass tube with a fritted end

was used to bubble HCl vapor through the solution for 2 h. The solution was then concentrated under reduced pressure and the white powder was dissolved in a minimal amount of boiling MeCN. The solution was allowed to cool and partially evaporate overnight. The solution was decanted, and the clear colorless crystals were washed with cold MeCN. They were crushed and dried on vacuum to give 0.973 (77%) of white powder (mp 200 °C). ^{1}H NMR (400 MHz, $CDCl_3$) δ 15.65 (s, br, 1H), 11.85 (s, 1H), 11.40 (s, 1H), 8.00 (t, *J* = 5.0 Hz, 1H), 7.85 (d, *J* = 7.4 Hz, 1H), 7.54 (d, *J* = 7.8 Hz, 2H), 7.28 (t, *J* = 8.3 Hz, 2H), 7.13-7.08 (m, 2H), 2.69 (s, 3H). $^{13}C\{^{1}H\}$ NMR (101 MHz, $CDCl_3$) δ 154.58, 150.06, 145.38, 136.91, 132.78, 129.04, 126.57, 124.66, 120.17, 117.45, 18.60. HRMS-QTOF: calcd for $C_{13}H_{14}N_3O^+$ $(M - Cl)^+$ 228.113, found 228.114.

3-phenyl-2-(3-phenylureido)pyridin-1-ium chloride (1c·Cl) A 250 mL Schlenk tube was charged with **2c** (0.634 g, 2.16 mmol) and 50 mL MeOH. A glass tube with a fritted end was used to bubble HCl vapor through the solution for 2 h. The solution was then concentrated under reduced pressure and the white powder was dissolved in a minimal amount of boiling MeCN. The solution was then cooled and partially evaporate overnight. The solution was decanted, and the clear colorless crystals were washed with cold MeCN. They were crushed and dried on vacuum to give 0.425 g (60%) of white powder (mp 186 °C). ^{1}H NMR (400 MHz, $CDCl_3$) δ 15.81 (s, br, 1H), 11.92 (s, 1H), 10.99 (s, 1H), 8.10 (d, *J* = 5.9 Hz, 1H), 7.92 (d, *J* = 7.5 Hz, 1H), 7.59-7.46 (m, 7H), 7.26-7.19 (m, 3H), 7.06 (t, *J* = 7.3 Hz, 1H). $^{13}C\{^{1}H\}$ NMR (101 MHz, $CDCl_3$) δ 154.39, 148.91, 145.72, 137.11, 135.06, 131.13, 130.49, 130.25, 130.05, 129.36, 128.97, 124.47, 120.40, 117.49. HRMS-QTOF: calcd for $C_{18}H_{16}N_3O^+$ $(M - Cl)^+$ 290.129, found 290.133.

2-(3-phenylureido)pyridin-1-ium tetrakis(3,5-bis(trifluoromethyl)phenyl)borate (1a·BARF) A 50 mL round bottom flask was charged with **1a·Cl** (0.200 g, 0.801 mmol), $NaBArF_{24}$ (0.710 g, 0.801 mmol), and anhydrous DCM (30 mL). The solution stirred at rt, under N_2 overnight. The solution was then cooled to -20 °C, and the fine precipitate was filtered. The filtrate was concentrated under reduced pressure, to yield a viscous pale-yellow oil. The oil was dried under vacuum, resulting in a foam. The foam was broken into a powder, dried under vacuum at 50 °C, to yield 0.720 g (83%) of fine white powder (mp 143 °C). ^{1}H NMR (400 MHz, CD_3CN) δ 14.46 (s, br, 1H), 9.46 (s, br, 1H), 8.29-8.22 (m, 2H), 8.19 (s, br, 1H), 7.69 (s, 8H), 7.67 (s, 4H), 7.48 (d, *J* = 7.7 Hz, 2H), 7.41 (t, *J* = 7.4 Hz, 3H), 7.34 (d, *J* = 8.8 Hz, 1H), 7.22 (t, *J* = 7.3 Hz, 1H). $^{13}C\{^1H\}$ NMR (101 MHz, CD_3CN) δ 162.60 (q, $^1J_{B-C}$ = 49.5 Hz), 153.83, 150.50, 147.61, 138.04, 137.49, 135.67, 130.14, 129.94 (qq, $^1J_{F-C}$ = 31.3, 2.0 Hz), 129.52, 126.14, 122.63 (q, $^2J_{C-F}$ = 272.7 Hz), 122.02, 119.95, 116.50. ^{19}F NMR (470 MHz, CD_3CN) δ -63.68. HRMS-QTOF: calcd for $C_{12}H_{12}N_3O^+$ $(M - C_{32}H_{12}BF_{24})^+$ 214.097, found 214.097.

3-methyl-2-(3-phenylureido)pyridin-1-ium tetrakis(3,5-bis(trifluoromethyl)phenyl)borate (1b·BARF) A 100 mL round bottom flask was charged with **1b·Cl** (0.422 g, 1.60 mmol), $NaBArF_{24}$ (1.42 g, 1.60 mmol), and anhydrous DCM (55 mL). The solution was stirred at rt, under N_2 overnight. The solution was then cooled to -20 °C, and the fine precipitate was filtered. The filtrate was concentrated under reduced pressure, to yield a viscous pale-yellow oil. The oil was dried under vacuum, resulting in a foam. The foam was broken into a powder, dried under vacuum at 50 °C, to yield 1.746 g (86%) of fine white powder (mp 126 °C). ^{1}H NMR (400 MHz,

CD_3CN) δ 14.64 (s, br, 1H), 8.45 (s, br, 1H), 8.22 (s, br, 1H), 8.15 (t, *J* = 6.5 Hz, 2H), 7.69 (s, 8H), 7.67 (s, 4H), 7.50 (d, *J* = 7.7 Hz, 2H), 7.42 (t, *J* = 7.5 Hz, 2H), 7.37 (t, *J* = 7.1 Hz, 1H), 7.22 (t, *J* = 7.3 Hz, 1H), 2.41 (s, 3H). $^{13}C\{^1H\}$ NMR (101 MHz, CD_3CN) δ 162.60 (q, $^1J_{B-C}$ = 50.0 Hz), 153.76, 149.28, 147.55, 137.53, 135.65, 135.54, 130.23, 129.92 (qq, $^1J_{F-C}$ = 31.8, 2.8 Hz), 129.50, 126.03, 125.93, 122.73 (q, $^2J_{C-F}$ = 272.8 Hz), 121.22, 119.65, 16.60. ^{19}F NMR (470 MHz, cd_3cn) δ -63.58 (s). HRMS-QTOF: calcd for $C_{13}H_{14}N_3O^+$ $(M - C_{32}H_{12}BF_{24})^+$ 228.113, found 228.115.

3-phenyl-2-(3-phenylureido)pyridin-1-ium tetrakis(3,5-bis(trifluoromethyl)phenyl)borate (1c·BARF) A 50 mL round bottom flask was charged with **1c·Cl** (0.200 g, 0.614 mmol), $NaBArF_{24}$ (0.544 g, 0.614 mmol), and anhydrous DCM (30 mL). The solution was allowed to stir at rt, under N_2 overnight. The solution was then cooled to -20 °C, and the fine precipitate was filtered. The filtrate was concentrated under reduced pressure, to yield a viscous pale-yellow oil. The oil was dried under vacuum, resulting in a foam. The foam was broken into a powder, dried under vacuum at 50 °C, to yield 0.708 g (82%) of fine white powder (mp 132 °C). ^1H NMR (400 MHz, CD_3CN) δ 14.94 (s, br, 1H), 8.46 (s, br 1H), 8.40 (s, br, 1H), 8.30 (dd, *J* = 6.1, 1.4 Hz, 1H), 8.17 (dd, *J* = 4.6, 1.4 H, 1H), 7.69 (s, 8H), 7.67 (s, 4H), 7.65-7.62 (m, 3H), 7.52-7.49 (m, 3H), 7.43 (d, *J* = 7.8 Hz, 2H), 7.38 (t, *J* = 8.4 Hz, 2H), 7.18 (t, *J* = 7.2 Hz, 1H). $^{13}C\{^1H\}$ NMR (101 MHz, CD_3CN) δ 162.57 (q, $^1J_{B-C}$ = 50.1 Hz), 153.74, 148.90, 147.61, 137.54, 137.24, 135.65, 132.60, 131.24, 131.02, 130.28, 130.20, 129.93 (qq, $^1J_{F-C}$ = 31.8, 2.9 Hz), 129.82, 129.50, 125.95, 122.73 (q, $^2J_{F-C}$ = 272.7 Hz), 121.05, 119.88. ^{19}F NMR

(470 MHz, cd_3cn) δ -63.68 (s). HRMS-QTOF: calcd for $C_{18}H_{16}N_3O^+$ $(M - C_{32}H_{12}BF_{24})^+$ 290.129, found 290.130.

Spectra

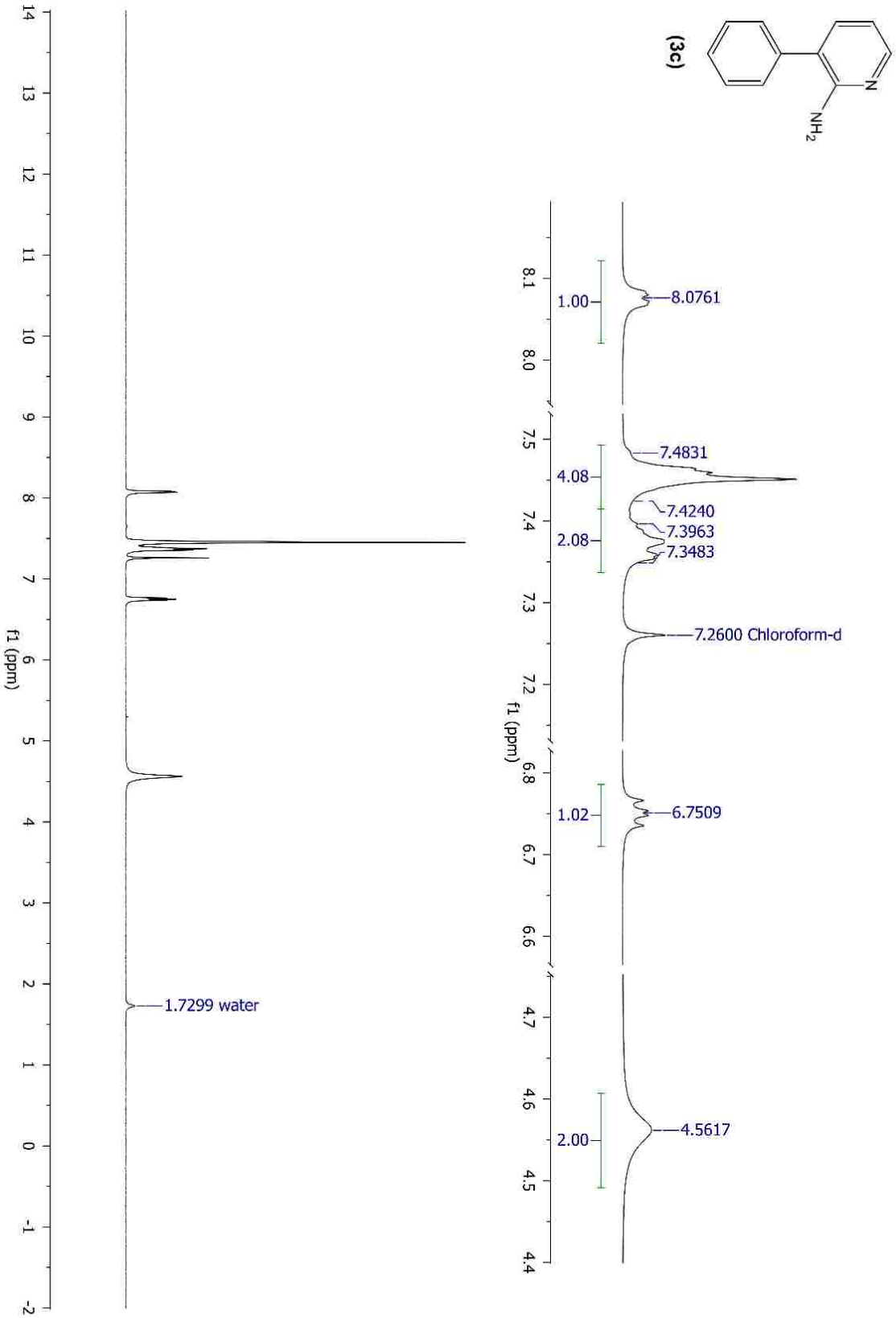
(3c)
N
NH2
f1 (ppm)
1.7299 water
8.0761
7.4831
7.4240
7.3963
7.3483
7.2600 Chloroform-d
6.7509
4.5617
1.00
4.08
2.08
1.02
2.00

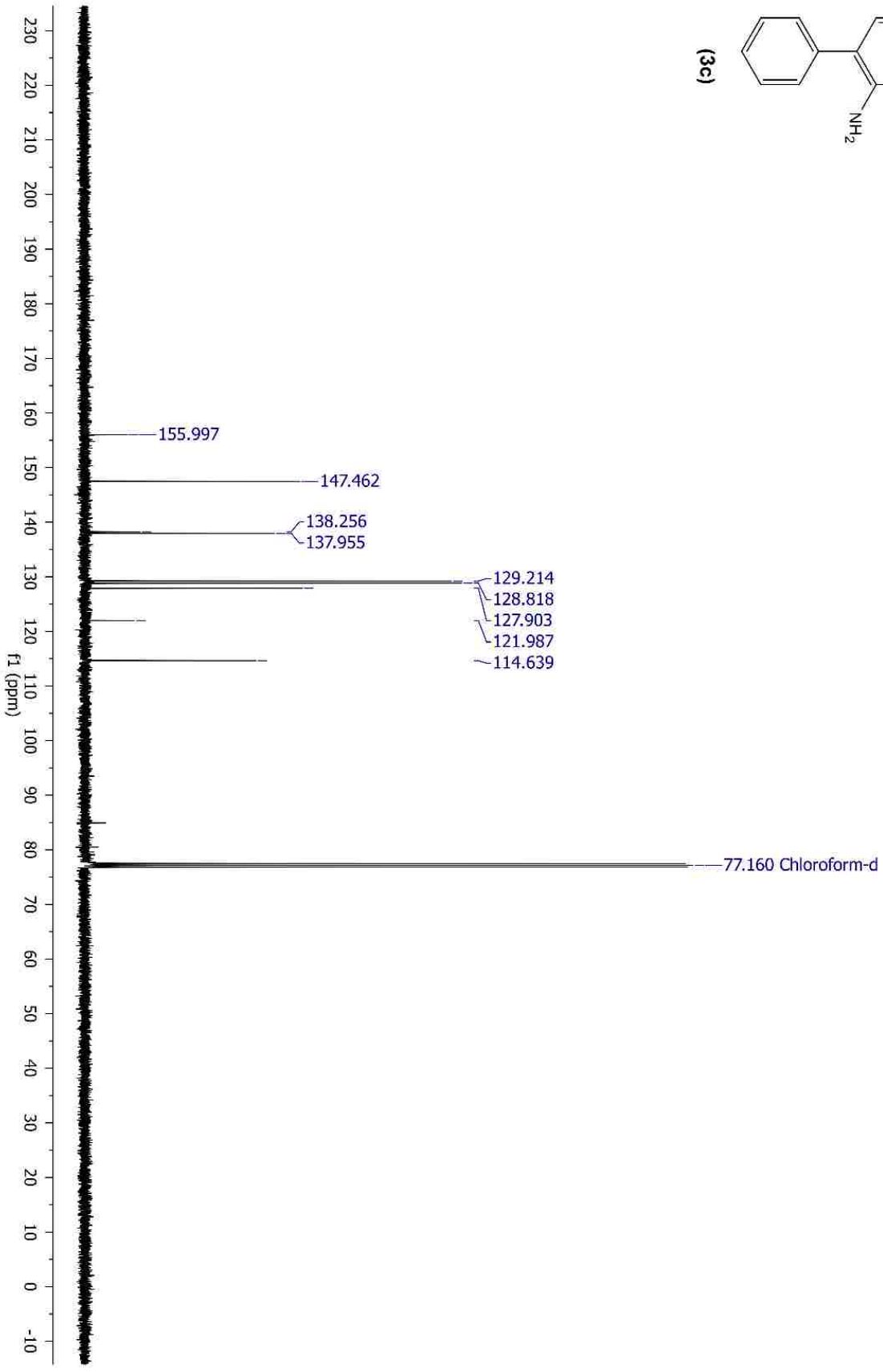
(3c)
NH2
N
155.997
147.462
138.256
137.955
129.214
128.818
127.903
121.987
114.639
77.160 Chloroform-d
f1 (ppm)
230
220
210
200
190
180
170
160
150
140
130
120
110
100
90
80
70
60
50
40
30
20
10
0
-10

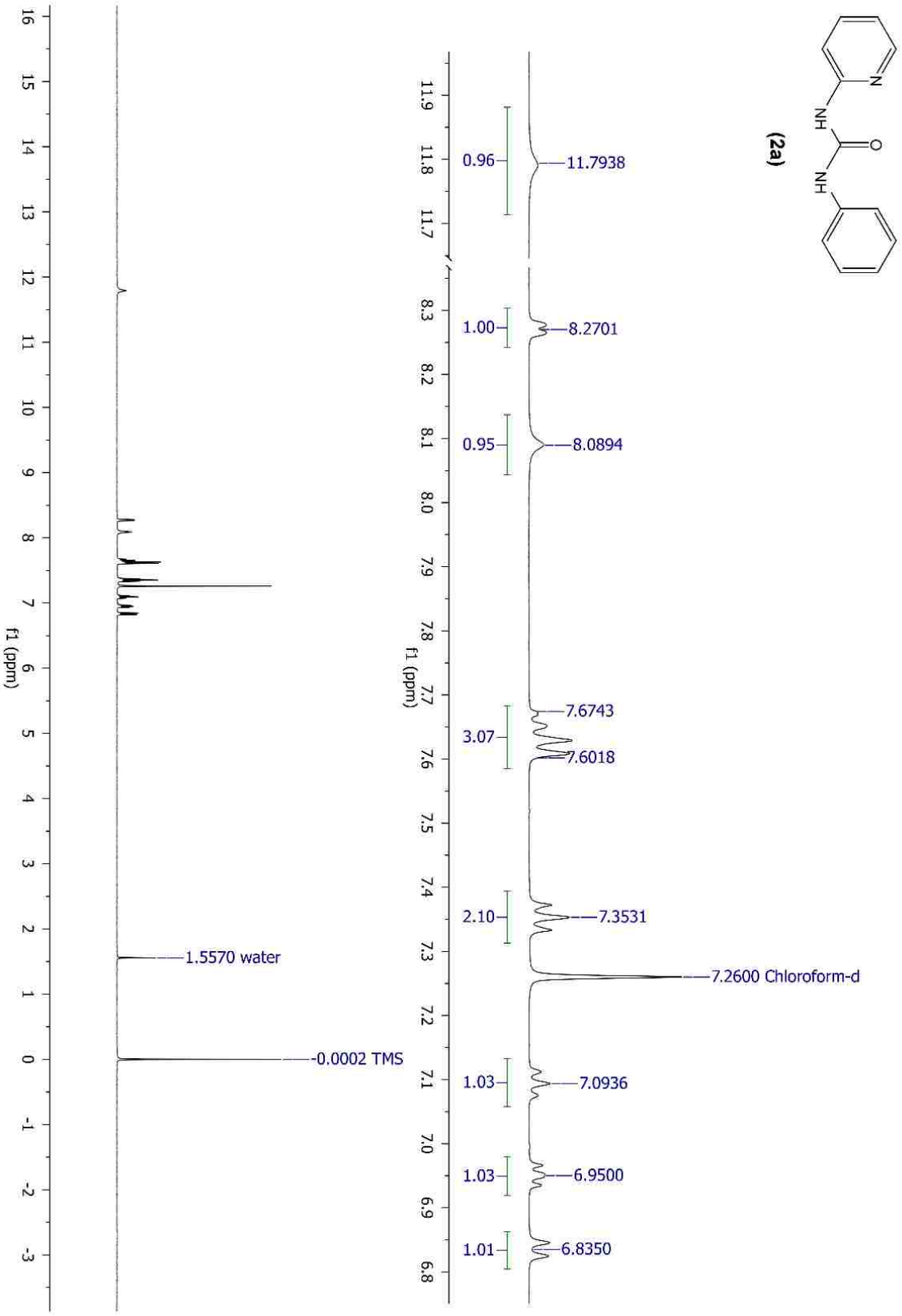
(2a)
11.7938
8.2701
8.0894
7.6743
7.6018
7.3531
7.2600 Chloroform-d
7.0936
6.9500
6.8350
1.5570 water
-0.0002 TMS
0.96
1.00
0.95
3.07
2.10
1.03
1.03
1.01
f1 (ppm)

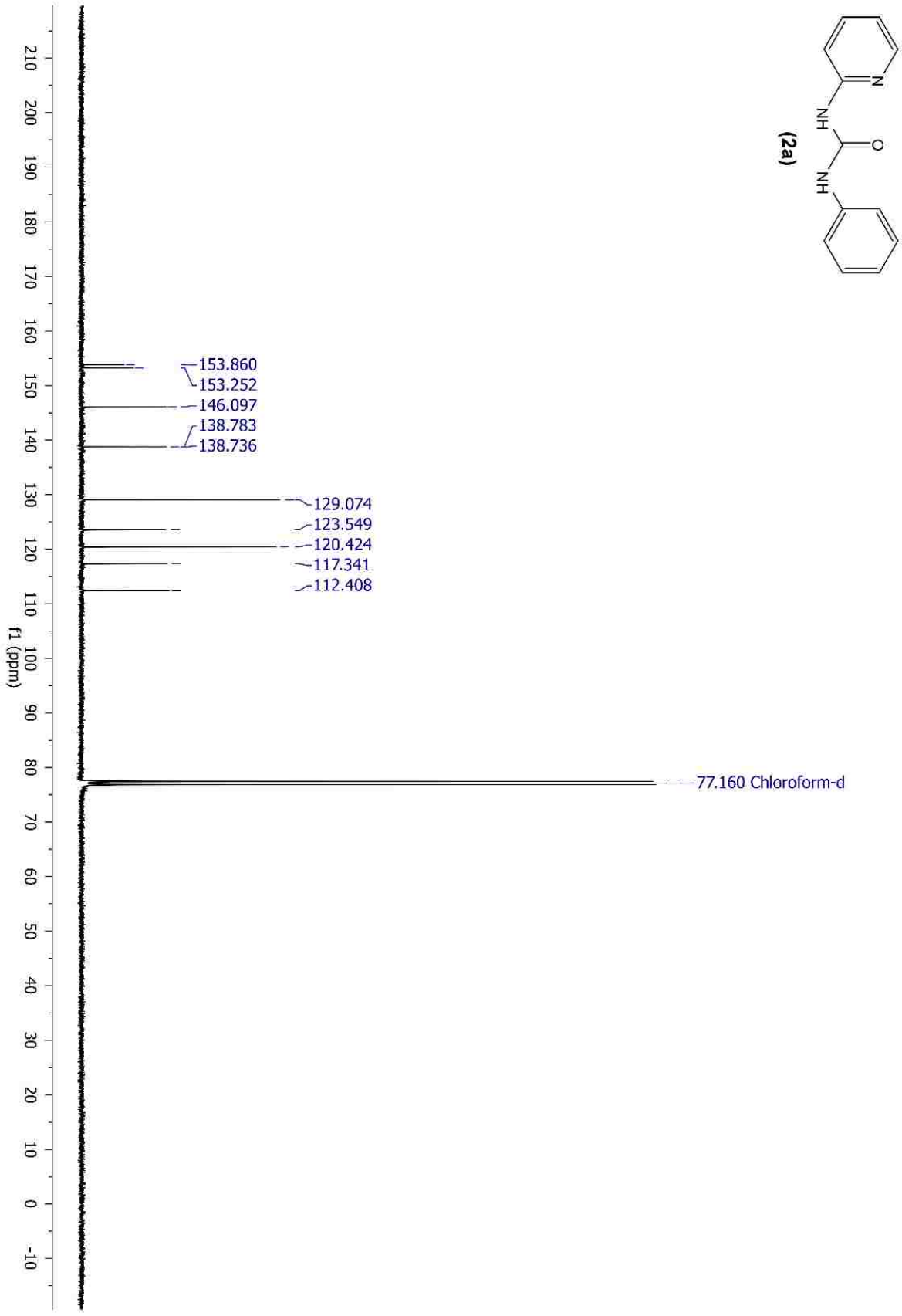
(2a)
153.860
153.252
146.097
138.783
138.736
129.074
123.549
120.424
117.341
112.408
77.160 Chloroform-d
f1 (ppm)

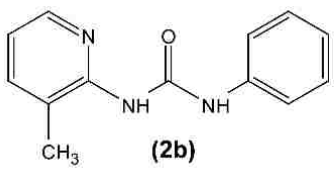
N
O
NH
NH
CH3

(2b)

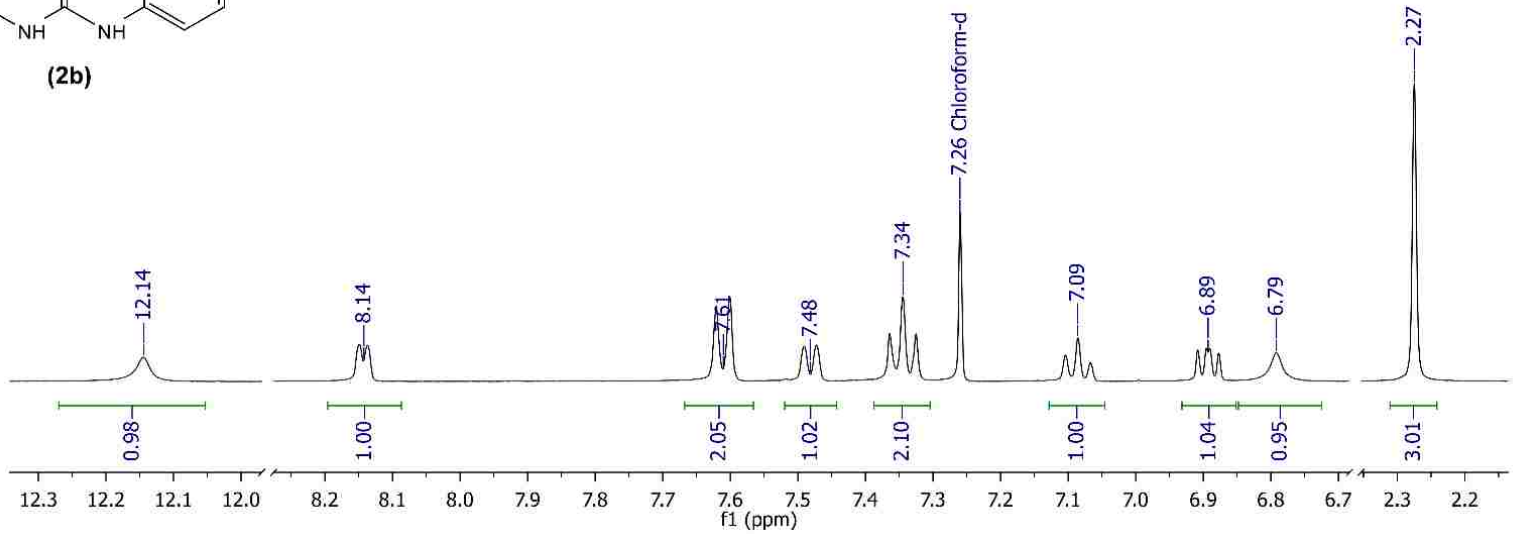
12.14
8.14
7.61
7.48
7.34
7.26 Chloroform-d
7.09
6.89
6.79
2.27
0.98
1.00
2.05
1.02
2.10
1.00
1.04
0.95
3.01
12.3 12.2 12.1 12.0 8.2 8.1 8.0 7.9 7.8 7.7 7.6 7.5 7.4 7.3 7.2 7.1 7.0 6.9 6.8 6.7 2.3 2.2
f1 (ppm)

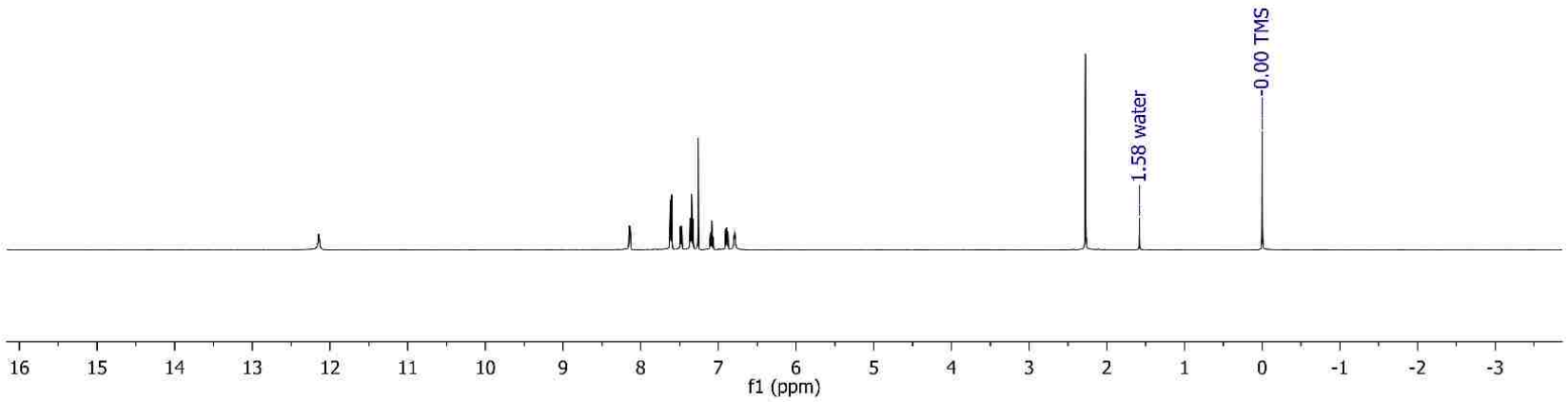
1.58 water
0.00 TMS
16 15 14 13 12 11 10 9 8 7 6 5 4 3 2 1 0 -1 -2 -3
f1 (ppm)

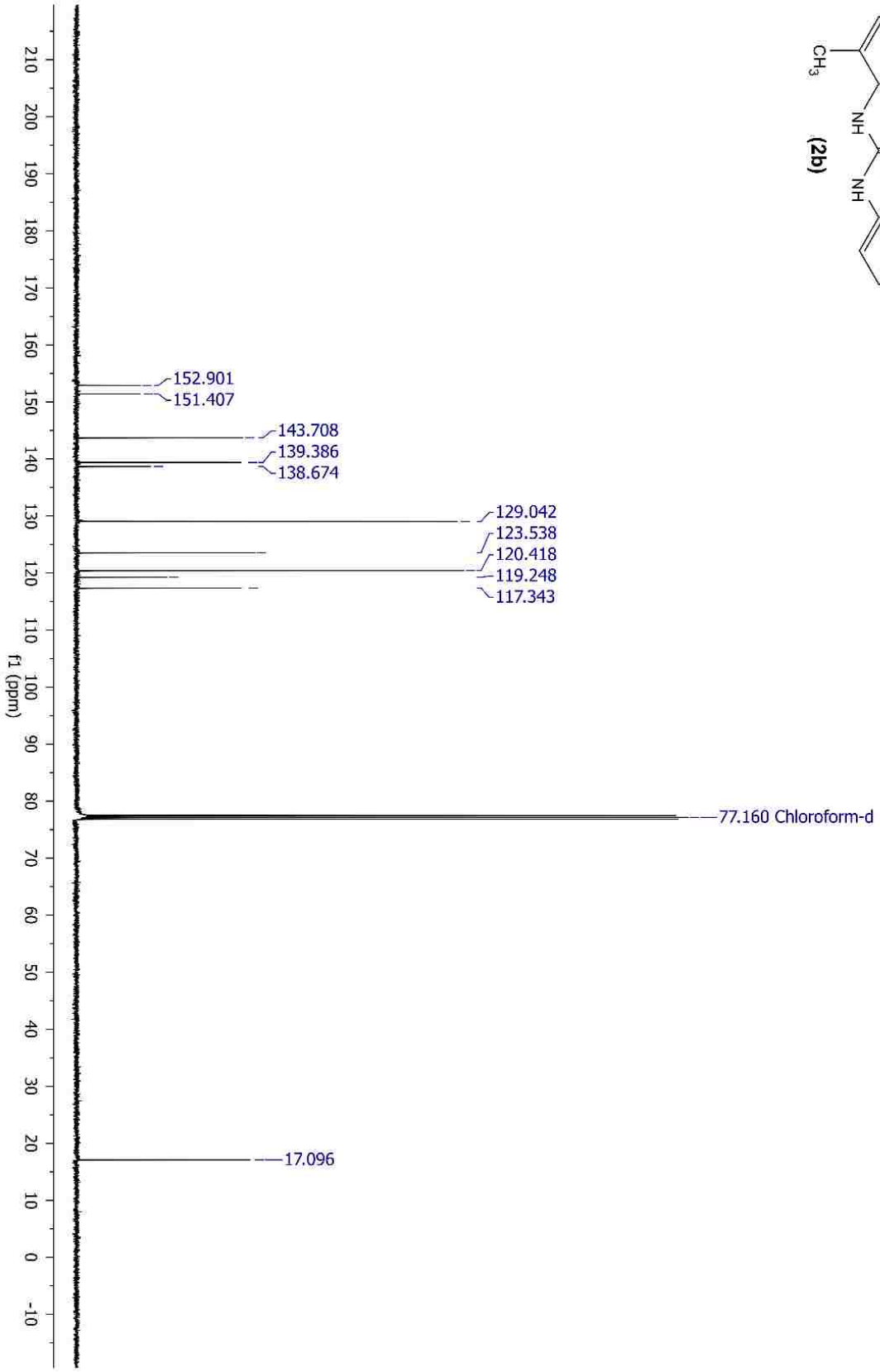
152.901
151.407
143.708
139.386
138.674
129.042
123.538
120.418
119.248
117.343
77.160 Chloroform-d
17.096
f1 (ppm)
(2b)

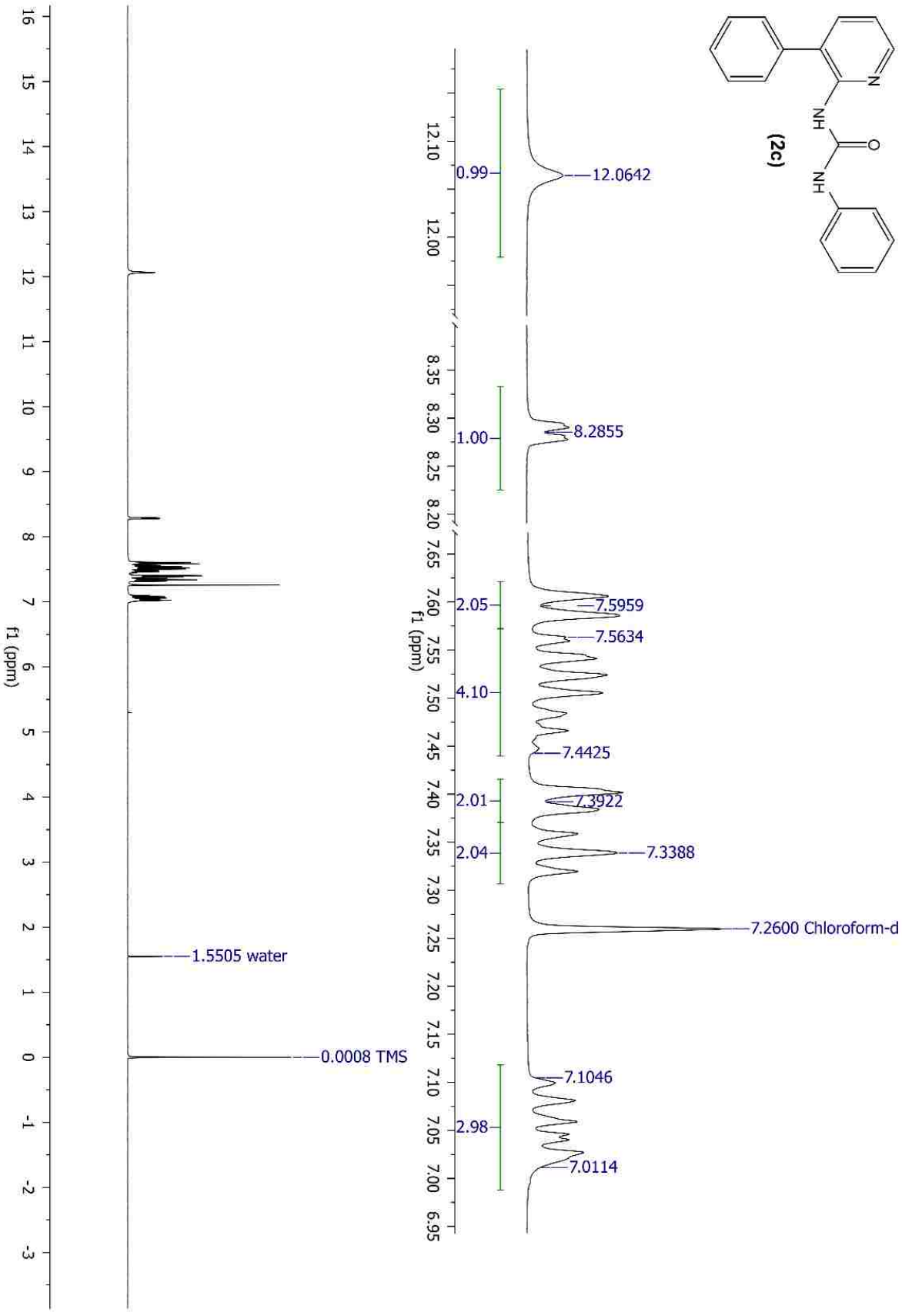
(2c)
12.0642
8.2855
7.5959
7.5634
7.4425
7.3922
7.3388
7.2600 Chloroform-d
7.1046
7.0114
0.99
1.00
2.05
4.10
2.01
2.04
2.98
1.5505 water
0.0008 TMS
f1 (ppm)

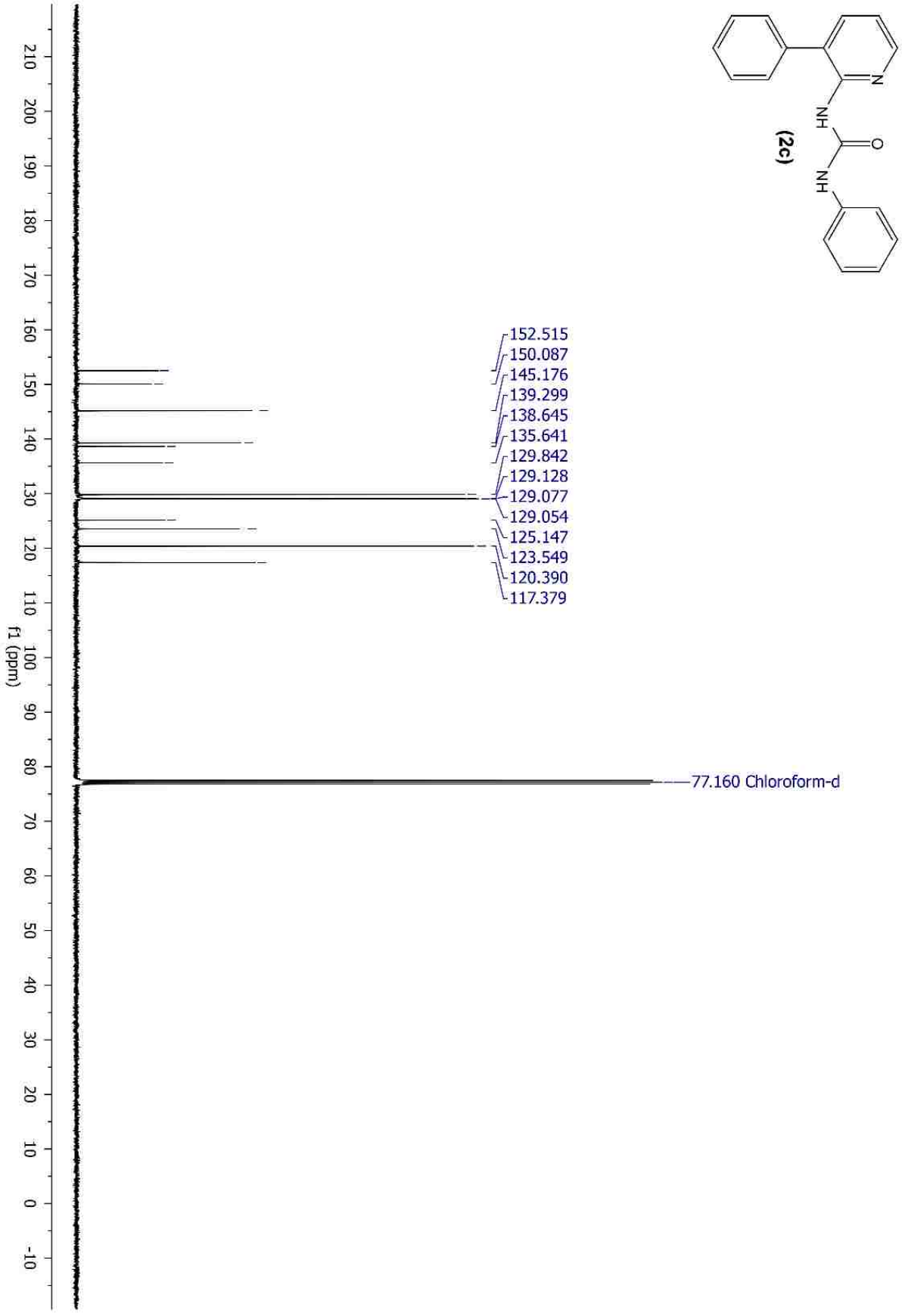
(2c)
152.515
150.087
145.176
139.299
138.645
135.641
129.842
129.128
129.077
129.054
125.147
123.549
120.390
117.379
77.160 Chloroform-d
f1 (ppm)

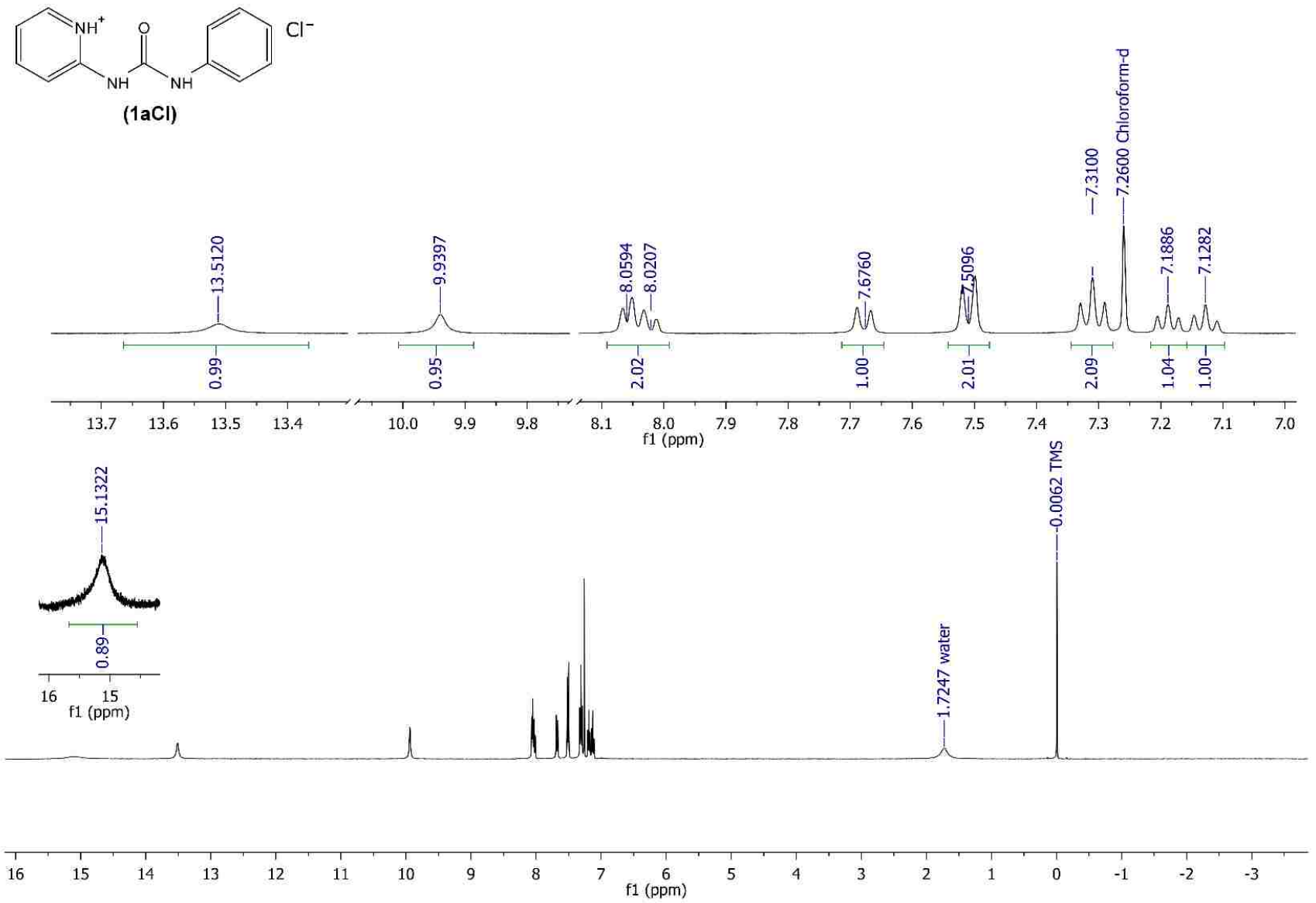
NH+
O
Cl−
NH
NH
(1aCl)
13.5120
9.9397
8.0594
8.0207
7.6760
7.5096
7.3100
7.2600 Chloroform-d
7.1886
7.1282
0.99
0.95
2.02
1.00
2.01
2.09
1.04
1.00
f1 (ppm)
15.1322
0.89
f1 (ppm)
1.7247 water
-0.0062 TMS
f1 (ppm)

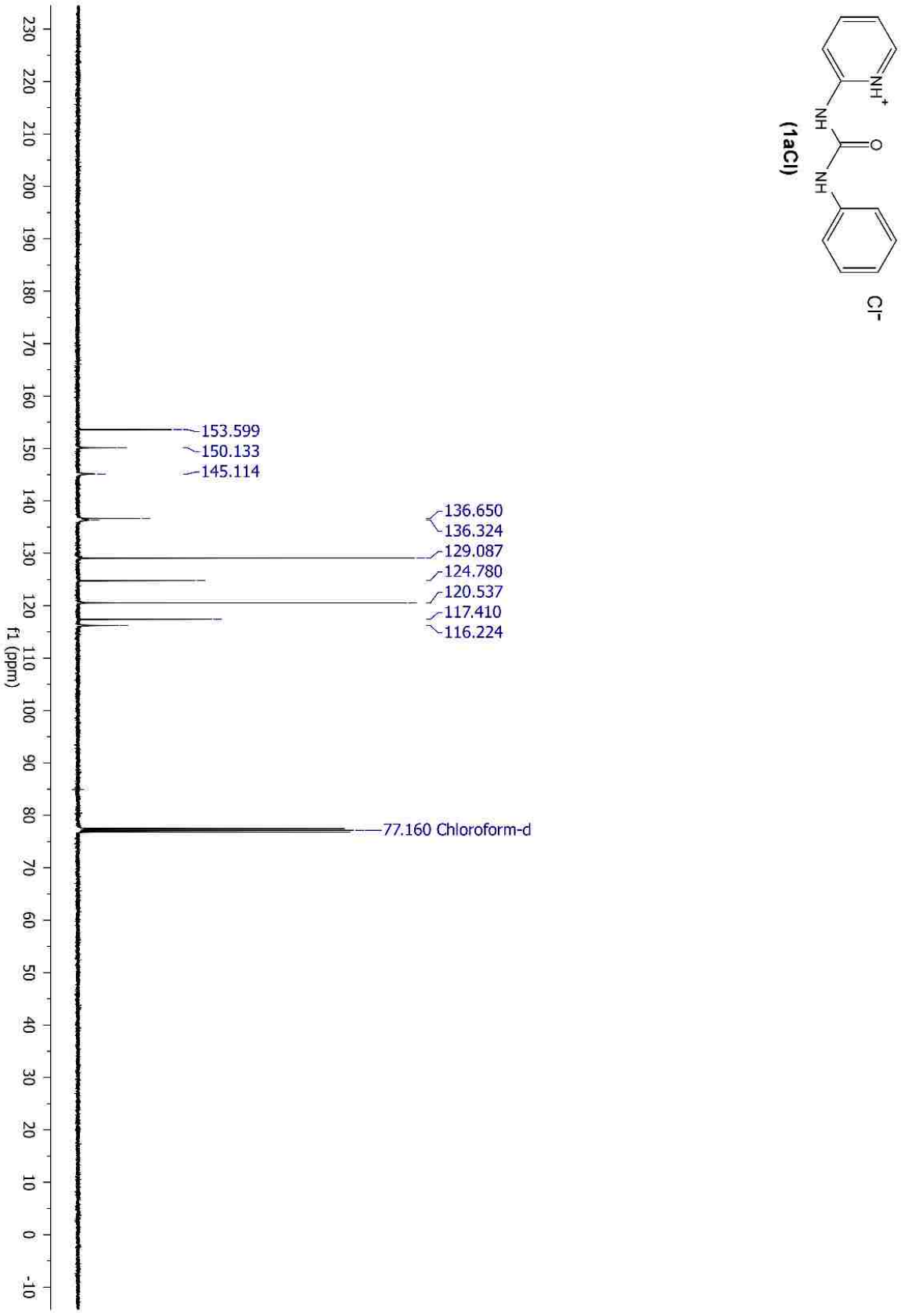
(1aCl)
Cl⁻
153.599
150.133
145.114
136.650
136.324
129.087
124.780
120.537
117.410
116.224
77.160 Chloroform-d
f1 (ppm)

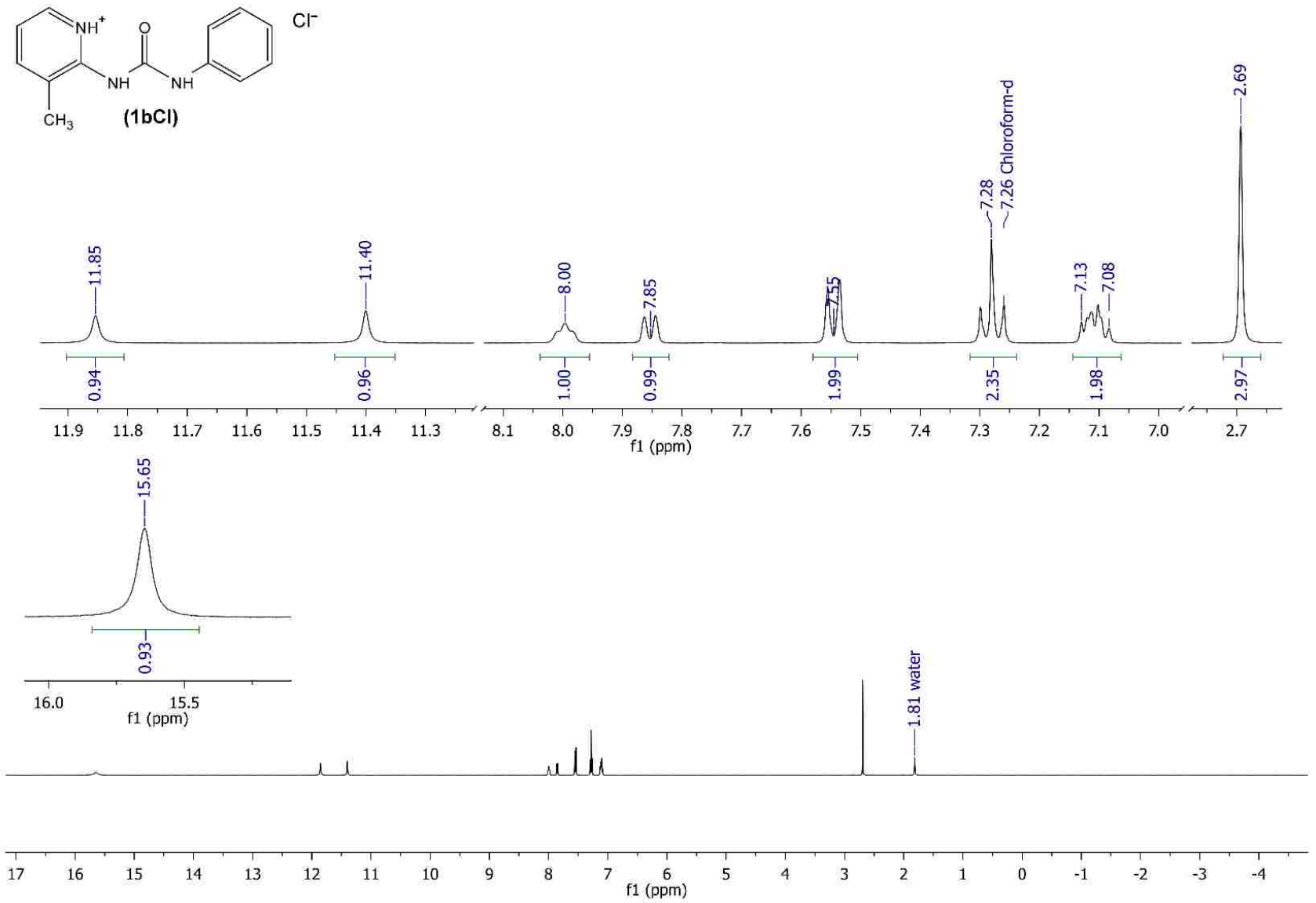
NH+
O
NH
NH
Cl-
CH3
(1bCl)
11.85
11.40
8.00
7.85
7.55
7.28
7.26 Chloroform-d
7.13
7.08
2.69
0.94
0.96
1.00
0.99
1.99
2.35
1.98
2.97
f1 (ppm)
15.65
0.93
16.0
15.5
f1 (ppm)
1.81 water
f1 (ppm)

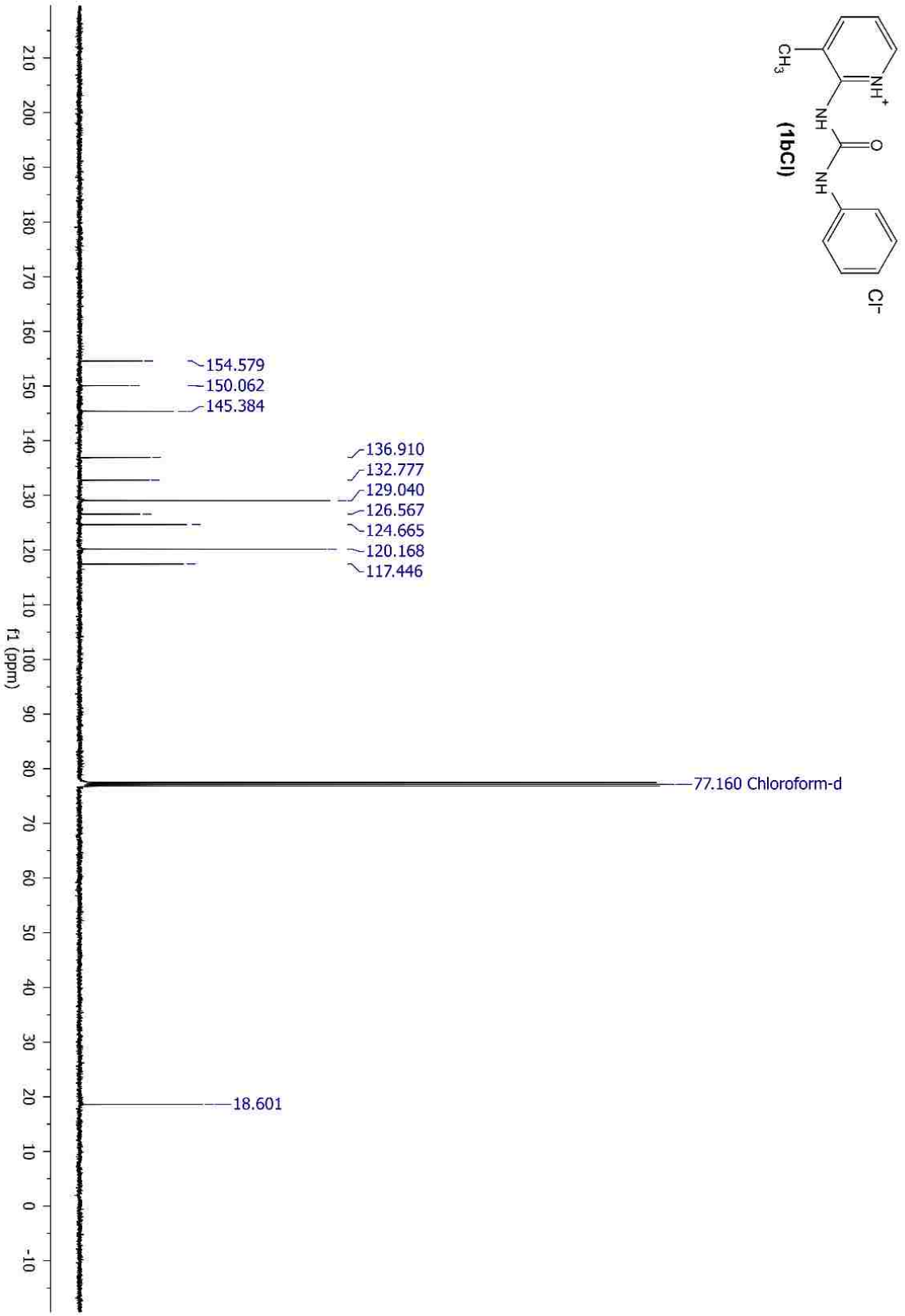
154.579
150.062
145.384
136.910
132.777
129.040
126.567
124.665
120.168
117.446
77.160 Chloroform-d
18.601
f1 (ppm)
(1bCl)
Cl⁻

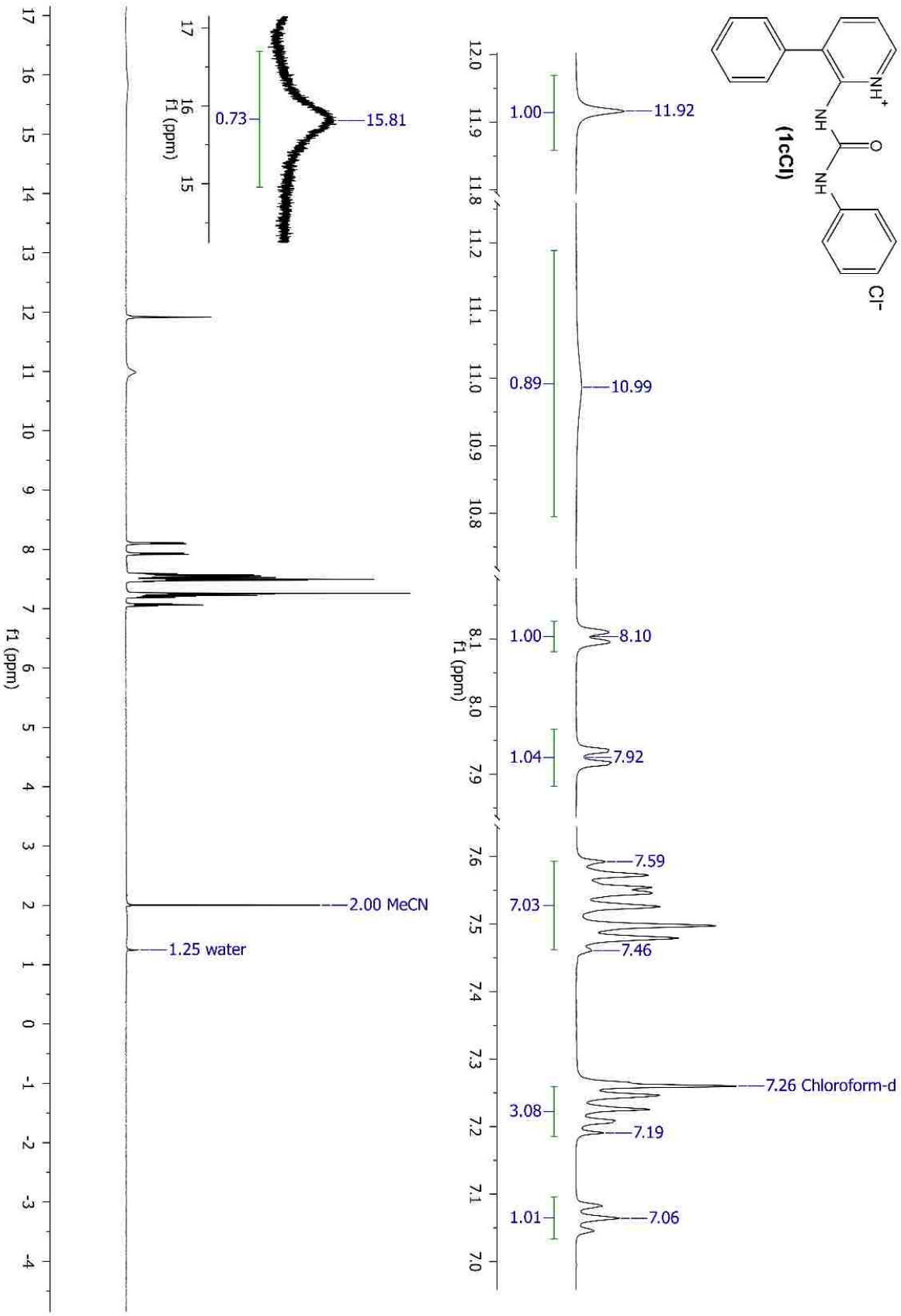
(1cCl)
Cl⁻
11.92
10.99
8.10
7.92
7.59
7.46
7.26 Chloroform-d
7.19
7.06
15.81
2.00 MeCN
1.25 water
f1 (ppm)

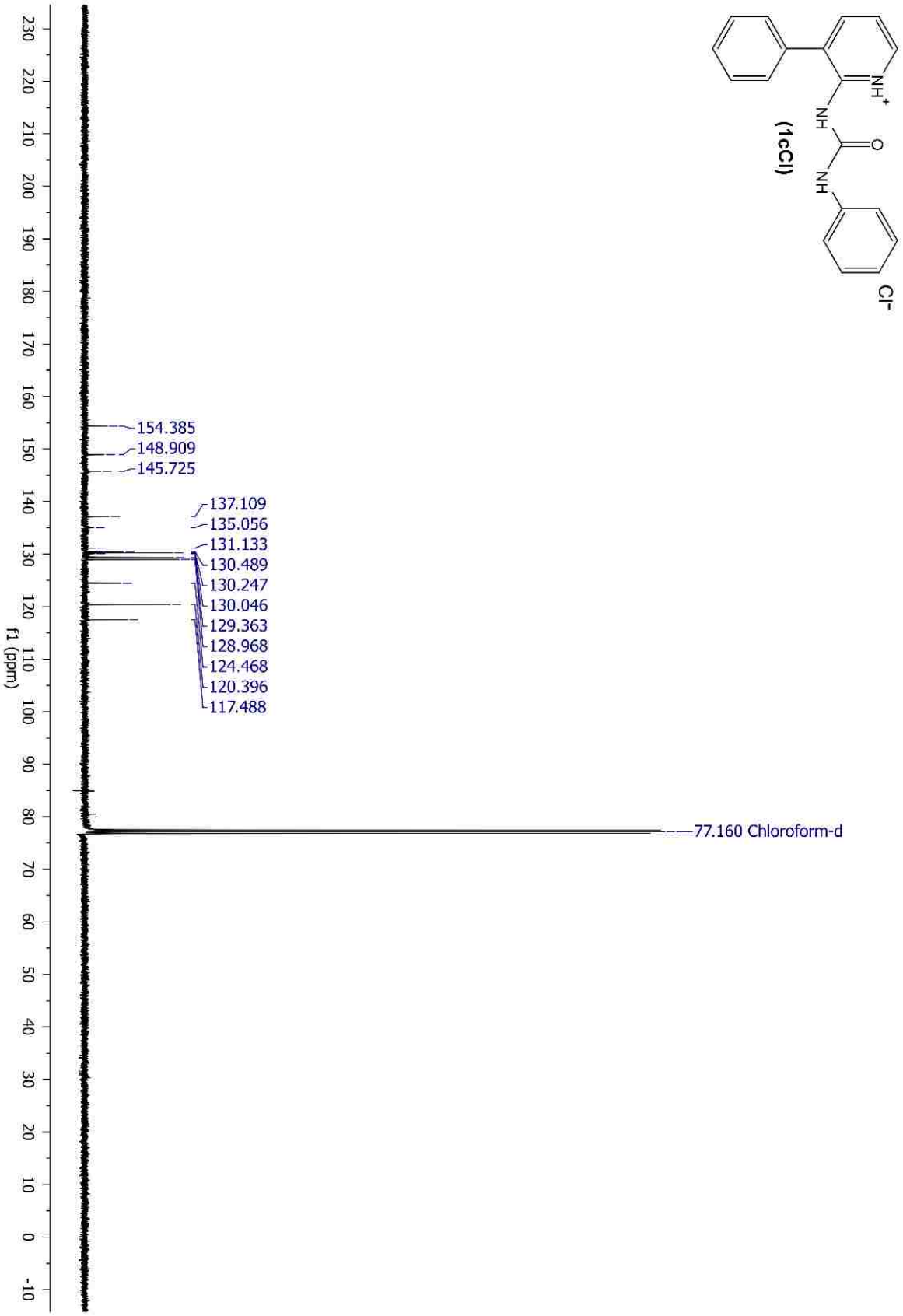
154.385
148.909
145.725
137.109
135.056
131.133
130.489
130.247
130.046
129.363
128.968
124.468
120.396
117.488
77.160 Chloroform-d
f1 (ppm)
230
220
210
200
190
180
170
160
150
140
130
120
110
100
90
80
70
60
50
40
30
20
10
0
-10
NH+
NH
O
NH
Cl-
(1cCl)

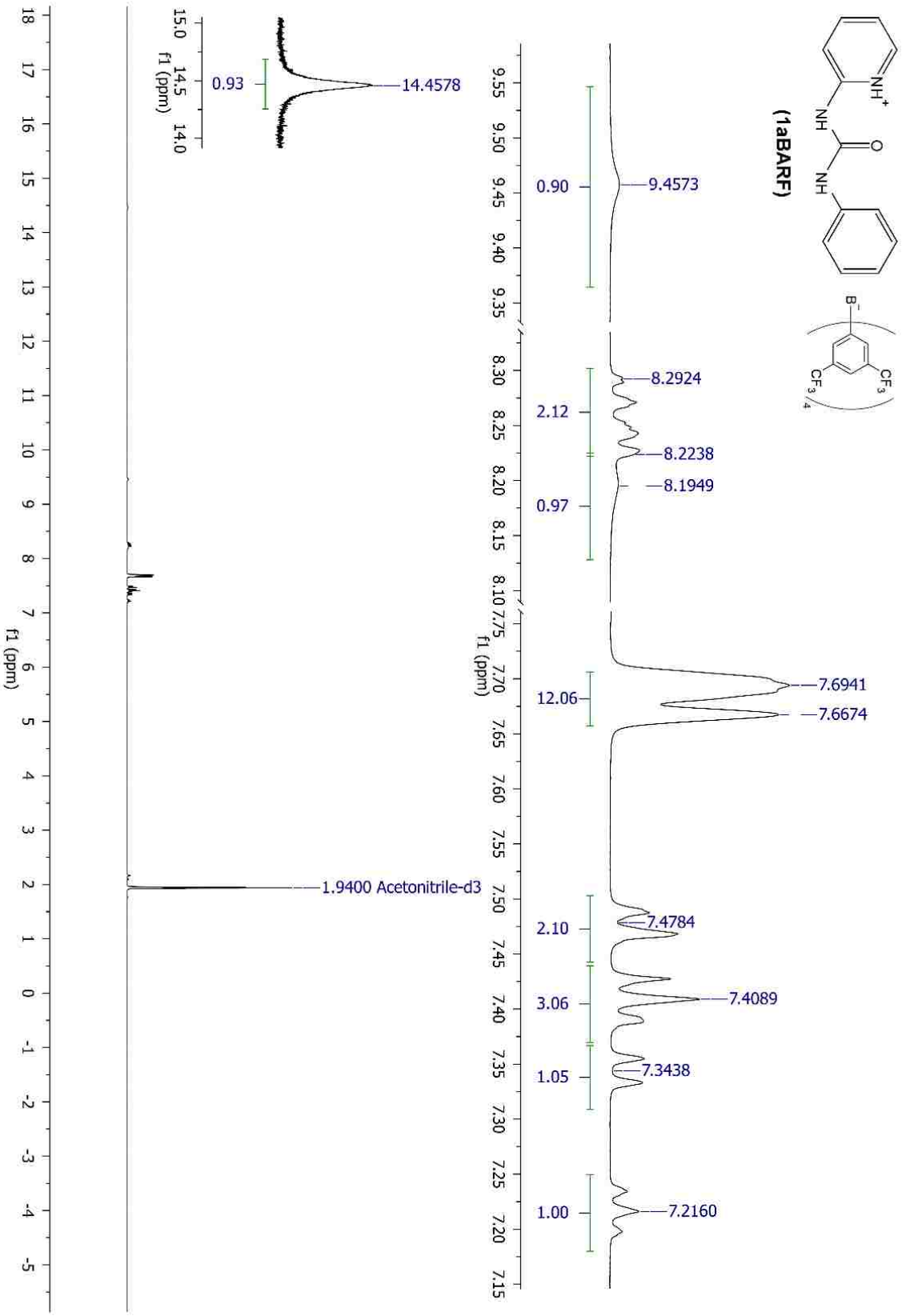
(1aBARF)
14.4578
0.93
1.9400 Acetonitrile-d3
9.4573
0.90
8.2924
8.2238
8.1949
2.12
0.97
7.6941
7.6674
12.06
7.4784
7.4089
7.3438
2.10
3.06
1.05
7.2160
1.00
f1 (ppm)

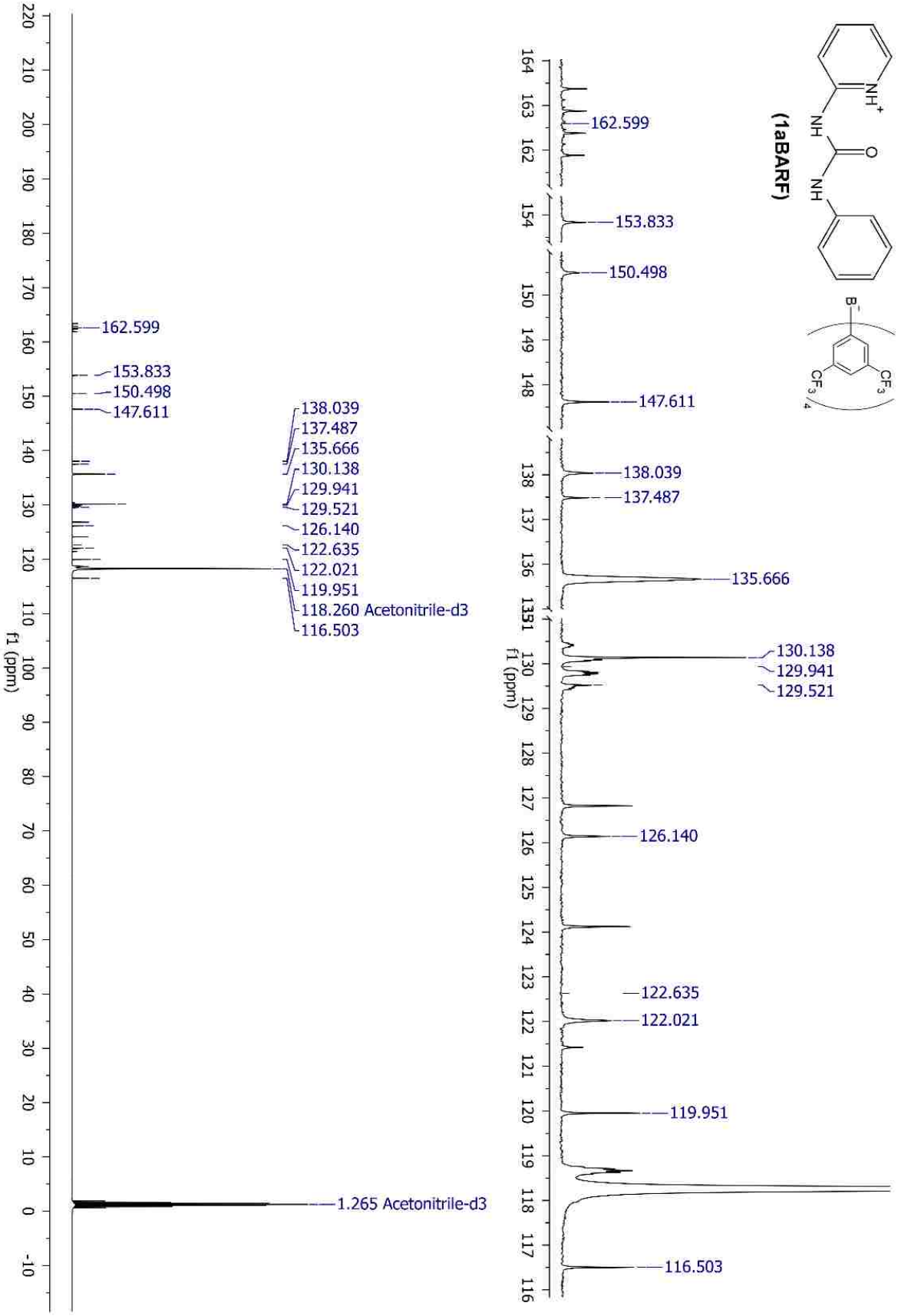
(1aBARF)
162.599
153.833
150.498
147.611
138.039
137.487
135.666
130.138
129.941
129.521
126.140
122.635
122.021
119.951
116.503
f1 (ppm)
162.599
153.833
150.498
147.611
138.039
137.487
135.666
130.138
129.941
129.521
126.140
122.635
122.021
119.951
118.260 Acetonitrile-d3
116.503
1.265 Acetonitrile-d3
f1 (ppm)

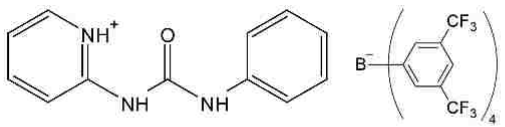
NH+
O
NH
NH
B−
CF3
CF3
4

(1aBARF)

-164.900 hexafluorobenzene
-63.680
30 20 10 0 -10 -20 -30 -40 -50 -60 -70 -80 -90 -100 -110 -120 -130 -140 -150 -160 -170 -180 -190 -200
f1 (ppm)

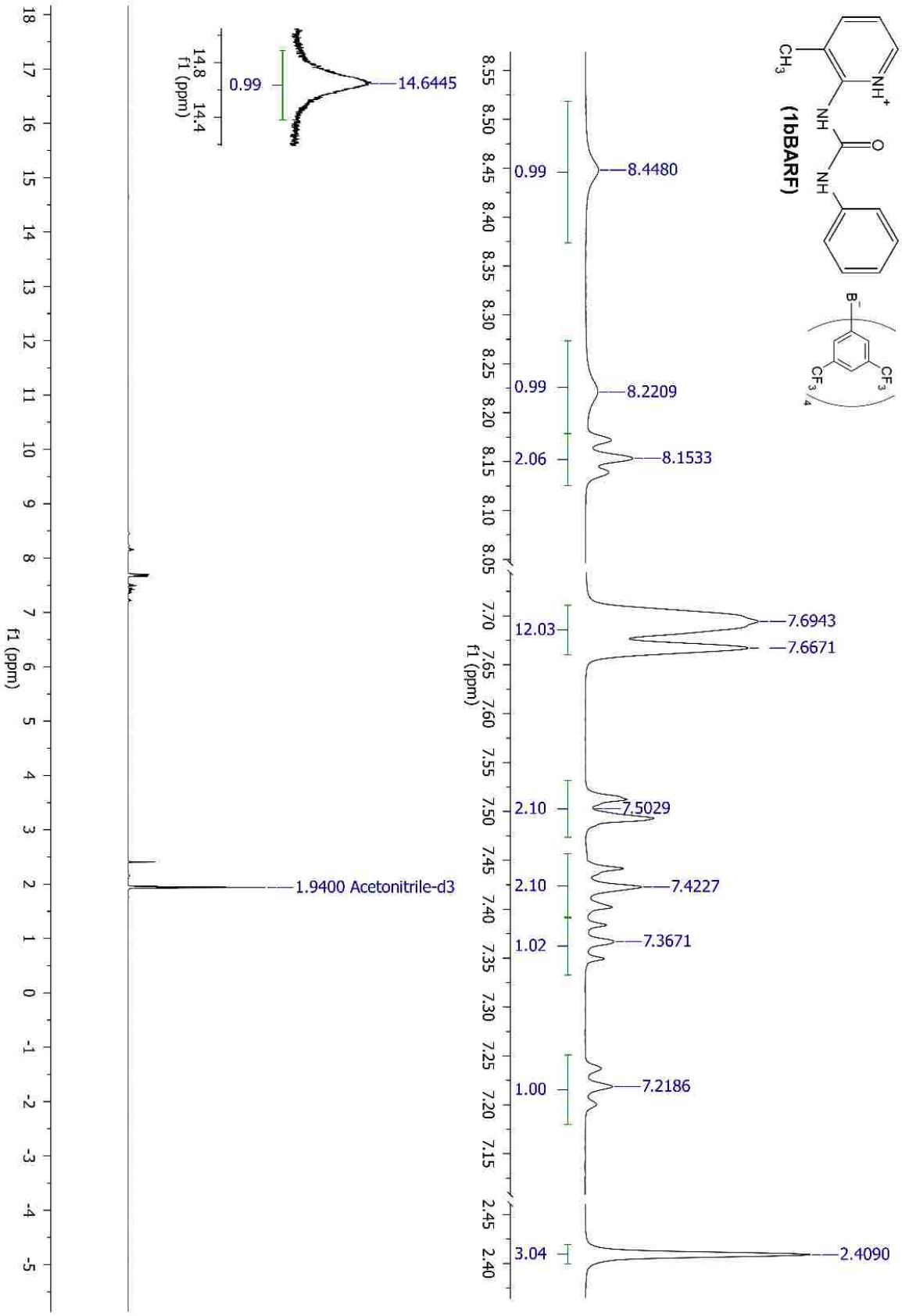
(1bBARF)
14.6445
0.99
1.9400 Acetonitrile-d3
8.4480
8.2209
8.1533
7.6943
7.6671
7.5029
7.4227
7.3671
7.2186
2.4090
0.99
0.99
2.06
12.03
2.10
2.10
1.02
1.00
3.04
f1 (ppm)

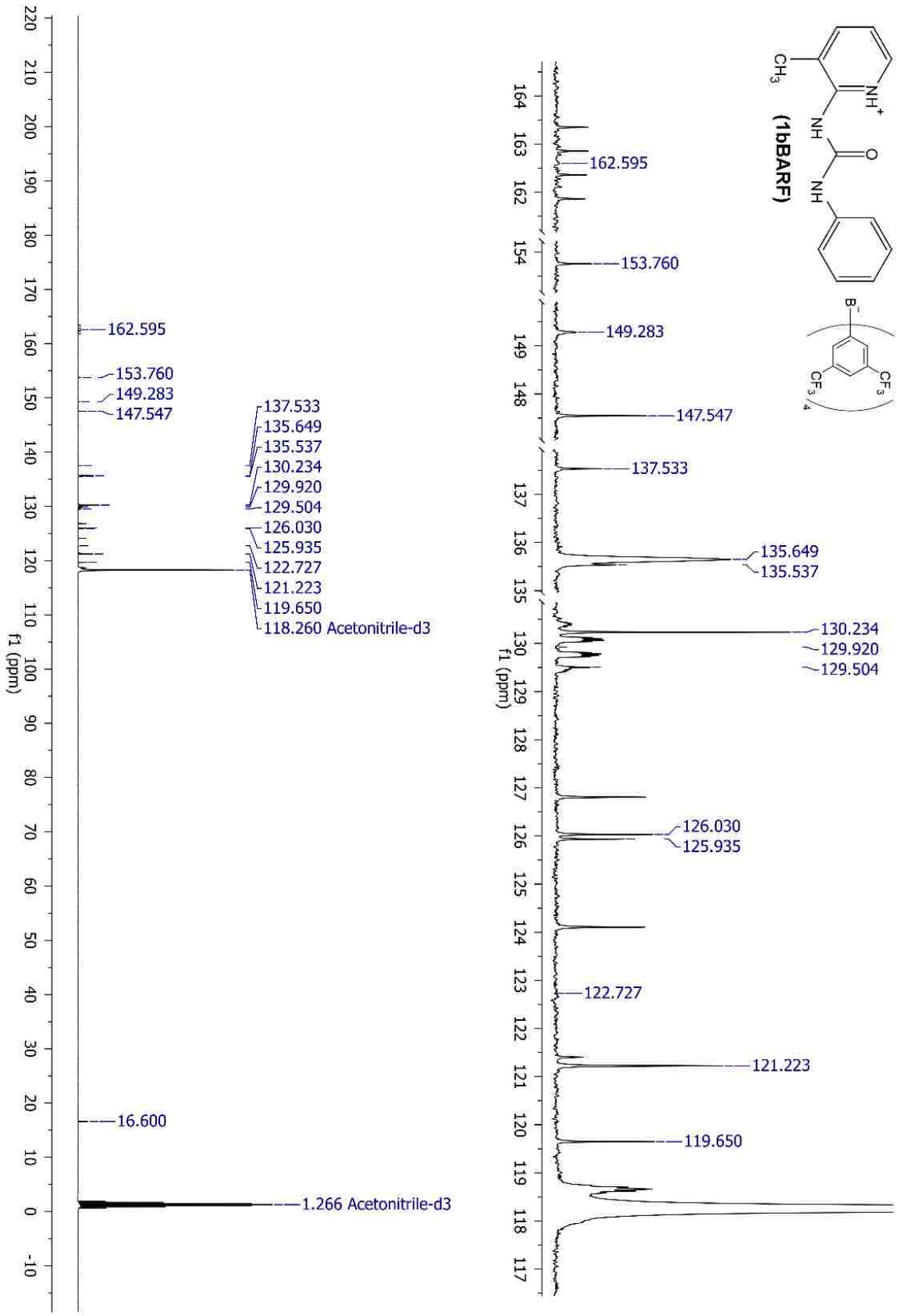
(1bBARF)
162.595
153.760
149.283
147.547
137.533
135.649
135.537
130.234
129.920
129.504
126.030
125.935
122.727
121.223
119.650
118.260 Acetonitrile-d3
16.600
1.266 Acetonitrile-d3
f1 (ppm)

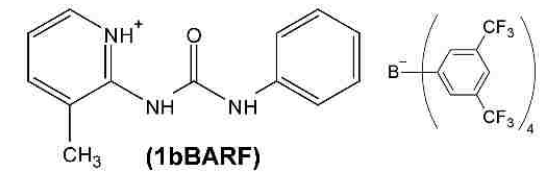
NH+
O
NH
NH
CH3

(1bBARF)

B-
CF3
CF3
4

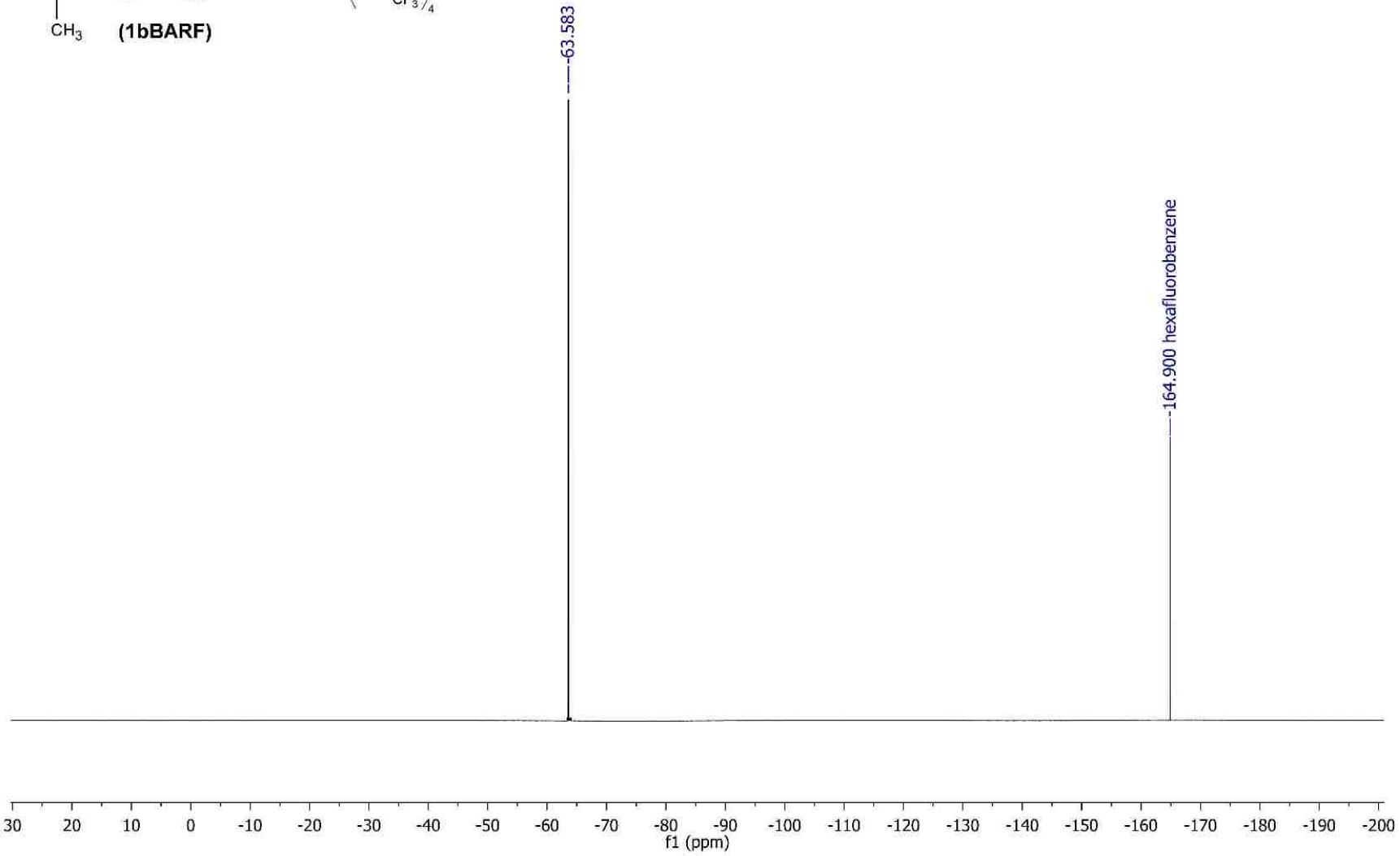
-63.583
-164.900 hexafluorobenzene
30
20
10
0
-10
-20
-30
-40
-50
-60
-70
-80
-90
-100
-110
-120
-130
-140
-150
-160
-170
-180
-190
-200
f1 (ppm)

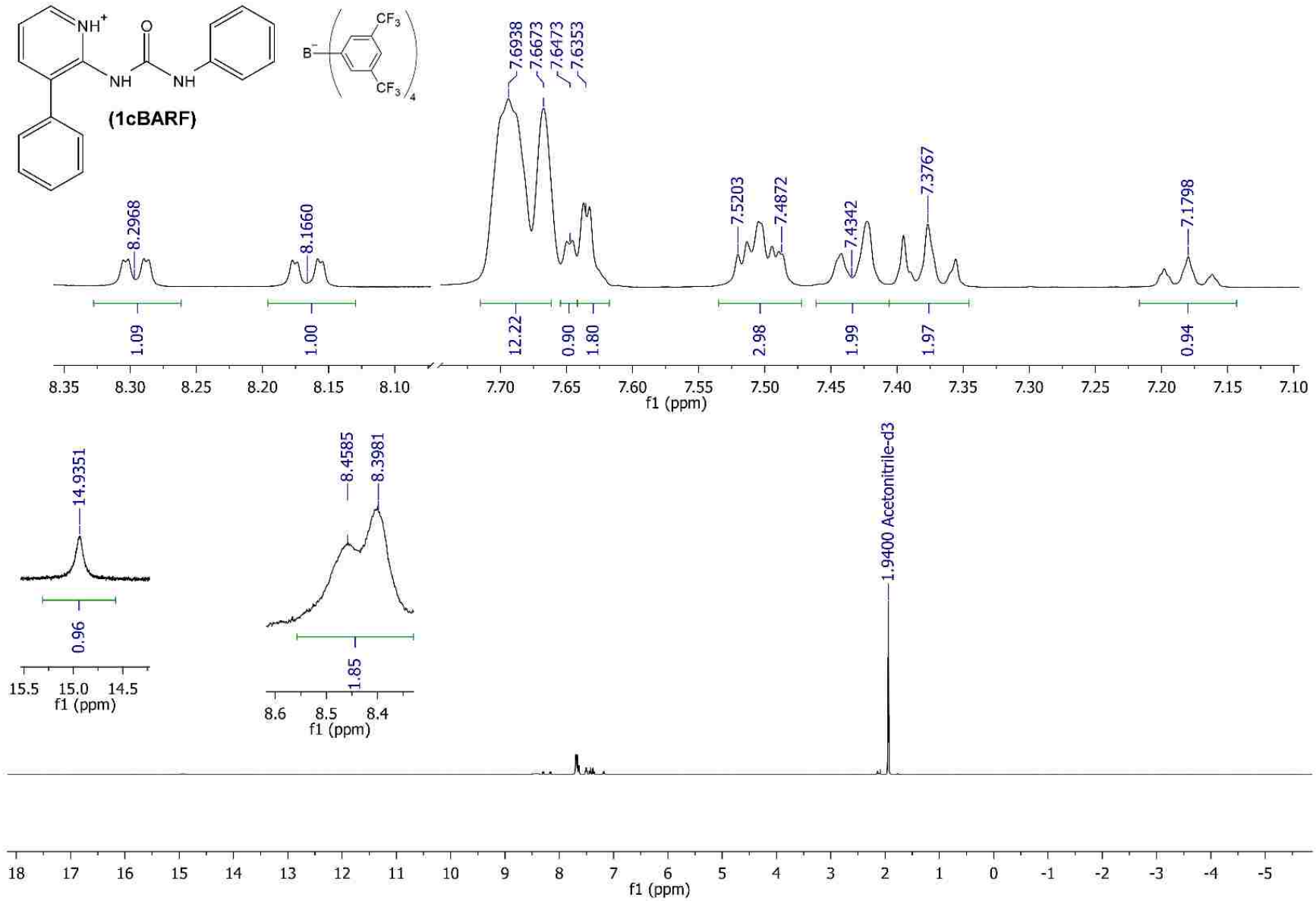
(1cBARF)
8.2968
8.1660
7.6938
7.6673
7.6473
7.6353
7.5203
7.4872
7.4342
7.3767
7.1798
1.09
1.00
12.22
0.90
1.80
2.98
1.99
1.97
0.94
f1 (ppm)
14.9351
0.96
8.4585
8.3981
1.85
1.9400 Acetonitrile-d3

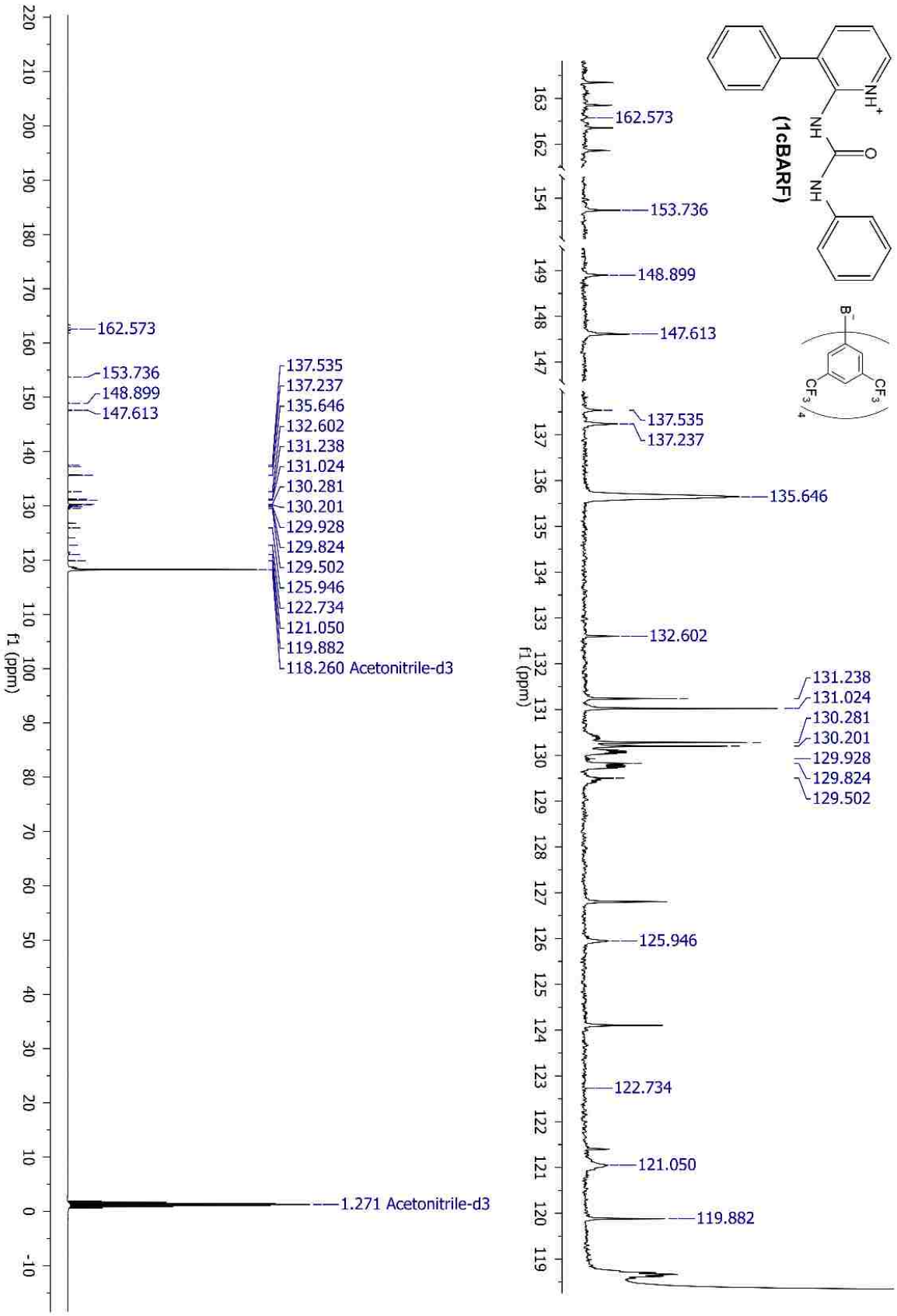
(1cBARF)
162.573
153.736
148.899
147.613
137.535
137.237
135.646
132.602
131.238
131.024
130.281
130.201
129.928
129.824
129.502
125.946
122.734
121.050
119.882
f1 (ppm)
162.573
153.736
148.899
147.613
137.535
137.237
135.646
132.602
131.238
131.024
130.281
130.201
129.928
129.824
129.502
125.946
122.734
121.050
119.882
118.260 Acetonitrile-d3
1.271 Acetonitrile-d3
f1 (ppm)

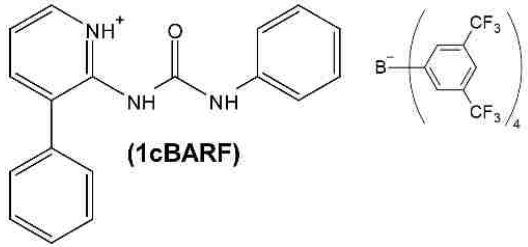
NH+
O
NH
NH

(1cBARF)

B−
CF3
CF3
4

-164.900 hexafluorobenzene
-63.676
30
20
10
0
-10
-20
-30
-40
-50
-60
-70
-80
-90
-100
-110
-120
-130
-140
-150
-160
-170
-180
-190
-200
f1 (ppm)

Catalysis Screens

Kinetics data: reactions with carbonyls, α,β-unsaturated carbonyls, and nitrosos

A stock solution was made by combining the carbonyl/nitroso, any other necessary reagents and dry $CDCl_3$ at room temperature. Concentrations were dependent on each reaction, and were calculated based on the conditions in the literature. After mixing, 50-100 mol% of the appropriate catalyst was added to a portion of the stock solution. The solution was transferred to an oven-dried NMR tube. Reaction progress was monitored by ^1H NMR by comparing a resonance from the starting material to a resonance of the product, if any appeared at all. No rate constants were determined for these reactions, as it was a qualitative screen for activity.

Kinetics data, N-methylindole and trans-β-nitrostyrene

A stock solution was made by combining *trans*-β-nitrostyrene (0.0160 g, 0.107 mmol), *N*-methylindole (0.0402 mL, 0.322 mmol), and dry $CDCl_3$ (4.200 mL) at room temperature. After mixing, 1.65 μmol of the appropriate catalyst was added to a 1.000 mL aliquot of the stock solution. The solution was transferred to an oven-dried NMR tube (screw-cap, PTFE septum). Reaction progress was monitored by ^1H NMR using the integration of the singlet methyl signals from *N*-methylindole and the product (3.751 and 3.087 ppm respectively). Second-order rate constants were calculated using the integrated rate law:

$$\ln\frac{[NMI][BNS]_0}{[NMI]_o[BNS]} = k([NMI]_0 - [BNS]_0)t$$

([NMI] = *N*-methylindole concentration at time t, $[NMI]_0$ = initial *N*-methylindole concentration, [BNS] = *trans*-β-nitrostyrene concentration at time t, $[BNS]_0$ = initial

trans-β-nitrostyrene concentration, ln = natural logarithm, k = rate constant, and t = time).

Raw kinetics NMR data: N-methylindole and trans-β-nitrostyrene

1aBARF		**1bBARF**		**1cBARF**	
% conversion	**t (min)**	**% conversion**	**t (min)**	**% conversion**	**t (min)**
Run 1		**Run 1**		**Run 1**	
35.065	28	15.966	56	1.961	20
55.556	50	22.481	82	3.846	45
79.339	94	24.812	95	8.257	86
89.362	133	27.536	110	10.714	127
99.033	342	57.082	313	24.812	331
100.000	447	63.636	379	31.034	439
100.000	543	-	-	34.641	536
Run 2		**Run 2**		**Run 2**	
35.484	30	16.667	59	1.961	23
56.332	53	22.481	84	3.846	47
80.732	96	25.373	98	7.407	87
90.119	136	28.571	112	11.504	129
99.269	344	57.265	315	24.242	332
100.000	449	63.100	382	29.078	443
100.000	545	-	-	32.886	538
Run 3		**Run 3**		**Run 3**	
35.065	32	17.355	61	2.913	25
53.704	54	22.481	86	3.846	49
76.247	98	25.373	100	7.407	92
88.221	139	29.078	114	10.714	131
99.039	345	57.447	318	23.664	339
100.000	451	63.504	383	28.571	445
100.000	547	-	-	33.333	540

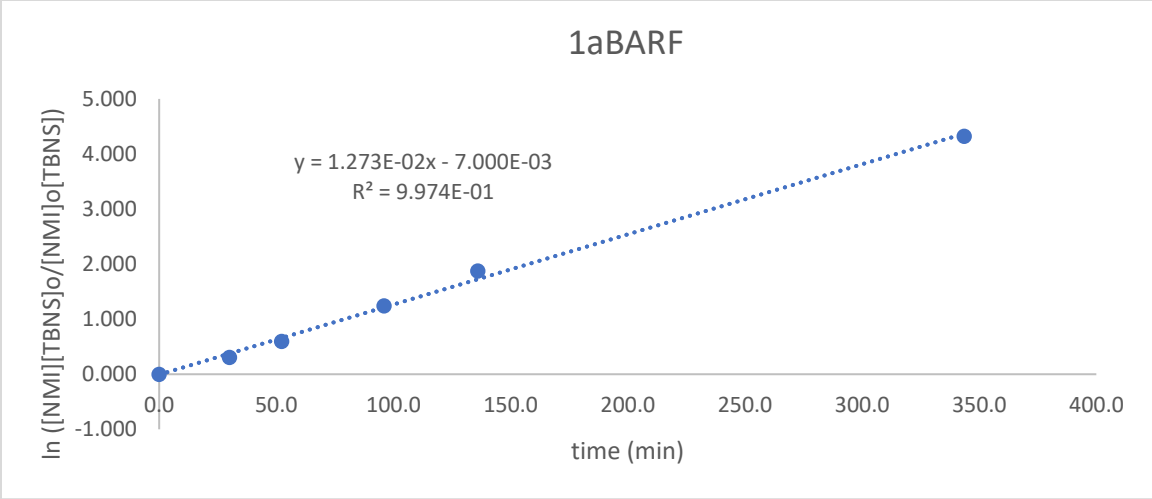
1aBARF
y = 1.273E-02x - 7.000E-03
R² = 9.974E-01
ln ([NMI][TBNS]o/[NMI]o[TBNS])
time (min)
5.000
4.000
3.000
2.000
1.000
0.000
-1.000
0.0
50.0
100.0
150.0
200.0
250.0
300.0
350.0
400.0

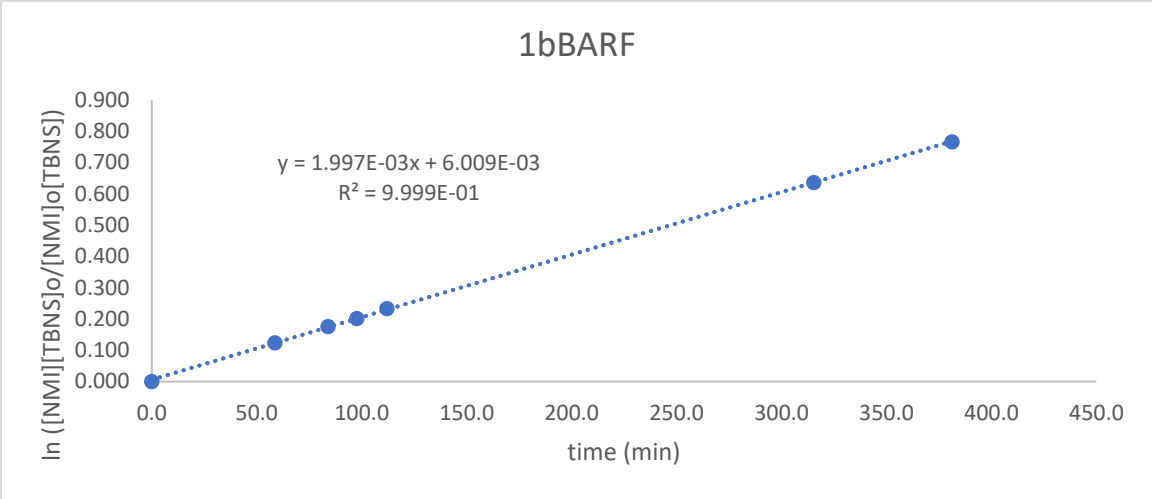
1bBARF
y = 1.997E-03x + 6.009E-03
R² = 9.999E-01
ln ([NMI][TBNS]o/[NMI]o[TBNS])
time (min)
0.900
0.800
0.700
0.600
0.500
0.400
0.300
0.200
0.100
0.000
0.0
50.0
100.0
150.0
200.0
250.0
300.0
350.0
400.0
450.0

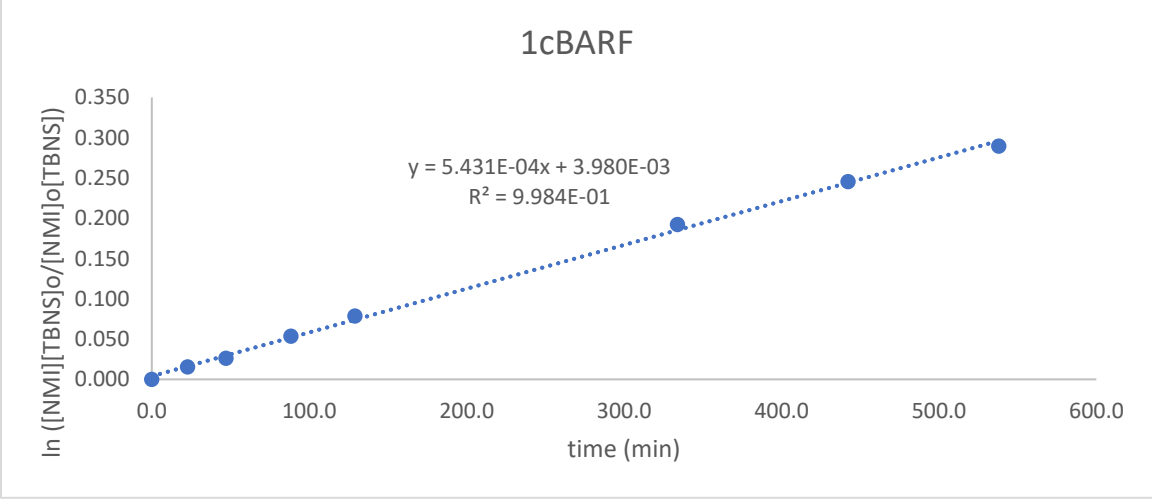
1cBARF
y = 5.431E-04x + 3.980E-03
R² = 9.984E-01
ln ([NMI][TBNS]o/[NMI]o[TBNS])
time (min)
0.350
0.300
0.250
0.200
0.150
0.100
0.050
0.000
0.0
100.0
200.0
300.0
400.0
500.0
600.0

Computations

GaussView[127] and Avogadro (an open source molecular editor and visualizer, available at https://avogadro.cc) were used to construct initial structures used in the computations. All density functional theory (DFT) calculations were performed using the Gaussian 09 suite.[126] All computations performed were in the gas phase, and no solvation model was applied to the systems. Geometry optimizations and frequency calculations were performed at the B3LYP/6-31G(d) level of theory. Frequency calculations confirmed that the optimized structures are minima. Single point energy calculations were performed at the B3LYP/6-31++G(d,p) level of theory. The structures of the pyridine-protonated ureas will be labeled as **1a**, **1b**, and **1c** (a = H, b = Me, c = Ph), consistently with the main text. No anions were included in the calculations. The *N*1-deprotonated structures were generated using the same geometry minimized structures as the appropriate protonated geometries of **1a**, **1b**, or **1c**, and will be labeled as **1a·zwit**, **1b·zwit**, and **1c·zwit** respectively. All energies are reported in Hartrees, and proton affinities were calculated from the difference between the deprotonated (zwitterionic) and protonated energies.

1a

Center Number	Atomic Number	Atomic Type	Coordinates (Angstroms) X	Y	Z
1	6	0	-5.025069	-0.691086	0.000000
2	6	0	-4.852009	0.706789	0.000000
3	6	0	-3.585805	1.264290	0.000000
4	6	0	-2.463333	0.417491	0.000000
5	7	0	-2.668079	-0.922739	0.000000
6	6	0	-3.903985	-1.485028	0.000000
7	1	0	-3.926055	-2.568214	0.000000
8	1	0	-6.010889	-1.139723	0.000000
9	1	0	-5.719876	1.358856	0.000000
10	1	0	-3.445800	2.340013	0.000000
11	7	0	-1.180659	0.900260	0.000000

12	6	0	0.000000	0.100604	0.000000
13	7	0	1.137668	0.824689	0.000000
14	6	0	2.489318	0.357305	0.000000
15	6	0	3.479913	1.347505	0.000000
16	6	0	4.823678	0.985230	0.000000
17	6	0	5.184864	-0.363221	0.000000
18	6	0	2.838425	-0.997710	0.000000
19	6	0	4.190923	-1.341830	0.000000
20	1	0	5.585361	1.758771	0.000000
21	1	0	6.232362	-0.647721	0.000000
22	1	0	2.075902	-1.763121	0.000000
23	1	0	4.463783	-2.392876	0.000000
24	1	0	3.203072	2.400377	0.000000
25	8	0	-0.087915	-1.128022	0.000000
26	1	0	-1.099483	1.909459	0.000000
27	1	0	1.057613	1.833911	0.000000
28	1	0	-1.796691	-1.483055	0.000000

E = -703.842956162

1b

Center Number	Atomic Number	Atomic Type	Coordinates (Angstroms) X	Y	Z
1	6	0	4.747583	-1.108833	0.000039
2	6	0	4.639288	0.293822	0.000072
3	6	0	3.410846	0.942091	0.000039
4	6	0	2.254036	0.125013	-0.000027
5	7	0	2.391725	-1.222342	-0.000062
6	6	0	3.593392	-1.851665	-0.000031
7	1	0	3.560067	-2.934289	-0.000068
8	1	0	5.713632	-1.598731	0.000063
9	1	0	5.543710	0.895314	0.000125
10	6	0	3.289486	2.443950	0.000075
11	7	0	0.988848	0.658932	-0.000061
12	6	0	-0.224203	-0.087866	-0.000102
13	7	0	-1.329797	0.686341	-0.000065
14	6	0	-2.700492	0.279407	-0.000020
15	6	0	-3.646839	1.312086	-0.000054
16	6	0	-5.005394	1.009669	-0.000011
17	6	0	-5.426186	-0.321331	0.000067
18	6	0	-3.109843	-1.058671	0.000060
19	6	0	-4.476271	-1.342702	0.000102
20	1	0	-5.731958	1.816326	-0.000039
21	1	0	-6.485267	-0.559101	0.000101
22	1	0	-2.382409	-1.857435	0.000087
23	1	0	-4.795070	-2.380742	0.000164
24	1	0	-3.324039	2.351801	-0.000115
25	8	0	-0.194762	-1.319384	-0.000036
26	1	0	0.947068	1.669322	-0.000024
27	1	0	-1.205175	1.690946	-0.000084
28	1	0	4.277531	2.908996	0.000104
29	1	0	2.759912	2.809493	0.889745

30	1	0	2.759943	2.809538	-0.889594
31	1	0	1.492305	-1.736691	-0.000121

E = -743.167656452

1c

Center Number	Atomic Number	Atomic Type	Coordinates (Angstroms) X	Y	Z
1	6	0	-3.300880	3.113524	-0.001689
2	6	0	-3.611741	1.741851	0.004126
3	6	0	-2.627663	0.758342	0.041817
4	6	0	-1.278097	1.199340	0.052153
5	7	0	-1.015908	2.528208	0.056834
6	6	0	-1.979394	3.483451	0.033504
7	1	0	-1.629023	4.508283	0.043903
8	1	0	-4.079053	3.866784	-0.021692
9	1	0	-4.651146	1.428320	-0.005357
10	6	0	-2.966182	-0.690466	0.036521
11	7	0	-0.226599	0.319645	0.032003
12	6	0	1.147951	0.674669	0.021694
13	7	0	1.974386	-0.392778	-0.031860
14	6	0	3.402624	-0.411527	-0.054303
15	6	0	3.999405	-1.675644	-0.145653
16	6	0	5.386228	-1.789781	-0.171114
17	6	0	6.184378	-0.646365	-0.105807
18	6	0	4.192445	0.741875	0.012448
19	6	0	5.581331	0.608080	-0.014679
20	1	0	5.839693	-2.773662	-0.242355
21	1	0	7.266155	-0.733534	-0.125676
22	1	0	3.734674	1.717961	0.082948
23	1	0	6.194443	1.502888	0.036871
24	1	0	3.381726	-2.570549	-0.197578
25	8	0	1.488092	1.858980	0.062805
26	1	0	-0.504152	-0.656166	0.005236
27	1	0	1.552774	-1.312049	-0.076278
28	1	0	-0.004841	2.755126	0.065751
29	6	0	-3.765864	-1.217108	-0.990820
30	6	0	-2.524103	-1.541989	1.066495
31	6	0	-2.874465	-2.892809	1.061048
32	6	0	-3.665279	-3.407665	0.032012
33	6	0	-4.111482	-2.567848	-0.990792
34	1	0	-4.727819	-2.964328	-1.791917
35	1	0	-4.104071	-0.570863	-1.796183
36	1	0	-1.950020	-1.139676	1.898356
37	1	0	-2.543839	-3.537046	1.870284
38	1	0	-3.938666	-4.458428	0.030647

E = -934.919132650

1a·zwit1

Center Number	Atomic Number	Atomic Type	Coordinates (Angstroms) X	Y	Z
1	6	0	-5.025070	-0.691082	0.000000
2	6	0	-4.852009	0.706793	0.000000

3	6	0	-3.585804	1.264293	0.000000
4	6	0	-2.463333	0.417493	0.000000
5	7	0	-2.668080	-0.922737	0.000000
6	6	0	-3.903986	-1.485025	0.000000
7	1	0	-3.926057	-2.568211	0.000000
8	1	0	-6.010890	-1.139718	0.000000
9	1	0	-5.719875	1.358860	0.000000
10	1	0	-3.445798	2.340016	0.000000
11	7	0	-1.180658	0.900261	0.000000
12	6	0	0.000000	0.100604	0.000000
13	7	0	1.137669	0.824688	0.000000
14	6	0	2.489318	0.357303	0.000000
15	6	0	3.479914	1.347502	0.000000
16	6	0	4.823679	0.985226	0.000000
17	6	0	5.184864	-0.363225	0.000000
18	6	0	2.838424	-0.997712	0.000000
19	6	0	4.190922	-1.341833	0.000000
20	1	0	5.585362	1.758767	0.000000
21	1	0	6.232361	-0.647726	0.000000
22	1	0	2.075901	-1.763123	0.000000
23	1	0	4.463781	-2.392880	0.000000
24	1	0	3.203074	2.400374	0.000000
25	8	0	-0.087916	-1.128022	0.000000
26	1	0	1.057614	1.833910	0.000000
27	1	0	-1.796692	-1.483054	0.000000

E = -703.444158402

1b·zwit1

Center Number	Atomic Number	Atomic Type	Coordinates (Angstroms) X	Y	Z
1	6	0	4.747583	-1.108833	0.000039
2	6	0	4.639288	0.293822	0.000072
3	6	0	3.410846	0.942091	0.000039
4	6	0	2.254036	0.125013	-0.000027
5	7	0	2.391725	-1.222342	-0.000062
6	6	0	3.593392	-1.851665	-0.000031
7	1	0	3.560067	-2.934289	-0.000068
8	1	0	5.713632	-1.598731	0.000063
9	1	0	5.543710	0.895314	0.000125
10	6	0	3.289486	2.443950	0.000075
11	7	0	0.988848	0.658932	-0.000061
12	6	0	-0.224203	-0.087866	-0.000102
13	7	0	-1.329797	0.686341	-0.000065
14	6	0	-2.700492	0.279407	-0.000020
15	6	0	-3.646839	1.312086	-0.000054
16	6	0	-5.005394	1.009669	-0.000011
17	6	0	-5.426186	-0.321331	0.000067
18	6	0	-3.109843	-1.058671	0.000060
19	6	0	-4.476271	-1.342702	0.000102
20	1	0	-5.731958	1.816326	-0.000039
21	1	0	-6.485267	-0.559101	0.000101
22	1	0	-2.382409	-1.857435	0.000087
23	1	0	-4.795070	-2.380742	0.000164

24	1	0	-3.324039	2.351801	-0.000115
25	8	0	-0.194762	-1.319384	-0.000036
26	1	0	-1.205175	1.690946	-0.000084
27	1	0	4.277531	2.908996	0.000104
28	1	0	2.759912	2.809493	0.889745
29	1	0	2.759943	2.809538	-0.889594
30	1	0	1.492305	-1.736691	-0.000121

E = -742.767136036

1c·zwit1

Center Number	Atomic Number	Atomic Type	Coordinates (Angstroms) X	Y	Z
1	6	0	-3.300880	3.113524	-0.001689
2	6	0	-3.611741	1.741851	0.004126
3	6	0	-2.627663	0.758342	0.041817
4	6	0	-1.278097	1.199340	0.052153
5	7	0	-1.015908	2.528208	0.056834
6	6	0	-1.979394	3.483451	0.033504
7	1	0	-1.629023	4.508283	0.043903
8	1	0	-4.079053	3.866784	-0.021692
9	1	0	-4.651146	1.428320	-0.005357
10	6	0	-2.966182	-0.690466	0.036521
11	7	0	-0.226599	0.319645	0.032003
12	6	0	1.147951	0.674669	0.021694
13	7	0	1.974386	-0.392778	-0.031860
14	6	0	3.402624	-0.411527	-0.054303
15	6	0	3.999405	-1.675644	-0.145653
16	6	0	5.386228	-1.789781	-0.171114
17	6	0	6.184378	-0.646365	-0.105807
18	6	0	4.192445	0.741875	0.012448
19	6	0	5.581331	0.608080	-0.014679
20	1	0	5.839693	-2.773662	-0.242355
21	1	0	7.266155	-0.733534	-0.125676
22	1	0	3.734674	1.717961	0.082948
23	1	0	6.194443	1.502888	0.036871
24	1	0	3.381726	-2.570549	-0.197578
25	8	0	1.488092	1.858980	0.062805
26	1	0	1.552774	-1.312049	-0.076278
27	1	0	-0.004841	2.755126	0.065751
28	6	0	-3.765864	-1.217108	-0.990820
29	6	0	-2.524103	-1.541989	1.066495
30	6	0	-2.874465	-2.892809	1.061048
31	6	0	-3.665279	-3.407665	0.032012
32	6	0	-4.111482	-2.567848	-0.990792
33	1	0	-4.727819	-2.964328	-1.791917
34	1	0	-4.104071	-0.570863	-1.796183
35	1	0	-1.950020	-1.139676	1.898356
36	1	0	-2.543839	-3.537046	1.870284
37	1	0	-3.938666	-4.458428	0.030647

E = -934.511643157

1a·zwit2

Center Number	Atomic Number	Atomic Type	Coordinates (Angstroms) X	Y	Z
1	6	0	-5.025069	-0.691086	0.000000
2	6	0	-4.852009	0.706789	0.000000
3	6	0	-3.585805	1.264290	0.000000
4	6	0	-2.463333	0.417491	0.000000
5	7	0	-2.668079	-0.922739	0.000000
6	6	0	-3.903985	-1.485028	0.000000
7	1	0	-3.926055	-2.568214	0.000000
8	1	0	-6.010889	-1.139723	0.000000
9	1	0	-5.719876	1.358856	0.000000
10	1	0	-3.445800	2.340013	0.000000
11	7	0	-1.180659	0.900260	0.000000
12	6	0	0.000000	0.100604	0.000000
13	7	0	1.137668	0.824689	0.000000
14	6	0	2.489318	0.357305	0.000000
15	6	0	3.479913	1.347505	0.000000
16	6	0	4.823678	0.985230	0.000000
17	6	0	5.184864	-0.363221	0.000000
18	6	0	2.838425	-0.997710	0.000000
19	6	0	4.190923	-1.341830	0.000000
20	1	0	5.585361	1.758771	0.000000
21	1	0	6.232362	-0.647721	0.000000
22	1	0	2.075902	-1.763121	0.000000
23	1	0	4.463783	-2.392876	0.000000
24	1	0	3.203072	2.400377	0.000000
25	8	0	-0.087915	-1.128022	0.000000
26	1	0	-1.099483	1.909459	0.000000
27	1	0	-1.796691	-1.483055	0.000000

E = -703.414849118

1b·zwit2

Center Number	Atomic Number	Atomic Type	Coordinates (Angstroms) X	Y	Z
1	6	0	4.747583	-1.108833	0.000039
2	6	0	4.639288	0.293822	0.000072
3	6	0	3.410846	0.942091	0.000039
4	6	0	2.254036	0.125013	-0.000027
5	7	0	2.391725	-1.222342	-0.000062
6	6	0	3.593392	-1.851665	-0.000031
7	1	0	3.560067	-2.934289	-0.000068
8	1	0	5.713632	-1.598731	0.000063
9	1	0	5.543710	0.895314	0.000125
10	6	0	3.289486	2.443950	0.000075
11	7	0	0.988848	0.658932	-0.000061
12	6	0	-0.224203	-0.087866	-0.000102
13	7	0	-1.329797	0.686341	-0.000065
14	6	0	-2.700492	0.279407	-0.000020

15	6	0	-3.646839	1.312086	-0.000054
16	6	0	-5.005394	1.009669	-0.000011
17	6	0	-5.426186	-0.321331	0.000067
18	6	0	-3.109843	-1.058671	0.000060
19	6	0	-4.476271	-1.342702	0.000102
20	1	0	-5.731958	1.816326	-0.000039
21	1	0	-6.485267	-0.559101	0.000101
22	1	0	-2.382409	-1.857435	0.000087
23	1	0	-4.795070	-2.380742	0.000164
24	1	0	-3.324039	2.351801	-0.000115
25	8	0	-0.194762	-1.319384	-0.000036
26	1	0	0.947068	1.669322	-0.000024
27	1	0	4.277531	2.908996	0.000104
28	1	0	2.759912	2.809493	0.889745
29	1	0	2.759943	2.809538	-0.889594
30	1	0	1.492305	-1.736691	-0.000121

E = -742.737811139

1c·zwit2

Center Number	Atomic Number	Atomic Type	Coordinates (Angstroms) X	Y	Z
1	6	0	-3.300880	3.113524	-0.001689
2	6	0	-3.611741	1.741851	0.004126
3	6	0	-2.627663	0.758342	0.041817
4	6	0	-1.278097	1.199340	0.052153
5	7	0	-1.015908	2.528208	0.056834
6	6	0	-1.979394	3.483451	0.033504
7	1	0	-1.629023	4.508283	0.043903
8	1	0	-4.079053	3.866784	-0.021692
9	1	0	-4.651146	1.428320	-0.005357
10	6	0	-2.966182	-0.690466	0.036521
11	7	0	-0.226599	0.319645	0.032003
12	6	0	1.147951	0.674669	0.021694
13	7	0	1.974386	-0.392778	-0.031860
14	6	0	3.402624	-0.411527	-0.054303
15	6	0	3.999405	-1.675644	-0.145653
16	6	0	5.386228	-1.789781	-0.171114
17	6	0	6.184378	-0.646365	-0.105807
18	6	0	4.192445	0.741875	0.012448
19	6	0	5.581331	0.608080	-0.014679
20	1	0	5.839693	-2.773662	-0.242355
21	1	0	7.266155	-0.733534	-0.125676
22	1	0	3.734674	1.717961	0.082948
23	1	0	6.194443	1.502888	0.036871
24	1	0	3.381726	-2.570549	-0.197578
25	8	0	1.488092	1.858980	0.062805
26	1	0	-0.504152	-0.656166	0.005236
27	1	0	-0.004841	2.755126	0.065751
28	6	0	-3.765864	-1.217108	-0.990820
29	6	0	-2.524103	-1.541989	1.066495
30	6	0	-2.874465	-2.892809	1.061048
31	6	0	-3.665279	-3.407665	0.032012
32	6	0	-4.111482	-2.567848	-0.990792

33	1	0	-4.727819	-2.964328	-1.791917
34	1	0	-4.104071	-0.570863	-1.796183
35	1	0	-1.950020	-1.139676	1.898356
36	1	0	-2.543839	-3.537046	1.870284
37	1	0	-3.938666	-4.458428	0.030647

E = -934.483985369

General crystallographic information for 2a, 2b, 2c, 1aCl, 1bCl, 1aTFA, 1bTFA, 1cTFA, 1aBARF, and 1cBARF·BNS

X-ray diffraction data for **2c**, **1a·BARF**, **1a·TFA**, **1b·TFA**, and, **1c·BARF·BNS** were collected at 100 K, while data for **1c·TFA**, **2b**, and **2a** were collected at were collected at 105 K, 110 K, and 115 K respectively. Data for all structures were collected on a Bruker D8 Venture using MoKα-radiation (λ = 0.71073 Å) except **1c·BARF·BNS** data which were collected using CuKα (λ = 1.54178 Å). All Data have been corrected for absorption using SADABS[7] area detector absorption correction program. Using Olex2, the structures (except **1c·BARF·BNS** SHELXD dual space direct methods) were solved with the SHELXT structure solution program using Direct Methods and refined with the SHELXL refinement package using least squares minimization. In all structures all non-hydrogen atoms were refined with anisotropic thermal parameters. Hydrogen atoms attached to heteroatoms were found from the residual density maps, placed, and refined with isotropic thermal parameters and exceptions to this are detailed below. All other hydrogen atoms in the investigated structures were located from difference Fourier maps but finally their positions were placed in geometrically calculated positions and refined using a riding model. Isotropic thermal parameters of the placed hydrogen atoms were fixed to 1.2 times the *U* value of the atoms they are linked to (1.5 times for methyl groups). Calculations and refinement of structures were carried out using

[7] Sheldrick, G. M. (1996). SADABS: Area Detector Absorption Correction; University of Göttingen, Germany.

APEX2,[8] APEX3,[9] SHELXTL, and Olex2 software. Individual structure refinement details and crystal growth conditions are given below. Crystallographic data for all structures are presented below.

2a – CCDC 1843472

Colorless rods were grown by slow evaporation of a methanol, trifluoroacetic acid solution of **2a.**

2b – CCDC 1843470

Colorless plates were grown by slow evaporation of a methanol, water, and trifluoroacetic acid solution of **2b.**

2c – CCDC 1843468

Colorless rods were grown by vapor diffusion of hexanes into an ethanol solution of **2c**.

1aCl – No CCDC

Diffraction quality crystals were grown by slow evaporation of an acetone and HCl (aq) solution of **1aCl**. The crystal selected was a clear colorless prism with dimensions of 0.14 mm x 0.14 mm x 0.10 mm.

1bCl – No CCDC

Diffraction quality crystals were grown by slow evaporation of an acetonitrile solution of **1bCl**. The crystal selected was a clear colorless prism with dimensions of 0.44 mm x 0.24 mm x 0.22 mm.

1aTFA – CCDC 1843469

[8] Bruker (2007). APEX2. Bruker AXS Inc., Madison, Wisconsin, USA.
[9] Bruker (2016). APEX3. Bruker AXS Inc., Madison, Wisconsin, USA.

Colorless prisms were grown by vapor diffusion of heptane into a dichloromethane solution of **1a·TFA.**

1bTFA – CCDC 1843471

Colorless plates were grown by vapor diffusion of toluene into a methanol/trifluoroacetic acid solution of **1b·TFA.**

1cTFA – CCDC 1843467

Colorless plates were grown by slow evaporation of an acetone, water and trifluoroacetic acid solution of **2c**.

The location of the hydrogen atom participating in the acid—acetate interaction was located from the difference map. The location of the residual electron density peak was ≈ 0.95Å from O4 and ≈1.5Å from O3. Upon refinement, the hydrogen atom moved slightly to a more central location between the oxygen atoms (≈1.0Å from O4). Due to this the O4-H4 bond length has been restrained using DFIX 0.95 0.01.

1aBARF – CCDC 1843473

Colorless prisms were grown from a toluene, and pentane solution of **1a·BARF.**

The structure was found to contain a disordered toluene molecule near an inversion center, and an indistinguishable solvent molecule roughly 2.6 Å from a water molecule. The toluene molecule was treated with a PART -1 and a site occupancy factor of 10.5000 instructions. Along with an AFIX 65 constraint on the ring and RIGU restraints led to a reasonable toluene model. Hydrogen atoms of the toluene were not found from the difference map and were placed in geometrically calculated positions and refined using a riding model. Isotropic thermal parameters of the placed hydrogen atoms were fixed

to 1.2 times the U value of the atoms they are linked to (1.5 times for methyl groups). The indistinguishable solvent is believed to be a partially occupied water and has been modeled as an oxygen atom (no hydrogens) with a site occupancy factor instruction of 10.2000. The location of the toluene near a special position and the partial occupancy of a third water molecule account for the non-integer values of the chemical formula. Numerous trifluoro methyl groups displayed disorder accounting for some of the checkcif thermal parameter alerts. These groups are likely best described as dynamic disorder but have been modeled over two positions.

1cBARF·BNS – CCDC 1843474

Colorless plates were grown by slow evaporation of a chloroform solution of **1cBARF·BNS.**

Hydrogen atoms attached to heteroatoms were found from the residual density maps. These hydrogen atoms when placed and refined resulted in unreasonable shortening of the N—H bond length. Given the lower resolution (1 Å) of the data and this shortening the decision was made to place the atoms in geometrically calculated positions riding on the parent atom.

The weakly diffracting sample dictated data collection to a theta(max) of 50.493°. This results in a lower ratio of measurements to refined parameters. An excessive and unnecessary use of constraints to improve this ratio could be employed, however this would not significantly change the results and therefore was not implemented in the refinement.

Crystallographic data for ureas

Identification code	**1a·TFA**	**1a·BARF**	**1c·BARF·BNS**	**1b·TFA**	**1c·TFA**	**2a**	**2b**	**2c**
Empirical formula	$C_{14}H_{12}F_3N_3O_3$	$C_{45.75}H_{28}BF_{24}N_3O_{2.1}$	$C_{58}H_{35}BF_{24}N_4O_3$	$C_{15}H_{14}F_3N_3O_3$	$C_{22}H_{17}F_6N_3O_5$	$C_{12}H_{11}N_3O$	$C_{13}H_{13}N_3O$	$C_{18}H_{15}N_3O$
Formula weight	327.27	1120.12	1302.71	341.29	517.39	213.24	227.26	289.33
Temperature/K	100	100	100	100	105	115	110	100
Crystal system	triclinic	triclinic	monoclinic	triclinic	triclinic	monoclinic	monoclinic	monoclinic
Space group	*P*-1	*P*-1	*P*2/*c*	*P*-1	*P*-1	*P*2$_1$/*c*	*C*2/*c*	*P*2$_1$/*n*
a/Å	8.5503(5)	13.3563(13)	37.9002(19)	6.7828(4)	8.7549(5)	5.5203(5)	27.2174(17)	5.6195(4)
b/Å	9.1631(5)	18.9881(18)	17.6328(9)	9.8879(6)	10.3102(6)	19.7229(18)	5.1498(3)	12.1789(8)
c/Å	10.1971(5)	21.291(2)	17.1111(8)	11.3335(7)	13.9306(8)	19.2215(17)	16.0655(10)	20.6621(14)
α/°	110.474(2)	64.635(2)	90	81.477(2)	104.100(3)	90	90	90
β/°	97.124(2)	84.966(3)	100.239(2)	82.468(2)	99.412(3)	96.753(5)	91.316(2)	93.152(2)
γ/°	106.199(2)	69.797(2)	90	83.006(2)	112.546(3)	90	90	90
Volume/Å^3	696.59(7)	4567.3(8)	11253.0(10)	741.16(8)	1079.02(11)	2078.2(3)	2251.2(2)	1411.96(17)
Z	2	4	8	2	2	8	8	4
ρ_{calc}g/cm^3	1.560	1.629	1.538	1.529	1.592	1.363	1.341	1.361
μ/mm^{-1}	0.138	0.168	1.339	0.133	0.147	0.091	0.088	0.087
F(000)	336.0	2245.0	5248.0	352.0	528.0	896.0	960.0	608.0
Crystal size/mm^3	0.30 × 0.20 × 0.06	0.20 × 0.18 × 0.15	0.31 × 0.18 × 0.04	0.37 × 0.20 × 0.01	0.10 × 0.10 × 0.03	0.40×0.05 × 0.03	0.55 × 0.20 × 0.02	0.20 × 0.20 × 0.15
Radiation	MoKα (λ = 0.71073)	MoKα (λ = 0.71073)	CuKα (λ = 1.54178)	MoKα (λ = 0.71073)	MoKα (λ = 0.71073)	MoKα (λ = 0.71073)	MoKα (λ = 0.71073)	MoKα (λ = 0.71073)
2Θ range for data collection/°	5.818 to 56.668	5.766 to 54.318	4.738 to 100.986	5.92 to 54.97	6.078 to 57.394	5.94 to 50.05	5.95 to 54.968	6.692 to 52.798
Index ranges	-11 ≤ h ≤ 11, -12 ≤ k ≤ 12, -13 ≤ l ≤ 13	-17 ≤ h ≤ 17, -24 ≤ k ≤ 24, -27 ≤ l ≤ 27	-37 ≤ h ≤ 37, -17 ≤ k ≤ 17, -17 ≤ l ≤ 17	-8 ≤ h ≤ 8, -12 ≤ k ≤ 12, -14 ≤ l ≤ 14	-11 ≤ h ≤ 11, -13 ≤ k ≤ 13, -18 ≤ l ≤ 18	-6 ≤ h ≤ 6, -23 ≤ k ≤ 23, -22 ≤ l ≤ 22	-34 ≤ h ≤ 34, -6 ≤ k ≤ 6, -20 ≤ l ≤ 20	-7 ≤ h ≤ 7, -15 ≤ k ≤ 15, -25 ≤ l ≤ 25
Reflections collected	34091	152257	149376	19923	32551	63272	14031	16818
Independent reflections	3476 [R_{int} = 0.0259, R_{sigma} = 0.0129]	20217 [R_{int} = 0.0514, R_{sigma} = 0.0425]	11746 [R_{int} = 0.0626, R_{sigma} = 0.0307]	3392 [R_{int} = 0.0388, R_{sigma} = 0.0317]	5568 [R_{int} = 0.0624, R_{sigma} = 0.0551]	3674 [R_{int} = 0.1168, R_{sigma} = 0.0467]	2581 [R_{int} = 0.0355, R_{sigma} = 0.0305]	2878 [R_{int} = 0.0454, R_{sigma} = 0.0358]
Data/restraints/parameters	3476/0/220	20217/353/1660	11746/102/1677	3392/94/252	5568/1/341	3674/0/305	2581/0/163	2878/0/207
Goodness-of-fit on F^2	1.043	1.017	1.017	1.021	1.021	1.034	1.036	1.050
Final R indexes [I>=2σ (I)]	R_1 = 0.0385, wR_2 = 0.0959	R_1 = 0.0511, wR_2 = 0.0979	R_1 = 0.0417, wR_2 = 0.1022	R_1 = 0.0423, wR_2 = 0.0932	R_1 = 0.0452, wR_2 = 0.0828	R_1 = 0.0481, wR_2 = 0.0910	R_1 = 0.0403, wR_2 = 0.0935	R_1 = 0.0417, wR_2 = 0.0805
Final R indexes [all data]	R_1 = 0.0447, wR_2 = 0.1003	R_1 = 0.0924, wR_2 = 0.1148	R_1 = 0.0575, wR_2 = 0.1104	R_1 = 0.0613, wR_2 = 0.1010	R_1 = 0.0884, wR_2 = 0.0942	R_1 = 0.0879, wR_2 = 0.1050	R_1 = 0.0601, wR_2 = 0.1017	R_1 = 0.0631, wR_2 = 0.0869
Largest diff. peak/hole / e Å^{-3}	0.55/-0.40	0.67/-0.47	0.42/-0.27	0.39/-0.20	0.37/-0.24	0.19/-0.22	0.30/-0.19	0.22/-0.19

Identification code	**1bCl**	**1aCl**
Empirical formula	$C_{13}H_{15}ClN_3O_{1.5}$	$C_{12}H_{13.74}ClN_3O_{1.87}$
Formula weight	272.73	265.37
Temperature/K	100	100
Crystal system	monoclinic	triclinic
Space group	C2/c	P-1
a/Å	14.6768(8)	8.8418(7)
b/Å	13.8211(8)	9.6416(7)
c/Å	14.5368(8)	15.6335(12)
α/°	90	74.147(2)
β/°	116.838(2)	76.129(2)
γ/°	90	86.302(2)
Volume/Å^3	2631.2(3)	1244.66(17)
Z	8	4
ρ_{calc}g/cm^3	1.377	1.416
μ/mm^{-1}	0.287	0.303
F(000)	1144.0	555.0
Crystal size/mm^3	0.44 × 0.24 × 0.22	0.14 × 0.14 × 0.1
Radiation	MoKα (λ = 0.71073)	MoKα (λ = 0.71073)
2Θ range for data collection/°	5.896 to 61.166	5.792 to 52.876
Index ranges	-20 ≤ h ≤ 20, -19 ≤ k ≤ 19, -20 ≤ l ≤ 19	-11 ≤ h ≤ 11, -12 ≤ k ≤ 12, -19 ≤ l ≤ 19
Reflections collected	33357	37794
Independent reflections	4044 [R_{int} = 0.0347, R_{sigma} = 0.0200]	5091 [R_{int} = 0.0433, R_{sigma} = 0.0325]
Data/restraints/parameters	4044/0/185	5091/51/375
Goodness-of-fit on F^2	1.032	1.044
Final R indexes [I>=2σ (I)]	R_1 = 0.0388, wR_2 = 0.0968	R_1 = 0.0403, wR_2 = 0.0821
Final R indexes [all data]	R_1 = 0.0485, wR_2 = 0.1025	R_1 = 0.0611, wR_2 = 0.0894
Largest diff. peak/hole / e Å^{-3}	0.52/-0.25	0.31/-0.25

REFERENCES

(1) van der Waals, J. D. Over de Continuitiet van Den Gas- En Valoeistoftoestand, Leiden University, **1873**.

(2) London, F. Zur Theorie Und Systematik Der Molekularkräfte. *Zeitschrift für Phys.* **1930**, *63*, 245–279.

(3) Eisenschitz, R.; London, F. Über Das Verhältnis Der van Der Waalsschen Kräfte Zu Den Homöopolaren Bindungskräften. *Zeitschrift für Phys.* **1930**, *60*, 491–527.

(4) Stone, A. J. *The Theory of Intermolecular Forces*; Oxford University Press: Oxford, **1997**.

(5) Kaplan, I. G. *Intermolecular Interactions*; Wiley: Chichester, **2006**.

(6) Leite, F. L.; Bueno, C. C.; Da Róz, A. L.; Ziemath, E. C.; Oliveira, O. N. *Theoretical Models for Surface Forces and Adhesion and Their Measurement Using Atomic Force Microscopy*; **2012**; Vol. 13.

(7) Minkin, V. I.; Osipov, O. A.; Zhdanov, Y. A. *Dipole Moments in Organic Chemistry*; Plenum Press: New York, 1970.

(8) Huggins, M. The Role of Hydrogen Bonds in Conduction by Hydrogen and Hydroxyl Ions. *J. Am. C* **1931**, *53*, 3190–3191.

(9) Latimer, W. M.; Rodebush, W. H. Polarity and Ionization from the Standpoint of the Lewis Theory of Valence. *J. Am. Chem. Soc.* **1920**, *42* (7), 1419–1433.

(10) Pauling, L. The Nature of the Chemical Bond. Application of Results Obtained from the Quantum Mechanics and from a Theory of Paramagnetic Susceptibility to the Structure of Molecules. *J. Am. Chem. Soc.* **1931**, *53* (4), 1367–1400.

(11) Pauling, L. *The Nature of the Chemical Bond, and the Structure of Molecules and Crystals; an Introduction to Modern Structural Chemistry*; Cornell University Press: Ithaca, **1939**.

(12) Arunan, E.; Desiraju, G. R.; Klein, R. A.; Sadlej, J.; Scheiner, S.; Alkorta, I.; Clary, D. C.; Crabtree, R. H.; Dannenberg, J. J.; Hobza, P.; et al. Definition of the Hydrogen Bond (IUPAC Recommendations 2011). *Pure Appl. Chem.* **2011**, *83* (8), 1637–1641.

(13) Jeffrey, G. A. *An Introduction to Hydrogen Bonding*; Oxford University Press: Oxford, **1997**.

(14) Atwood, J. L.; Barbour, L. J.; Jerga, A. Organization of the Interior of Molecular Capsules by Hydrogen Bonding. *Proc. Natl. Acad. Sci.* **2002**, *99* (8), 4837–4841.

(15) Tepper, R.; Schulze, B.; Görls, H.; Bellstedt, P.; Jäger, M.; Schubert, U. S. Preorganization in a Cleft-Type Anion Receptor Featuring Iodo-1,2,3-Triazoles As Halogen Bond Donors. *Org. Lett.* **2015**, *17* (23), 5740–5743.

(16) Marie, A.; Riel, S.; Decato, D. A.; Sun, J.; Massena, C. J.; Jessop, M. J.; Berryman, O. B. The Intramolecular Hydrogen Bonded–halogen Bond: A New Strategy for Preorganization and Enhanced Binding. *Chem. Sci.* **2018**, 5828–5836.

(17) Kim, M. J.; Lee, H. W.; Moon, D.; Jeong, K. S. Helically Foldable Diphenylureas as Anion Receptors: Modulation of the Binding Affinity by the Chain Length. *Org. Lett.* **2012**, *14* (19), 5042–5045.

(18) Custelcean, R. Urea-Functionalized Crystalline Capsules for Recognition and Separation of Tetrahedral Oxoanions. *Chem. Commun.* **2013**, *49*, 2173.

(19) Bredig, G.; Fiske, P. S. Durch Katalysatoren Bewirkte Asymmetrische Synthese. *Biochem. Z.* **1912**, *46*, 7–23.
(20) Hajos, Z. G.; Parrish, D. R. Asymmetric Synthesis of Bicyclic Intermediates of Natural Product Chemistry. *J. Org. Chem.* **1974**, *39* (12), 1615–1621.
(21) Sigman, M. S.; Jacobsen, E. N. Schiff Base Catalysts for the Asymmetric Strecker Reaction Identified and Optimized from Parallel Synthetic Libraries. *J. Am. Chem. Soc.* **1998**, *120*, 4901–4902.
(22) Sigman, M. S.; Vachal, P.; Jacobsen, E. N. A General Catalyst for the Asymmetric Strecker Reaction. *Angew. Chem. Int. Ed.* **2000**, *39* (7), 1279–1281.
(23) Curran, D. P.; Kuo, L. H. Altering the Stereochemistry of Allylation Reactions of Cyclic α-Sulfinyl Radicals with Diarylureas. *J. Org. Chem.* **1994**, *59*, 3259–3261.
(24) Curran, D. P.; Kuo, L. H. Acceleration of a Dipolar Claisen Rearrangement by Hydrogen Bonding to a Soluble Diaryl Urea. *Tetrahedron Lett.* **1995**, *36* (37), 6647–6650.
(25) Schreiner, P. R.; Wittkopp, A. H-Bonding Additives Act Like Lewis Acid Catalysts. *Org. Lett.* **2002**, *4*, 217–220.
(26) Wittkopp, A.; Schreiner, P. R. Metal-Free, Noncovalent Catalysis of Diels-Alder Reactions by Neutral Hydrogen Bond Donors in Organic Solvents and in Water. *Chem. A Eur. J.* **2003**, *9*, 407–414.
(27) List, B.; Lerner, R. A.; Barbas, C. F. Proline-Catalyzed Direct Asymmetric Aldol Reactions. *J. Am. Chem. Soc.* **2000**, *122* (10), 2395–2396.
(28) Gröger, H.; Wilken, J. The Application of L-Proline as an Enzyme Mimic and Further New Asymmetric Syntheses Using Small Organic Molecules as Chiral Catalysts. *Angew. Chem. Int. Ed.* **2001**, *40* (3), 529–532.
(29) Merino, P.; Tejero, T. Organocatalyzed Asymmetric α-Aminoxylation of Aldehydes and Ketones - An Efficient Access to Enantiomerically Pure α-Hydroxycarbonyl Compounds, Diols, and Even Amino Alcohols. *Angew. Chem. Int. Ed.* **2004**, *43* (23), 2995–2997.
(30) Houk, K. N.; List, B. Asymmetric Organocatalysis. *Acc. Chem. Res.* **2004**, *37* (8), 487–487.
(31) Movassaghi, M.; Jacobsen, E. N. The Simplest "Enzyme." *Science* **2002**, *298*, 1904–1905.
(32) McDougal, N. T.; Schaus, S. E. Asymmetric Morita-Baylis-Hillman Reactions Catalyzed by Chiral Brønsted Acids. *J. Am. Chem. Soc.* **2003**, *125* (40), 12094–12095.
(33) Yamada, Y. M. A.; Ikegami, S. Efficient Baylis-Hillman Reactions Promoted by Mild Cooperative Catalysts and Their Application to Catalytic Asymmetric Synthesis. *Tetrahedron Lett.* **2000**, *41* (13), 2165–2169.
(34) Matsui, K.; Takizawa, S.; Sasai, H. Bifunctional Organocatalysts for Enantioselective Aza-Morita-Baylis-Hillman Reaction. *J. Am. Chem. Soc.* **2005**, *127* (11), 3680–3681.
(35) Hine, J.; Linden, S. M.; Kanagasabapathy, V. M. 1,8-Biphenylenediol Is a Double-Hydrogen-Bonding Catalyst for Reaction of an Epoxide with a Nucleophile. *J. Am. Chem. Soc.* **1985**, *107* (4), 1082–1083.

(36) Kelly, T. R.; Meghani, P.; Ekkundi, V. S. Diels-Alder Reactions: Rate Acceleration Promoted by a Biphenylenediol. *Tetrahedron Lett.* **1990**, *31*, 3381–3384.
(37) Corey, E. J.; Grogan, M. J. Enantioselective Synthesis of α-Amino Nitriles from *N* -Benzhydryl Imines and HCN with a Chiral Bicyclic Guanidine as Catalyst. *Org. Lett.* **1999**, *1* (1), 157–160.
(38) Schuster, T.; Kurz, M.; Göbel, M. W. Catalysis of a Diels-Alder Reaction by Amidinium Ions. *J. Org. Chem.* **2000**, *65* (6), 1697–1701.
(39) Schuster, T.; Bauch, M.; Dürner, G.; Göbel, M. W. Axially Chiral Amidinium Ions as Inducers of Enantioselectivity in Diels-Alder Reactions. *Org. Lett.* **2000**, *2* (2), 179–181.
(40) Bach, T.; Bergmann, H.; Harms, K. Enantioselective Intramolecular [2+2]-Photocycloaddition Reactions in Solution. *Angew. Chem. Int. Ed.* **2000**, *39* (13), 2302–2304.
(41) Grosch, B.; Orlebar, C. N.; Herdtweck, E.; Kaneda, M.; Wada, T.; Inoue, Y.; Bach, T. Enantioselective [4+2]-Cycloaddition Reaction of a Photochemically Generated o-Quinodimethane: Mechanistic Details, Association Studies, and Pressure Effects. *Chem. A Eur. J.* **2004**, *10* (9), 2179–2189.
(42) Bach, T.; Aechtner, T.; Neumüller, B. Enantioselective Norrish Yang Cyclization Reactions of N-(ω-Oxo-ω-Phenylalkyl)-Substituted Imidazolidinones in Solution and in the Solid State. *Chem. A Eur. J.* **2002**, No. 11, 2464–2475.
(43) Aechtner, T.; Dressel, M.; Bach, T. Hydrogen Bond Mediated Enantioselectivity of Radical Reactions. *Angew. Chem. Int. Ed.* **2004**, *43* (43), 5849–5851.
(44) Takemoto, Y.; Kuraoka, S.; Hamaue, N.; Aoe, K.; Hiramatsu, H.; Iwata, C. Enantioselective Cu-Catalyzed 1,4-Addition of Me3 Al to a 4,4-Disubstituted Cyclohexa-2,5-Dienone. *Tetrahedron* **1996**, *52* (45), 14177–14188.
(45) Huang, Y.; Unni, A. K.; Thadani, A. N.; Rawal, V. H. Single Enantiomers from a Chiral-Alcohol Catalyst. *Nature* **2003**, *424* (6945), 146.
(46) Du, H.; Zhao, D.; Ding, K. Enantioselective Catalysis of the Hetero-Diels-Alder Reaction between Brassard's Diene and Aldehydes by Hydrogen-Bonding Activation: A One-Step Synthesis of (S)-(+)-Dihydrokawain. *Chem. A Eur. J.* **2004**, *10* (23), 5964–5970.
(47) Akiyama, T.; Itoh, J.; Yokota, K.; Fuchibe, K. Enantioselective Mannich-Type Reaction Catalyzed by a Chiral Brønsted Acid. *Angew. Chem. Int. Ed.* **2004**, *43* (12), 1566–1568.
(48) Uraguchi, D.; Terada, M. Chiral Brønsted Acid-Catalyzed Direct Mannich Reactions via Electrophilic Activation. *J. Am. Chem. Soc.* **2004**, *126* (17), 5356–5357.
(49) Rueping, M.; Sugiono, E.; Azap, C.; Theissmann, T.; Bolte, M. Enantioselective Brønsted Acid Catalyzed Transfer Hydrogenation: Organocatalytic Reduction of Imines. *Org. Lett.* **2005**, *7* (17), 3781–3783.
(50) Tian, S. K.; Chen, Y.; Hang, J.; Tang, L.; McDaid, P.; Deng, L. Asymmetric Organic Catalysis with Modified Cinchona Alkaloids. *Acc. Chem. Res.* **2004**, *37* (8), 621–631.
(51) McDaid, P.; Chen, Y.; Deng, L. A Highly Enantioselective and General Conjugate Addition of Thiols to Cyclic Enones with an Organic Catalyst. *Angew. Chem. Int.*

Ed. **2002**, *41* (2), 338–340.
(52) Iwabuchi, Y.; Nakatani, M.; Yokoyama, N.; Hatakeyama, S. Chiral Amine-Catalyzed Asymmetric Baylis− Hillman Reaction: A Reliable Route to Highly Enantiomerically Enriched (α-Methylene-β-Hydroxy) Esters. *J. Am. Chem. Soc* **1999**, *121* (13), 10219–10220.
(53) Li, H.; Wang, Y.; Tang, L.; Deng, L. Highly Enantioselective Conjugate Addition of Malonate and β-Ketoester to Nitroalkenes: Asymmetric C-C Bond Formation with New Bifunctional Organic Catalysts Based on Cinchona Alkaloids. *J. Am. Chem. Soc.* **2004**, *126* (32), 9906–9907.
(54) Desiraju, G. R.; Ho, P. S.; Kloo, L.; Legon, A. C.; Marquardt, R.; Metrangolo, P.; Politzer, P.; Resnati, G.; Rissanen, K. Definition of the Halogen Bond (IUPAC Recommendations 2013). *Pure Appl. Chem.* **2013**, *85* (8), 1711–1713.
(55) Hassel, O.; Hvoslef, J.; Vihovde, E. H.; Sörensen, N. A. The Structure of Bromine 1,4-Dioxanate. *Acta Chemica Scandinavica*. 1954, pp 873–873.
(56) Clark, T.; Hennemann, M.; Murray, J. S.; Politzer, P. Halogen Bonding: The σ-Hole: Proceedings of "Modeling Interactions in Biomolecules II", Prague, September 5th-9th, 2005. *J. Mol. Model.* **2007**, *13* (2), 291–296.
(57) Politzer, P.; Murray, J. S.; Clark, T. Halogen Bonding and Other σ-Hole Interactions: A Perspective. *Phys. Chem. Chem. Phys.* **2013**, *15* (27), 11178.
(58) Clark, T.; Politzer, P.; Murray, J. S. Correct Electrostatic Treatment of Noncovalent Interactions: The Importance of Polarization. *WIREs Comput. Mol. Sci.* **2015**, *5* (2), 169–177.
(59) Stasyuk, O. A.; Sedlak, R.; Hobza, P. Comparison of the DFT-SAPT and Canonical EDA Schemes for the Energy Decomposition of Various Types of Noncovalent Interactions. *J. Chem. Theory Comput.* **2018**.
(60) Riley, K. E.; Hobza, P. Investigations into the Nature of Halogen Bonding Including Symmetry Adapted Perturbation Theory Analyses. *J. Chem. Theory Comput.* **2008**, *4* (2), 232–242.
(61) Chudzinski, M. G.; Taylor, M. S. Correlations between Computation and Experimental Thermodynamics of Halogen Bonding. *J. Org. Chem.* **2012**, *77* (7), 3483–3491.
(62) Huber, S. M.; Scanlon, J. D.; Jimenez-Izal, E.; Ugalde, J. M.; Infante, I. On the Directionality of Halogen Bonding. *Phys. Chem. Chem. Phys.* **2013**, *15* (25), 10350.
(63) Kilah, N. L.; Wise, M. D.; Beer, P. D. Crystallographic Implications for the Design of Halogen Bonding Anion Receptors. *Cryst. Growth Des.* **2011**, *11* (10), 4565–4571.
(64) Cavallo, G.; Metrangolo, P.; Milani, R.; Pilati, T.; Priimagi, A.; Resnati, G.; Terraneo, G. The Halogen Bond. *Chem. Rev.* **2016**, *116* (4), 2478–2601.
(65) Raatikainen, K.; Cavallo, G.; Metrangolo, P.; Resnati, G.; Rissanen, K.; Terraneo, G. In the Pursuit of Efficient Anion-Binding Organic Ligands Based on Halogen Bonding. *Cryst. Growth Des.* **2013**, *13*, 871–877.
(66) Rissanen, K. Halogen Bonded Supramolecular Complexes and Networks. *CrystEngComm* **2008**, *10* (9), 1107.
(67) Troff, R. W.; Mäkelä, T.; Topič, F.; Valkonen, A.; Raatikainen, K.; Rissanen, K. Alternative Motifs for Halogen Bonding. *Eur. J. Org. Chem.* **2013**, 1617–1637.

(68) Arman, H. D.; Gieseking, R. L.; Hanks, T. W.; Pennington, W. T. Complementary Halogen and Hydrogen Bonding: Sulfur···iodine Interactions and Thioamide Ribbons. *Chem. Commun.* **2010**, *46* (11), 1854–1856.
(69) Walsh, R. B.; Padgett, C. W.; Metrangolo, P.; Resnati, G.; Hanks, T. W.; Pennington, W. T. Crystal Engineering through Halogen Bonding: Complexes of Nitrogen Heterocycles with Organic Iodides. *Cryst. Growth Des.* **2001**, *1* (2), 165–175.
(70) Aakeröy, C. B.; Fasulo, M.; Schultheiss, N.; Desper, J.; Moore, C. Structural Competition between Hydrogen Bonds and Halogen Bonds. *J. Am. Chem. Soc.* **2007**, *129* (45), 13772–13773.
(71) Alvarez, S. A Cartography of the van Der Waals Territories. *Dalt. Trans.* **2013**, *42* (24), 8617–8636.
(72) Vargas Jentzsch, A.; Hennig, A.; Mareda, J.; Matile, S. Synthetic Ion Transporters That Work with Anion-π Interactions, Halogen Bonds, and Anion-Macrodipole Interactions. *Acc. Chem. Res.* **2013**, *46* (12), 2791–2800.
(73) Molina, P.; Zapata, F.; Caballero, A. Anion Recognition Strategies Based on Combined Noncovalent Interactions. *Chem. Rev.* **2017**, *117* (15), 9907–9972.
(74) Tepper, R.; Schubert, U. S. Halogen Bonding in Solution: Anion Recognition, Templated Self-Assembly, and Organocatalysis. *Angew. Chem. Int. Ed.* **2018**, *57* (21), 6004–6016.
(75) Lorenzo Gualandi, Elisabetta Mezzina, Paola Franchi, M. L. Nitroxide Radical Spin Probes for Exploring Halogen-Bonding Interactions in Solution. *Chem. A Eur. J.* **2016**, *22*, 16017–16021.
(76) Jungbauer, S. H.; Schindler, S.; Herdtweck, E.; Keller, S.; Huber, S. M. Multiple Multidentate Halogen Bonding in Solution, in the Solid State, and in the (Calculated) Gas Phase. *Chem. A Eur. J.* **2015**, *21*, 13625–13636.
(77) Massena, C. J.; Wageling, N. B.; Decato, D. A.; Martin Rodriguez, E.; Rose, A. M.; Berryman, O. B. A Halogen-Bond-Induced Triple Helicate Encapsulates Iodide. *Angew. Chem. Int. Ed.* **2016**, *55* (40), 12398–12402.
(78) Amendola, V.; Bergamaschi, G.; Boiocchi, M.; Fusco, N.; Rocca, M. V. La; Linati, L.; Presti, E. Lo; Mella, M.; Metrangolo, P.; Miljkovic, A. Novel Hydrogen- and Halogen-Bonding Anion Receptors Based on 3-Iodopyridinium Units. *RSC Adv.* **2016**, *6*, 67540–67549.
(79) Chakraborty, S.; Duttaa, R.; Ghosh, P. Halogen Bonding Assisted Selective Removal of Bromide. *Chem. Commun.* **2015**, *51*, 14793–14796.
(80) Ruiz-Botella, S.; Vidossich, P.; Ujaque, G.; Peris, E.; Beer, P. D. Tripodal Halogen Bonding Iodo-Azolium Receptors for Anion Recognition. *RSC Adv.* **2017**, *7*, 11253–11258.
(81) Langton, M. J.; Robinson, S. W.; Marques, I.; Félix, V.; Beer, P. D. Halogen Bonding in Water Results in Enhanced Anion Recognition in Acyclic and Rotaxane Hosts. *Nat. Chem.* **2014**, *6* (12), 1039–1043.
(82) Walter, S. M.; Kniep, F.; Herdtweck, E.; Huber, S. M. Halogen-Bond-Induced Activation of a Carbon-Heteroatom Bond. *Angew. Chem. Int. Ed.* **2011**, *50* (31), 7187–7191.

(83) Breugst, M.; Heiden, D. von der; Schmauck, J. Novel Noncovalent Interactions in Catalysis: A Focus on Halogen, Chalcogen, and Anion-π Bonding. *Synthesis* **2017**, *49* (15), 3224–3236.
(84) Breugst, M.; Detmar, E.; Von Der Heiden, D. Origin of the Catalytic Effects of Molecular Iodine: A Computational Analysis. *ACS Catal.* **2016**, *6* (5), 3203–3212.
(85) Yang, X. J.; Zhang, Y. Sen. Molecular Iodine: A Powerful Catalyst for the Knoevenagel Condensation of Isatins with Malononitrile. *J. Chem.* **2013**, 4 pages.
(86) Kniep, F.; Jungbauer, S. H.; Zhang, Q.; Walter, S. M.; Schindler, S.; Schnapperelle, I.; Herdtweck, E.; Huber, S. M. Organocatalysis by Neutral Multidentate Halogen-Bond Donors. *Angew. Chem. Int. Ed.* **2013**, *52* (27), 7028–7032.
(87) Jungbauer, S. H.; Walter, S. M.; Schindler, S.; Rout, L.; Kniep, F.; Huber, S. M. Activation of a Carbonyl Compound by Halogen Bonding. *Chem. Commun.* **2014**, *50* (47), 6281.
(88) Bulfield, D.; Huber, S. M. Halogen Bonding in Organic Synthesis and Organocatalysis. *Chem. A Eur. J.* **2016**, *22* (41), 14434–14450.
(89) Saito, M.; Kobayashi, Y.; Tsuzuki, S.; Takemoto, Y. Electrophilic Activation of Iodonium Ylides by Halogen-Bond-Donor Catalysis for Cross-Enolate Coupling. *Angew. Chem. Int. Ed.* **2017**, *56* (26), 7653–7657.
(90) Chan, Y. C.; Yeung, Y. Y. Halogen Bond Catalyzed Bromocarbocyclization. *Angew. Chem. Int. Ed.* **2018**, *57* (13), 3483–3487.
(91) Matsuzawa, A.; Takeuchi, S.; Sugita, K. Iodoalkyne-Based Catalyst-Mediated Activation of Thioamides through Halogen Bonding. *Chem. Asian J.* **2016**, 11, 2863–2866.
(92) Bew, S. P.; Fairhurst, S. A.; Hughes, D. L.; Legentil, L.; Liddle, J.; Pesce, P.; Nigudkar, S.; Wilson, M. A. Organocatalytic Aziridine Synthesis Using F^+ Salts. *Org. Lett.* **2009**, *11* (20), 4552–4555.
(93) Kazi, I.; Guha, S.; Sekar, G. CBr4as a Halogen Bond Donor Catalyst for the Selective Activation of Benzaldehydes to Synthesize α,β-Unsaturated Ketones. *Org. Lett.* **2017**, *19* (5), 1244–1247.
(94) Zhang, Z.; Schreiner, P. R. (Thio)Urea Organocatalysis—What Can Be Learnt from Anion Recognition? *Chem. Soc. Rev.* **2009**.
(95) Hay, B. P.; Gutowski, M.; Dixon, D. A.; Garza, J.; Vargas, R.; Moye, B. A. Structural Criteria for the Rational Design of Selective Ligands: Convergent Hydrogen Bonding Sites for the Nitrate Anion. *J. Am. Chem. Soc.* **2004**, *126* (25), 7925–7934.
(96) Robertson, C. C.; Perutz, R. N.; Brammer, L.; Hunter, C. A. A Solvent-Resistant Halogen Bond. *Chem. Sci.* **2014**, *5* (11), 4179–4183.
(97) Zapata, F.; Caballero, A.; White, N. G.; Claridge, T. D. W.; Costa, P. J.; Félix, V.; Beer, P. D. Fluorescent Charge-Assisted Halogen-Bonding Macrocyclic Halo-Imidazolium Receptors for Anion Recognition and Sensing in Aqueous Media. *J. Am. Chem. Soc.* **2012**, *134* (28), 11533–11541.
(98) Frassineti, C.; Ghelli, S.; Gans, P.; Sabatini, A.; Moruzzi, M. S.; Vacca, A. Nuclear Magnetic Resonance as a Tool for Determining Protonation Constants of Natural Polyprotic Bases in Solution. *Anal. Biochem.* **1995**, *231* (2), 374–382.
(99) Hirose, K. A Practical Guide for the Determinaation of Binding Constants. *J. Incl.*

Phenonena Mol. Recognit. Chem. **2001**, *39*, 193–209.
(100) Thordarson, P. Determining Association Constants from Titration Experiments in Supramolecular Chemistry. *Chem. Soc. Rev.* **2011**.
(101) Bryant, R. G. The NMR Time Scale. *J. Chem. Ed.* **1983**, *60* (1), 933–935.
(102) Riel, A. M. S.; Jessop, M. J.; Decato, D. A.; Massena, C. J.; Nascimento, V. R.; Berryman, O. B. Experimental Investigation of Halogen-bond Hard–soft Acid–base Complementarity. *Acta Crystallogr. Sect. B* **2017**, *73*, 203–209.
(103) Platts, J. A.; Howard, S. T.; Bracke, B. R. F. Directionality of Hydrogen Bonds to Sulfur and Oxygen. *J. Am. Chem. Soc.* **1996**, *118*, 2726–2733.
(104) Simón, L.; Goodman, J. M. Enzyme Catalysis by Hydrogen Bonds: The Balance between Transition State Binding and Substrate Binding in Oxyanion Holes. *J. Org. Chem.* **2010**, *75* (6), 1831–1840.
(105) Etter, M. C.; Urbañkzyk-Lipkowska, Z.; Zia-Ebrahimi, M.; Panunto, T. W. Hydrogen Bond Directed Cocrystallization and Molecular Recognition Properties of Diarylureas. *J. Am. Chem. Soc.* **1990**, *112*, 8415–8426.
(106) Amendola, V.; Fabbrizzi, L.; Mosca, L. Anion Recognition by Hydrogen Bonding: Urea-Based Receptors. *Chem. Soc. Rev.* **2010**, *39* (10), 3889.
(107) Connon, S. J. Organocatalysis Mediated by (Thio)Urea Derivatives. *Chem. A Eur. J.* **2006**.
(108) Maes, J.; Rauws, T. R. M.; Maes, B. U. W. Synthesis of C8-N9 Annulated Purines by Iron-Catalyzed C-H Amination. *Chem. A Eur. J.* **2013**, *19* (28), 9137–9141.
(109) Bolte, M.; Kühl, C.; Lüning, U. N,N'-Bis(6-Methyl-2-Pyridyl)Urea. *Acta Crystallogr. Sect. E* **2001**, *E57*, 502–504.
(110) Ganesh, M.; Seidel, D. Catalytic Enantioselective Additions of Indoles to Nitroalkenes. *J. Am. Chem. Soc.* **2008**, *130* (49), 16464–16465.
(111) Rashdan, S.; Light, M. E.; Kilburn, J. D. Pyridyl Thioureas as Switchable Anion Receptors. *Chem. Commun.* **2006**, *3*, 4578.
(112) Velinova, V.; Angelova, O.; Kossev, K. N-(2-Pyridyl)Urea. *Acta Crystallogr.* **1997**, *C53*, 1273–1275.
(113) So, S. S.; Burkett, J. A.; Mattson, A. E. Internal Lewis Acid Assisted Hydrogen Bond Donor Catalysis. *Org. Lett.* **2011**, *13*, 716–719.
(114) Fan, Y.; Kass, S. R. Electrostatically Enhanced Thioureas. *Org. Lett.* **2016**, *18*, 188–191.
(115) Thadani, A. N.; Stankovic, A. R.; Rawal, V. H. Enantioselective Diels-Alder Reactions Catalyzed by Hydrogen Bonding. *Proc. Natl. Acad. Sci. U. S. A.* **2004**, *101*, 5846–5850.
(116) McCooey, S. H.; Connon, S. J. Urea- and Thiourea-Substituted Cinchona Alkaloid Derivatives as Highly Efficient Bifunctional Organocatalysts for the Asymmetric Addition of Malonate to Nitroalkenes: Inversion of Configuration at C9 Dramatically Improves Catalyst Performance. *Angew. Chem. Int. Ed.* **2005**, *44*, 6367–6370.
(117) Simón, L.; Goodman, J. M. Enzyme Catalysis by Hydrogen Bonds: The Balance between Transition State Binding and Substrate Binding in Oxyanion Holes. *J. Org. Chem.* **2010**, *75*, 1831–1840.

(118) Shokri, A.; Wang, X. Bin; Kass, S. R. Electron-Withdrawing Trifluoromethyl Groups in Combination with Hydrogen Bonds in Polyols: Brønsted Acids, Hydrogen-Bond Catalysts, and Anion Receptors. *J. Am. Chem. Soc.* **2013**, *135* (25), 9525–9530.
(119) Hanwell, M. D.; Curtis, D. E.; Lonie, D. C.; Vandermeerschd, T.; Zurek, E.; Hutchison, G. R. Avogadro: An Advanced Semantic Chemical Editor, Visualization, and Analysis Platform. *J. Cheminform.* **2012**, *4* (8), 1–17.
(120) Bates, R. G.; Pinching, G. D. Acidic Dissociation Constant of Ammonium Ion at 0 to 50 C, and the Base Strength of Ammonia. *J. Res. Natl. Bur. Stand. (1934).* **1949**, *42*, 419.
(121) Uddin, N.; Choi, T. H.; Choi, C. H. Direct Absolute pK_a Predictions and Proton Transfer Mechanisms of Small Molecules in Aqueous Solution by QM/MM-MD. *J. Phys. Chem. B* **2013**, *117*, 6269–6275.
(122) Yakelis, N. A.; Bergman, R. G. Safe Preparation and Purification of Sodium Tetrakis[(3,5-Trifluoromethyl)Phenyl]Borate (NaBArF24): Reliable and Sensitive Analysis of Water in Solutions of Fluorinated Tetraarylborates. *Organometallics* **2005**, *24* (16), 3579–3581.
(123) Byrne, P.; Turner, D. R.; Lloyd, G. O.; Clarke, N.; Steed, J. W. Gradual Transition from NH··· Pyridyl Hydrogen Bonding to the NH··· O Tape Synthon in Pyridyl Ureas. *Cryst. Growth Des.* **2008**, *8* (9), 3335–3344.
(124) McGuirk, C. M.; Mendez-Arroyo, J.; D'Aquino, A. I.; Stern, C. L.; Liu, Y.; Mirkin, C. A. A Concerted Two-Pron Approach to the in Situ Allosteric Regulation of Bifunctional Catalysis. *Chem. Sci.* **2016**, *7*, 6674–6683.
(125) Tobe, Y.; Utsumi, N.; Nagano, A.; Sonoda, M.; Naemura, K. Synthesis of Butadiyne-Bridged [4n] Metacyclophanes Having Exo-Annular t-Butyl Groups. *Tetrahedron* **2001**, *57* (38), 8075–8083.
(126) M. J. Frisch; Trucks, G. W.; Schlegel, H. B.; Scuseria, G. E.; Robb, M. A.; Cheeseman, J. R.; Scalmani, G.; Barone, V.; Mennucci, B.; Petersson, G. A.; et al. Gaussian 09, Revision C.01. Gaussian Inc.: Wallingford CT **2010**.
(127) Dennington, R.; Keith, T.; Millam, J. GaussView, v. 5.0.9. Semichem Inc.: Shawnee Mission KS **2009**.